

From Soot to Space: Using Quantum Mechanical Methods to Investigate Combustion and
Astrochemical Processes

by

Josie E. Hendrix

A dissertation submitted in partial satisfaction of the

requirements for the degree of

Doctor of Philosophy

in

Chemistry

in the

Graduate Division

of the

University of California, Berkeley

Committee in charge:

Professor Martin Head-Gordon, Chair

Professor Teresa Head-Gordon

Professor Ehud Altman

Fall 2022

From Soot to Space: Using Quantum Mechanical Methods to Investigate Combustion and
Astrochemical Processes

Copyright 2022
by
Josie E. Hendrix

Abstract

From Soot to Space: Using Quantum Mechanical Methods to Investigate Combustion and Astrochemical Processes

by

Josie E. Hendrix

Doctor of Philosophy in Chemistry

University of California, Berkeley

Professor Martin Head-Gordon, Chair

Theoretical models and simulations that describe chemical systems at the quantum mechanical level of electrons and nuclei have become essential components supporting experimental chemistry. The use of adequately accurate quantum mechanical simulations can help guide experiments in the laboratory, or assist in the interpretation of experimental results. Density functional theory (DFT) in particular has become the most widely used method in electronic structure due to generally good performance for a moderate computational cost. The work in this thesis primarily involves the application of DFT and other electronic structure methods to explore chemical processes in the realms of astrochemistry and combustion chemistry. For all studies, we employ the generally accurate ω B97X-V density functional, and in some cases bolster our results using coupled-cluster methods with singles, doubles and perturbative triples correction (CCSD(T)). In Chapter 2, we characterize the cation, anion, and radical isomers of C_4H_4N , as well as reaction pathways that may lead to these isomers. Small, nitrogenated species such as C_4H_4N may be important precursors to prebiotic molecules formed in non-Earth environments such as the atmosphere of Titan, a moon of Saturn. In Chapter 3, we investigate more Earthly processes that may lead to incipient soot particles during incomplete combustion reactions of hydrocarbons. Specifically, rate constants for hydrogen ejection reactions are calculated and reaction sequences are modeled for a suite of polycyclic aromatic hydrocarbons that are postulated to be quite important in radical-chain reaction pathways leading to soot. In Chapter 4, we return to the interstellar medium, this time exploring surface reactions on cold, icy grains. To this end, we explore the optimized complex geometries and binding energies of astrochemically relevant neutral closed-shell, neutral open-shell, anionic and cationic small molecules to water clusters of up to four waters. Such quantities are important for constructing accurate models of interstellar reaction chemistry, where cold grains play an important role in the production and observed abundances of gas-phase species.

To my family, especially Bailey, and my dear friends
For supporting me always

Contents

Contents	ii
List of Figures	iv
List of Tables	ix
1 Introduction	1
1.1 The Schrödinger equation and general electronic structure	2
1.2 Hartree-Fock Theory	3
1.3 Density Functional Theory	7
1.4 Correlated Wavefunction Methods	11
1.5 Semi-Empirical Methods	15
1.6 Outline	17
2 The Cation, Anion, and Radical Isomers of C₄H₄N	20
2.1 Introduction	20
2.2 Methods	22
2.3 Results and Discussion	24
2.4 Conclusions	40
3 Characterization of Hydrogen Ejection Processes from Hydrocarbons	42
3.1 Introduction	42
3.2 Methods	45
3.3 Results and Discussion	47
3.4 Conclusions	56
4 Binding Energies and Motifs for Astrochemically Relevant Molecules	59
4.1 Introduction	59
4.2 Methods	62
4.3 Results and Discussion	63
4.4 Conclusions	78
Bibliography	80

A	Supplementary Information: The Cation, Anion, and Radical Isomers of C₄H₄N	105
A.1	Vibrational frequencies and IR intensities for A ⁻ , A [•] , and F ⁺	106
A.2	A comparison of DFT energies and CCSD(T)/CBS results	109
A.3	Optimized geometries for C ₄ H ₄ N	111
B	Supplemental Information: Characterization of Hydrogen Ejection Processes from Hydrocarbons	118
C	Supplementary Information: Binding Energies and Motifs for Astrochemically Relevant Molecules	130
C.1	Binding Energies of lowest-energy conformers	131
C.2	Coordinates for lowest energy conformers	136
C.3	Alternative conformers and relative energies	181

List of Figures

- 1.1 Jacob’s Ladder of density functionals. Functionals improve in their ability to accurately reproduce chemical data as the ladder ascends, with the inclusion of the density gradient, occupied and virtual orbitals, etc. 9
- 2.1 Structures of C_4H_4N in the closed-shell anionic state. Isomer (A^-) was found to be the energetic minimum, stabilized by a favorable 6π aromatic electron arrangement. Energetic differences are calculated with respect to (A^-) in kcal/mol. 25
- 2.2 Bond lengths (**I.**) and Natural Charges (**II.**) for anionic (A^-) calculated in ω B97X-V /aug-cc-pVTZ. Charges indicated on carbon atoms are a sum of the C–H moiety. The aromatic nature of the ring leads to a planar structure with lengthened $C_\alpha=C_\beta$ and slightly shortened $C_\beta-C_\beta$ and $C_\alpha-N$ (compared to pyrrole). 26
- 2.3 Structures of C_4H_4N in the radical configuration; relative energies are calculated with respect to (A^\bullet) in kcal/mol. Similar to the anionic state, (A^\bullet) is the lowest energy structure. Though electron removal has resulted in loss of complete aromaticity, (A^\bullet) still benefits from some delocalization of the remaining 5π electrons over the ring. 28
- 2.4 Comparison of molecular orbitals and electron configuration between (A^-) (left) and (A^\bullet) (right). The HOMO of anionic (A^-) is similar to the SOMO of the corresponding radical species, indicating electron removal from the anionic occurs from $2p_z$ orbitals on nitrogen that contribute to the π system. The $2p_y$ orbitals are largely undisturbed and contribute to the planarity of (A^\bullet). 29
- 2.5 Bond lengths (**I.**) and Natural charges (**II.**) for radical (A^\bullet) calculated in ω B97X-V /cc-pVTZ. Charges indicated on carbon atoms are a sum of the C–H moiety. Electron removal from anionic (A^-) has disrupted the aromaticity of the heterocycle, inducing small structural changes in the radical and reflecting the depletion of bonding character between α and β carbons. 30
- 2.6 Spin densities calculated for isomers (A^\bullet), (B^\bullet), and (C^\bullet). Electron spin is relatively delocalized in (A^\bullet), while it is highly localized for (B^\bullet) and (C^\bullet). 31
- 2.7 Structures of C_4H_4N in the cationic state; relative energies are expressed in kcal/mol. Heterocyclic (A), the global minimum on both anionic and radical potential energy surfaces, is now reduced to an anti-aromatic arrangement with 4π electrons in the ring, destabilizing the structure. The global minimum for the cationic surface was found to be (F^+), a linear structure reminiscent of cyanoallene. 32

- 2.8 Electronic configuration (**I.**), Natural charges (**II.**), and bond lengths (**III.**) for cationic (A^+). Charges indicated on carbon atoms are a sum of the C–H moiety. Half-filled orbitals contribute to the destabilization of this structure. In response, the $C_\alpha=C_\beta$ bonds elongate to 1.518 Å, close to a typical C–C single bond. 33
- 2.9 Bond lengths (**I.**) and Natural charges (**II.**) for cationic (F^+). Charges indicated on carbon atoms are a sum of the C–H moiety. This carbocation is of C_s symmetry, and is stabilized by electronic donation from the neighboring nitrogen and C–H σ bond to vacant p orbitals of the positively charged carbon. 34
- 2.10 Formation of anionic (A^-) from pyrrole via photodissociation. Dehydrogenation of the apical N follows excitation via energetic UV radiation, and electron attachment yields the stable anionic isomer. 36
- 2.11 Schematic reaction path to anionic (A^-) via CN^- and CH_3CCH . Both propyne and cyano anion have been detected in Titan’s ionosphere, and could feasibly react to produce anionic (A^-). The desired product (A^-) is stabilized relative to reactants by over 50 kcal/ mol. 37
- 2.12 Schematic pathway to anionic (A^-) via CN^\bullet and CH_3CCH . The presence of CN^\bullet in Titan’s ionosphere is predicted by several models to be significant. Reaction between this radical and propyne, could proceed similarly to the reaction depicted in Figure 10, with electron attachment to an intermediate species to form the desired product, which is stabilized by nearly 140 kcal/ mol. 38
- 2.13 Schematic representation of cyanoallene formation via the reaction of propyne (CH_3CCH) and cyano radical (CN^\bullet). The relevant transition state has been characterized by Balucani et al. and occurs through a submerged energetic barrier. This reaction is exothermic by about 18 kcal/mol, in good agreement with the aforementioned calculations. Structures were here optimized and energies calculated at the $\omega B97X-V$ /aug-cc-pVTZ level of theory. 39
- 2.14 Protonation of cyanoallene to form isomer (F^+). The excess energy may be emitted as a photon, or dispersed via collisions with a third body in the dense atmosphere of Titan. Structures were here optimized at the $\omega B97X-V$ /aug-cc-pVTZ level of theory. 40
- 3.1 Schematic illustration of the accepted steps beginning soot formation: (I) growth of gas-phase precursors, (II) particle inception and (III) particle growth. Hot hydrogen ejection (right inset) may speed reactions in radical-based mechanisms contributing to soot inception and growth [171]. This process may also assist dimer stabilization, growth at radical centers, and soot-particle inception. 43

3.2	Bond dissociation energies for selected open and closed shell parent hydrocarbon species - isomers are indicated by a roman numeral. Ejection is examined from free edge (FE) and zig-zag (ZZ) sites, indicated in red. Breaking C–H bonds to eject H from closed shell species is quite energetically costly, but barriers are markedly smaller for open-shell species, diminishing to between 25 and 50% of a saturated C–H bond energy for species I–V . All energies are corrected for zero-point energy (ZPE).	47
3.3	Ejection rates as a function of temperature and bond dissociation energy. Ejection occurs rapidly from ZZ sites of I–V , but more slowly from FE sites. For the most part, rates scale with C–H bond energies; C–H bonds in multi-ring radicals break more easily than those in small closed-shell species.	49
3.4	Schematic illustration of the CHRCR-inspired pathway from RSR vinylcyclopentadienyl to indenyl. V is initially formed via ring-closure, and various decomposition pathways are available, including immediate hydrogen ejection and fast isomerization to stable isomers. From nearly all C ₉ H ₉ isomers explored here, ejection as a primary route of hydrogen loss is rapid - for indene, spontaneous ejection is slower, and abstraction may be the preferred route in high-pressure scenarios.	52
3.5	Free energy barriers for sequential H ejection from isomers II , IV , and V . Significantly lower barriers to initial ejection from ZZ sites make this the preferred pathway, and the second ejection is typically more costly.	55
4.1	Zero point corrected DFT binding energies calculated for a set of closed-shell neutral molecules. As expected, non-polar molecules such as hydrocarbons exhibit weaker binding to water clusters, while molecules with a stronger dipole such as NH ₃ and H ₂ CO have binding energies that are nearly on par with water-water interactions.	63
4.2	Zero point corrected binding energies calculated using DFT for a set of neutral, open-shell molecules. Despite their reactive unpaired electrons, most open-shell species do not exhibit binding energies stronger than their neutral counterparts, nor do they <i>spontaneously</i> react in a significant way with H ₂ O in the water cluster.	66
4.3	Minima for H [•] , NO [•] , and CH ₃ [•] bound to water clusters of size <i>n</i> =3 and 4 waters. These three molecules bind only weakly to the clusters. The strongest hydrogen bonding interactions are still between water molecules, and minima configurations of these are undisturbed by the guest.	67
4.4	Minima for structures of NH ₂ [•] , OH [•] , and HCO [•] bound to water clusters of size <i>n</i> =3 and 4 waters. Hydrogen bonding interactions between the heavy atom of the guest molecule and hydrogen atoms of water are indicated by dashed lines. These guest molecules bind strongly and exhibit similar structures - hydrogen bond interactions generally become closer in distance as the number of waters in the cluster increases, resulting in steadily increasing binding strengths for NH ₂ [•] and OH [•]	68

4.5	Zero point corrected binding energies for cationic closed-shell molecules with water calculated using DFT. All ions tested here bind to water clusters significantly more strongly than neutral or radical molecules. The molecules with the strongest binding energies (NH_2^+ , CH_3^+ , HCO^+) react with water as the cluster size increases to form new solvated products and a free proton. Neutral H_2O is included as a reference point.	70
4.6	Optimized geometries for the lowest-energy conformers of NH_2^+ bound to water monomer, dimer, trimer, and tetramer. Close interaction between NH_2^+ and H_2O produces protonated hydroxylamine without a barrier; as the water cluster size grows, the potential for proton sharing increases, and hydroxylamine is deprotonated.	71
4.7	Optimized minima CH_3^+ bound to clusters of $n=1-4$ water molecules. Like NH_2^+ , CH_3^+ reacts with one of the water molecules to form a new species (methanol).	72
4.8	Zero point corrected binding energies for a set of anionic molecules calculated using DFT. The magnitude of binding energies exhibited by anions is greater than closed and open-shell neutrals, but less than that of cationic molecules in the previous section. Analogously to cations, the strongest binders are CH_3^- , NH_2^- , and HCO^- . Neutral H_2O is included as a reference point.	73
4.9	Hydrogen bonding (marked with dashed lines) for anionic conformers of CN^- , NO^- , and HCO_3^- with $n=3$ waters. NO^- and HCO_3^- maximize the number of hydrogen bonds formed between guest and water molecules, and thus have larger binding energies than CN^-	73
4.10	NH_2^- reactivity with water clusters of size $n=1-4$. NH_2^- acts as a strong base to barrierlessly deprotonate water, forming NH_3 and OH^- . The resulting hydroxyl anion clusters with the remaining water molecules in familiar structures, while newly formed NH_3 interacts less strongly.	74
4.11	Minima geometries of HCO^- interacting and reacting with $n=1-4$ water molecules. Different reactions occur with differing numbers of H_2O ; in the case of $n=2$ waters, HCO^- reacts with one water to form hydroxymethanolate, $\text{H}_2\text{COH}(\text{O})^-$, which is the conjugate base of methane diol, $\text{H}_2\text{C}(\text{OH})_2$. For $n > 3$ waters however, HCO^- deprotonates a water molecule to form formaldehyde and OH^-	75
4.12	Starting structures versus and their resulting optimized geometries for two conformers of NH_2^+ bound to water tetramer. Initial approach of the guest molecule via N results in a different configuration than approach via the H atoms of NH_2^+ . Both conformers form hydroxylamine, but form different composite structures with the remaining waters and shared proton. Energy differences are indicated with respect to the global minimum in kcal/mol.	76
4.13	Minima and next-lowest conformers of HCO^+ bound to water dimer and tetramer shown in conjunction with their respective starting structures. Energy differences are indicated with respect to the minima in kcal/mol.	76

B.1	Potential energy surface (PES) for sample CHRCR reaction sequence from vinylcyclopentadienyl to indenyl. Energetic barriers are expressed in kcal/mol. Isomerization barriers are shown for species (I).	118
C.1	DFT binding energies for closed-shell neutral molecules, zero point corrected. . .	131
C.2	DFT binding energies for open-shell neutral molecules, zero point corrected. . .	133
C.3	DFT binding energies for closed-shell cationic molecules, zero point corrected. . .	134
C.4	DFT binding energies for closed-shell anionic molecules, zero point corrected. . .	135

List of Tables

2.1	Adiabatic electron affinities and ionization energies (eV) relative to the radical species for all isomers, calculated using single point energies (CCSD(T)/CBS) of all isomers. All species (except perhaps G) are stabilized by electron gain. Ionization of radical (A [•]) requires significant energy, while ionization of radical (F [•]) is markedly more feasible.	35
3.1	Hydrogen ejection rates, both canonical and microcanonical, for C ₉ H ₉ species illustrated in Figure 4. Canonical rates are computed at 1600K; Microcanonical rates assume reactants at a temperature of 1600K. Rate units are in s ⁻¹ unless otherwise indicated.	53
4.1	Comparison of (zero-point corrected) ω B97X-V/def2-qzvppd and CCSD(T)/aug-cc-pVTZ binding energy values for select structures, reported in kcal/mol. General agreement is observed between the methods, and trends are preserved. . . .	65
A.1	Vibrational frequencies and IR intensities for A ⁻	106
A.2	Vibrational frequencies and IR intensities for A [•]	107
A.3	Vibrational frequencies and IR intensities for F ⁺	108
A.4	Relative energies of anionic isomers A-G, calculated both using the CCSD(T)/CBS scheme and the indicated density functional ω B97X-V in the aug-cc-pVTZ basis.	109
A.5	Relative energies of radical isomers A-G, calculated both using the CCSD(T)/CBS scheme and the indicated density functional ω B97X-V in the aug-cc-pVTZ basis. Structures were optimized using the latter DFT methodology, except in the cc-pVTZ basis.	110
A.6	Relative energies of cationic isomers A-G, calculated both using the CCSD(T)/CBS scheme and the indicated density functional ω B97X-V in the aug-cc-pVTZ basis. Structures were optimized using the latter DFT methodology, except in the cc-pVTZ basis.	110
B.1	Canonical RRKM rate constants for C ₁₃ H ₁₁ (II)	119
B.2	Canonical RRKM rate constants for C ₁₃ H ₁₁ (IV)	120
B.3	Canonical RRKM rate constants for C ₁₃ H ₁₀ (II)	121
B.4	Canonical RRKM rate constants for C ₁₃ H ₁₀ (IV)	122

B.5	Canonical RRKM rate constants for C_9H_9 (V)	123
B.6	Canonical RRKM rate constants for C_9H_9 (V) and C_9H_8 (V)	124
B.7	Canonical RRKM rate constants for C_9H_9 isomers	125
B.8	Canonical RRKM rate constants for indene, cyclopentadiene, and propyne. . . .	126
B.9	Canonical RRKM rate constants for triplet cyclopentadiene and triplet toluene .	127
B.10	Ordered energy barriers to ejection at 1600K	127
B.11	Microcanonical rate constants for select species. "Cutoff 500" indicates that a low frequency cutoff was included - frequencies less than 500 are set to $500cm^{-1}$. Monte Carlo sampling was used to determine the vibrational energy of reactant species preceding C_9H_9 . "Avg E" indicates the average thermal energy of reac- tants, and BDE indicates the barrier to dissociation in kcal/mol.	128
B.12	$k(E)$ calculated using MESMER for C_9H_9 (V)	129
C.1	Tabulated binding energies (in kcal/mol) for closed-shell neutral molecules with clusters of size $n=1-4$, zero point corrected.	132
C.2	Tabulated binding energies (in kcal/mol) for open-shell neutral molecules with clusters of size $n=1-4$, zero point corrected.	133
C.3	Tabulated binding energies (in kcal/mol) for closed-shell cationic molecules with clusters of size $n=1-4$, zero point corrected.	134
C.4	Tabulated binding energies (in kcal/mol) for closed-shell anionic molecules with clusters of size $n=1-4$, zero point corrected.	135

Acknowledgments

Naturally, I must begin by thanking Prof. Martin Head-Gordon, who I've had the pleasure of studying under over the past five and a half years. When I first met Martin, it was over a Skype call with a spotty connection - he was (and remains) a distinguished professor and figurehead in the electronic structure community. I was a first year graduate student in way over my head and knew...none of this about him. To me, he was a friendly face and knowledgeable mentor who graciously welcomed me into his research group despite my severely lacking knowledge of quantum chemistry. Through all these years of graduate school, Martin has been exceptionally patient and supportive, even when I felt that I was not cut out for a PhD. Thank you Martin, for helping me to grow exponentially as a graduate student, sharing your incredible wisdom and knowledge about the field, and most importantly, always being kind.

Next in line to thank are my mentors in the Head-Gordon group and beyond, who have been an essential part of my journey to finishing the PhD. In the M. Head-Gordon group alone, there are several people who have been essential. I'd like to thank Dr. Tamar Stein for taking me under her wing during my first year of graduate school and helping me get started in QChem. Another important mentor has been Dr. Diptarka Hait - thank you for working with me on our combustion project, teaching me everything about density functional theory before my qualifying exam (and beyond), and knowing almost everything about electronic structure. We're glad you're only an Uber ride away! I'm lucky to have you not only as a coworker, but a valued friend. And of course, thanks to Prof. Christopher Stein for being an amazing leader for the DFTB project. You have always been helpful and supportive, and never made me feel stupid. I'd also like to thank my collaborators Prof. Hope Michelsen (at CU Boulder), Dr. Partha Bera (NASA), and Dr. Timothy Lee (NASA). Thank you all for sharing your wisdom with me and for being amazing collaborators - I'm so lucky to have worked with all of you. Rest in peace Dr. Lee, you were gone too soon and I know you'd be happy to see our latest paper out in the world. I also need to thank Profs. Amy Prieto and Martin McCullough from my undergraduate studies at Colorado State University - you were both essential mentors to me, and I wouldn't have even considered graduate school without your guidance. To Amy in particular, thank you for pushing me to apply to Berkeley, even though I was highly skeptical about my chances - this would have never been possible without you.

An enormous, group-sized thank you to all my coworkers in the Head-Gordon group. All of you have been amazing colleagues, and I'm so lucky to work with such an incredible group of people. Thank you for all of your support troubleshooting QChem, which is truly a team effort. More meaningfully perhaps, thank you for all the great times we had when we should've been doing work but weren't. You made the dismal basement office a slightly better place. A special shout-out to my office-mates Richard and Elliot, for always listening to me complain and being generally great people to share an office with. Finally, thank you to the super cool office administrators who have kept me on track and saved me from some of the pain of Berkeley bureaucracy - Jessie, you were always so kind, helpful, and

knowledgeable! And Shobit, thanks for being an energetic and enthusiastic presence who was always quick to help out, and Gnocchi thanks you for giving him many neck massages.

I wouldn't have made it this far without the support of my amazing friends. I'm so grateful for the fast friends I made in my cohort, with a special shout-out to Abdul, Jonathan, Bryan, and David - the first semester of quantum brought us together in suffering, and luckily our friendship has held out for the rest of the years too. Thank you Jenna for always being a happy face. I'm amazingly grateful to Becca, Wendy, Richard, and Tim for living within a one-block radius, proofreading parts of this thesis, introducing me to aggressive new music (thanks Tim), throwing me German chocolate from your balcony (thanks Becca), and always being willing to dog-sit Gnocchi. Thanks to Nikhil, Kartavya and Yannick, the O.G. dogsitters and best upstairs neighbors ever. My life would be so much less bright without all of you in it. And finally, a heartfelt thank you to my best friend Michelle - even though you live hundreds of miles away, our phone conversations lifted my spirits and I miss you all the time.

I'm lucky to count my family as my number one fans. I'd like to thank Bruce and Dawn for supporting me in every way possible to this point. Without you, I wouldn't have made it this far, or had so many amazing opportunities. Thank you for our weekly conversations, even when we're just reporting the same old stuff over and over, and for always welcoming me back home with open arms and a full fridge when I need a break. Bailey, you're hands down my favorite sister. Thank you for being there for me and for sharing our single brain cell occasionally. The PhD aside, I literally wouldn't be here by now without my family's support - thank you for believing in me, both in graduate school and in my own growth as a functional, happy, healthy human. And to one of my essential supporters, my dog Gnocchi - thank you for emotionally supporting me and everyone else in the office for the past two years, though I think you need the emotional support as much as we do. Group meeting won't be half as interesting without your snoring.

Chapter 1

Introduction

In the same way that classical physics can quantify the forces that influence matter in the macroscopic world, quantum mechanics has its own sets of equations and rules to describe the motions of electrons in molecules. While this analogy is too coarse for most theoreticians who devote their lives to creating models approximating nuclear and electronic phenomena, it's a good place to start when describing the field of electronic structure to a relative, a classroom of undergraduates, or the occasional armchair expert in general quantum mechanics. Naturally, our work as electronic structure "chemists" is much more complex.

Electronic structure and quantum chemistry are subfields of chemistry that heavily utilize mathematics and physics to describe the interactions of subatomic particles (namely nuclei and electrons), which in turn are responsible for macroscopic chemical phenomena. In this way, while our work can seem a far cry from 'traditional' chemistry, theory, simulation and experiment have become an inseparable trio. Theoretical chemistry and chemical simulations offer a window of understanding into electronic phenomena that are otherwise unexplainable - these insights both guide experimental projects and further understanding of their results from a sub-atomic perspective. With the general progress of technology, our ability to accurately describe and interrogate chemical systems has improved immensely. While computational methods are forever doomed to balance between high accuracy and computational affordability (though perhaps not forever, with the rise of powerful quantum computers), a multitude of choices are available in various combinations of the two, from highly accurate (sometimes exact) methods that can treat small systems to heavily coarse-grained empirical models that can provide reasonable treatment of systems comprising thousands of atoms.

The interplay between electronic structure theory and real-world phenomena is highlighted by several projects outlined in this dissertation, specifically in the realms of astrochemistry and combustion processes. In particular, we will use quantum mechanical methods to elucidate structures of pre-biotic molecules in planetary atmospheres, model reaction pathways leading to soot precursors in combustion flames, and calculate binding energies of astrochemical species to amorphous ice surfaces. To better understand the theoretical underpinnings of the methods used in these studies and the implications of our results therein, we will first discuss the fundamentals of electronic structure and explore the methodology

used to perform these calculations.

1.1 The Schrödinger equation and general electronic structure

It is impossible to begin any discussion of electronic structure without introducing the core prerogative of all electronic structure methods: solving the Schrödinger equation.

$$\hat{H}\Psi(\mathbf{r}, \mathbf{R}) = E\Psi(\mathbf{r}, \mathbf{R}) \quad (1.1)$$

The time-independent Schrödinger equation, originally proposed in its time-dependent form by E. Schrödinger himself in 1926 [1], takes the form of an eigenvalue problem where Ψ is the wavefunction description of a system, and \hat{H} is the Hamiltonian, an operator that corresponds to the total energy of this system. Ψ are the eigenfunctions of \hat{H} that depend on electronic and nuclear positions (\mathbf{r} and \mathbf{R} respectively), and E are the energy eigenvalues of Ψ obtained through application of the Hamiltonian. Since the Hamiltonian is a linear operator, any arbitrary wavefunction Ψ can be described by a linear combination of eigenstates. In the analogous chemical picture, the wavefunction Ψ describes the chemical system built from a combination of molecular orbitals.

Molecules are composed of electrons and nuclei, both of which influence their chemical properties but move on very different timescales due to huge differences in mass. If we consider the full Hamiltonian for N electrons and M nuclei, this takes the following form:

$$\hat{H} = -\sum_{i=1}^N \frac{1}{2} \nabla_i^2 - \sum_{A=1}^M \frac{1}{M_A} \nabla_A^2 - \sum_{i=1}^N \sum_{A=1}^M \frac{Z_A}{r_{iA}} + \sum_{i=1}^N \sum_{j>i}^N \frac{1}{r_{ij}} + \sum_{A=1}^M \sum_{B>A}^M \frac{Z_A Z_B}{R_{AB}} \quad (1.2)$$

$$= \hat{T}_e + \hat{T}_{\text{nuc}} + \hat{V}_{\text{en}} + \hat{V}_{\text{ee}} + \hat{V}_{\text{nn}} \quad (1.3)$$

In Eq. 1.2, \hat{T}_e and \hat{T}_{nuc} are the kinetic energy operators for electrons and nuclei respectively. \hat{V}_{en} , \hat{V}_{ee} and \hat{V}_{nn} are the potential energy operators corresponding to electron-nuclei, electron-electron, and nuclei-nuclei repulsion. r_{iA} , r_{ij} and R_{AB} denote the inter-particle distances between electrons and nuclei, electrons and electrons, or nuclei and nuclei. Please note that atomic units are used throughout this thesis.

Since we are most interested in electronic motion, it is useful to separate the motions of electrons and nuclei in the molecular wavefunction. To do this, the Born-Oppenheimer approximation is invoked, allowing for separation of electronic and nuclear coordinates by assuming that the (relatively) massive nuclei are fixed in position relative to electrons in motion [2].

$$\Psi = \psi_e(\mathbf{r}; \mathbf{R})\phi(\mathbf{R}) \quad (1.4)$$

Application of the Born-Oppenheimer approximation gives a wavefunction in the form of Equation 1.4, where separated electron and nuclear coordinates are denoted by \mathbf{r} and \mathbf{R}

respectively, which are implicitly coordinate vectors of lengths $3N$ and $3M$. Naturally electronic motion is still influenced by the nuclei; while Ψ depends explicitly on electronic coordinates \mathbf{r} , it depends only parametrically on the nuclear coordinates. Different arrangements of nuclei will result in a changed Ψ , and \hat{V}_{nn} is included in the total energy expression. Simplifying our expression to focus on electronic motion results in the electronic Schrödinger equation:

$$\hat{H}_{el} = - \sum_{i=1}^N \frac{1}{2} \nabla_i^2 - \sum_{i=1}^N \sum_{A=1}^M \frac{Z_A}{r_{iA}} + \sum_{i=1}^N \sum_{j>i}^N \frac{1}{r_{ij}} = \hat{T}_e + \hat{V}_{en} + \hat{V}_{ee} \quad (1.5)$$

Here the indices i, j and N correspond to the index and total number of electrons, A and M for the same quantities of nuclei, and Z the charge of electrons or nuclei as indicated. In simpler notation, three main operators emerge: the kinetic energy of electrons (\hat{T}_e), electron-nuclei repulsion (\hat{V}_{en}), and electron-electron repulsion (\hat{V}_{ee}). For the remainder of this thesis, we will abandon most explicit effects resulting from nuclear motion and use the electronic Schrödinger equation. Substituting the operator in Eq. 1.5 into Eq. 1.1, we can solve for E (now E_{el}) to construct a potential energy surface for a given Ψ , which provides useful information such as equilibrium geometries, vibrational frequencies, and other essential quantities.

While the Schrödinger equation is an undeniably important cornerstone of electronic structure, it's important to remember that we can rarely identify the exact form of Ψ . Different strategies to accurately approximate Ψ and solve the Schrödinger equation lead to a plethora of electronic structure methods for modelling chemical systems. Next, we will examine those methods which are most relevant to the work presented in this thesis.

1.2 Hartree-Fock Theory

One of the most fundamental methods to approximate the Schrödinger equation is Hartree-Fock theory, which is a cornerstone of molecular-orbital (MO) theory. In this framework, electronic motion is described by single-particle functions that do not depend on the instantaneous movement of other electrons [3]. Due to the multitude and complexity of electron interactions, the only system that is entirely, exactly solvable with the Schrödinger equation is for one electron in one orbital; most commonly, H^\bullet or H_2^+ . The wavefunction for such a system can be modelled mathematically:

$$\Psi(r) = \phi(r) \quad (1.6)$$

Here, $\phi(r)$ is a function describing the molecular orbital in which the single electron resides. Additionally, $\phi(r)$ may be broken down further into a spin orbital χ which expresses both the spatial part of the molecular orbital ($\phi(r)$) and spin configuration of the electron ($\sigma(\omega)$):

$$\chi(x) = \phi(r)\sigma(\omega) \quad (1.7)$$

In constructing $\Psi(r)$ for multi-electron systems, one might naively choose to express $\Psi(r)$ as a product of multiple $\phi(r)$ - which is referred to as a Hartree Product [4]. However, this simple representation cannot fulfill a fundamental constraint of the wavefunction: antisymmetry. Electrons are fermions, and as such the wavefunction describing these fermions must be antisymmetric with respect to exchange of electron coordinates. To construct an expression that satisfies this antisymmetry constraint, we can build a trial wavefunction in the form of a Slater determinant [5].

$$\Phi_0(x_1, x_2, \dots, x_n) = \frac{1}{\sqrt{n!}} \det \begin{vmatrix} \chi_1(x_1) & \chi_1(x_2) & \cdots & \chi_1(x_n) \\ \chi_2(x_1) & \chi_2(x_2) & \cdots & \chi_2(x_n) \\ \vdots & \vdots & \ddots & \vdots \\ \chi_n(x_1) & \chi_n(x_2) & \cdots & \chi_n(x_n) \end{vmatrix} \quad (1.8)$$

In this construction, the rows of the determinant denote the one-electron spin orbitals χ , while the columns index the spatial coordinates; this determinant can also be expressed more concisely in ket form as $|\chi_1\chi_2\dots\chi_n\rangle$ for representations of n particles.

Now prepared with a reasonable trial wavefunction to use in Eq. 1.1, we can begin to solve for a more accurate energy of the wavefunction. As we can tell from Eq. 1.1, the energy values are entirely dependent on the wavefunction expression. We can reformulate the spatial part (molecular orbital) of our wavefunction as a linear combination of known atomic orbitals $\phi_\mu(r_j)$:

$$\psi_{i,\sigma}(r_j) = \sum_{\mu}^N C_{\mu i,\sigma} \phi_{\mu}(r_j) \quad (1.9)$$

In Eq. 1.9, $\phi_{\mu}(r_j)$ are generally modelled in the form of an atom-centered Gaussian function, or as plane waves in the case of periodic systems, and μ indexes the basis function. This expansion is formulated to modify the differential expression into an algebraic one. $C_{\mu i,\sigma}$ are the unique molecular orbital coefficients. Variation of these directly influences the energy eigenvalues of the orbital, and thus the total energy of the wavefunction. In other words, variational optimization of $C_{\mu i,\sigma}$ will lead to optimization of E ; this is known as the variational principle:

$$E_0 \leq \frac{\langle \Phi(C) | H | \Phi(C) \rangle}{\langle \Phi(C) | \Phi(C) \rangle} = E(C) \quad (1.10)$$

Solved in this way, we additionally know that the molecular orbital-dependent energy $E(C)$ gleaned from minimization of molecular orbital coefficients will always be greater than or equal to the true ground state energy E_0 , which would only be known if we were able to exactly determine the particle wavefunction.

The electronic Hamiltonian \hat{H}_{HF} can be split into both one and two particle components.

$$\hat{f}(i) = \hat{h}(i) + v(i, j) \quad (1.11)$$

$$\hat{h}(i) = -\frac{1}{2}\nabla_i^2 - \sum_{A=1}^M \frac{Z_A}{r_{iA}} \quad (1.12)$$

$$v(i, j) = \frac{1}{r_{ij}} \quad (1.13)$$

The one-particle term $\hat{h}(i)$ contains one-particle kinetic energy and electron-nuclear potential energy effects, while the two-particle operator depicts two-electron interactions.

Substitution of the Slater determinant into Eq. 1.10 and the use of the Hartree-Fock Hamiltonian components leads to the following energy expression:

$$E_{HF} = \sum_{i=1}^N \langle \chi_i | \hat{h} | \chi_i \rangle + \sum_{i < j}^n [\langle \chi_i \chi_j | \chi_i \chi_j \rangle - \langle \chi_i \chi_j | \chi_j \chi_i \rangle] \quad (1.14)$$

In terms of spin orbitals χ_i , the energy breaks down into several recognizable inner products; $\langle \chi_i | \hat{h} | \chi_i \rangle$ consists of the energy dependent on the one-electron operator. The second contribution are the two-electron, four-center integrals:

$$\langle \chi_i \chi_j | \chi_i \chi_j \rangle = \int \int \chi_i^*(x_1) \chi_j^*(x_2) \frac{1}{r_{12}} \chi_i(x_1) \chi_j(x_2) dx_1 dx_2 \quad (1.15)$$

$$\langle \chi_i \chi_j | \chi_j \chi_i \rangle = \int \int \chi_i^*(x_1) \chi_j^*(x_2) \frac{1}{r_{12}} \chi_j(x_1) \chi_i(x_2) dx_1 dx_2 \quad (1.16)$$

These two electron integrals are referred to as Coulomb and Exchange integrals (often denoted as J and K).

To determine the ground-state Hartree-Fock energy, we must minimize the energy expression with respect to the spin orbitals, while accounting for the constraint that all molecular orbitals remain orthonormal to each other. Performing this minimization results in the following eigenvalue problem:

$$\hat{f}(x_1)\psi_i(x_1) = \epsilon_i\psi_i(x_1) \quad (1.17)$$

Where:

$$\hat{f}_\sigma(x_1) = \hat{h}(x_1) + \sum_{i=1}^N [J(x_1) - K(x_1)] \quad (1.18)$$

With these expressions, we are ready to set up the generalized matrix form of the eigenvalue problem. Using the definition of overlap matrix S ($S_{\mu\nu} = \langle \phi_\mu | \phi_\nu \rangle$) and substituting the expansion of Ψ with molecular orbital (MO) coefficients given in Eq. 1.4, we can represent the eigenvalue expression as Roothaan-Hall equations [6]:

$$FC = SC\epsilon \quad (1.19)$$

Where F is the Fock matrix, C the MO coefficients, and ϵ the diagonal matrix of orbital eigenvalues (energies) in the atomic orbital (AO) basis. With one more step, the Fock expression can be simplified by introducing the density matrix P :

$$P_{\mu\nu,\sigma} = \sum_{i=1}^{n_\sigma} C_{\mu i,\sigma} C_{\nu i,\sigma} \quad (1.20)$$

$$F_{\mu\nu,\sigma} = \hat{h} + \sum_{\lambda}^N \sum_{\eta}^N \langle \phi_{\mu} \phi_{\lambda} | \phi_{\nu} \phi_{\eta} \rangle (P_{\lambda\eta,\alpha} + P_{\lambda\eta,\beta}) - \sum_{\lambda}^N \sum_{\eta}^N \langle \phi_{\mu} \phi_{\lambda} | \phi_{\eta} \phi_{\nu} \rangle (P_{\lambda\eta,\sigma}) \quad (1.21)$$

Commonly, atomic orbital basis functions are not already orthonormal, which is a key requirement of the theory. To remedy this, we introduce a transformation matrix X to perform a unitary transformation of these orbitals. X can be defined in multiple ways - here, we define an X appropriate for performing canonical orthogonalization of the atomic orbitals [7].

$$X = U S^{-1/2} \quad (1.22)$$

Using Eq. 1.22, a new set of orthogonal orbitals can be constructed, and substituted into Eq. 1.19:

$$C' = X^{-1}C \quad (1.23)$$

$$F X C' = S X C' \epsilon \quad (1.24)$$

$$(X' F X) C' = (X' S X) C' \epsilon \quad (1.25)$$

$$F' C' = C' \epsilon \quad (1.26)$$

While this eigenvalue problem appears simple enough, the equation must be minimized in an iterative manner since F_{σ} depends on the molecular orbitals (specifically variation of their coefficients C_{σ}) and vice versa. To solve Eq. 1.19 iteratively, we use a self-consistent field (SCF) procedure to find the solution of the Hartree-Fock equations. The steps of the SCF procedure are the following:

1. Specify a target molecule (or system of molecules) and essential quantities such as the basis set, nuclear coordinates, and number of electrons in the system.
2. Pre-compute S and core hamiltonian \hat{h} , neither of which depend on the density matrix $P_{\mu\nu}$.
3. Use S to create transformation matrix X .
4. Create an initial guess for density matrix $P_{\mu\nu}$.
5. Using $P_{\mu\nu}$, construct the Fock matrix and compute E_{HF} .
6. Using X and F , compute F' and solve for MO coefficients C'

7. Construct new density matrix $P_{\mu\nu}$ from C' ; if the density matrix is converged, return the final energy and quit. If not converged, return to the 5th step and iterate until convergence.

Solving the Hartree-Fock equations variationally results in ground-state energies that capture most contributions needed to reproduce the *true* ground-state electronic energy. However, a great simplification in Hartree-Fock is ignorance of the fact that electron motions are correlated - that is to say, electrons avoid each other spontaneously. This accounts for the difference between the exact ground state energy E_0 and the computed Hartree-Fock energy:

$$E_{corr} = E_0 - E_{HF} \quad (1.27)$$

While Hartree-Fock is clearly very useful, the neglect of correlation energy is concerning and can lead to quite erroneous results when applied to real chemical systems. Therefore, the development of new methods beyond the limited capabilities of Hartree-Fock has been incredibly important for the advancement of electronic structure theory. Hartree-Fock (HF) theory models the wavefunction as a single determinant and minimizes the total energy with respect to molecular orbitals. Other post-HF wavefunction methods can describe molecular systems with greater accuracy - however, this comes at the price of increasing computational cost. Hartree-Fock itself scales as N^4 with basis set (where N is the number of basis functions in the system and molecule size is fixed), and $O(N^2-N^3)$ with molecule size. Other increasingly sophisticated choices scale as N^5 and beyond.

One important and widely used method that boasts moderate affordability and has its own unique solutions for the problem of capturing this electron correlation energy is Density Functional Theory (DFT), which we will explore in the following section.

1.3 Density Functional Theory

The birth of density-functional theory in the 1960's [8, 9] was fueled by several important motivations. One was the development of an electronic structure method beyond Hartree-Fock that accounted for electron correlation. Another was to explore how modelling systems in terms of the electron density rather than depending on costly determinants - both goals could improve computational scaling and results.

Density functional theory is constructed to depend only on the electron density ρ for computation of ground state energies. Some of the earliest renditions of density-based methodology modelled kinetic energy, local exchange and correlation energies using forms that are corrected only for the uniform electron gas (UEG) [10–12]. Unfortunately, this model failed to reproduce atomic shell structure, which is obviously quite important for modelling real molecules. Truly usable ideas weren't proposed until at least the mid-1900's. Modern DFT is built upon two key theorems, first proposed by Kohn and Sham in 1964 [8, 9]. Considering a system of electrons moving under the influence of some external potential v_{ext} :

Hohenberg-Kohn Thm. 1: The external potential v_{ext} is a unique functional of the ground state electronic density $\rho(\mathbf{r})$ of a given system; since the external potential is associated with the full many-particle ground state, this too is a functional of $\rho(\mathbf{r})$.

Hohenberg-Kohn Thm. 2: The electron density that minimizes the total DFT energy is the true ground state electron density, and the associated ground state energy can be solved variationally.

Due to the one-to-one mapping between external potential v_{ext} and ρ delineated in the first theorem, the DFT energy expression can be written as a function of the electron density. Much like Hartree-Fock (but now in terms of $\rho(\mathbf{r})$), there are several main operators contributing to the energy functional: electron kinetic energy \hat{T}_e , electron-electron interactions \hat{V}_{ee} , and electron-nuclear interactions \hat{V}_{ne} .

$$E[\rho(\mathbf{r})] = \hat{T}_e[\rho(\mathbf{r})] + \hat{V}_{ee}[\rho(\mathbf{r})] + \hat{V}_{ne}[\rho(\mathbf{r})] \quad (1.28)$$

$$\hat{V}_{ee}[\rho(\mathbf{r})] = J[\rho(\mathbf{r})] + K[\rho(\mathbf{r})] \quad (1.29)$$

The electron-electron potential energy \hat{V}_{ee} can be further broken down into Coulomb and exchange contributions, indicated as $J[\rho(\mathbf{r})]$ and $K[\rho(\mathbf{r})]$ respectively.

The classical electron Coulomb repulsion and electron-nuclear terms in the energy functional that can be computed in familiar forms:

$$J[\rho(\mathbf{r})] = \frac{1}{2} \int \int \frac{\rho(r_1)\rho(r_2)}{r_{1,2}} dr_1 dr_2 \quad (1.30)$$

$$\hat{V}_{ne}[\rho(\mathbf{r})] = - \sum_{A=1}^M \int \frac{Z_A}{\mathbf{r} - \mathbf{R}_A} \rho(\mathbf{r}) dr \quad (1.31)$$

Unfortunately, the remaining terms $\hat{T}_e[\rho(\mathbf{r})]$ and $K[\rho(\mathbf{r})]$ do not have exact solutions. Early attempts to compute the kinetic energy term were made in the Thomas-Fermi model [10, 13], the form of which has been known since the 1930's:

$$\hat{T}_e[\rho(\mathbf{r})] = \frac{3}{10} (3\pi^2)^{2/3} \int \rho(\mathbf{r})^{5/3} dr \quad (1.32)$$

In this form, $\hat{T}_e[\rho(\mathbf{r})]$ is exact, but only for the uniform electron gas, which is only very rarely useful for modeling actual chemical systems. To circumvent this issue, Kohn and Sham improved the formulation of the kinetic energy term. In their design, the kinetic energy is approximated by a fabricated system of non-interacting electrons having the same density as the exact wave function - this is accomplished by reintroducing a single determinant to $\hat{T}_e[\rho(\mathbf{r})]$. The inclusion of these orbitals does come with slightly increased computational cost (compared to orbital-free DFT [14–17]), but despite this, Kohn-Sham DFT (KS-DFT) has become the most popular variety because of dramatically improved accuracy.

With inclusion of orbitals $\phi(r)$ in the kinetic energy term, the electron density takes the form:

$$\rho(\mathbf{r}) = \sum_i^N |\phi_i|^2 \quad (1.33)$$

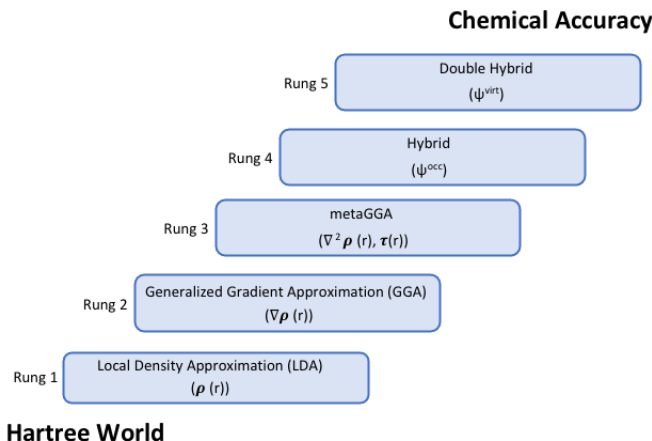


Figure 1.1: Jacob’s Ladder of density functionals. Functionals improve in their ability to accurately reproduce chemical data as the ladder ascends, with the inclusion of the density gradient, occupied and virtual orbitals, etc.

And the non-interacting kinetic energy term can be expressed in terms of the Slater determinant Φ_s as:

$$\hat{T}_e = \langle \Phi_s | \hat{T} | \Phi_s \rangle = -\frac{1}{2} \sum_{i=1}^N \int \phi_i^* \nabla^2 \phi_i dr \quad (1.34)$$

This form of the kinetic energy is exact for the non-interacting reference, but not exact for the fully interacting system ($\hat{T}[\rho(\mathbf{r})]$). Furthermore, there is still one unknown term: the electron exchange energy $K[\rho(\mathbf{r})]$, to which no such simple approximation is yet formulated. This discrepancy between $\hat{T}[\rho(\mathbf{r})]$ and the one used in KS-DFT is bundled with the undefined exchange contribution $K[\rho(\mathbf{r})]$ to define the exchange-correlation energy, denoted as $Q[\rho(\mathbf{r})]$ in Eq. 1.35.

$$E_{XC} = (\hat{T}[\rho(\mathbf{r})] - \hat{T}_e[\rho(\mathbf{r})] + Q[\rho(\mathbf{r})]) \quad (1.35)$$

Formulation of an effective E_{XC} term is the main driver in the development of modern DFT functionals. This is achieved by including additional terms that better model changes in electron density which affect the energy of actual chemical systems. Different research groups have developed increasingly sophisticated functionals with inclusions such as the gradient of the density ($\nabla \rho(\mathbf{r})$), the square of the gradient, exact Hartree-Fock exchange, and more [18]. These progressive improvements result in a hierarchy of density functionals commonly referred to as ”Jacob’s Ladder”, spanning from the primordial ’Earth’ of Hartree-Fock theory into the ’Heaven’ of chemical accuracy.

As shown in Figure 1.1, the rungs of this ladder begin with the simplest of density functional - the Local Density Approximations (LDA or LSDA for spin-density) which models E_{XC} depending only on the total electron density $\rho(\mathbf{r})$. Well-known species in this category

include VWN5 [19], PZ81 [20], and PW92 [21]. These LSDA functionals capture important details such as molecular binding, but have rather poor performance for most chemical systems (with the exception of very uniform samples such as nearly free electron metals), since they are only exact for a non-varying density (the uniform electron gas) [22].

At Rung 2, inclusion of the gradient of the density $\nabla\rho(\mathbf{r})$ gives rise to Generalized Gradient Approximation (GGA) functionals [23, 24], such as PW91 [21] and the well-known PBE [25]. Inclusion of the density gradient offers significant enhancements in performance compared to LSDA [18]. The introduction of GGAs was the leap that made Kohn-Sham DFT useful for chemistry.

Further notable improvements arise at rungs three and higher with meta-GGAs (such as M06-L [26]), hybrids (such as ω B97X-V [27]), and double hybrids (such as ω B97M(2) [28]) with inclusion of the square gradient, occupied orbitals, and virtual orbitals respectively. Many of the density functionals of rungs 4 and 5 have proven themselves to be quite effective for many chemical problems [18].

It's important to remember that unlike in wavefunction theory, the 'improvement' of density functionals does not necessarily lead to a true hierarchy of accuracy for a given molecule or system; there is no guarantee that similar formulations of E_{XC} will produce systematically more accurate results across all calculations. Functional development often involves extensive fitting of semi-empirical parameters to match benchmark experimental data (such as bonded or non-bonded interactions), or a combinatorial approach that includes a delicate balance of terms to render a functional both high-performing and highly transferrable. This makes such functionals semi-empirical in nature. While taking a semi-empirical route to E_{XC} can indeed be very successful for chemical modelling, some have argued that reliance on parameter fitting for functional development has actually taken density functional theory further from the true functional form [29, 30]. Regardless of the contention and competition surrounding the development of well-performing functionals, interest in and usage of DFT still remains at an all-time high as far as quantum mechanical methods are concerned.

With a satisfactory form of E_{XC} obtained, the Fock operator for KS-DFT can be constructed and solved similarly to Hartree-Fock theory:

$$\hat{f}_{\sigma}^{KS-DFT}(r_1) = -\frac{1}{2} \sum_{i=1}^N \nabla_i^2 - \sum_A \frac{Z_A}{|r - R_A|} + \int \frac{\rho(\mathbf{r}')}{|r - r'|} dr' + v_{xc,\sigma}(r) \quad (1.36)$$

The main difference from the Hartree Fock operator is of course the exchange-correlation potential, which takes the form:

$$v_{xc,\sigma}(r) = \frac{\delta E_{XC}[\rho(\mathbf{r})]}{\delta \rho_{\sigma}(r)} \quad (1.37)$$

With this Fock operator, we can once again set up an eigenvalue problem, and iteratively improve Kohn-Sham orbitals and energies:

$$\hat{f}_{\sigma}^{KS-DFT}(r_1)\psi_{i,\sigma}(r_1) = \epsilon_{i,\sigma}\psi_{i,\sigma}(r_1) \quad (1.38)$$

$$F^{KS}C^{KS} = SC^{KS}\epsilon^{KS} \quad (1.39)$$

1.4 Correlated Wavefunction Methods

In the previous section, we explored density functional theory, which offers a good compromise between accuracy and efficiency for electronic structure calculations. Electron correlation effects, which are missing in Hartree-Fock, are captured in the E_{XC} term of density functionals. Though DFT is the main electronic structure method used in this thesis, we must include a brief discussion regarding other correlated wavefunction methods beyond Hartree-Fock, as these are essential for obtaining benchmark, high-accuracy results for molecular energies and other quantities that are extremely important for the following chapters of this thesis. Wavefunction methods are commonly used in conjunction with DFT for routine investigations; structural optimizations and initial energies are obtained with DFT for a lower computational cost, and final energies are computed at a higher level (and higher cost) with the best wavefunction method one can afford - this strategy is used for the studies outlined in chapters 2, 3, and 4 of this thesis. Unlike DFT, correlated wavefunction methods are systematically improvable, but these improvements come at a steep computational price that makes them difficult to employ for routine calculations. The levels of theory differ in how they treat electron correlation, and we will cover the basics of the three most relevant for understanding the basic concepts of wavefunction theory and its use in this thesis: configuration interaction, coupled-cluster methods, and perturbation theory.

Configuration Interaction

Without the effects of correlation, Hartree-Fock (HF) is a limited method for performing electronic structure calculations. As 'simple' a problem as modelling the dissociation of H_2 produces incorrect results, though qualitatively correct results may be obtained with the use of unrestricted HF. One major improvement over HF methods for modelling electron correlation is configuration interaction (CI), which is conceptually perhaps the simplest electronic structure method to understand from a theory perspective, but one of the most computationally expensive to carry out [4], at least when one is aiming for high accuracy.

Recall from HF the form of the ground state wavefunction Ψ , constructed from one Slater determinant composed of spin orbitals χ .

$$|\Phi_0\rangle = |\chi_1\chi_2\cdots\chi_n\rangle \quad (1.40)$$

Given a system of n electrons, using an N -dimensional basis set, the solutions to the Roothaan equations of Hartree-Fock yield n occupied spin orbitals (denoted with indices i, j, k, \dots) and $2N - n$ virtual spin orbitals (denoted with indices a, b, c, \dots). While the wavefunction expression of HF was limited to a single Slater determinant, one could imagine constructing a more accurate wavefunction using multiple Slater determinants using the HF expression as a reference; these additional Slater determinants can arise from replacing occupied orbitals χ_i with virtual orbitals χ_a in varying combinations. Inclusion of many determinants not only allows for representation of excited states, but can also improve accuracy of the the ground state wavefunction.

If we take Φ_0 as the ground-state reference determinant, we can denote a single excitation of an electron in occupied orbital i to unoccupied orbital a as $c_i^a \Phi_i^a$, where c_i^a is a scalar amplitude associated with the new wavefunction. These excitations can similarly be expressed mathematically in terms of raising and lowering 'ladder' operators \hat{a} and \hat{a}^\dagger :

$$\sum_{ia} c_i^a \hat{a}_a^\dagger \hat{a}_i \Phi_0 = \sum_{ia} c_i^a \Phi_i^a \quad (1.41)$$

By acting on different combinations of occupied and virtual orbitals to produce multiple excited Slater determinants, a new and much more sophisticated wavefunction can be constructed:

$$\Phi_0 = c_0 \Phi_0 + \sum_{ia} c_i^a \Psi_i^a + \sum_{i<j,a<b} c_{ij}^{ab} \Phi_{ij}^{ab} + \sum_{i<j<k,a<b<c} c_{ijk}^{abc} \Phi_{ijk}^{abc} + \dots \quad (1.42)$$

If all possible excited Slater determinants of the system are included, this full-CI wavefunction can be optimized through the linear variational method, and exact energies for both ground and excited states can be procured by diagonalizing the full hamiltonian. Unfortunately, as one might guess from simply looking at Eq. 1.42 and trying to write out all possible determinants to complete the wavefunction basis, use of full-CI becomes computationally intractable quite quickly even for small molecules. Therefore, truncations of full-CI are often employed to make calculations on small and medium-sized molecules usable. For example, one might truncate the full wavefunction to only include up to double excitations (CISD) or triple excitations (CISDT). However, there are consequences for truncation; exclusion of select determinants results in a wavefunction that is not independent of the reference wavefunction. Thus, one must choose a reasonable reference that has good overlap with the true ground state wavefunction. Additionally, truncation results in calculations that are not size consistent; for example, use of CISD would be able to accurately model two isolated molecules each with a double excitation, but not the both of them together as one non-interacting system - the quadruple excitation resulting from combination of the double excitations would be excluded. Therefore, we must regretfully save exact, full-CI calculations for only the smallest of molecules. Workarounds to full-CI are improving; take for example the rise in interest for so-called "selected" CI methods - these are particularly useful for strongly correlated systems, and in principle they can be converged to the full-CI energy [31]. One relevant and recent example is Adaptive Sampling CI, or ASCI [32]. ASCI is built upon the framework of full-CI quantum Monte-Carlo (FCIQMC) algorithms, which are built to achieve good chemical accuracy on large-scale determinant spaces (no longer limited to diatomic molecule sizes!). Development of the algorithms central to ASCI allows for calculations on difficult problems (for example Cr_2) on drastically improved timescales compared to FCI. These advancements offer excellent alternatives to full-CI that preserve the excellent results of this method as far as chemical accuracy. In the following sections, we will consider still other options that are even more computationally tractable.

Coupled-Cluster Methods

Coupled-Cluster methods (CCM) seek to preserve some of the accuracy of CI methods while mitigating the size-consistency error that results from truncating them. Like configuration interaction, coupled-cluster utilizes excitation operators to build excited determinants, indicated in a concise notation as \hat{T} for any number of excitations:

$$\hat{T}_1 = \sum_{ia} t_i^a \hat{a}_a^\dagger \hat{a}_i \quad (1.43)$$

$$\hat{T}_2 = \sum_{ijab} t_{ij}^{ab} \hat{a}_b^\dagger \hat{a}_a^\dagger \hat{a}_j \hat{a}_i \quad (1.44)$$

The coupled-cluster formalism works in much the same way as CI, applying these operators to the ground state (reference) wavefunction Φ_0 . However, these operators are contained in an exponential ansatz acting on Φ_0 :

$$|\Psi_{CC}\rangle = e^{\hat{T}_1 + \hat{T}_2 + \dots} |\Phi_0\rangle = e^{\hat{T}} |\Phi_0\rangle \quad (1.45)$$

This preserves the same information as far as constructing excited state wavefunctions, truncation of coupled-cluster operators at different orders does not incur the same size-consistency issues as truncation of CI methods does. This exponential ansatz allows for separability of the wavefunction in the case of non-interacting systems; this is evident in expansion of the exponential:

$$e^{\hat{T}_A + \hat{T}_B} = e^{\hat{T}_A} + e^{\hat{T}_B} \quad (1.46)$$

The main cost of coupled-cluster theory comes from the computation of so-called "t-amplitudes", which result from products of excited determinants. For the following chapters of this thesis, CCSD(T) is frequently used to obtain accurate molecular energies for determination of experimentally relevant values. This formulation of coupled cluster includes single and double excitations in the ansatz, as well as a perturbative triples correction (indicated by the (T)). For most quantum chemists, CCSD(T) is considered the gold standard for accuracy [33, 34], since full CCSDT or higher CC methods such as CCSDT(Q), etc. and full-CI are too expensive to apply to most chemical systems. The use of CCSD(T) with an adequate basis set is still limited to systems of tens of atoms (especially if heavy atoms are involved), but presents a significant improvement over its more costly predecessors.

Perturbation Theory

The last wavefunction-based method we will cover is perturbation theory, which takes a rather different approach to the electron correlation problem than configuration interaction or coupled cluster theories. Recall, once again, the Hartree-Fock Hamiltonian and its solutions, which contain inadequate electron correlation. The HF wavefunction and its eigenvalues are of course exact solutions to the HF Fock operator, \hat{F} . If we assume that a given wavefunction

Ψ is near enough to $\Psi_{0,HF}$, we can rewrite the Hamiltonian to include perturbations (W) that models electron correlation:

$$\hat{H} = \hat{F}_{HF} + \lambda W \quad (1.47)$$

λ is a dimensionless parameter. If we expand the exact wavefunction in terms of the HF wavefunction and energy, we obtain, up to an arbitrary order:

$$\Psi = \Psi_0 + \lambda\Psi^{(1)} + \lambda^2\Psi^{(2)} + \lambda^3\Psi^{(3)} \quad (1.48)$$

$$E = E_0 + \lambda E^{(1)} + \lambda^2 E^{(2)} + \lambda^3 E^{(3)} \quad (1.49)$$

By substituting these expressions back into the Schrödinger equation and collecting terms by orders of λ , we obtain systems of equations for the zeroth, first, and arbitrary orders that expand the Schrödinger equation to incorporate orders of perturbation W . Multiplying these through with Ψ_0 yields expressions for the Møller-Plesset perturbation theory [35] energy corrections to order n (demonstrated here to 2nd order only):

$$E_0 = \langle \Psi_0 | \hat{F} | \Psi_0 \rangle \quad (1.50)$$

$$E^{(1)} = \langle \Psi_0 | W | \Psi_0 \rangle \quad (1.51)$$

$$E^{(2)} = \langle \Psi_0 | W | \Psi^{(1)} \rangle \quad (1.52)$$

Møller-Plesset perturbation theory, or MP n , is the most commonly used 'flavor' of perturbation theory, particularly MP2 to second order. To model the energy contribution of MP2, we first consider the first order wavefunction expanded in the basis of zeroth order states:

$$\Psi^{(1)} = \sum_{ia} t_i^a \Phi_i^a + \sum_{i<j,a<b} t_{ij}^{ab} \Phi_{ij}^{ab} \quad (1.53)$$

Utilizing this expansion and combining with the first order expansion of $H\Psi = E\Psi$ yields a first order wavefunction consisting only of double substitutions (Φ_{ij}^{ab}) and associated matrix elements, and spin orbital energies, which may be used to model the second order energy correction in a similar manner:

$$E_{MP2} = -\frac{1}{4} \sum_{ab}^{virt} \sum_{ij}^{occ} \frac{|\langle ab || ij \rangle|^2}{\epsilon_a + \epsilon_b - \epsilon_i - \epsilon_j} \quad (1.54)$$

In this expression, the denominator indicates the difference in orbital energies. In the limit where this denominator approaches zero, the MP2 energy diverges, but for closed-shell energies and properties MP2 is usually accurate (with results somewhere between Hartree-Fock theory and CCSD). The computational scaling of MP2 is lower than configuration interaction or coupled cluster, but still higher than density functional theory. However, it remains widely used as one of the simplest wavefunction theories beyond Hartree-Fock with substantially improved performance.

1.5 Semi-Empirical Methods

In the previous sections, we have covered a number of different computational methods that present varying levels of computational accuracy and cost. Highly accurate wavefunction methods such as full configuration interaction can deliver excellent results, but only for relatively small systems (tens of atoms) even without a complete basis set. Coupled-cluster theory, with CCSD(T) being the gold-standard method of electronic structure, is somewhat more feasible in this regard but still comes at a steep computational cost ($O(N^7)$ for CCSD(T)). Density functional theory offers a more attractive option - well-developed functionals can offer good accuracy for most calculations at a cost of only $O(N^3)$, and progress has been made to produce linear-scaling DFT [36–39], making this method a great choice for systems of hundreds of atoms.

However, many chemical systems relevant to atmospheric reactions, interstellar chemistry, biological processes and more far exceed the system size limits offered by even the most affordable of these methods. For example, models of protein residues in solution can easily involve the interactions of thousands of atoms. So, how is one to successfully apply quantum mechanical methods to study such systems?

One useful work-around for treatment of large, many-molecule systems are semi-empirical (SE), self-consistent field (SCF) methods. These have their roots in rigorous SCF theories such as Hartree-Fock or DFT, but employ approximations for the most computationally demanding portions (for example, the two-electron integrals). This allows for reasonably good treatment of very large systems while still enjoying (at least partially) some rigor of a fully developed quantum mechanical method. There are several different flavors of SE methodology that have enjoyed usage for a variety of chemical applications, and development continues to make these even more useful; all generally share several key features [40]:

1. Minimal basis set: To save computational effort, semi-empirical methods usually model molecules in a minimal basis set. That is to say, usually only a single basis function is provided for each valence orbital. Core orbitals are removed from explicit consideration.
2. Extensive parameterization: As mentioned above, approximations for integral calculations are crucial to preserve the speed of SE methods. To do this, many methods invoke a library of atomic or atom-pairwise parameters to model the quantities that would normally be calculated using these integrals. Typically, only a quadratic number of integrals are evaluated at most.
3. Rooted in well-established theory: Most basic methodology of the parent theory is preserved.

Several well-established SE methods have arisen from Hartree-Fock theory. Recall the most computationally demanding portions of the Hartree Hamiltonian, which are the two-

electron integrals:

$$F_{\mu\nu,\sigma}^{HF} = \sum_{\lambda} \sum_{\eta} \langle \phi_{\mu} \phi_{\lambda} | \phi_{\eta\eta} \phi_{\sigma} \rangle (P_{\lambda\eta,\alpha} + P_{\lambda\eta,\beta}) - \sum_{\lambda} \sum_{\eta} \langle \phi_{\mu} \phi_{\lambda} | \phi_{\eta\eta} \phi_{\sigma} \rangle (P_{\lambda\eta,\sigma}) \quad (1.55)$$

One of the earliest renditions was the zero-differential overlap (ZDO) approximation [41], which bypasses calculation of all two electron integrals except those of type $\langle \mu\mu | \nu\nu \rangle$, drastically reducing the number of integral calculations and reducing computational overhead by a whole order of magnitude (scaled by system size). In later approximations such as the complete neglect of differential overlap (CNDO), ZDO is further scaled down by applying the Magata-Nishimoto approximation to parametrize the $\langle \mu\mu | \nu\nu \rangle$ integrals [42]. The intermediate neglect of differential overlap (INDO) family also parametrizes integrals centered on the same atom [43]. Finally, the neglect of differential-diatomic overlap (NDDO) approximations retain integrals of type $\langle \mu\lambda | \eta\nu \rangle$ but also employ an approximate Fock matrix that simplifies the Roothaan-Hall equations substantially [44].

Naturally, undertaking so many approximations means introducing a generous amount of error. In addition to adopting errors associated with the parent theory of Hartree-Fock (lack of electron correlation, etc.), elements that enhance the speed of calculations also affect the accuracy. Usage of a minimal basis set means limitations when it comes to accurately modeling molecules, especially in situations where polarizability of the electron cloud is important (such as for non-covalent interactions) [40]. And predictably, highly parametrized methods generally work best on sets of molecules similar to those that were used to optimize the fitted parameters, which may also only be established for a limited library of atoms or atomic interactions.

While SE methods developed in the basis of Hartree-Fock do not enjoy extensive usage today, methodologies based on DFT, usually called Density Functional Theory Tight-Binding (DFTB) approaches, have taken off in terms of popularity and usefulness.

As we explored in previous chapters, DFT constructs the energy expression as a function of the electron density ($E[\rho]$). DFTB uses the core concepts of energy expression, but is built as an expansion around density fluctuations $\delta\rho$:

$$E[\rho] = E^{(0)}[\rho_0] + E^{(1)}[\rho_0, \delta\rho] + E^{(2)}[\rho_0, (\delta\rho)^2] + E^{(3)}[\rho_0, (\delta\rho)^3] + \dots \quad (1.56)$$

Different formulations of DFTB truncate the energy expansion at varying orders. The zeroth order density ρ_0 is taken to be that of the superposition of non-interacting atoms, and thus gives rise to a repulsive potential that is necessary in some form for all DFTB expressions. DFTB1 [45], truncated at first order, can be used to calculate band energies. DFTB2 [46, 47], which includes second order density fluctuations, is most widely used and requires self-consistent iterations to calculate the changes incurred in higher multipole moments of atoms with these fluctuations. This term also includes approximations of the Coulomb and exchange energy E_{xc} , though importantly only within a restricted formalism.

Inclusion of higher-order terms of the expansion have been finely tuned and successfully used in modern DFTB software packages. Grimme and coworkers in particular have developed the widely used "xtb" software that includes increasingly complex functionality and

parameterizations of the energy expression [48]. Other packages such as DFTB+ are also available [49]. Most formulations of DFTB are formally closed-shell in nature; however, extensions have emerged that adapt the DFTB energy and hamiltonian to treat unrestricted molecular orbitals [50, 51]. DFTB is utilized in Chapter 4 of this thesis as a rapid, low-cost method to generate conformers for candidate guest molecule-water cluster complexes. Specifically, the CREST software developed by Grimme and co-workers [52] built on the framework of GFN2-xTB was used for this purpose.

1.6 Outline

In this thesis, we utilize density functional theory and other quantum mechanical methods to explore a wide range of chemical problems in astrochemistry and combustion chemistry. All of these projects are performed in collaboration with field experts, and represent noteworthy examples of how computational chemistry can assist scientific advances that occur on a macroscopic scale. The first chapter, originally published in the *Journal of Physical Chemistry A*, explores the formation and evolution of nitrogen containing pre-biotic molecules in non-Earth environments such as the atmosphere of Titan. The second chapter, currently in peer review at the journal *Proceedings of the National Academy of Sciences*, involves modelling of hydrogen ejection reactions relevant for soot formation processes during incomplete combustion. This chapter contains hydrogen-loss rate constant calculations and models formation pathways to polycyclic aromatic hydrocarbons that are likely to be important precursors to incipient soot particles. Finally, the third chapter (as of yet unpublished) returns to space and contains calculations of binding energies and characterization of binding motifs for neutral, radical, and ionic interstellar molecules. These quantities are essential for creating accurate chemical models of interstellar chemistry, especially that which happens on the surface of icy grains.

Chapter 2

Nitrogen-containing ions and molecules in the gas phase have been detected in non-Earth environments such as dark molecular clouds, and more recently in the atmosphere of Saturn’s moon Titan. These molecules may serve as precursors to larger heterocyclic structures that provide the foundation of complex biological molecules. On Titan, molecules of mass-to-charge ratio 66 have been detected by the Cassini mission, and species of the empirical formula C_4H_4N may contribute to this signature. Characterization of structural minima of C_4H_4N and their spectral signatures may not only assist astronomers with detection of these molecules, but also allow us to postulate novel synthetic routes to pre-biotic molecules that have C_4H_4N precursors or intermediates. To this end, we have characterized seven isomers of C_4H_4N in anionic, neutral radical, and cationic states using density functional theory. Structures were optimized using the range-separated hybrid ω B97X-V with the cc-pVTZ and aug-cc-pVTZ basis sets. We have found through our optimizations that anionic and radi-

cal C_4H_4N favor cyclic structures with aromatic and quasi-aromatic electron arrangements, respectively. Interestingly, our calculations indicate that ionization from the radical surface to the cation induces significant changes in structural stability, and the global minimum for positively charged isomers is $CH_2CCHCNH^+$, a bent species reminiscent of cyanoallene. Select formation pathways to these structures from Titan's existing or postulated gas-phase species, reactions which are also relevant for other astrophysical environments, are discussed. By characterizing C_4H_4N isomers, we have identified energetically stable anionic, radical, and cationic structures that may be present in Titan's atmosphere and dark molecular clouds. The content of this chapter has been published in the *Journal of Physical Chemistry A* (JE Hendrix, PP Bera, TJ Lee, and M Head-Gordon, *J. Phys. Chem. A* **124** 2001-2013 (2020)[53]

Chapter 3

Polycyclic aromatic hydrocarbons (PAHs) play a major role in combustion chemistry, as well as the chemistry of the interstellar medium. Production (or activation) of radical PAHs and propagation of their resulting reactions requires efficient dehydrogenation - but what is the preferred method of hydrogen loss? Unimolecular hydrogen ejection (i.e. direct C-H bond fission) and bimolecular radical abstraction are two main candidate pathways. To characterize the role of H ejection, particularly as a driver for molecular-weight growth in radical-centric hydrocarbon growth mechanisms, this work reports electronic structure calculations establishing that C-H bond strengths span a broad range of energies, going down to below 30 kcal/mol in some C_9-C_{13} PAH radicals. At $T > 1200K$, calculated thermal rates of hydrogen ejection from weak C-H bonds at zig-zag sites on PAH radicals are significantly faster than typical H-abstraction rates. These results are highly relevant in the context of chain reactions of radical species, and soot inception under fuel-rich combustion conditions. Furthermore, calculated microcanonical rates that include the additional internal energy associated with bond formation (e.g. ring closure to yield C_9H_9) yield significantly higher rates than those associated with full thermalization. These microcanonical considerations are relevant to the astrochemical processes associated with hydrocarbon growth and processing in the low density interstellar environment. The content of this chapter is under peer review at the journal *Proceedings of the National Academy of Sciences*.

Chapter 4

Reactions occurring on the surfaces of icy dust grains, which are found in diverse interstellar environments from cold molecular clouds to the plumes of Enceladus, are important for driving chemistry in the interstellar medium (ISM). Due to frigid temperatures, many species bind to the surface of these grains, where they may go on to react with other adsorbates and potentially release new products back into the gas phase. These surface processes are heavily influenced by the mode of binding, and the molecular binding energy, which are thus key quantities to include in models describing interstellar chemical processes. How-

ever, both structures and binding energies are as yet missing or incompletely characterized, especially for species such as radicals and ions. To address this, we report computational searches for optimal structures and binding energies for sets of neutral, open-shell, cationic, and anionic molecules of astrochemical relevance with clusters of $n=1-4$ water molecules. The calculations used reliable density functionals for geometry optimization, and CCSD(T) single point coupled cluster calculations for refinement of calculated binding energies. Efforts were made to characterize all relevant low energy structures identified by conformer searches as well as a range of initial guesses. For neutral closed and open-shell molecules, functional-group dependent trends are apparent - molecules with strong dipoles and potential for hydrogen bonding are more tightly bound to water clusters. The unpaired electron in open-shell species has little effect on binding energies, giving only a slight enhancement for some species. For closed-shell cationic and anionic species, barrierless reactions with water clusters occur for several species, indicating radical-free routes to alternative products that could result from condensation of these molecules onto amorphous ice surfaces. Such direct chemical processing can be understood as a consequence of acid-base properties of the species involved.

Chapter 2

The cation, anion, and radical isomers of C_4H_4N : Computational characterization and implications for astrophysical and planetary environments

2.1 Introduction

The emergence of biomolecules on early Earth is an intriguing topic and the chemical origins of life have not been fully resolved. Groundbreaking experiments performed by Miller in the mid-1950's under reducing conditions showed that complex organic molecules can form from small inorganic precursors in the presence of electric discharge [54], supporting the possibility of biomolecule formation in the atmosphere of primitive Earth. Since this iconic experiment, our understanding of chemistry in early Earth environments has continued to grow, and multiple synthetic routes leading to complex organic species have emerged [55–64].

Though these complex molecules have been shown to form without pre-existing complex organic material, the particular atmospheric conditions of our young planet are not entirely certain. Thus, it is important to consider a variety of alternative conditions supporting biomolecule origin. Exogenous delivery of key precursors to Earth from extraterrestrial environments is one example. Complex organic molecules have been found in many astrophysical environments including interstellar molecular clouds, protoplanetary nebulae, and primitive solar system bodies [65]. Particularly, the existence of these molecules (including pristine amino acids and sugars) has been confirmed in meteoric samples of extraterrestrial origin [66–69], implying that exogenous delivery of organic molecules during or after the formation of the solar system is a viable pathway that could have precluded biomolecule formation on early Earth and potentially contributed to the origins of life on this planet. Direct formation

of these nucleobases on interstellar cold grains has been shown to occur when ices containing the appropriate precursors undergo UV irradiation [70–75]. Additionally, these compounds could be synthesized in the gas phase and condense onto cold grains for delivery to early planetary systems..

Gas-phase reactions are more likely to occur in environments such as the circumstellar envelopes of dying stars, dark molecular clouds, and select planetary atmospheres where particle densities are higher than in the diffuse interstellar medium [76–78]. As well as illuminating formation pathways to complex species that could be delivered exogenously to Earth through meteorites, some of these processes serve as useful templates when considering the atmospheric conditions of early Earth. Low temperatures typical of these environments disfavor particle growth through neutral-neutral reactions between closed-shell members, which require large activation barriers; however, reactions involving radicals and ions proceeding through small or submerged energetic barriers have been shown to produce complex nitrogen-containing molecules [79–82]. Ion-molecule chemistry between atomic nitrogen and cyclic precursors can generate nitrogenated polycyclic aromatic hydrocarbons (PANH) [83, 84], and cyclization reactions of smaller nitrogenated and hydrocarbon species are also quite possible [78, 85].

A planetary body of particularly rich nitrile chemistry is the ionosphere of Titan, Saturn’s moon. Titan’s dense atmosphere, composed primarily of nitrogen (94 - 98%) and methane (1.8 - 6.0%) [86], is exposed to UV and extreme-UV radiation as well as energetic electrons from Saturn’s magnetosphere [86]; this particular combination favors molecular interactions involving and producing nitrogen-containing molecules. Understanding processes occurring in Titan’s atmosphere that could lead to complex nitrogenated organics is important for species identification both here and in molecular clouds, and these may mimic reactions that took place in a primitive Earth environment.

The recent Cassini-Huygens mission, equipped with an ion neutral mass spectrometer (INMS), performed a fly-by of Titan and collected data on neutral, cationic, and anionic species up to several hundred daltons in size [87–91]. Accurate identification of new nitrogen-containing species in remote environments such as the atmosphere of Titan is experimentally difficult, and often relies on theoretical groundwork when existing molecular information is limited. Here, we explore the lower mass end of the INMS readings (<100 daltons), and specifically direct our investigation to the measured signal at m/z 66 [92–95]. There are several stoichiometries that could potentially contribute to this mass peak (e.g. C_4H_4N , $C_2N_3^-$, $C_5H_6^+$, $C_3H_2N_2$, etc. [95–98]), belonging to hydrocarbons or nitriles due to the atmospheric composition. We choose to focus our attention on isomers of the empirical formula C_4H_4N due to its potential to form heterocyclic ring structures.

Similar characterizations of C_4H_5N and C_4H_3N isomers have been performed to identify energetically favorable arrangements [99, 100]. For example, C_4H_5N is by far most stable in ring form as pyrrole [100]. This aromatic 5 membered ring contains 6π electrons; the apical nitrogen is sp^2 hybridized in the molecular plane, leaving its lone pair to delocalize into the aromatic system. Linear species of C_4H_3N (isomers of which have been detected in the interstellar medium [101–103]) have been studied by Custer et al. [99], who found that

methylcyanoacetylene CH_3CCCN was the most stable isomer of those tested. The preferred structures of each chemical formula are good indicators of which isomers are most likely to be present in cold extraterrestrial environments.

Changes in the electronic structure of these molecules influence isomer stability and reactivity. Multiple potential energy surfaces are available to C_4H_4N depending on the mechanism of formation: anionic or neutral radical species may form via deprotonation or dehydrogenation of cyclic C_4H_5N , while protonation of C_4H_3N leads to cationic $C_4H_4N^+$. In the open-shell radical or closed-shell ionic form, molecules such as C_4H_4N are especially reactive and could initiate reactions producing the larger heterocyclic structures that compose biomolecules. Reactions involving pyrrole and pyridine (the six-membered aromatic analog) have been experimentally probed in this vein [79, 80, 104].

Because chemistry in cold extraterrestrial environments is driven primarily by radical-radical and ion-radical reactions (as well as those between a closed shell species and an ion or radical), characterizing C_4H_4N in different electronic states will help us identify which species are likely to participate in pathways leading to biologically relevant molecules. Thus, we present a systematic exploration of select C_4H_4N isomers in their cationic, anionic, and radical forms. The relative stability of these structures in each electronic state is discussed, as well as select formation routes via the uni-molecular or bi-molecular reactions of available species. By characterizing C_4H_4N , we produce structures that will narrow the field of candidate molecules that may contribute to the observed mass data from Cassini INMS, and thus help guide the identification of new species. In the process, we hope to also gain a better understanding of how unique cationic, anionic, or radical isomers could contribute to the synthesis of complex organics. This will help us understand not only processes occurring in the rich atmosphere of Titan or that of early Earth, but also in cold molecular clouds where nitrogen-containing molecules may form in the gas phase and deposit onto the cold grains of meteorites for delivery to planetary bodies.

2.2 Methods

Seven isomers of C_4H_4N (see Chapter 2.3 for optimized radical structures, which deviated the least from starting geometries) were chosen based on their presence in both the chemical physics and combustion literature [100, 105–107]. Though we recognize that these seven isomers are not fully representative of all possible configurations, the number of species was limited to likely low-energy structures to lessen computational cost and focus on adequate characterization of individual species. Full geometry optimizations were performed for structures of all seven isomers and several relevant precursors using unrestricted density functional theory (DFT), a widely used method for quantum mechanical calculations by virtue of its impressive accuracy at low computational cost. Our DFT calculations were performed on an ultra-fine integration grid of 99 radial points and 590 angular points. Optimizations of starting structures A-G were performed using the ω B97X-V functional [27]. The range-separated hybrid ω B97X-V has been shown to out-perform many other existing functionals

for calculations on numerous relevant systems [108–111]. Inclusion of range-separation helps mitigate the infamous ‘self-interaction error’ inherent to DFT, which can lead to inaccuracies in energetics, especially in radical systems such as the ones studied here [112, 113]. Each structure was allowed to relax from the initial geometry on the appropriate potential energy surface: anion, neutral radical, and singlet cation. Isomers are referred to by distinguishing letter and charge symbol hereafter (e.g. A^- , A^\bullet , and A^+ for anionic, neutral radical, and cationic isomer A).

Cationic and radical isomers were optimized with ω B97X-V in the cc-pVTZ basis. Because the use of diffuse functions is generally recommended for DFT calculations involving anions, anionic structures were optimized using the larger aug-cc-pVTZ basis set. Inclusion of sufficient diffuse functions in aug-cc-pVTZ better captures the ‘tail behavior’ of atomic orbitals farther from the atom’s nucleus, a crucial feature for structures with excess electron density [114]. Natural Population Analysis [115] was performed using ω B97X-V in aug-cc-pVTZ. To confirm that the equilibrium geometries of the isomers were indeed minima and obtain zero point energies, vibrational frequency analyses were performed for cations and radicals at the ω B97X-V/cc-pVTZ level, and for anions at the ω B97X-V/aug-cc-pVTZ level. Vibrational constants and intensities are provided in the Supplemental Information (Appendix A). Because the accuracy of the isomer energies was crucial for the purposes of this study, single-point energies were calculated for isomers A-G of the cation, radical, and anion at the coupled cluster level, including up to triple excitations using CCSD(T) [116]. In conjunction with second-order Møller-Plesset perturbation theory with the resolution of the identity approximation (RI-MP2) [117, 118] in progressively larger basis sets, energies were extrapolated to the complete basis set limit (CBS) using the following scheme:

$$\begin{aligned} E(\text{CCSD}(T)/\text{CBS}) = & \\ E(\text{HF}/\text{cc-pV5Z}) + E^{\text{corr}}(\text{RI-MP2}/\text{CBS}_{3,4,5}) + & \\ E^{\text{corr}}(\text{CCSD}(T)/\text{cc-pVTZ}) - & \\ E^{\text{corr}}(\text{RI-MP2}/\text{cc-pVTZ}) + & \\ \text{ZPE}(\omega\text{B97X-V}/\text{cc-pVTZ}) & \end{aligned}$$

Here, the $E^{\text{corr}}(\text{RI-MP2}/\text{CBS}_{3,4,5})$ term contains the complete basis extrapolation using cc-pVTZ through cc-pV5Z:

$$\begin{aligned} E^{\text{corr}}(\text{RI-MP2}/\text{cc-pVNZ}) = & \\ E^{\text{corr}}(\text{RI-MP2}/\text{CBS}_{3,4,5}) + AN^{-3} & \end{aligned}$$

The variable N corresponds to the basis set cardinal number [119], which here is 5. For anionic structures, the same scheme was followed using aug-cc-pVNZ.

In exploring potential formation pathways of the lowest-energy structures, the freezing-string method was utilized to generate a guess for transition state structures [120]. Once a suitable transition state was located, its initial structure and Hessian were further improved

using the partitioned-rational function optimization eigenvector following method [121]. All this is done in ω B97X-V with cc-pVTZ or aug-cc-pVTZ as individually indicated.

All calculations were performed using the Q-Chem 5 software package [122].

2.3 Results and Discussion

Anionic isomers

Figure 2.1 shows the energetic ordering of structures on the closed-shell anionic potential energy surface.

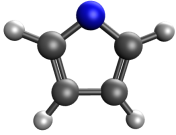
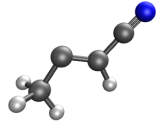
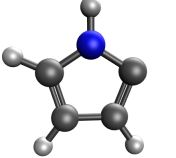
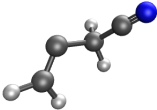
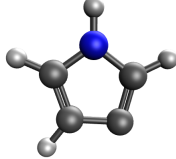
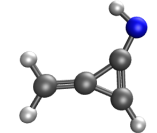
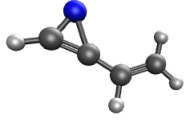
Isomer (Formula)	Structure	Relative Energy
A^- ($c-C_4H_4N$)		0.00
E^- (CH_3CCHCN)		33.28
B^- ($c-C_\alpha C_3H_3NH$)		36.59
D^- (CH_2CCH_2CN)		42.72
C^- ($c-C_\beta C_3H_3NH$)		46.91
F^- ($CH_2CCHCNH$)		56.34
G^- ($CH_2CHCCHN$)		84.26

Figure 2.1: Structures of C_4H_4N in the closed-shell anionic state. Isomer (A^-) was found to be the energetic minimum, stabilized by a favorable 6π aromatic electron arrangement. Energetic differences are calculated with respect to (A^-) in kcal/mol.

The energetic differences of the anionic isomers were computed with respect to cyclic isomer (A^-), which was found to be the most stable structure (energetic minimum). Electronically, (A^-) is isoelectronic to pyrrole. Pyrrole and $C_4H_4N^-$ are aromatic heterocycles, each with a total of 6π electrons; four π electrons are contributed by carbon atoms in the conjugated 5-member ring, and the remaining two are donated from the nitrogen's lone pair.

In neutral pyrrole, the nitrogen atom has an in-plane trigonal configuration, bonding to the surrounding α carbons and a single hydrogen; the remaining lone electron pair occupies $2p_z$ out-of-plane, contributing to the 6π aromatic ring system [123]. Deprotonation of pyrrole occurs at the apical nitrogen, as the electronegativity difference between N and H makes this proton the most acidic. In the anionic C_4H_4N (structure (A^-)), the aromatic configuration is retained. Due to this favorable electronic arrangement, isomer (A^-) is by far the favored structure on the anionic surface - the second lowest energy structure (E^-) lies 33 kcal/mol above (A^-) in energy and is quasi-linear, stabilized by several resonance structures. Most of the negative charge in (E^-) is localized on the carbon at which the molecule sharply bends; because of (E^-)'s shape, electron density centered on this carbon is spatially separated from the lone electron pair on nitrogen, decreasing steric interactions between the respective electron clouds. To the point, cyclic (B^-) (deprotonated at the α carbon) is slightly destabilized by comparison.

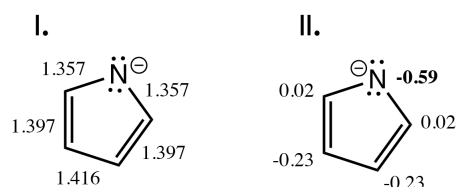


Figure 2.2: Bond lengths (**I.**) and Natural Charges (**II.**) for anionic (A^-) calculated in ω B97X-V/aug-cc-pVTZ. Charges indicated on carbon atoms are a sum of the C-H moiety. The aromatic nature of the ring leads to a planar structure with lengthened $C_\alpha=C_\beta$ and slightly shortened $C_\beta-C_\beta$ and $C_\alpha-N$ (compared to pyrrole).

Figure 2.2 shows bond lengths and natural charges in anionic isomer (A^-), the global minimum for this set. The 6π aromatic conjugation of the structure results in a shortened 1.416 Å $C_\beta-C_\beta$ (vs 1.424 Å), a lengthened 1.397 Å $C_\alpha=C_\beta$ (vs 1.371 Å), and shortened 1.357 Å $C_\alpha-N$ (vs 1.370 Å) bond (compared to those in neutral pyrrole), culminating in a planar structure with C_{2v} symmetry. These slight deviations from parent pyrrole (optimized at the same level of theory) are due largely to the extra electron density of the anionic lone pair atop the apical nitrogen, which also drives the 109.7° $C_\alpha-N-C_\alpha$ angle in pyrrole to a more acute 105.0° in deprotonated (A^-). Natural charges reflect the spread of electron density across the ring, with negative charge centered mostly at nitrogen as expected, but also distributed in a good proportion to the β carbons.

Structural stability depends highly on the deprotonation site in the anionic C_4H_4N cyclic isomers. Deprotonation of the heteroatom to form (A^-) is clearly the most favorable process - as discussed previously, the distinct difference in electronegativity along the N-H bond makes this proton highly acidic. Deprotonation at an α or β carbon in the ring is comparatively more difficult, despite the similarities in N-H and C-H bond enthalpies (both 338 kJ/mol [124]). Structures (B^-) and (C^-) (with C-H bond cleavage at α and β sites,

respectively) lie over 35 kcal/mol higher in energy than (A^-). Deprotonation at the α carbon in (B^-) is preferred over a similar process at the β site in (C^-), with the latter relatively destabilized by about 10 kcal/mol. In general, electrophilic substitutions to five-member heterocyclic rings favor attack at the α carbon. Compared to the β site, substitution at the α carbon leads to a greater number of intermediate resonance structures, allowing for more facile charge delocalization and a more stabilized product [125]. Due to this effect and the proximity of the electron-withdrawing heteroatom, the hydrogen atom at the α carbon is more acidic than that at the β carbon, favoring α deprotonation of the cycle. These effects stabilize (B^-) relative to (C^-).

Radical isomers

For the radical electronic configuration, (A^\bullet) is once again found to be the global minimum as shown in Figure 2.3. Interestingly, quasi-linear isomer (E^\bullet) is nearly equivalent in energy to cyclic radical isomers (B^\bullet) and (C^\bullet), which all lie approximately 25 kcal/mol above (A^\bullet) in energy. The relative energetics of isomers (B^\bullet) and (C^\bullet) with respect to (A^\bullet) indicate that the location of the radical electron influences heterocycle stability. With the exception of (E^\bullet), other linear and semi-linear isomers of C_4H_4N are found to be subsequently higher in energy than their cyclic counterparts on the radical PES, though with energetic differences less dramatic than in the anionic case.

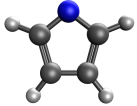
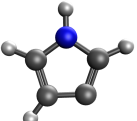
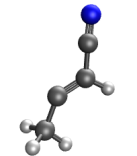
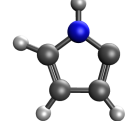
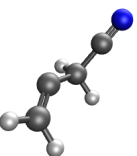
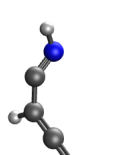
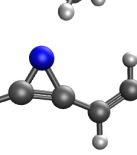
Isomer (Formula)	Structure	Relative Energy
A [•] (c-C ₄ H ₄ N)		0.00
C [•] (c-C _β C ₃ H ₃ NH)		24.72
E [•] (CH ₃ CCHCN)		24.79
B [•] (c-C _α C ₃ H ₃ NH)		25.12
D [•] (CH ₂ CCH ₂ CN)		28.81
F [•] (CH ₂ CCHCNH)		44.29
G [•] (CH ₂ CHCCHN)		53.91

Figure 2.3: Structures of C_4H_4N in the radical configuration; relative energies are calculated with respect to (A[•]) in kcal/mol. Similar to the anionic state, (A[•]) is the lowest energy structure. Though electron removal has resulted in loss of complete aromaticity, (A[•]) still benefits from some delocalization of the remaining 5π electrons over the ring.

Recent calculations performed by Sah et al. on a variety of five-membered heterocyclic species found that radicals centered at the heteroatom were favored over those located on nearby α or β carbon atoms - unpaired electrons on heteroatoms can delocalize across the π orbitals of the ring more easily [105]. For dehydrogenated pyrrole species (C_4H_4N), these authors optimized heteroatom, α carbon, and β carbon centered radicals (corresponding to

our (A^\bullet), (B^\bullet), and (C^\bullet)) at several levels of theory, and our computed energetic differences are in good agreement.

The particular stability of (A^\bullet) can be rationalized in a way similar to the anionic analog. Recall the nature of the apical nitrogen - in both pyrrole and the aforementioned anionic counterpart, N is sp^2 hybridized and maintains a trigonal configuration within the molecular plane. In anionic (A^-), nitrogen has two electron pairs. One occupies the $2p_y$ orbitals to maintain the sp^2 arrangement, and the other resides in $2p_z$ out of the molecular plane, contributing to the aromatic ring system. (A^-) is isoelectronic to cyclopentadienyl anion, which has degenerate π molecular orbitals due to the D_{5h} symmetry of the molecule [126]. However, inclusion of a nitrogen atom in the ring reduces the overall symmetry to C_{2v} in pyrrole and (A^-), and the π orbitals are no longer energetically degenerate [127]. Due to their hybridization and non-participation in the π system, nitrogen's $2p_y$ orbitals lie lower in energy than the $2p_z$ orbitals. Because of this, electron removal from (A^-) to form the radical (A^\bullet) occurs from $2p_z$ - this disturbs the aromaticity of the cycle, but the radical electron can still delocalize over the ring, resulting in a pseudo-aromatic 5π arrangement. Considering the stabilization of $2p_y$ and the observation that (A^\bullet) suffers no distortion from the x-y plane, it is reasonable to assert that the unpaired electron of the radical occupies $2p_z$ and the lone pair of $2p_y$ remains intact.

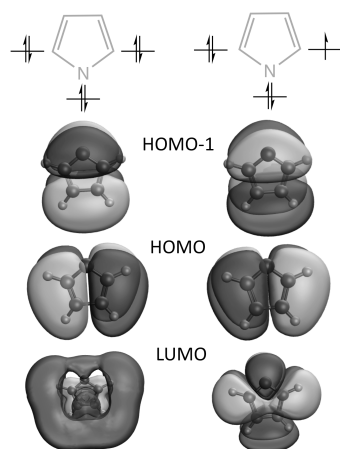


Figure 2.4: Comparison of molecular orbitals and electron configuration between (A^-) (left) and (A^\bullet) (right). The HOMO of anionic (A^-) is similar to the SOMO of the corresponding radical species, indicating electron removal from the anionic occurs from $2p_z$ orbitals on nitrogen that contribute to the π system. The $2p_y$ orbitals are largely undisturbed and contribute to the planarity of (A^\bullet).

The orbitals shown in Figure 2.4 support this picture. The highest occupied molecular orbital (HOMO) of anionic (A^-) and singly occupied molecular orbital (SOMO) of radical (A^\bullet) show similar shapes, indicating a similar contribution from the atomic orbitals.

The molecular orbitals of these heterocycles and their occupations have been previously appraised; Gianola et al. investigated the electronic structure of pyrrolide anion and its corresponding radical in detail, noting the clear bonding character between α and β carbons [127]. In our systems, this interaction is particularly strong in the anion, and removal of an electron to form the radical reduces bonding character. This manifests as a slight lengthening of the central $C_\alpha=C_\beta$ bonds highlighted in Figure 2.5. Though these structural changes occur due to the loss of aromaticity in radical (A^\bullet), decreased interaction between α and β carbons does not completely destabilize the ring.



Figure 2.5: Bond lengths (I.) and Natural charges (II.) for radical (A^\bullet) calculated in ω B97X-V/cc-pVTZ. Charges indicated on carbon atoms are a sum of the C–H moiety. Electron removal from anionic (A^-) has disrupted the aromaticity of the heterocycle, inducing small structural changes in the radical and reflecting the depletion of bonding character between α and β carbons.

Figure 2.5 shows the bond lengths and Natural charges of isomer (A^\bullet) in the radical configuration. Though (A^\bullet) is pseudo-aromatic and stabilized on the radical surface, the loss of complete aromaticity is reflected in the bond lengths and charge distribution.

Stretching and shortening of bonds in radical (A^\bullet) reflects fluctuations of electron density. Compared to anionic (A^-), there is a slight lengthening of the 5-member heterocycle, as the $C_\alpha=C_\beta$ bonds stretch by 0.059 Å while $C_\alpha-N$ and $C_\beta-C_\beta$ shorten by 0.017 and 0.061 Å respectively.

While the loss of bonding character between α and β carbons manifests in $C_\alpha=C_\beta$ lengthening, the apical $C_\alpha-N-C_\alpha$ angle remains nearly unaltered from the aromatic anion ring at 104.6°, indicating that the position of the lone pair atop N remains undisturbed and providing further support for the proposed 5π electronic arrangement.

As shown in Figure 2.5 II., charge differences between ring atoms have become more pronounced than in the anionic case of (A^-). These changes in charge distribution go hand-in-hand with the altered bond lengths. Stretching of $C_\alpha=C_\beta$ in (A^\bullet) brings the p orbitals of the α carbons closer to nitrogen, donating some of their electron density to the more electronegative atom. As a consequence, α carbons have taken on a noticeable positive charge, and are quite charge separated from their neighboring nitrogen.

The β carbons of (A^\bullet) pull closer together at a distance nearing that of a carbon-carbon double bond. Like the α carbons, β carbons have become more positive than nitrogen (by 0.48 charge units, versus their 0.36 charge unit difference in (A^-)). Though the effect is

less drastic, α and β carbons themselves are charge separated to a greater degree as bonding character between them decreases.

Additionally, spin density delocalization contributes to the stability of (A^\bullet) and helps explain the relative stabilities of cyclic isomers (B^\bullet) and (C^\bullet). As shown in Figure 2.3, there is a ~ 25 kcal/mol difference in energy between (A^\bullet) and the other cyclic isomers, though (B^\bullet) and (C^\bullet) less than 1 kcal/mol apart. This is in contrast to anionic (B^-) and (C^-) isomers, which were energetically separated by about 10 kcal/mol (with relative stabilization of (B^-)).

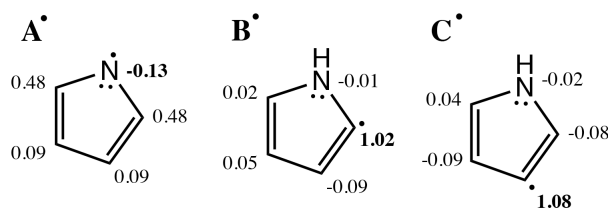


Figure 2.6: Spin densities calculated for isomers (A^\bullet), (B^\bullet), and (C^\bullet). Electron spin is relatively delocalized in (A^\bullet), while it is highly localized for (B^\bullet) and (C^\bullet).

For dehydrogenation reactions of pyrrole to form the radical, acidity of the departing hydrogen is less predictive of the preferred reaction site than it is for deprotonation reactions; since isomers (A^\bullet), (B^\bullet), and (C^\bullet) are carrying a radical electron, spin densities help explain some of the observed stability trends, shown in Figure 2.6. Highly localized electron spin results in a very reactive species, while delocalized spin conversely stabilizes a structure [105]. Figure 2.6 shows the distribution of spin between the two α carbons in (A^\bullet), contributing to the stability of the structure. Conversely, (B^\bullet) and (C^\bullet) show highly localized spin densities at their respective dehydrogenation sites, and spin is localized to the same degree in each, so α dehydrogenation is not particularly favored over the β site, and vice versa.

Cationic isomers

Removal of another electron from the C_4H_4N radical surface results in the singlet cationic electronic configuration. Ionization is accompanied by more major shifts in the stability ordering of these isomers shown in Figure 2.7.

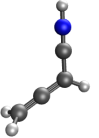
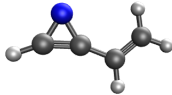
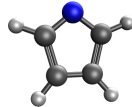
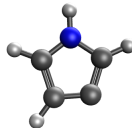
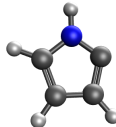
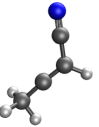
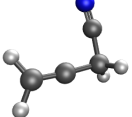
Isomer (Formula)	Structure	Relative Energy
F^+ ($CH_2CCHCNH$)		0.00
G^+ ($CH_2CHCCHN$)		25.28
A^+ ($c-C_4H_4N$)		26.40
C^+ ($c-C_\beta C_3H_3NH$)		35.24
B^+ ($c-C_\alpha C_3H_3NH$)		36.66
E^+ (CH_3CCHCN)		39.02
D^+ (CH_2CCH_2CN)		39.53

Figure 2.7: Structures of C_4H_4N in the cationic state; relative energies are expressed in kcal/mol. Heterocyclic (A), the global minimum on both anionic and radical potential energy surfaces, is now reduced to an anti-aromatic arrangement with 4π electrons in the ring, destabilizing the structure. The global minimum for the cationic surface was found to be (F^+), a linear structure reminiscent of cyanoallene.

Previously, cyclic (A) was found to be the global minimum on the radical and anionic potential energy surfaces; however, in the cationic case, (G^+) and (F^+) are found to be lower in energy. Similar to the anion/radical transition, transition from radical (A^\bullet) to the cation can occur via electron removal from either the $2p_y$ or $2p_z$ of nitrogen, and once again this removal occurs from the higher energy $2p_z$ orbitals. Nitrogen's lone pair continues to occupy $2p_y$ and planarity is retained; however, (A^+) is now left relatively higher in energy due to its

anti-aromatic 4π electron arrangement.

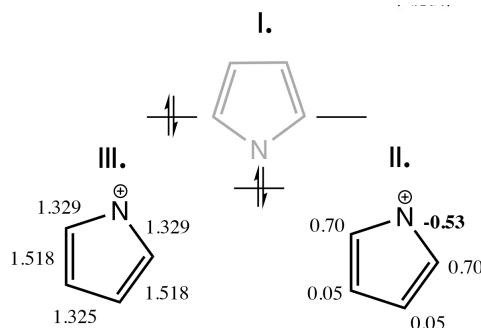


Figure 2.8: Electronic configuration (**I.**), Natural charges (**II.**), and bond lengths (**III.**) for cationic (A^+). Charges indicated on carbon atoms are a sum of the C–H moiety. Half-filled orbitals contribute to the destabilization of this structure. In response, the $C_\alpha=C_\beta$ bonds elongate to 1.518 Å, close to a typical C–C single bond.

Cationic (A^+) was found to be a transition state structure, and the now half-filled molecular orbitals contribute to structural distortion that lowers the overall energy of the molecule. Despite its stretched and strained structure, the singlet cation was found to be lower in energy than the triplet configuration, though the singlet-triplet gap is small (~ 5.2 kcal/mol).

As shown in Figure 2.8, the $C_\alpha=C_\beta$ bonds have lengthened significantly compared to aromatic pyrrole or anionic (A^-), approaching the length one would expect from a C–C single bond. Since (A^+) is now antiaromatic, the bonding character between α and β carbons established for anionic and radical species [127] is disrupted completely. Similar phenomena have been discussed in detail for the isoelectronic cyclopentadienyl cation [126, 128], another planar C_{2v} ring with modes of distortion leading to lower symmetry (more energetically stable) structures [129].

The stabilization of (G^+) compared to (A^+) is slightly surprising - however, structural strain within the three-membered ring is mitigated by electron delocalization, as the ring is aromatic by the $4n+2$ rule, where here $n=0$. In isoelectronic 3-membered carbocations such as cyclopropenyl, structures are stabilized by delocalization of the 2π electrons residing in the ring system, which can spread into empty 2p orbitals of the positively charged carbon atoms [130, 131]. Azirinyli cation, a three-membered ring with an apical nitrogen atom, has recently been investigated in the interstellar context and was found to be the most stable structural isomer of the formula $C_2H_2N^+$ [132].

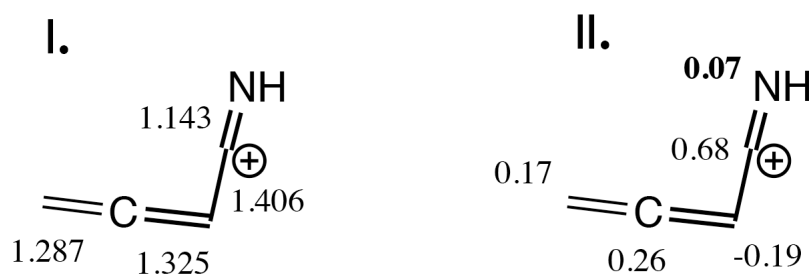


Figure 2.9: Bond lengths (**I.**) and Natural charges (**II.**) for cationic (F^+). Charges indicated on carbon atoms are a sum of the C–H moiety. This carbocation is of C_s symmetry, and is stabilized by electronic donation from the neighboring nitrogen and C–H σ bond to vacant p orbitals of the positively charged carbon.

The global minimum on the singlet cationic surface was found to be (F^+), a highly conjugated quasi-linear isomer with C_s symmetry. As shown in Figure 2.9, the unsaturated carbon participating in the C=N double bond (C_2) carries most of the positive charge. Hyperconjugation and resonance contribute to the stability of this carbocation. The empty p orbital on C_2 can accept electron density from the nearby C–H σ bond; this stabilizing interaction results in a lower-energy electron occupancy versus the isolated positively charged p orbital. Structurally, this manifests as the slight shortening of the C_2 – C_3 single bond. Similarly, a non-negligible amount of electron density from the lone pair on nitrogen interacts with the C_2 empty p orbital, again stabilizing the positively charged carbon atom and shortening the C=N double bond to a length approaching that of a C≡N triple bond.

Ionization energies and electron affinities

Table 2.1 shows the adiabatic electron affinities and ionization energies of all isomers studied here as compared to the radical form in units of eV. Unsurprisingly, electron attachment to radical (A^\bullet) forming anionic (A^-) is highly favorable, as this leads to 6π electrons in the ring. Energetic stabilization through anion formation decreases with structural stability of the anionic isomer. Electron affinity for isomer (F^\bullet) was not included in this table due to the significant structural rearrangement that occurs upon electron gain (See e.g. Fig. 2.1 or Fig. 2.3 for comparison between the structures).

Table 2.1: Adiabatic electron affinities and ionization energies (eV) relative to the radical species for all isomers, calculated using single point energies (CCSD(T)/CBS) of all isomers. All species (except perhaps G) are stabilized by electron gain. Ionization of radical (A^\bullet) requires significant energy, while ionization of radical (F^\bullet) is markedly more feasible.

Isomer	EA	IE
A	2.21	9.20
B	1.68	8.54
C	1.18	8.48
D	1.57	8.51
E	1.80	8.67
F	—	6.05
G	0.83	6.67

An interesting trend has emerged regarding ionization states of isomer (F). On the anionic surface, previously linear (F) rearranges to adopt a central 3-membered ring, promoting delocalization of negative charge. These structural adaptations require significant energy. In contrast, ionization to the cationic state supports the original linear arrangement.

Astrochemistry Implications

In the previous sections, we calculated low-energy structures of cationic, radical, and anionic isomers, providing a structural starting point for further identification of species that may be present in Titan’s atmosphere and elsewhere. Providing highly accurate ro-vibrational data using theoretical methods for use in conclusive species identification is a challenging prospect [133, 134], and though accurate structures provided here may be used for this purpose, producing high-accuracy ro-vibrational data is not our ultimate goal in this work. However, because calculated vibrational frequencies and intensities in addition to molecular structures are still useful to provide astronomers with a solid foundation for deconvoluting measurable ro-vibrational data from small molecules, we provide vibrational frequencies and intensities for the energetic minima of each C_4H_4N state in the SI.

Small nitrogen-containing molecules such as C_4H_4N may be found in molecular clouds or in the ionospheres of planetary bodies such as Titan, and perhaps even existed in the young atmosphere of our own Earth long ago. In Titan’s nitrogen-rich atmosphere, many energy sources are available to initiate the formation of radicals and ions, including short wavelength ultraviolet (UV) radiation, extreme ultraviolet radiation (EUV) and an energetic flux of electrons from Saturn’s magnetosphere [86]. Nitriles produced in the upper atmosphere through photochemistry involving N_2 and CH_4 [135–137] presumably combine through ion-neutral or radical chemistry to form more complex species, contributing to the organic haze surrounding this planetary moon [138].

Here, we investigate several relevant formation pathways leading to ions of C_4H_4N and their preferred structures.

Astrochemical Implications - Anion species

The Cassini-Huygens mission identified a number of nitrogen-containing anionic species in Titan's atmosphere, including anions of this molecular weight ($m/z = 66$) [95]. Though cyclic species such as isomers (A), (B), and (C) have yet to be unambiguously observed in the gas phase, precursors such as pyrrole and other N-heterocycles have been detected as products in plasma-discharge, H-NMR, and other experiments performed in Titan-like conditions or on tholin mixtures [139, 140].

With these observations in mind, the presence of pyrrole (C_4H_5N) in Titan's haze (or elsewhere in the interstellar medium) cannot be discounted, and we thus consider the direct formation of anionic (A^-) from this hydrogenated five member ring to be a viable possibility.

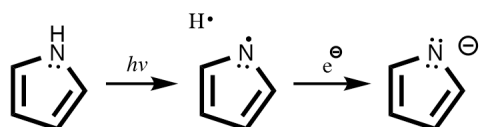


Figure 2.10: Formation of anionic (A^-) from pyrrole via photodissociation. Dehydrogenation of the apical N follows excitation via energetic UV radiation, and electron attachment yields the stable anionic isomer.

Figure 2.10 depicts the formation of anionic (A^-) through photodissociation of pyrrole and subsequent electron attachment. The photofragmentation and dynamics of excited state pyrrole have been extensively studied [141–152] (and references therein). Irradiation of ground state pyrrole (S_0 (1A_1)) at wavelengths from 238–250nm (corresponding to photons of energy $>4.8\text{eV}$) excites the molecule into the $^1\pi\sigma^*$ (1A_2) excited state from which hydrogen atoms are ejected quickly with high kinetic energy, yielding the ground state radical (A^\bullet) [141, 151, 152]; though this is formally electric-dipole forbidden, this mode intensifies by borrowing vibrational energy from higher energy states [143, 151]. At shorter excitation wavelengths, ejection can also occur after direct excitation to the $^1\pi\pi^*$ state (1B_2), which accesses the $^1\pi\sigma^*$ (1A_2) energetic state via a conical intersection [142, 151]. Slower hydrogen ejection can occur from a "vibrationally hot" pyrrole ground state S_0 , where additional energy is dispersed to the many vibrational modes of the heterocycle [143, 151, 152]. In Titan's atmosphere, long wave UV radiation ($>155\text{nm}$) pierces down to intermediate altitudes (nearing 500km), providing an adequate energy source for the photodissociation of pyrrole.

After formation of the ground state radical (A^\bullet), the high electron affinity of this species (see Table 2.1) makes it a good candidate for thermal electron attachment. Processes such as radiative electron attachment (REA) have been investigated as a viable pathway to anion formation in Titan's atmosphere [153]. With many vibrational modes to disperse excess energy, (A^\bullet) could efficiently form (A^-) through this process, depicted in the second step of Figure 2.10. Additionally, the atmosphere is dense enough [92] to support third body interactions that may assist in diffusing the newly formed molecule's energy.

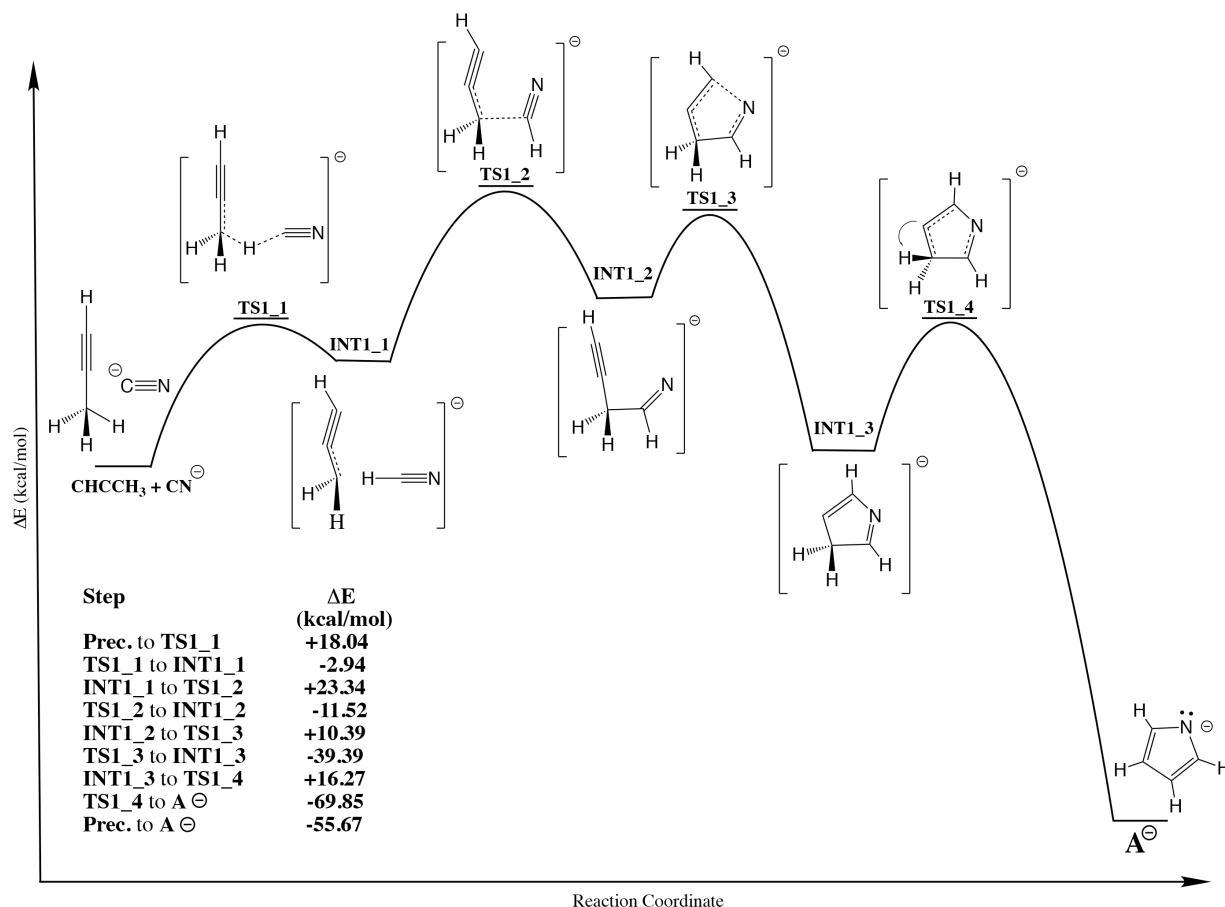


Figure 2.11: Schematic reaction path to anionic (A^-) via CN^- and CH_3CCH . Both propyne and cyano anion have been detected in Titan's ionosphere, and could feasibly react to produce anionic (A^-). The desired product (A^-) is stabilized relative to reactants by over 50 kcal/mol.

Alternatively, formation of anionic (A^-) is possible through recombination of smaller hydrocarbon species. Figure 2.11 shows the energetic profile for reaction between CN^- and propyne. Though barrier heights for cyclization were not calculated, anionic (A^-) is stabilized by more than 50 kcal/mol compared to the reactants alone. Both precursors have been detected in molecular clouds [154, 155] and more recently in Titan's atmosphere: the signatures of various negative ions including CN^- were observed by Cassini-Huygens [88, 89] and heavier hydrocarbons including propyne have been detected at lower altitudes [156]. Though accurate densities for many anionic species are not readily available, several models calculate cyanide anion to be ubiquitous in the ionosphere [153]. Chemical reactions between this species and available hydrocarbons could lead to more complex anionic nitriles such as (A^-).

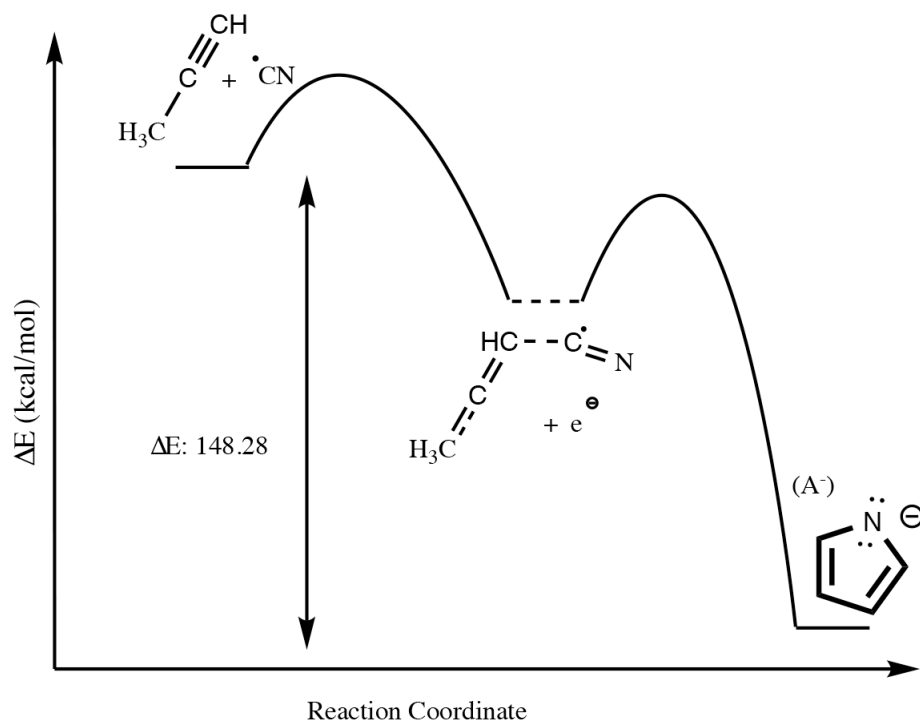


Figure 2.12: Schematic pathway to anionic (A^-) via CN^\bullet and CH_3CCH . The presence of CN^\bullet in Titan's ionosphere is predicted by several models to be significant. Reaction between this radical and propyne, could proceed similarly to the reaction depicted in Figure 10, with electron attachment to an intermediate species to form the desired product, which is stabilized by nearly 140 kcal/mol.

Formation of anions such as (A^-) through electron attachment to radical species is also possible. Reactions of radicals proceed rapidly through small or negligible barriers [81], which is crucial in the cold environment of Titan's atmosphere or dense molecular clouds. Reactions of CN^\bullet with propyne (shown in Figure 2.12) and other small hydrocarbons have been characterized experimentally [157], though heterocycle formation is not discussed in these works. Thermal electron attachment to an intermediate in the reaction pathway could potentially lead to anionic C_4H_4N (A^-) under appropriate conditions.

Astrochemical Implications - Cationic species

Positively charged ions are also ubiquitous on Titan and in other extraterrestrial environments. The aforementioned energy sources (solar radiation and energetic electrons from Saturn's magnetosphere) ionize N_2 and CH_4 , the main constituents composing the upper atmosphere. These ions react with neutrals to create a variety of charged hydrocarbon species.

Molecular mass data obtained during the fly-by of Titan includes traces linked to cations [92–94] - the mass peak appearing at m/z 66 has been investigated by several models [138, 158], and is assigned by some to be $CH_2CCHCNH^+$, our isomer (F^+). Because we found (F^+) to be the global minimum cationic structure in our calculations, we propose that isomer (F^+) is quite likely to contribute to this signal.

Cationic isomers of C_4H_4N such as (F^+) could be interesting precursors to larger structures. As shown by values in Table 2.1, ionization to the cationic state requires significant energy, but sources of radiation are plentiful in this environment and ions are readily formed from their parent neutrals. Several potential reaction pathways have been included in models for cationic C_4H_4N . [138, 158]

One likely formation route to (F^+) is through protonation of allenyl cyanide (cyanoallene, CH_2C_2HCN), which has been detected in the interstellar medium [101] and is predicted in Titan's ionosphere. Isomers of the empirical formula C_3H_3N are most stable as methylcyanoacetylene (CH_3CCCN), but cyanoallene (CH_2C_2HCN , direct precursor to (F^+)) only lies about 2.4 kcal/mol higher in energy [99]. This species has also been detected extraterrestrially near the Taurus Molecular Cloud (TMC-1) [102, 103].

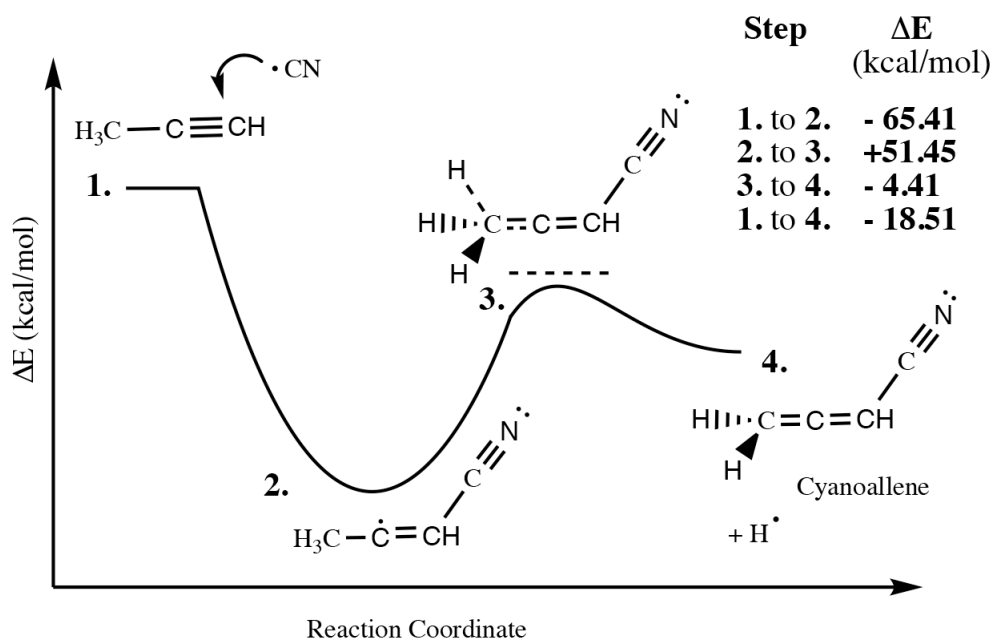


Figure 2.13: Schematic representation of cyanoallene formation via the reaction of propyne (CH_3CCH) and cyano radical (CN^\bullet). The relevant transition state has been characterized by Balucani et al. and occurs through a submerged energetic barrier. This reaction is exothermic by about 18 kcal/mol, in good agreement with the aforementioned calculations. Structures were here optimized and energies calculated at the $\omega B97X-V$ /aug-cc-pVTZ level of theory.

The formation of cyanoallene may occur through reactions between precursors discussed above, namely propyne (CH_3CCH) and cyano radical (CN^\bullet). The reaction of cyano radical with propyne has been investigated experimentally and theoretically [159]. Balucani et al. used a combination of crossed beam experiments and *ab initio* calculations to characterize products and transition states. Reaction of cyano radical with CH_3CCH to form products including CH_2CCHCN (cyanoallene) is barrierless and exothermic overall [159]. When examined at the $\omega B97X-V/cc-pVTZ$ level of theory, the geometries and energetics of key structures along this reaction path (shown in Figure 2.13) are in good agreement with Baculani's calculations.

Because the reaction depicted in Figure 2.13 is barrierless, it could feasibly occur in the cold environments of Titan's atmosphere or molecular clouds. Formation of isomer (F^+) ($CH_2CCHCNH^+$) from cyanoallene would simply require protonation of the neutral species. Due to their high proton affinities, nitriles are good acceptors for H^+ [158].

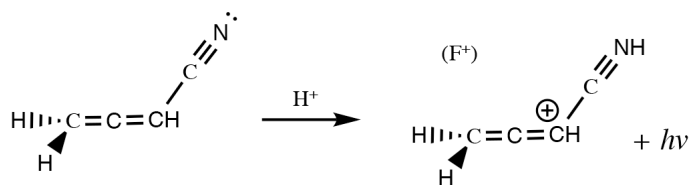


Figure 2.14: Protonation of cyanoallene to form isomer (F^+). The excess energy may be emitted as a photon, or dispersed via collisions with a third body in the dense atmosphere of Titan.

Structures were here optimized at the $\omega B97X-V/aug-cc-pVTZ$ level of theory.

Figure 2.14 shows the protonation of cyanoallene to form isomer (F^+). Cyanoallene has a high proton affinity (over 8eV). Excess energy resulting from this process could be emitted as a photon from isomer (F^+), or be dispersed through third body interactions in the dense atmosphere of Titan.

2.4 Conclusions

In this work, we have investigated isomers of C_4H_4N in cationic, neutral radical, and anionic states to determine the structures of C_4H_4N that could be present in Titan's atmosphere or molecular clouds. We found the energetic ordering of isomers to change with electronic state; that is, the most stable structures for anionic isomers were different from those same configurations on the cationic PES. For anionic species, the global minimum was found to be (A^-). This cyclic isomer, analogous in structure to deprotonated pyrrole, is an aromatic ring containing six π electrons. Negative charge is well distributed between the electronegative nitrogen atom and β carbons of the ring. On the radical PES, (A^\bullet) remains the most stable isomer, preserving a quasi-aromatic five π arrangement after electron removal from

the anion. Lengthening of the central $C_\alpha=C_\beta$ bonds occurs as bonding character between α and β carbons decreases. Electron density again centers on the apical nitrogen and β carbons, though charge discrepancy between ring members is more pronounced.

Upon ionization to the cationic state, structural trends in stability present for anionic and radical isomers change notably. Previously stable (A) now has only four π electrons in the cationic ring, creating an unfavorable anti-aromatic arrangement. In contrast to the anionic and radical species, linear isomer (F^+) was found to be the global minimum on the cationic surface. Hyperconjugation contributes to the stability of this structure, and the terminal nitrogen can donate electron density into empty p orbitals of the carbocation.

(A), the most stable C_4H_4N isomer of those studied here for anions and radicals, could form through numerous feasible mechanisms. Though the presence of N-heterocycles such as pyrrole is unconfirmed in Titan's atmosphere or the interstellar medium, photoexcitation of pyrrole leads to homolytic dehydrogenation of the apical nitrogen, leaving the ground state radical (A^\bullet). Radiative electron attachment to this species, which has a high electron affinity, would result in the aromatic (A^-). Other pathways, such as cyclization reactions between CN and propyne, could similarly lead to (A^-) or (A^\bullet). We found that one such pathway involving CN^- was not particularly feasible, as it passed through high energy transition states and intermediates over the course of cyclization. However, a similar reaction involving *radical chCN was not hindered in this way. All barriers were submerged beneath the energy of reactants for the radical*

By characterizing C_4H_4N in anionic, radical, and cationic states, we identified lowest-energy structures of each respective type that could be present in non-Earth environments. We have found that anionic (A^-) and cationic (F^+) isomers are global minima on their respective potential energy surfaces. Either of these species can form from reactions between smaller molecules that are readily available in some interstellar environments such as dense molecular clouds. Our work indicates that these ionic isomers of C_4H_4N may be synthesized in Titan's atmosphere and contribute to the molecular mass data collected by the Cassini INMS. Given the reactivity of ionic species in this environment, molecules such as anionic (A^-) and cationic (F^+) could go on to participate in the formation of complex organics.

Additionally, we've highlighted that the formation of these molecules through reactions involving radicals can pass through submerged barriers, and are thus quite feasible in cold, energy deficient environments. Radical (A), potentially formed via the radical-neutral pathway shown in Fig. 2.12 could have similar reactivity to its precursors and is a very interesting candidate to explore when contemplating the formation mechanisms of nitrogenated PAH. Our results are a contribution towards better understanding species present and chemistry occurring in the atmosphere of Titan (and perhaps that of early Earth), dense molecular clouds, or other extraterrestrial sources. Further studies interrogating C_4H_4N and other nitrogen-containing ions are needed to continue to probe the composition and chemistry of Titan's atmosphere and beyond.

Chapter 3

Hydrogen ejection from hydrocarbons: Characterization and relevance in soot formation and interstellar chemistry

3.1 Introduction

Soot particles, composed primarily of carbon, are produced during the incomplete combustion or pyrolysis of hydrocarbons and are released into the environment from sources such as internal combustion engines, coal-powered industries, wildfires, after-harvest burning, and cook stoves common in developing countries [160, 161]. Soot particles have detrimental effects on the environment, contributing to worldwide air pollution and global warming [160, 161]. They also present a significant hazard to human health, leading to cardiopulmonary and neurological illnesses and deaths [162–165]. On the other hand, synthesized soot particles (carbon black) have a variety of useful commercial applications, particularly as a filler to modify material properties [166, 167].

Soot formation begins with the production of molecular precursors, including polycyclic aromatic hydrocarbons (PAHs). These molecular precursors, via as of yet incompletely characterized processes, [168–171] form solid nanoscale (or sometimes larger) particles. For large enough species, growth can occur via physical condensation of large PAHs held together through van der Waals-type forces, while chemical linkage through covalent bond formation is presumably required for the inception step associated with formation of the smallest particles. [172]. The structure and stoichiometry of these particles evolves as they undergo surface growth and lose hydrogen to become more carbonized. Incipient particles can form loosely-bound agglomerates [172]), which eventually evolve into mature soot particles (referred to as aggregates). The process of particle inception alone is a complex balance of kinetic and thermodynamic factors that existing chemical models cannot fully replicate [170, 171].

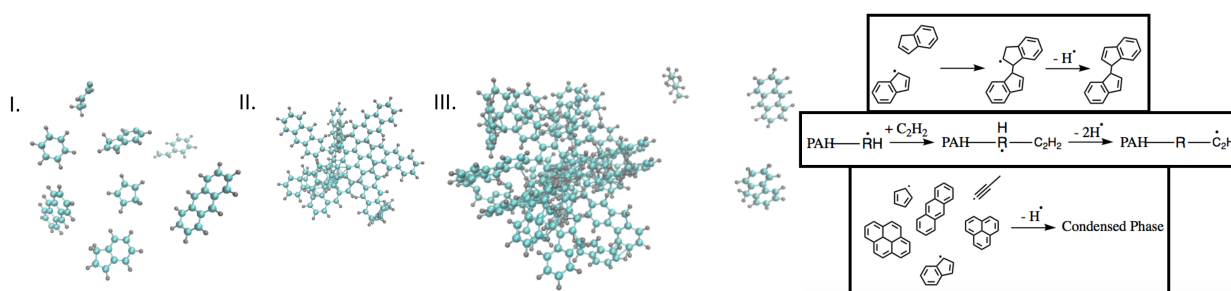


Figure 3.1: Schematic illustration of the accepted steps beginning soot formation: (I) growth of gas-phase precursors, (II) particle inception and (III) particle growth. Hot hydrogen ejection (right inset) may speed reactions in radical-based mechanisms contributing to soot inception and growth [171]. This process may also assist dimer stabilization, growth at radical centers, and soot-particle inception.

Figure 3.1 depicts these generally accepted steps to begin soot formation. The coupling between PAH growth and soot inception has been studied extensively; see e.g. Refs 170 and 173 for excellent reviews. There are numerous kinetic models for soot formation and particle inception [169, 174–177], as well as physical condensation processes and reactivity studies of PAHs [178–181]. However, despite decades of investigation, the detailed mechanisms underlying these processes, particularly at inception, are not yet fully understood. [170, 171] There are conflicting hypotheses for the events leading to (and following) particle inception (step II in Figure 3.1). Most involve chemical condensation pathways via reactive PAHs, like the recently proposed “*clustering of hydrocarbons by radical-chain reactions*” (CHRCR) [171] mechanism. The CHRCR mechanism hypothesizes that radical-chain reactions involving persistent resonance-stabilized radicals (RSRs) lead to clustering of species without depletion of the radical pool (which is continually regenerated). Open-shell PAHs serve as clustering centers at which particle inception may be initiated, which is in line with recent evidence that small to medium sized PAHs may actually contribute to particle inception [182, 183] (in contrast to previously held beliefs that only larger PAHs (e.g. pyrene, coronene, and beyond) participate in these processes). Although a collection of theoretical and experimental evidence supports this mechanism [171, 184–191], it has yet to be fully validated.

In mechanisms such as CHRCR, growth paths to larger hydrocarbons and hydrocarbon clusters require effective dehydrogenation to propagate the fast growth of molecular precursors or to generate RSRs that may be important during inception. What is the preferred method of dehydrogenation for these RSR-fuel adducts? Bimolecular abstraction by a radical, or unimolecular C-H bond fission using internal energy to eject a hydrogen atom are the two principal candidates.

Growth models such as HACA (Hydrogen Abstraction - Carbon (acetylene) Addition), widely regarded as an essential mechanism in combustion chemistry, rely on bimolecular abstraction of H atoms from precursor molecules (such as PAHs) by small radicals [171, 192,

193]. The rates of such processes are bounded by the collision frequency between the reactant and the abstracting radical. Molecular growth in CHRCR and other models involving covalent clustering requires repeated H abstractions and therefore necessitates persistently high local concentrations of abstractors. Furthermore, the reverse process of radical (often hydrogen) addition to a newly dehydrogenated species occurs at a similar rate as abstraction [193]. Experimental results have even suggested that concentrations of small radicals are inversely related to soot-volume fractions under soot formation conditions [194–196], implying that radicals such as H^\bullet may directly affect or be affected by soot growth. In hot, dense regions of the flame where radicals are readily available, abstraction is likely to be the major player; however, in regions where radicals are depleted (i.e. the post-flame region, or for hydrocarbon growth in extremely sparse environments such as the interstellar medium, other mechanisms may be needed that do not rely so heavily on two-body collisions.

The alternative dehydrogenation mechanism to abstraction is ejection (unimolecular C-H bond fission) of H atoms from hot (or excited) molecules. Such processes dissipate excess energy generated by covalent bond formation. Hydrogen loss from hydrocarbon intermediates in the combustion flame is certainly not a novel process, and has been acknowledged in many other combustion mechanisms (see e.g. Refs 197, 198, 199); however, this essential process rarely receives attention as a key propagator pulling forward molecular-weight growth, a role it may perform in mechanisms such as CHRCR [171], as attested by Johansson et al. in their seminal paper. Thermal loss of H atoms from hydrocarbons is known to lead to significant concentrations of atomic hydrogen in flames [194, 196, 200, 201]. Hydrogen elimination through bimolecular reactions and unimolecular hydrocarbon decomposition is a critical component of the pyrolytic cracking of hydrocarbon fuels and is one of the first steps in ignition [196, 202–206]. Accurate representation of hydrogen-atom sources is important in combustion models, particularly for predicting soot-precursor concentrations [192] and even for soot surface growth [207]; however, reaction inventories included in chemical kinetic combustion models are far from complete. Inclusion of vetted and validated chemical reactions is drastically reduced in models that predict abundances of larger hydrocarbons (C9 and above) and soot because of the computational cost and the sheer multitude of viable hydrocarbons that may be present in combustion environments [177, 208]. It is thus important to identify and include reactions that impact precursor and particle formation and growth, and characterize dehydrogenation processes, both for combustion and interstellar reactions. Several useful databases have already been compiled for quantities such as bond dissociation energy using large-scale techniques such as machine learning (see e.g. Ref 209). Because the generation of hydrogen atoms and chemical activation of stable species through abstraction [210, 211] are inexorably related, kinetic models for fuel combustion and soot formation must be able to accurately predict H concentrations under a wide range of conditions.

Efficient dehydrogenation is also imperative for chemical growth reactions in the interstellar medium (ISM). In fact, processes leading to PAHs in combustion environments are often the blueprint for similar processes in the ISM [212]. Carbonaceous dust in the outflows of asymptotic giant branch (AGB) stars may form through clustering of PAHs, analogous to soot particle inception [212, 213]. In cold molecular clouds [214, 215] and planetary

atmospheres (such as that of Titan [216, 217]), PAHs have been detected despite limited sources of energy, low temperatures, and low pressures. Radical-radical and radical-neutral reactions involving RSRs are often barrierless [213, 218, 219], and are likely to contribute to the formation of larger PAHs in the ISM. This hypothesis once again begs the question of how PAHs dehydrogenate to form reactive, open-shell species. Studies have shown hydrogen loss is a decomposition pathway following UV excitation in interstellar PAHs [212, 220, 221]. In the absence of sufficient abstractors to perform dehydrogenation in the ISM, other processes must be at play to promote radical formation, and should be further studied to understand the reaction pathways that lead to interstellar PAHs, and their subsequent chemical evolution.

In this work, we revisit H ejection in the context of formation and conversion of hydrocarbons large enough to serve as clustering centers for soot-particle inception or reactions of interstellar RSRs. We report H ejection rates for selected open and closed-shell hydrocarbon species and analyze how this process compares to H abstraction over a range of temperatures. Specifically, we focus on H ejection in the context of CHRCR pathways involving RSRs associated with (but not limited to) this mechanism, and identify and tabulate trends in C–H bond strength and ejection rates based on hydrocarbon structure, which may be useful for kinetic models. To complete the picture, we examine the role of H ejection in a prototypical CHRCR reaction sequence modeling the formation of the RSR indenyl, and discuss the competition of various decomposition pathways. Finally, we explore microcanonical and canonical H ejection rate regimes that may be expected for various sizes of hydrocarbons.

3.2 Methods

All electronic structure calculations were performed in the methodological framework of Kohn-Sham density functional theory (DFT) using the Q-Chem 5 software package [122]. Geometry optimizations and harmonic vibrational frequencies were obtained using the ω B97X-V functional [27], a range-separated functional that is the most accurate of its class for main group chemistry [222], and the def2-SVPD basis set [223]. Single point energies at the optimized geometries were subsequently computed with ω B97X-V and the larger def2-TZVPD basis set. To validate the good accuracy of our DFT methods, single point energies (and corresponding H ejection rates) were calculated for species (**V**) using composite method G4(MP2) [224]. We found our numerics to be in good agreement, please see the SI for comparative values. Local exchange-correlation integrals were evaluated on an ultrafine integration grid consisting of 99 radial points and 590 angular points. Nuclear contributions to the free energy were estimated using a modified quasi rigid-rotor harmonic-oscillator model (RRHO)[225] with a cutoff of 100 cm^{-1} . All energies are zero-point corrected using unmodified, harmonic vibrational frequencies. To determine the transition state for concerted H_2 loss from **V**, the freezing string method [226] was employed to obtain initial structures, followed by optimization of the resulting saddle point using the partitioned-rational function optimization eigenvector following method [227] and verification via a frequency calculation.

Thermal rate constants for H ejection were computed using variational transition state theory with RRKM theory [228] (at constant T for canonical rates, and constant E for microcanonical ones) for unimolecular reactions in the 500-2000K temperature range. Vibrational and rotational partition functions were computed within the harmonic oscillator and rigid rotor approximations. We note that use of anharmonic frequencies was found to have negligible impact for H ejection from propyne, indicating that the harmonic oscillator approximation was adequate.

The total energy available to the system for microcanonical rate calculations was estimated via Monte-Carlo sampling over the Boltzmann distribution for the translational and vibrational degrees of freedom for the reactants at the chosen initial temperature. Through this, we obtain a distribution $p(E)$ where E is the total energy of the system. A rate constant $k(E)$ could be computed for each E via RRKM theory. The relevant numbers and densities of state were computed with the Bayer-Swinehart direct count method [229]. Unaltered harmonic frequencies were used without recourse to the quasi RRHO model. Afterwards, the average rate could simply be computed as $k = \int k(E)p(E)dE$.

Structures and RRKM rates are available for each relevant molecule in the Supplementary Information (Appendix B). Rate constants computed with MESMER [230] for hydrogen ejection from species V are also available in Appendix B.

3.3 Results and Discussion

Variations in C-H bond strengths

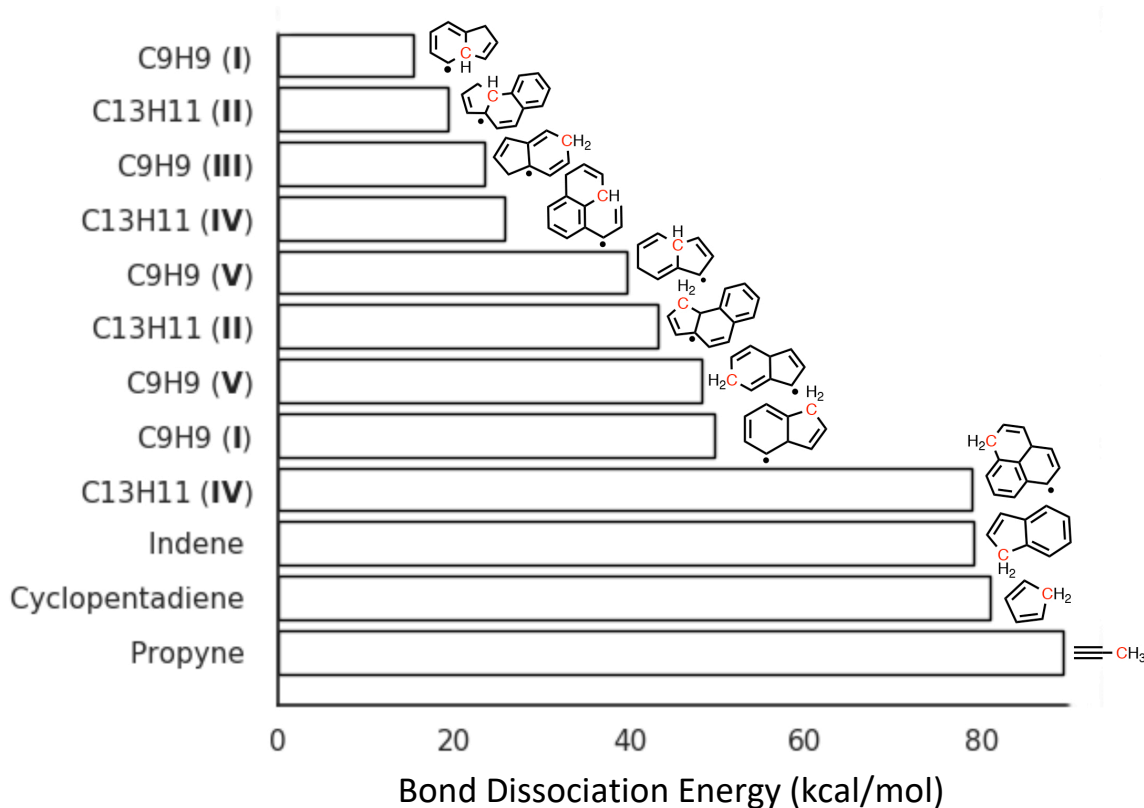


Figure 3.2: Bond dissociation energies for selected open and closed shell parent hydrocarbon species - isomers are indicated by a roman numeral. Ejection is examined from free edge (FE) and zig-zag (ZZ) sites, indicated in red. Breaking C–H bonds to eject H from closed shell species is quite energetically costly, but barriers are markedly smaller for open-shell species, diminishing to between 25 and 50% of a saturated C–H bond energy for species I–V. All energies are corrected for zero-point energy (ZPE).

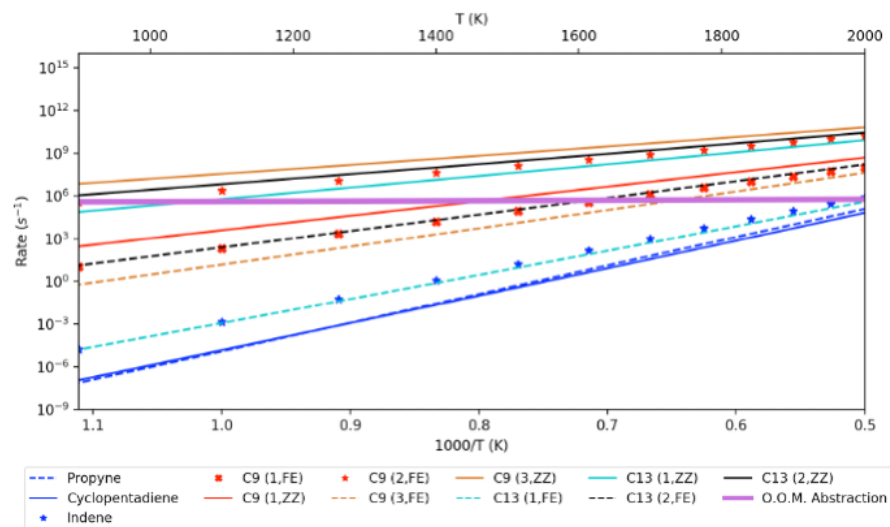
The stability and unreactivity of the C–H bond is the *raison d'être* for the entire field of C–H activation.[231] While C–H bond strength is viewed as a characteristic of the associated bonding environment, values are typically quoted in the range between 85 kcal/mol and 115 kcal/mol for closed shell molecules.[232] The strongest C–H bond is 133 kcal/mol for acetylene [233, 234]. By contrast, radicals sometimes have far lower C–H bond energies, as exemplified by the ethyl radical, at 36 kcal/mol [235, 236]. What are the implications for formation and processing of RSR species? Figure 3.2 displays the energetic cost of homolytic C–H bond cleavage for a number of conjugated hydrocarbons, showing a tremendous range

of bond energies. Notably, a few of these conjugated radicals have C–H bond strengths well below 30 kcal/mol. Several of these molecules (such as indene and cyclopentadiene) are prominent species involved in combustion reactions [237–239]. Others are documented or postulated intermediates or precursors leading to molecules commonly generated during pyrolysis, and may give rise to open-shell species important for inception and growth pathways driven by reactions of RSRs. C₁₃H₁₁ isomers **IV** and **II** are precursors to their respective C₁₃H₁₀ counterparts 1H-phenalene [240] and cyclopentanaphthalene [241], which have been detected in high yields during pyrolysis experiments [242]. Phenalenyl (C₁₃H₉), an RSR indicated to be important for soot inception [171], follows from decomposition of 1-H phenalene [240, 243]. C₉H₉ isomers such as **I**, **III**, and **V** form as intermediates on the path to indene [171, 244, 245].

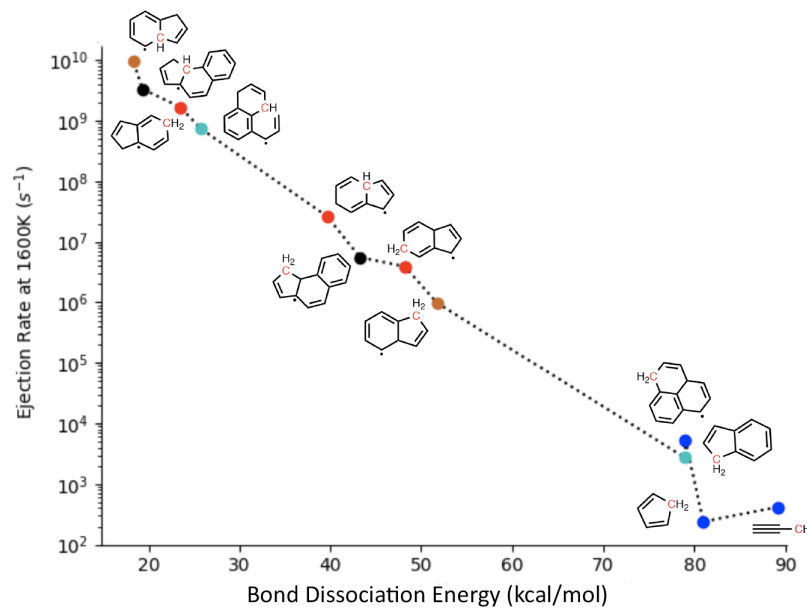
The relative stability of R–H and R + H determine C–H bond strength via R–H → R• + H• to create a radical product R• or R–H → R + H• to yield a closed shell product R. Well-known factors such as the degree of substitution at the product radical site modulate the characteristic C–H bond strengths. The formation of a C=C bond upon fission of the weakest C–H bond in •C₂H₅ largely determines its very low bond strength. Aromaticity in the closed shell product is the key driving force behind the weakest C–H bond strengths shown in Figure 3.2, consistent with the bond energy of 22 kcal/mol for •C₆H₇ → C₆H₆ + H.[246] Apart from such effects, increasing the size of the hydrocarbon (or adding rings to a PAH) generally has little effect on C–H bond strength [247, 248]. For open-shell systems and reactive intermediates, where H ejection can lead to formation of (relatively) stable, closed-shell products, greater delocalization of electron density lessens (sometimes dramatically) the cost of C–H bond cleavage (Figure 3.2); in fact, within structural groups (ie C₉H₉ or C₁₃H₁₁), trends in decreasing C-H bond strength emerge based on the location of the bond and the aromaticity of the local environment. The hydrocarbons presented above can be roughly classified into three categories: small fuel molecules, larger radicals attributed to CHRCR processes, and closed-shell precursors to PAHs. The rate of unimolecular H ejection is strongly dependent on the strength of the C–H bonds being broken.

Hydrogen ejection rates

H ejection rates (computed using variational transition state theory (VTST[249])) for various species are presented here. The nature of the product influences the relationship between C–H bond strength and ejection rates. Figure 3.3b directly compares bond dissociation energies related to ejection with ejection rates at 1600K; for the most part, larger values lead to slower rates.



(a) Canonical rates ($k_{\infty}(T)$) of hydrogen ejection for open and closed shell hydrocarbon species as a function of temperature, showing cross-over with an order of magnitude (OOM) abstraction rate estimate. The abstraction rate is almost certainly an overestimate, and real abstraction rates will vary with temperature.



(b) Rates of hydrogen ejection plotted on a logarithmic scale against the free energy barrier to ejection.

Figure 3.3: Ejection rates as a function of temperature and bond dissociation energy. Ejection occurs rapidly from ZZ sites of **I-V**, but more slowly from FE sites. For the most part, rates scale with C–H bond energies; C–H bonds in multi-ring radicals break more easily than those in small closed-shell species.

C-H bond energies for many closed-shell hydrocarbons (such as cyclopentadiene [199, 250–253] and indene [254–258]) have been previously reported; these bonds are strong and generally hard to break with thermal energy alone. Our computed BDE for cyclopentadiene is in good agreement with previous literature [252, 253], adding confidence to the relative accuracy of the bond strengths reported here. Propyne and cyclopentadiene must both overcome high energetic barriers exceeding 80 kcal/mol to break a C–H bond (Figure 3.2), making H ejection from small closed-shell hydrocarbons difficult and slow even at elevated flame temperatures. Temperatures as high as 2000 K are necessary to attain millisecond scale ejection rates (Figure 3.3a), despite the formation of RSRs like propargyl and cyclopentadienyl. Larger closed-shell species such as indene exhibit only slight increases in ejection rates compared to their smaller relatives. Figure 3.3a shows that indene (C_9H_8) loses H to form indenyl only an order of magnitude faster than cyclopentadiene. Though hot spots in combustion flames may initiate H ejection from such species, the high energetic cost of breaking this C–H bond through thermal energy alone makes such a process less likely than abstraction in most flame regions.

Certain circumstances and environments may influence the efficacy of hydrogen loss from these species. In the interstellar context, photon absorption may incur hydrogen loss [259]. Particularly, electronic excitation of molecules can promote reactivity and decrease C-H bond strength in some hydrocarbons as singly excited states essentially act as diradicals [181]. We have found that triplet cyclopentadiene loses hydrogen easily; the free energy barrier for this process has a magnitude of around 26 kcal/mol at 1600K, over 60% less than the cost of H loss for ground state cyclopentadiene. A similar calculation on toluene produced analogous results. This is certainly useful information when considering hydrogen loss processes in the interstellar medium and in situations where molecules may have diradical character. However, in the combustion context, the likelihood of forming such an excited state is debatable.

In contrast to the smaller, closed-shell molecules, open-shell species have much faster H ejection rates due to formation of extensively conjugated (typically aromatic) products. The cases considered in Fig. 3.2 have much weaker C–H bond strengths ranging from 20–56 kcal/mol, corresponding to the much faster H ejection rates depicted in Figure 3.3a.

Hydrogen ejection rates for open-shell C_9H_9 isomers (precursors to indene) are calculated to be very competitive with abstraction even at relatively low flame temperatures, losing a hydrogen atom several orders of magnitude faster than indene despite similar size and composition. As temperature approaches 1600K, hydrogen ejection from the ZZ site of **V** (studied in Ref. 171 as an intermediate in the CHRCR mechanism) occurs on the microsecond timescale, several orders of magnitude faster than abstraction. Other isomers of C_9H_9 eject even faster. **III** (accessible via a single H migration from **V**) ejects hydrogen at a microsecond rate at 1200K and **I** (an intermediate in the reaction of benzyl and C_2H_2 [244, 245]) loses H even more rapidly with an extremely low free energy barrier to ejection from the ZZ site (Figure 3.3b).

As demonstrated for **I** and **V**, there is considerable site sensitivity to ejection rates, which are influenced by sterics and (de)aromatization. Loss of ZZ hydrogen from $C_{13}H_{11}$ isomers

occurs readily on the order of microseconds at relatively low temperatures (1000 to 1200K), as a result of aromatizing rings. Ejection from **IV** leaves two of the three benzene rings aromatic, with multiple resonance structures available. Similarly, the very rapid ejection from **II** aromatizes two six-membered rings and one five-membered ring. By contrast, ejection from free-edge (FE) sites on each of these molecules leads to less extensive conjugation and is hence markedly slower, as shown in Figure 3.3b.

Abstraction of hydrogen atoms by free radicals is the main competitive process to hydrogen ejection. Assuming a free H^\bullet radical concentration [200] of 10^{15} cm^{-3} and a reaction cross section radius of 2.5 \AA (roughly twice normal C–H bond lengths), abstraction occurs at a rate of $\sim 2 \times 10^6 \text{ s}^{-1}$ at 2000 K. The abstraction rate shown in Figure 3.3a is demonstrative of this - note that this is an order of magnitude approximation based on peak H^\bullet concentration, and is an upper limit assuming that all collisions lead to successful abstraction, if not a generous overestimate. Actual abstraction rates will vary with temperature, hydrocarbon concentrations, and variations in H^\bullet partial pressure [260–264]. It is clear from Figure 3.3a that at typical flame temperatures, H abstraction by free radicals is much more likely for stable hydrocarbons than H ejection. On the other hand, at temperatures above 1600K, ejection rates for most reactive intermediates are easily greater than hydrogen abstraction. Dehydrogenation via abstraction is an appealing route due to extremely low free energy barriers ($< 20 \text{ kcal/mol}$), which makes for extremely fast rates of hydrogen loss; however, there are clearly many factors that decrease the effectiveness of these processes. Abstraction events require collision of the abstractor and target molecule, where the collision frequency is linearly dependent on radical concentration but has only a \sqrt{T} dependence on temperature. A high enough abstractor concentration is necessary to produce an abstraction-dominated environment, as radicals are generally quite reactive, and a very high concentration would lead to pairwise radical annihilation - while the primary reaction zones of combustion systems generally have a persistently high free-radical equilibrium, this is not achievable for all relevant environments in which hydrocarbon growth may occur. Some environments, such as the post-flame zone in combustion and the interstellar medium, simply cannot maintain high enough small-radical concentrations to promote an abstraction-dominated environment, indicating that other processes such as H ejection may be quite important for propagating reactions.

To this point, we have demonstrated that canonical hydrogen ejection rates from open-shell hydrocarbons occurs rapidly at a range of temperatures relevant for combustion, and that these rates are much faster than competing dehydrogenation processes such as abstraction. While ZZ ejection is already fast from isomers **I** - **V** at thermal equilibrium (Figure 3.3a), it is likely to be faster still under combustion conditions.

Hydrogen ejection and the first steps of CHRCR

A large focus of this paper is to explore hydrogen ejection as a viable sub-mechanism of the CHRCR pathway that pulls forward molecular-weight growth, regenerates radical species, and produces new local abstractors. To put our findings into better context, we have explored

an early reaction sequence of the CHRCR pathway involving C_9H_9 isomers included in our study.

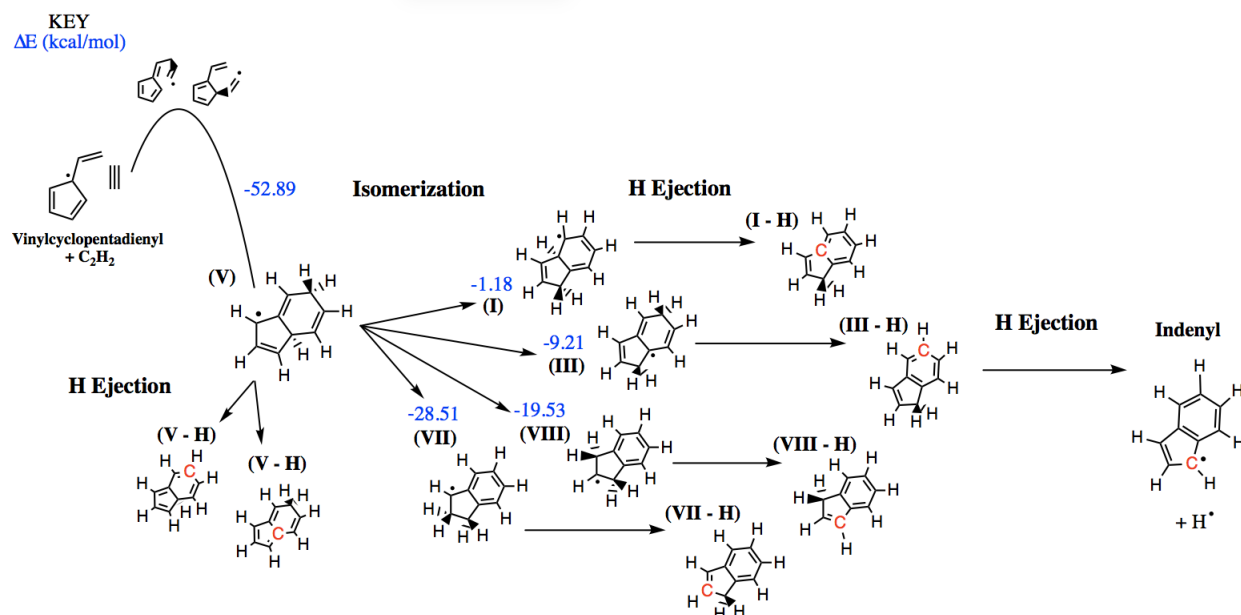


Figure 3.4: Schematic illustration of the CHRCR-inspired pathway from RSR vinylcyclopentadienyl to indenyl. **V** is initially formed via ring-closure, and various decomposition pathways are available, including immediate hydrogen ejection and fast isomerization to stable isomers. From nearly all C_9H_9 isomers explored here, ejection as a primary route of hydrogen loss is rapid - for indene, spontaneous ejection is slower, and abstraction may be the preferred route in high-pressure scenarios.

Figure 3.4 depicts an example cyclization reaction between acetylene and vinylcyclopentadienyl producing **V** and various reaction steps involving H ejection. Vinylcyclopentadienyl was identified as an important RSR in the experiments of Johansson et al. [171] that may play an important role in the CHRCR pathway and others. The initial product of cyclization is C_9H_9 isomer **V**, for which several decomposition pathways are available. The most plausible scenarios for **V** are: 1) dehydrogenate via collision with an abstractor, 2) fall apart into smaller hydrocarbons, 3) eject hydrogen to form a closed-shell species, or 4) isomerize via H migration to a lower energy C_9H_9 isomer.

The first point has been discussed previously; collisions of **V** with small abstractors such as H^{\bullet} occur on the order of $10^6 s^{-1}$, which is dependent on the density of abstractors and scales only as \sqrt{T} with temperature. H ejection on the other hand becomes exponentially faster with increasing temperature, and under combustion conditions is a more rapid dehydrogenation route for many molecules (including **V**). The second scenario, falling apart into

Table 3.1: Hydrogen ejection rates, both canonical and microcanonical, for C_9H_9 species illustrated in Figure 4. Canonical rates are computed at 1600K; Microcanonical rates assume reactants at a temperature of 1600K. Rate units are in s^{-1} unless otherwise indicated.

Species	Canonical ejection rate	Microcanonical ejection rate
V (ZZ site)	2.64E07	1.29E09
I	9.67E09	1.34E11
III	1.68E09	3.08E10
VIII	1.09E08	1.38E10
VII	8.59E06	2.41E09

smaller hydrocarbon species, is unlikely. The newly formed C–C bonds of **V** during ring closure are fairly strong, and breaking these immediately into smaller fragments is thermodynamically unfavorable. This leaves ejection and isomerization as plausible decomposition routes for **V**.

The canonical ejection rate from the ZZ site of **V** occurs on the order of $10^7 s^{-1}$ at 1600K. This rate is fast, but the actual rate of H ejection is likely faster. To determine the behavior of **V** in the reaction context, we have computed microcanonical rates to account for the effects of internal energy gained via C–C bond formation (~ 52 kcal/mol from ring closure), as well as the contribution from the thermal vibrational energy of each reactant (~ 70 kcal/mol, assuming a local temperature of 1600K). Accounting for this excess energy, the ZZ site rate of ejection from **V** increases to $1.33 \times 10^9 s^{-1}$, a few orders of magnitude greater than the canonical rate.

Given the great amount of internal energy **V** has accumulated after ring closure, rapid isomerization to a more stable isomer is also a viable (and likely) result. As depicted in Figure 3.4, several lower-lying C_9H_9 isomers are available (**I**, **III**, **VII**, and **VIII**). Canonical hydrogen ejection rate constants are already quite rapid for some of these species, and excess internal energy from the preceding reaction scheme speeds hydrogen loss to an even greater degree, as values show in Table 3.1. Internal energy provides at least an order of magnitude boost to hydrogen ejection rates for **V** and other C_9H_9 isomers. Consider a likely sequence from vinylcyclopentadienyl \rightarrow **V** \rightarrow **VII** and on. **V** is initially formed with ~ 52 kcal/mol energy, and rapidly isomerizes to the most stable isomer **VII**, which lies almost 30 kcal/mol downhill. Even after isomerization, hydrogen ejection from the isomer (in this case **VII**) occurs on the order of $10^9 s^{-1}$. These rapid microcanonical rates serve to show that even after reorganization to lower-lying isomers, hydrogen ejection from C_9H_9 is much faster than other hydrogen loss methods such as abstraction.

The rate of H ejection generalizes well to similar reaction schemes. Replacing vinylcyclopentadienyl with benzyl, which is a common candidate for assignment of m/z 91 in combustion spectra and an important combustion intermediate [244], forms the initial C_9H_9 intermediate **I**, from which H ejection may occur. Considering the C–C bond formation energy and that which is available vibrationally from each reactant, the rate of H ejection

from **I** is $3.4 \times 10^{10} \text{ s}^{-1}$. This evidence for the viability of H ejection suggests that it could be relevant for pathways involving other RSRs, not just following reactions of vinylcyclopentadienyl.

The microcanonical rate for H ejection from **V** and other C_9H_9 isomers is rapid, and few factors will be influential enough to significantly slow these processes. Dissipation of energy through collisions with inert gas molecules, or through a natural dispersal of energy through vibrational modes may inhibit the efficiency of hydrogen ejection, but even these should not change the rate to a huge degree. Considering a generous cross sectional impact area for C_9H_9 with a diameter of several C–H bonds, collisions with an inert gas such as N_2 occur on the order of 10^9 s^{-1} at 1 bar pressure. The effective temperature of **V** is calculated to decrease by less than 15 K per collision (assuming perfectly inelastic behavior); thus, it would take at least 10 collisions to have a significant decrease in energy. Therefore, we are confident that the computed microcanonical rates are a good estimate for immediate H ejection, which will take place before collisions can dissipate excess internal energy, and thus the rate.

Molecules such as C_9H_9 are small enough that the internal energy from C–C bond formation processes should remain local for long enough to fuel H ejection processes at the microcanonical rates computed above. However, such rates may not be as accurate as hydrocarbons grow in size and energy quickly equilibrates over many vibrational modes. Recent literature has addressed the differentiation between microcanonical and canonical regimes when computing vibrational energies for hydrocarbons of varying size; larger hydrocarbons have increasingly large densities of states, and after a certain threshold, choosing a threshold energy is less valid [265]. Our computed microcanonical H ejection rate for a slightly larger hydrocarbon, **IV** (see Fig 3.2 at the zig-zag site), is still fast at $9.3 \times 10^9 \text{ s}^{-1}$. As hydrocarbons approach 100 atoms or more, or internal reaction threshold energies greater than $\sim 100 \text{ kcal/mol}$ [265], canonical rate constants are a better choice.

Hydrogen ejection is without a doubt a rapid process that is very likely to occur along the CHRCR reaction pathways. However, the efficacy of the second hydrogen ejection (as shown in Figure 3.4, where closed-shell species (now indene) lose a hydrogen to become indenyl) is less certain. In Figures 3.3a and 3.2, we demonstrated that H ejection for closed-shell species is slow due to higher C–H bond strengths. Indene, for example, has a bond dissociation energy of nearly 80 kcal/mol. Even with significant thermal energy from the flame, hydrogen ejection is unlikely to be quite as competitive with abstraction compared to the C_9H_9 species. In areas where abstractor concentrations are high, collision with an abstractor seems more likely than spontaneous hydrogen ejection for a closed-shell species. Hydrogen ejection may of course still occur from indene (albeit not as quickly as for C_9H_9), and this may be important in low-pressure regions to propagate reaction sequences leading to the next radical clustering center. In this way, ejection and abstraction processes are likely to both be at play in the CHRCR mechanism, depending on the conditions in which the reaction sequence is taking place. Abstraction itself may be initiated and sped up by ejection events in a pseudo-unimolecular manner, as we'll explore in the next section.

Sequential H ejection and processes of larger PAHs

Hydrogen ejection from open-shell species results in a closed-shell molecule, which needs to lose another H atom to re-form a radical. This is a significant factor in the ability of CHRCR mechanisms to propagate reactions, which at their culmination produce PAH radicals postulated by the CHRCR mechanism and others to participate in inception events [171], which ultimately contribute to soot formation. While to this point we have focused on a single H ejection event, we now ask another question: can sequential ejections from a single molecule drive molecular growth? In environments where small radical abstractors are scarce, such processes may be vital for continuation of the chain reaction.

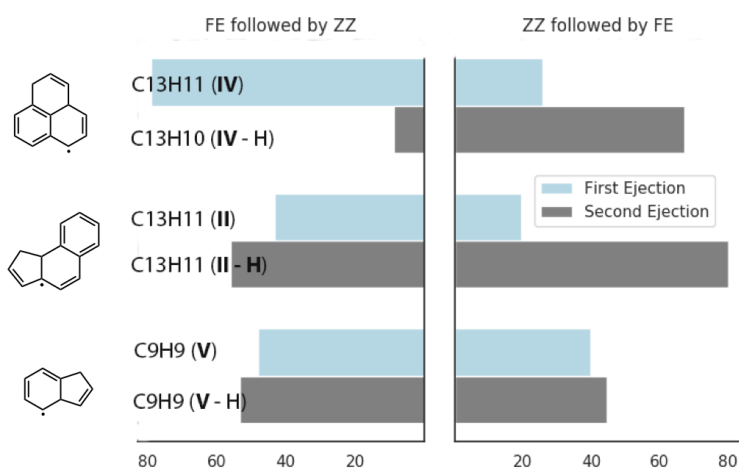


Figure 3.5: Free energy barriers for sequential H ejection from isomers **II**, **IV**, and **V**. Significantly lower barriers to initial ejection from ZZ sites make this the preferred pathway, and the second ejection is typically more costly.

Sequential hydrogen loss from either $C_{13}H_{11}$ or C_9H_9 isomers results in a new RSR (via a closed-shell intermediate) and two H atoms. Figure 3.5 demonstrates the differences in bond dissociation energies between the first and second H ejections from isomers **II**, **IV**, and **V**. As seen previously, initial ZZ ejections are easier than those from FE sites, indicating that this will be the preferred ejection pathway. In almost all cases, ejection of a second hydrogen atom (from closed-shell $C_{13}H_{10}$ and C_9H_8 isomers) is more costly than the first ejection. These larger closed-shell hydrocarbons have C–H bond strengths similar to small species such as propyne and cyclopentadiene (Figure 3.2).

These effects are due to the molecular environment - initial H ejections that lead to stable aromatic rings are low barrier, and thus occur quickly, as depicted in Figure 3.5. This stability-driven site preference leads to the high energetic cost for the second ejection. For example, initial ejection from the ZZ site of **IV** is fast, with a free energy barrier of only about ~ 25 kcal/mol, resulting in closed-shell $C_{13}H_{10}$ (**IV - H**) and leading to two aromatic rings.

The second ejection to form $C_{13}H_9$ is over twice as costly - while this open-shell product benefits from many resonance structures, hydrogen loss does not stabilize this molecule relative to the parent, as aromatization of all three six-membered rings is not feasible. This logic may be extended to sequential ejection from **II**, and explains why initial FE ejections are so difficult. Interestingly, **V** has similar barriers to first and second ejections, with the latter being only slightly more costly regardless of initial ejection site. This may result from competition between the favorable aromatization of the six-membered ring and loss of some closed-shell stability.

Sequential H ejection thus appears difficult as a stand-alone process in many cases from an energetic standpoint, particularly for high-temperature and pressure combustion events. Large bond dissociation energies in the closed-shell species lead to slower rates of H ejection. In instances where abstractor concentrations are adequately high, reaction propagation in the CHRCR context will likely require an abstraction event to lose the second hydrogen atom.

In some cases, multiple dehydrogenations via H ejection may be more viable. One scenario where sequential H ejections may be a more useful pathway is in the post-flame region of combustion flames. Soot nucleation continues into this region, despite low abstractor abundances, requiring pathways that proceed without the need for abstraction [170]. Despite the slow speed of the second ejection, it may still occur faster than abstraction in this case, since abstraction processes depend directly on the concentrations of small radicals, which influences the likelihood of collision. Another similar scenario is in the interstellar medium, where collisions will be even rarer for most systems. And finally, the success of the first ejection may promote an abstraction on the same molecule - the first ejection creates a $H\cdot$ radical in close proximity to the parent molecule that may abstract a second hydrogen atom. This would effectively result in H_2 loss without any change in the overall radical concentration. Concerted H_2 loss via a single transition state is possible from species such as **V**, with free energy barriers slightly larger than those for cleaving the weakest C–H bond (see SI for transition state structure). It is important to note here that given the slow rate of the second H ejection (if it occurs), this overall process will not enhance the modelled rate of soot formation in most reactive zones of the combustion flame.

3.4 Conclusions

The data presented in this paper highlights several important concepts. We have tabulated C–H bond strengths for a variety of open and closed-shell hydrocarbons, and found a striking range of values that depend highly on the species and the structural characteristics. We have observed that C–H bond strengths for normal valent, closed-shell molecules have high bond dissociation energies which typically fall into the expected range. In sharp contrast, open-shell species (even with similar structural characteristics) have much smaller bond dissociation energies, down to as low as 20-30 kcal/mol in some cases.

This range of C–H bond strengths directly effects hydrogen ejection rates - our results

show that the significance of hydrogen ejection depends strongly on the nature of the hydrocarbon molecule, as well as other factors such as the temperature and concentrations of hydrogen abstractors. These data indicate that H ejection is energetically costly and rather slow for most closed-shell species, but open-shell molecules, particularly those thought to be intermediates in CHRCR growth pathways, can eject hydrogen atoms rapidly in a site-specific manner, with rates of H loss from zig-zag sites outstripping those from free edge sites. The high ejection rates from sp^3 sites in multi-ring radical species are particularly noteworthy, as PAHs are widely thought to be key precursors to incipient soot particles [170, 175, 266–270]. Rates of H ejection and the associated C–H bond strengths are heavily influenced by general factors such as the gain (or loss) of aromaticity in molecular rings, suggesting that families of similarly structured hydrocarbons should exhibit predictable trends in ejection rates [181].

Our results indicate that small bond dissociation energies in PAH radicals contribute to fast hydrogen ejection rates - this process can occur rapidly at combustion temperatures and potentially help propagate reaction pathways. Since hydrogen loss from closed-shell species for a given reaction sequence is comparatively slow, we theorize that hydrogen ejection and hydrogen abstraction are both critical processes acting to propagate the CHRCR pathway.

Hydrogen ejection may be a key process in radical-driven mechanisms acting in several stages of these soot growth pathways. Prior to inception, loss of H atoms by ejection from thermally excited or post-cyclization precursors and intermediates allows for rapid growth of PAHs and RSRs, which in turn encourages fast intermolecular reaction rates and speeds radical chain reactions. Characterization of a CHRCR reaction sequence in this work modeled the relevance of dehydrogenation of intermediate via ejection. During the inception event, stabilization of dimers and larger structures (such as the clusters at radical growth centers proposed by CHRCR) following covalent bond formation may occur more quickly via hot hydrogen ejection [171, 271] and negate the need for collisional stabilization. H ejection may also play a role in later stages of soot formation, where new mechanisms are emerging that promote soot mass growth in the absence of high H atom concentrations (e.g. Ref. 272 and others); for example, fast hydrogen loss from the surfaces of incipient and partially aged particles creates radical sites where 3-dimensional growth occurs to eventually form the complex aggregate that is mature soot.

Rapid rates of hydrogen loss for open-shell intermediates are also relevant for PAH formation processes in the interstellar medium, either in hot or cold regions, where abstractors and energetic collisions are scarce. Under conditions where hydrogen ejection is a preferred pathway acting in radical-chain reactions, the radicals are regenerated - this may also help explain the prevalence of particle inception and growth in the secondary reaction zone of combustion flames (and perhaps in environments such as cold molecular clouds or planetary atmospheres), where radicals are depleted and activation of a hydrocarbon by H abstraction is far less likely [170].

The data presented here provide numerical evidence that hydrogen ejection is a significant piece of current radical-driven models, sometimes acting alongside hydrogen abstraction, that contributes to multiple stages of soot formation and growth, and even radical-driven

processes that act in the formation of large interstellar PAHs. Our results demonstrate the need for further investigation to systematically explore the role of hydrogen ejection in models containing radical chain reactions contributing to inception and formation of soot particles.

Chapter 4

Computational exploration of the binding motifs and binding energies of neutral molecules, radicals and ions with small water clusters

4.1 Introduction

Molecular reactions in the interstellar medium range (ISM) from relatively simple to amazingly elaborate. The existence of *any* chemistry is somewhat astounding; given the generally inhospitable nature of space, successful chemical reactions seem improbable in most interstellar environments. Temperatures are often cold (usually 10's of K in dense molecular clouds), which means that most reactions must proceed without thermal activation. In addition, low number densities of reactant molecules make collisions far less likely, thus drastically decreasing opportunities for two-body reactions to occur. Despite these adverse conditions, many types of reaction chemistry are active in the ISM that produce a diverse array of products. The presence of diatomic molecules in the ISM was confirmed as early as the 1930's [273, 274], with the detection of polyatomic molecules and complex organics following soon after in the late 1960's [275–277]. The diverse field of astrochemistry was thus born in pursuit of unravelling the details of interstellar chemical reactions.

The two main production routes to most interstellar species are gas-phase chemistry and surface reactions, and both must be accounted for when considering molecular abundances in the ISM [278–280]. While gas-phase chemistry is responsible for many interstellar reactions, grain surfaces are at least equally important, especially for production of complex organic molecules (COMs) in diverse interstellar environments. In fact, it is widely accepted that molecules as fundamental as H_2 , H_2O , CO_2 , and others have abundances that cannot be attributed to gas-phase reactions alone. For example, H_2 formation in the gas phase requires inefficient processes; radiative association of two hydrogen atoms is not a viable route, and

production of H_2 from these atomic constituents requires sequences of radiative electron attachment to hydrogen atoms ($\text{H} + \text{e}^- \rightarrow \text{H}^- + \text{h}\nu$) followed by associative detachment upon combination ($\text{H}^- + \text{H} \rightarrow \text{H}_2 + \text{e}^-$) to form H_2 [281]. These observations have led to the conclusion that surface reactions (such as those occurring on icy grains) play an important role in H_2 formation [282, 283], along with production of a manifold of other species. Synthesis of novel and increasingly complex organics can be instigated by condensation of PAH onto grain surfaces, where processing via stellar radiation can promote reactions that yield interesting products, even pre-biotic molecules such as nucleobases [284, 285].

Icy grains are prevalent in the frigid ISM, and can originate from multiple sources - a few relevant examples include cold molecular clouds, inside the snowline of the proto-planetary disks, in planetary atmospheres, and in the gaseous plumes of Enceladus. Most grains from the former sources, particularly molecular clouds, are particles of interstellar dust coated in an icy mantle. This mantle is mainly composed of H_2O , but also contains other atomic and molecular species that freeze-out onto the grains. The water freeze-out process influences the composition of the amorphous ice and thus reactions that occur there [286]. The example of Enceladus, an icy moon of Saturn, is a unique environment and an interesting site that may host complex organics and their precursors. Analysis of ejecta from vents at the surface of Enceladus has shown evidence of macromolecular material that may be produced from hydrothermal activity in the sub-surface ocean, or possibly formed on the ice grains from deposited precursors [287–289].

Grain surface chemistry is dependent on elementary processes including molecular binding, diffusion, surface reaction, dissociation, and thermal and non-thermal desorption. These processes are critically important for understanding phenomena from core collapse to planetesimal formation, and are typically included for proto-planetary disk modelling. The binding energy directly influences desorption efficiency, which in turn affects the gas-phase abundance and reaction potential after cold grain production. Unfortunately, many parameters such as these that are dependent on the binding energies (especially of radicals and ions to ice) are unavailable, and are therefore assumed from literature values of similar species. In addition to excluding accurate binding energies for many species, models often make coarse-grained assumptions about processes such as diffusion that are influenced by binding energies. While diffusion coefficients are often calculated as a fraction of the binding energy, diffusion behavior of molecules can vary greatly and should be evaluated on a case-by-case basis. While the important molecular binding energies with one or two water molecules are included in the PPD simulations, many of these values for radicals are not available, and the ions are not at all considered in the proto-planetary disk models. Inclusion of the binding energies of such species to amorphous ice analogs will result in a significant improvement in the outcome of protoplanetary disk (PPD) simulations.

Experimentally, binding energies are usually determined using techniques such as temperature programmed desorption (TPD), where target species are adsorbed to and desorbed from a particular substrate in a controlled way [290]. Although this method can provide useful data, it's highly dependent on the reactivity of the target species and the nature of the substrate among other experimental parameters. Experimental data for reactive species

(ie radicals as well as ions) are limited since these typically have fairly short lifetimes in laboratory.

Computationally, the same challenges of modeling reactive species and building a suitable grain surface remain. Periodic density functional theory (DFT), molecular dynamics and mixed QM/MM approaches have been used to describe amorphous water surface and compute molecular binding energies, which gives insight into the range of binding sites available on an ice grain [291, 292]. A growing library of existing data is available for binding energies of molecules with smaller water clusters, usually in the range of one to ten waters [293]; calculations of this size are tractable at a high level of theory [294–296]. Other authors have performed fitting procedures between computed and experimental binding energies to bootstrap their way to larger water clusters [297]. Recently, Bovolenta et al. have made Python libraries available for reliable, systemic calculation of binding energies based upon DFT and other methods [298]. Clearly the database for small molecule binding energies to water and amorphous ice is already available and growing; however, less information is available when it comes to ionic and radical species, which as mentioned above is disadvantageous for proto-planetary disk models.

In this work, we seek to remedy some of the holes in literature data by presenting the results of a computational exploration of the binding motifs (i.e. preferred mode of binding) and the associated binding energy for sets of neutral, radical, cationic, and anionic molecules relevant for reactions occurring on icy grains. These grains can be those originating from the southern Enceladean plumes, from near the midplanes of protoplanetary disks inside their snowlines, from inside dark molecular clouds in the ISM or on icy surface of meteorites. Our aim is to provide reliable binding energies of species so as to address several questions that are not yet considered adequately in the existing literature: 1) How does the binding energy and the preferred mode of binding of a molecule to water change between open and closed-shell molecules? 2) How do the binding energies and associated structures of closed-shell cations and anions compare to their neutral counterparts? 3) What electronic structure or functional group- dependent trends are apparent in the binding energies of these species to small water clusters, and how do they affect potential reactivity of the molecules in question? 4) How do the binding energies change during the water freeze-out process? Using high-level *ab initio* DFT and Coupled-Cluster methods, we have identified low-lying cluster geometries for guest molecules bound with $n=1-4$ water molecules, and compared trends in binding energies that result from changes in functional groups, ionization, and other electronic structure modifications. Our results expand the existing data for binding energies of small neutral, radical, and ionic molecules in a meaningful and systematic way, and provide insight into how the electronic structure influences binding energies and therefore reactivity of these species during the water freeze-out process.

4.2 Methods

Suites of neutral, open-shell, cationic, and anionic guest molecules were chosen with consideration to 1. Species that have been detected in cold molecular clouds or planetary atmospheres, 2. Species that are postulated to be present in such environments, and 3. Species that have been indicated as important for astrochemical modeling that display a good range of functional groups, and thus varied chemical properties. Binding energies were computed for a total of 25 distinct species with water clusters of $n=1-4$ water(s).

Water cluster structures have been well described in the existing literature [299–302]. In order to sample conformers associated with multiple binding sites on a given water cluster in an effective way, we utilized automated conformer generation with CREST [52]. CREST is supported by Grimme’s GFN2-xTB tight-binding software [303], and provides a rapid avenue for conformer generation. For neutral and open-shell guest molecules with $n=1-4$ water(s), 50-100 conformer geometries were computed with CREST, and the 10 with lowest energy were selected for further analysis and optimization. For open-shell and ionic guest molecules, CREST was not used due to observed poor results for these types; instead, conformer starting structures were generated using a chemically intuitive starting point or inspired by literature structures if these were available.

Unique conformers established during pre-screening for each molecule were selected for geometry optimization using DFT at the ω B97X-V/def2-svpd level [27]. Vibrational frequency calculations were performed at the same level of theory to ensure that minima were successfully found. Single point energies for the conformers that were found to be the energetic minima for a given guest molecule-water complex were refined with the same functional in the larger def2-qzvppd basis set to reduce basis set incompleteness error (BSIE) as well as to mitigate basis set superposition error (BSSE)[18]. All calculations were performed using the Q-Chem 6 software package [122]. ZPVE corrections were included at the ω B97X-V/def2-svpd level. Binding energies were calculated using the following scheme:

$$\Delta E_{\text{bind}} = E_{\text{complex}} - E_{\text{guest}} - E_{\text{water}}$$

Here, E_{complex} is the energy of the bound guest/water complex, E_{molecule} the energy of the guest molecule, and E_{water} the energy of the water cluster minima for a given number of water molecules.

To achieve a potentially higher level of computational accuracy, optimized geometries at the ω B97X-V/def2-svpd level were also used to calculate single-point energies using the CCSD(T)/aug-cc-pVTZ method. All the coupled cluster energies were evaluated using the MOLPRO quantum chemistry package [304], and include F12 corrections [305, 306] to improve basis set convergence and mitigate BSSE. DFT calculated zero-point vibrational energies were used for the ZPVE corrections of the CCSD(T) energies. We shall subsequently see that there is good agreement between the DFT and coupled-cluster binding energies, which serves to validate both protocols.

4.3 Results and Discussion

In the following sections the binding energies of the closed shell neutral molecules, neutral radicals, cations and anions with one to four water molecules are presented. A discussion of the trends and their implications for various astrophysical environments are presented after that. For each molecule, radical, or ions, many low-lying conformers or isomers were identified with (size $n=1-4$) water clusters. Only the lowest-lying cluster is presented here for comparison. All the other structures and their relative energies are presented in the Supplementary Information (Appendix C).

Neutrals

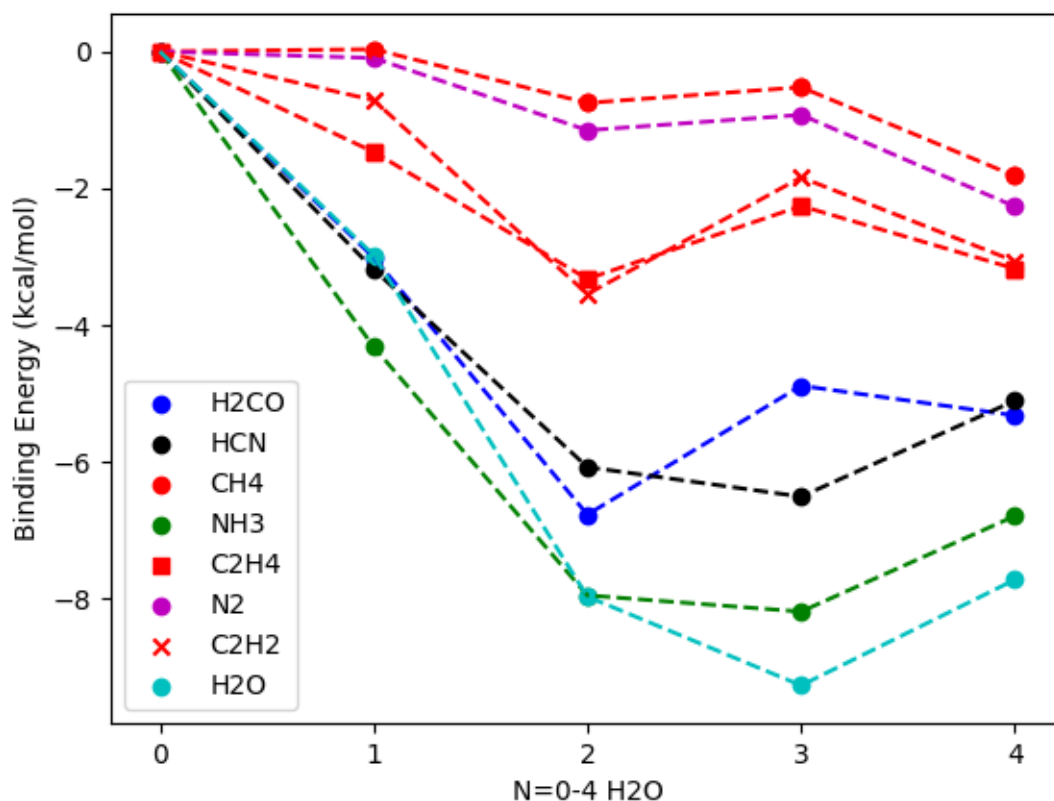


Figure 4.1: Zero point corrected DFT binding energies calculated for a set of closed-shell neutral molecules. As expected, non-polar molecules such as hydrocarbons exhibit weaker binding to water clusters, while molecules with a stronger dipole such as NH₃ and H₂CO have binding energies that are nearly on par with water-water interactions.

Figure 4.1 shows trends in binding energies between neutral molecules and water clusters of up to four water molecules. As seen from this figure, the binding energy of the guest to the cluster generally increases as the water cluster grows. With a large enough number of molecules, water interacts most strongly with itself, forming well documented structures from the monomer to the pentamer [300, 301]. The most powerful binding forces are hydrogen bonds optimized for the maximum amount of $\text{H}_2\text{O} \cdots \text{H}-\text{OH}$ interaction, leading to tightly bound structures and a peripherally attached guest molecule.

Hydrocarbons are the least tightly bound group, here modelled by CH_4 , C_2H_2 , and C_2H_4 . CH_4 , without any π -system, barely interacts with the water at all, leading to only weakly bound complexes for all water cluster sizes. In these cases, the water complex is bound in its lowest-energy (non-interacting with CH_4) configuration, adjacent to the guest molecule. Notably, despite being linear hydrocarbons without means for strong hydrogen bonding networks, C_2H_2 and C_2H_4 do bind more strongly than their cousin CH_4 . For the $n=3$ and $n=4$ water cases, the water mostly interacts with itself, forming only weak interactions between water's oxygen and H-C bonds in the hydrocarbon. Interactions are most obvious in the $N=2$ water case, where there is some attraction between the hydrogen atoms of the water and the double or triple C-C bonds of each hydrocarbon, i.e. interaction with the π system ($\pi \cdots \text{H}-\text{OH}$). A similarly weak binding is seen for N_2 ; while the nitrogen can interact with the O-H of water, the molecule has no dipole moment, and thus interactions are weak with individual water molecules.

Polar molecules H_2CO , HCN , and NH_3 are more tightly bound to the water clusters. H_2CO and HCN have two sites that can interact via hydrogen bonding with water, with electron deficient H atoms at one end and electron rich O and N atoms respectively at the other. For HCN , the $\text{NCH} \cdots \text{OH}_2$ interaction is dominant, as has been documented in previous literature [307–309].

Notably, the curves for NH_3 and H_2O are quite similar in shape and magnitude. The chemical structure and potential for hydrogen bonding of NH_3 is somewhat akin to that of H_2O , with an electron rich nitrogen atom in place of oxygen; as evidenced by the cluster structures with $n=1-3$ waters, the structural formations of NH_3 and water clusters are analogous to water with itself, leading to similar general trends in binding energies and maximizing hydrogen bonding. In previous literature, the global minimum of NH_3 with four waters was found to be a cyclic structure; while we have included this conformer and a number of other documented low-lying isomers in our analysis [310, 311], we have identified an alternative lower energy structure where NH_3 interacts with the water cluster through hydrogen bonding without forming a pentamer-like complex. The minimum used here, with NH_3 bonded to the water tetramer by a $\text{HO}-\text{H} \cdots \text{NH}_3$ hydrogen bond but not incorporated into the cluster, is also used by Das et al [293]. The latter is more representative of a guest molecule approaching an existing water cluster structure, while the hydrogen-bonded pentamer (analogous to the 5-water cluster) is more indicative of a structure where the guest molecule has integrated fully into the cluster, or where waters are added sequentially and relaxed.

Table 4.1: Comparison of (zero-point corrected) ω B97X-V/def2-qzvppd and CCSD(T)/aug-cc-pVTZ binding energy values for select structures, reported in kcal/mol. General agreement is observed between the methods, and trends are preserved.

Molecule	Monomer		Dimer		Trimer	
	DFT	CCSD(T)	DFT	CCSD(T)	DFT	CCSD(T)
H ₂ CO	-3.009	-3.141	-6.768	-6.947	-4.884	-4.838
HCN	-3.184	-3.241	-6.074	-5.992	-6.505	–
CH ₄	-0.032	-0.111	-0.752	-0.981	-0.522	-0.752
NH ₃	-4.315	-4.364	-7.948	-8.098	-8.185	–
C ₂ H ₄	-1.468	-1.453	-3.323	–	-2.258	-2.568
N ₂	-0.095	-0.440	-1.152	-1.549	-0.926	-1.243
C ₂ H ₂	-0.711	-0.886	-3.545	–	-1.840	-2.045
H ₂ O	-2.974	-3.198	-7.966	-8.248	-9.264	–

Table 4.1 compares the binding energies calculated with DFT to those acquired with CCSD(T). In general, the agreement between the two is very good. For the guest molecule bound to a single water molecule, discrepancies between DFT and CCSD(T) are less than 0.4 kcal/mol for all guest molecules tested here, with N₂ binding showing the largest deviations. As the water cluster size increases, errors in DFT compared to CCSD(T) scarcely change. Indeed, given that BSIE is smaller for the DFT calculations than the CCSD(T) calculations, while correlation errors are smaller for CCSD(T) than for ω B97X-V, it is unclear which should be considered more accurate. The generally very good agreement can be considered as a cross-validation of both sets of results.

Radicals

Somewhat surprisingly, many open-shell neutral species (Figure 4.2) have binding energies very similar to their closed-shell counterparts; despite their reputation as highly reactive, none of the radicals studied here spontaneously reacted with members of the water cluster. Of course there are other minima that are separated by barriers from the structures characterized here: for instance the H₂O \cdots H $\dot{\text{C}}$ cluster has another local minimum corresponding to HO $\dot{\text{C}}\cdots$ H₂ but we did not consider these highly activated rearrangements.

In agreement with previous literature, H $\dot{\text{C}}$ is the weakest binder and interacts remotely with the water cluster for all structures via dispersion forces; even at cluster sizes of four waters, H $\dot{\text{C}}$ binds at a magnitude of only \sim 1 kcal/mol. Structures of H $\dot{\text{C}}$ bound to clusters of $n=3$ and $n=4$ waters are shown in Figure 4.3. Previously calculated binding energies for H $\dot{\text{C}}$ with four waters are even lower, significantly less than 1 kcal/mol [293] - this discrepancy could be accounted for by the inclusion of zero point corrections in our study, which were neglected by Das et al. The NO $\dot{\text{C}}$ radical also behaves only as a spectator to the water clusters, especially as they grow in size, and is bound with a strength of \sim 2.5 kcal/mol at

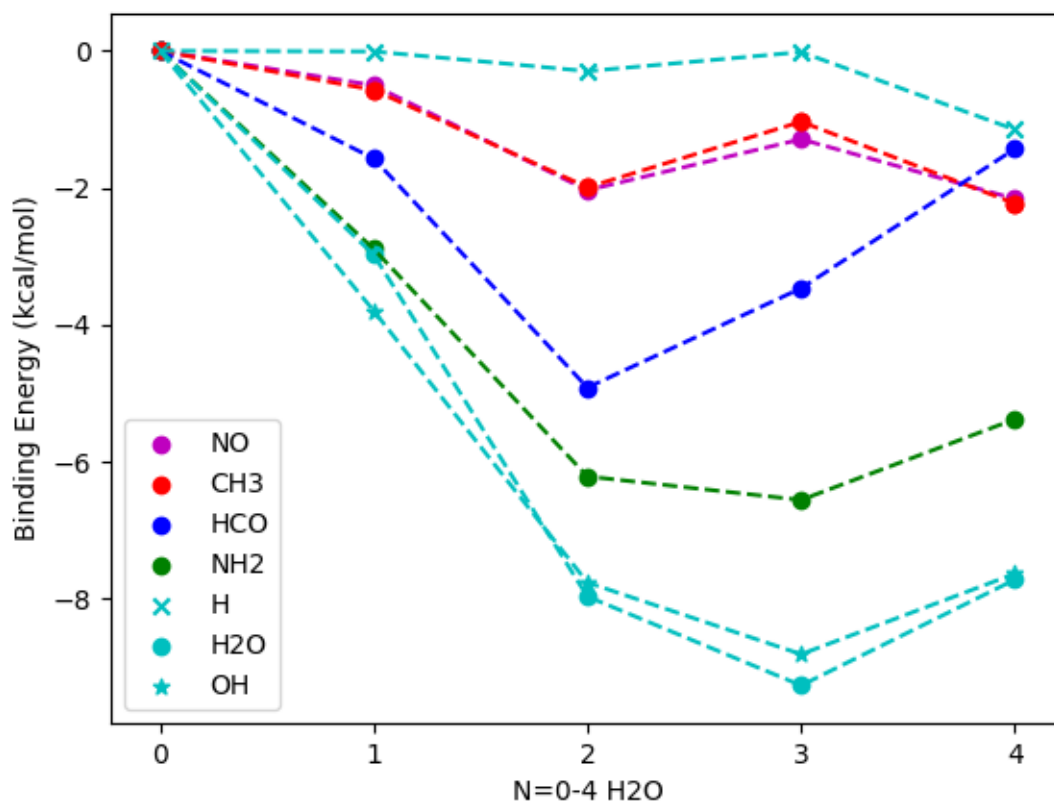


Figure 4.2: Zero point corrected binding energies calculated using DFT for a set of neutral, open-shell molecules. Despite their reactive unpaired electrons, most open-shell species do not exhibit binding energies stronger than their neutral counterparts, nor do they *spontaneously* react in a significant way with H_2O in the water cluster.

the largest cluster size. Chemically, this lack of interaction is easily explainable due to the lack of a strong dipole in NO^\bullet , which leaves hydrogen bonding interactions within the waters of the cluster itself as the strongest forces at play.

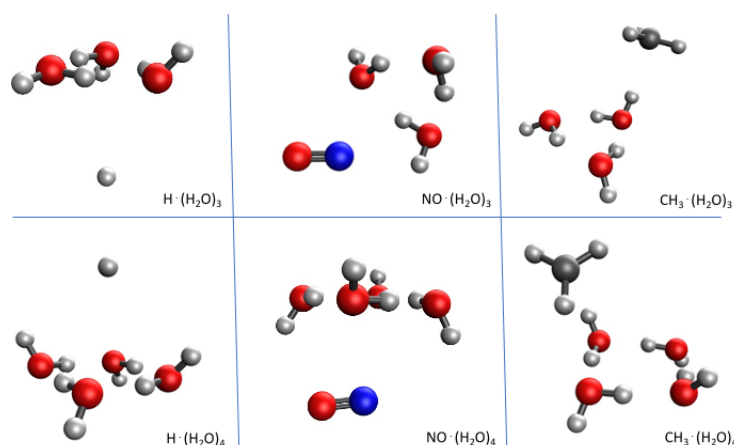


Figure 4.3: Minima for H^\bullet , NO^\bullet , and CH_3^\bullet bound to water clusters of size $n=3$ and 4 waters. These three molecules bind only weakly to the clusters. The strongest hydrogen bonding interactions are still between water molecules, and minima configurations of these are undisturbed by the guest.

Similarly, open-shell hydrocarbon species are bound to water clusters through weak dispersion forces. CH_3^\bullet , the dehydrogenated analogue of CH_4 , binds only slightly more than the neutral analog to water clusters, and hydrogen bonding amongst the waters prevails over any interaction from the guest molecule. The pattern of binding between dehydrogenated radical CH_3^\bullet and neutral CH_4 for water clusters of increasing size is strikingly similar. While CH_3^\bullet binds with a slightly greater strength to all clusters (by approx. 0.5-1 kcal/mol), binding strength for both CH_4 and CH_3^\bullet increases from cluster sizes of 1-2 waters, decreases slightly for interaction with 3 waters, then increases slightly for 4 waters. The magnitudes of these interactions scale similarly as well - for the largest cluster, CH_3^\bullet is bound by approx. 3 kcal/mol (only ~ 0.1 kcal/mol stronger than CH_4). These analogous trends for molecules of similar functional groups between the open and closed-shell molecule sets are apparent for several species, including several that bind with greater strength.

Stronger binders HCO^\bullet and NH_2^\bullet also exhibit patterns in binding that are similar to their neutral cousins H_2CO and NH_3 . NH_2^\bullet (like NH_3) acts as a hydrogen bond acceptor and actively participates in the water cluster. In the lowest-lying tetramer geometry, NH_2 incorporates to form a complex nearly identical to the minima geometry of the water pentamer, a structure that has also been observed as a low-lying conformer for NH_3 [308, 311]. The $\text{O}-\text{H}\cdots\text{N}$ distance in this structure is quite short at $\sim 1.8\text{\AA}$, while usual $\text{O}-\text{H}\cdots\text{N}$ hydrogen bonding distances are slightly longer [312]. The similar hydrogen bonding patterns shown in clusters containing guest molecules with $\text{N}-\text{H}$ and $\text{O}-\text{H}$ functional groups lead to binding strengths that are quite similar for NH_2^\bullet , NH_3 , and H_2O , both in magnitude and curve shape with increasing numbers of water. The hydroxyl radical OH^\bullet also binds in a similar pattern to water with itself (with a nearly identical magnitude of binding energy), and has been investigated more thoroughly in previous literature [313].

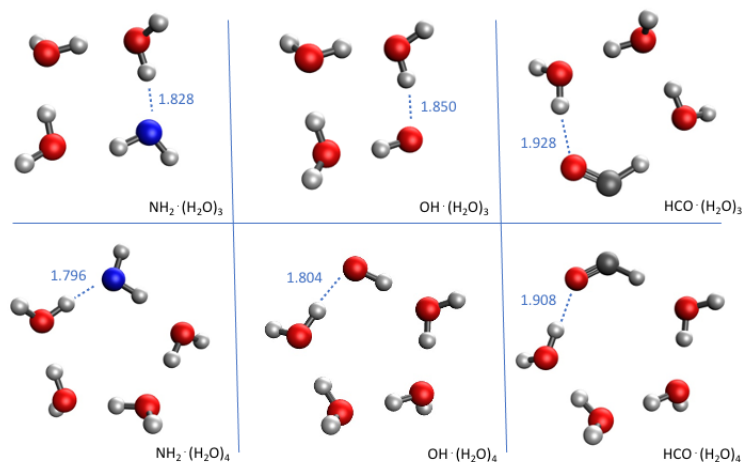


Figure 4.4: Minima for structures of NH_2^\bullet , OH^\bullet , and HCO^\bullet bound to water clusters of size $n=3$ and 4 waters. Hydrogen bonding interactions between the heavy atom of the guest molecule and hydrogen atoms of water are indicated by dashed lines. These guest molecules bind strongly and exhibit similar structures - hydrogen bond interactions generally become closer in distance as the number of waters in the cluster increases, resulting in steadily increasing binding strengths for NH_2^\bullet and OH^\bullet .

Comparatively, HCO^\bullet is an interesting case. Like NH_2^\bullet , HCO^\bullet maximizes hydrogen bonding with water molecules to form cyclic structures for $n=2$ waters and above (shown bound to the water trimer and tetramer in Fig. 4.4). However, while the binding strengths for nitrogenated guest molecules such as NH_2^\bullet generally increase as the water cluster size grows, HCO^\bullet experiences a dramatic decrease after $n=2$ waters. The hydrogen bonding interactions for the $\text{C}=\text{O}$ bond of HCO^\bullet are notable - however, they are still not as strong as those of the $\text{OH}_2\cdots\text{O}-\text{H}$ bond of H_2O with OH^\bullet or the $\text{OH}_2\cdots\text{N}-\text{H}_2$ bond of NH_2^\bullet , so despite similarities in structure, the interactions between this molecule and water clusters are not as robust. The strength of hydrogen bonding tracks well with $\text{X}\cdots\text{H}$ bond distances, where X is the atom acting as a hydrogen bond acceptor on the guest molecule. Hydrogen bonds for NH_2^\bullet , OH^\bullet , and HCO^\bullet are indicated in Figure 4.4 for the water trimer and tetramer. For both NH_2^\bullet and OH^\bullet , $\text{X}\cdots\text{H}$ hydrogen bond distances shorten notably upon addition of a water molecule to the cluster. Previous work on species such as the peroxy radical supports the observation that an unpaired electron can influence hydrogen bonding of radicals to water, with hydrogen bonding effects strengthened or diminished depending on the bonding angle and relative positioning of the unpaired electron [314, 315].

Overall, many the neutral open-shell molecules behave similarly to the neutral closed-shell ones; despite having an unpaired electron, hydrogen-bonding interactions between water molecules generally win out over interactions with the guest molecule, unless the guest has a significant ability to act as a hydrogen bond donor or acceptor.

Cations

There are in-numberable studies regarding the binding energies of cationic species to water. Charged water clusters have been a highly active area of research [316–318], as are hydrated alkali ions [319–323] and other molecules [324–327]. There are many careful benchmark-level studies of the complexes formed by simple cations, such as the alkali metal ions, and also hydronium and ammonium, with small water clusters. Cations are considered to be major contributors to interstellar chemistry, but their inclusion in astrochemical models has been limited. From a chemical viewpoint, cations of the AH_{n+1}^+ form considered here can be viewed as acids whose conjugate base is a neutral AH_n molecule. Such acids can be very strong, and can in some cases initiate barrierless chemical reactions, as will be discussed below.

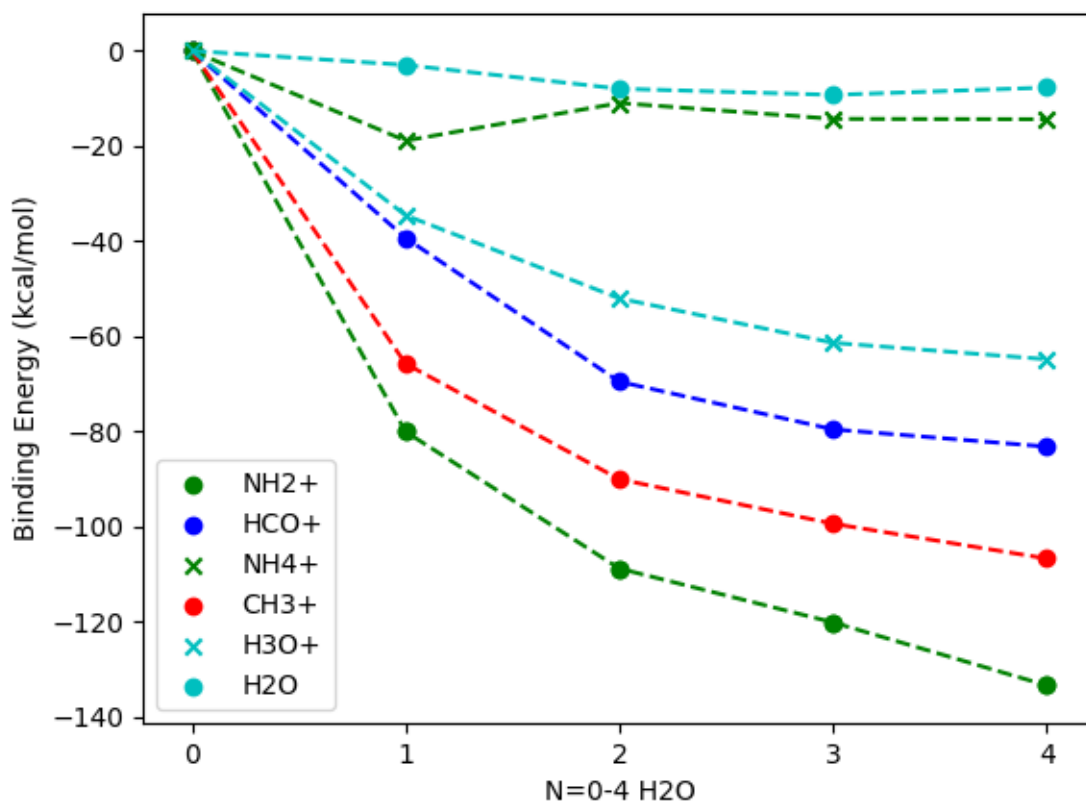


Figure 4.5: Zero point corrected binding energies for cationic closed-shell molecules with water calculated using DFT. All ions tested here bind to water clusters significantly more strongly than neutral or radical molecules. The molecules with the strongest binding energies (NH_2^+ , CH_3^+ , HCO^+) react with water as the cluster size increases to form new solvated products and a free proton. Neutral H_2O is included as a reference point.

Compared to neutral closed and open-shell molecules in the previous sections, cations exhibit the largest magnitude of binding energies to water clusters, plotted in Figure 4.5. The binding of water with itself, which was generally the strongest guest binder, is conversely the weakest binder here. As the water cluster size grows from $n=1-4$ water molecules, binding energies with all cationic guest molecules smoothly increase, and begin to plateau between $n=3$ and 4 waters. Substantial binding energies observed in these cations can be attributed to intense electrostatic interactions (both permanent and induced), as well as partial charge-transfer to the electrophilic cation. All these factors promote reactivity with water and, in some cases, initiate barrierless acid-base chemistry.

The weakest binders from this set of cationic molecules (NH_4^+ and H_3O^+) still have binding energies at least twice that of their non-protonated counterparts NH_3 and H_2O .

NH_4^+ is the only molecule of this set that undergoes no further reaction or dissociation when solvated; the lowest energy structures of NH_4^+ with water clusters maximize hydrogen bonding interactions between the protons of NH_4^+ and the oxygen molecules of H_2O , but no protons are lost to the water cluster, and no new chemical bonds are formed. This lack of reactivity has been noted in previous studies of solvated NH_4^+ in clusters containing up to six waters [328]. The dramatic effect of even modest acid/base chemistry on binding energies for a given cation is immediately apparent in H_3O^+ - this molecule effectively shares a proton with the other H_2O in the cluster. The strongest binders CH_3^+ and NH_2^+ go a step farther and barrierlessly react with members of the water cluster to form new compounds, as discussed in detail below.

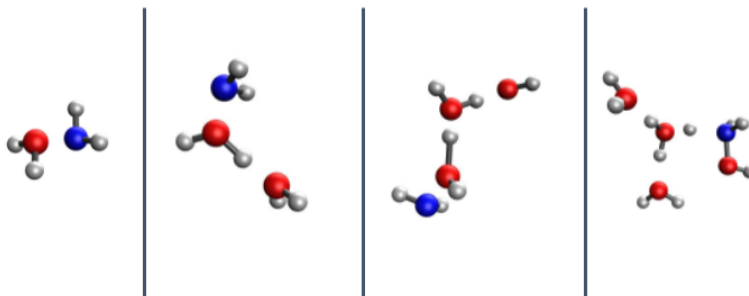


Figure 4.6: Optimized geometries for the lowest-energy conformers of NH_2^+ bound to water monomer, dimer, trimer, and tetramer. Close interaction between NH_2^+ and H_2O produces protonated hydroxylamine without a barrier; as the water cluster size grows, the potential for proton sharing increases, and hydroxylamine is deprotonated.

Figure 4.6 depicts the optimized, lowest energy conformers of NH_2^+ with clusters of $n=1-4$ waters. With one water, NH_2^+ closely interacts with H_2O to form what closely resembles protonated hydroxylamine; the N–O distance of this complex is 1.49\AA , while hydroxylamine itself is just shy of this at around 1.37\AA . As the number of waters in the cluster increases, the N–O bond distance in this hydroxylamine moiety decreases to 1.43, 1.42, and 1.40\AA for $n=2, 3,$ and 4 waters respectively. As the N–O bond distance decreases, a proton from the bonded O–H is pulled away at increasing O–H distances to interact with other free H_2O . At $n=4$ waters, hydroxylamine is fully realized; the three remaining waters interact through hydrogen bonding and a proton is shared between the nitrogen of hydroxylamine (formerly NH_2^+) and a water molecule. The difference in binding energy magnitudes between the two NH cations (NH_2^+ and NH_4^+) is quite striking - by contrast, NH_4^+ is non-reactive with water molecules in the cluster. For interactions of NH_4^+ with water trimer and tetramer, the $\text{H}_3\text{N}-\text{H}\cdots\text{OH}_2$ bonds are slightly lengthened (by $0.02-0.04\text{\AA}$), but not at lengths long enough to break the N–H bond and donate a proton into the water cluster. Unlike NH_2^+ , no N–O bond is formed to create a new species.

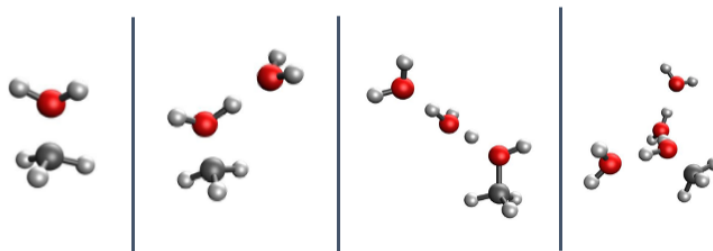


Figure 4.7: Optimized minima CH_3^+ bound to clusters of $n=1-4$ water molecules. Like NH_2^+ , CH_3^+ reacts with one of the water molecules to form a new species (methanol).

A competitor for strongest binder is CH_3^+ , which reacts with water molecules to form protonated methanol, CH_3OH_2^+ or a composite closely resembling methanol with H_3O^+ (shown in Figure 4.7). In a similar trend to NH_2^+ , bond distances between the closest interacting water molecule and the carbon atom of CH_3^+ decrease to 1.50, 1.47, and 1.44 Å with $n=1-3$ waters. Interestingly, the trend is slightly changed in the case of the water tetramer, and C–O bond length again increases slightly to 1.45 Å; another low-lying conformer where methanol is fully realized in the tetramer case lies approx. 3 kcal/mol higher in energy.

Anions

We have also explored binding motifs and computed binding energies for selection of closed-shell anionic species. Generally, anions exhibit stronger binding energies compared to neutral molecules with similar functional groups, but do not bind as strongly to water clusters as cations. Broadly, one can view the anions, A^- as the deprotonated conjugate base of a neutral molecule, AH . In some cases they are strong enough bases to barrierlessly deprotonate water.

Figure 4.8 shows trends in binding energy for seven selected anionic species. Weaker binders amongst the anions include NO^- , CN^- , and HCO_3^- . NO^- is a relatively weak binder to just one water (compared to CN^- and HCO_3^-), but binds more strongly to dimer, trimer, and tetramer water clusters in its lowest energy conformations. For one water, the $\text{OH}_2 \cdots \text{N}$ or $\text{OH}_2 \cdots \text{O}$ hydrogen bonds occur at similar distances (1.74, 1.7, and 1.72 Å) for CN^- , HCO_3^- , and NO^- respectively, and at direct angles. Increased binding energies in CN^- and HCO_3^- are likely due to the stronger dipole of the C–N and C–O bonds. Binding energies with the water dimer are fairly similar for the three molecules, but divergences occur when binding to the water trimer. At $n=3$ waters, both HCO_3^- and NO^- bind far more strongly to the waters than CN^- , as they maintain a higher count of hydrogen bonds.

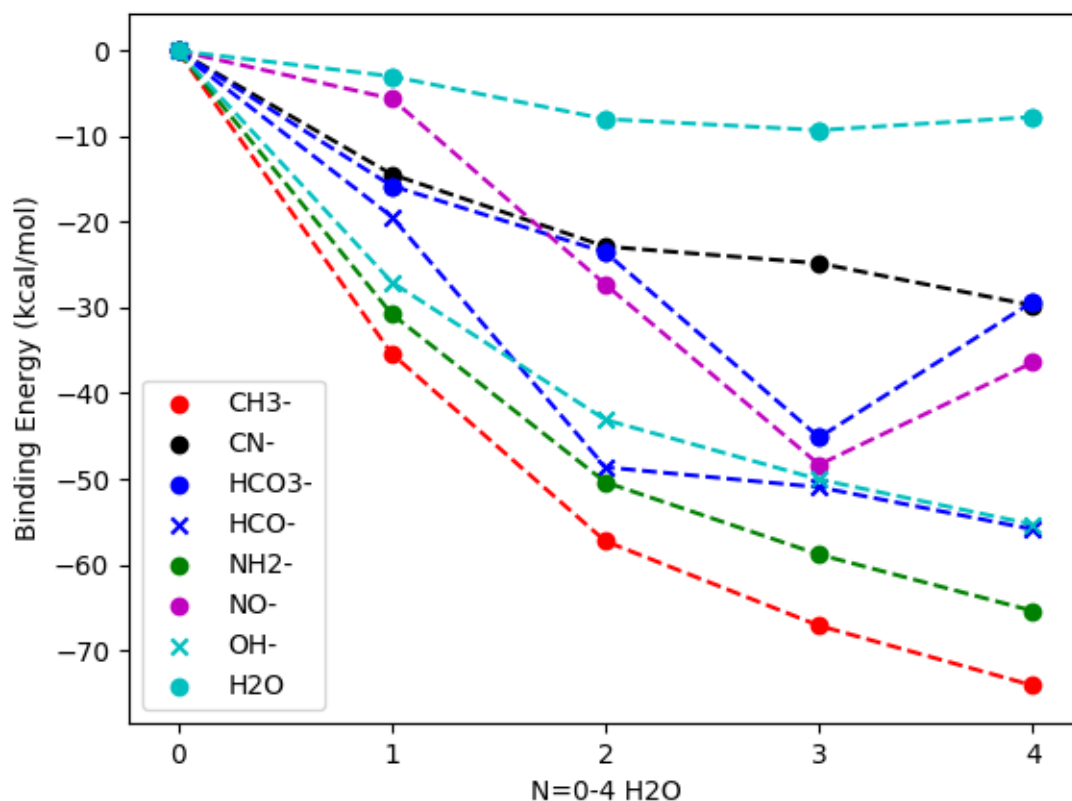


Figure 4.8: Zero point corrected binding energies for a set of anionic molecules calculated using DFT. The magnitude of binding energies exhibited by anions is greater than closed and open-shell neutrals, but less than that of cationic molecules in the previous section. Analogously to cations, the strongest binders are CH_3^- , NH_2^- , and HCO^- . Neutral H_2O is included as a reference point.

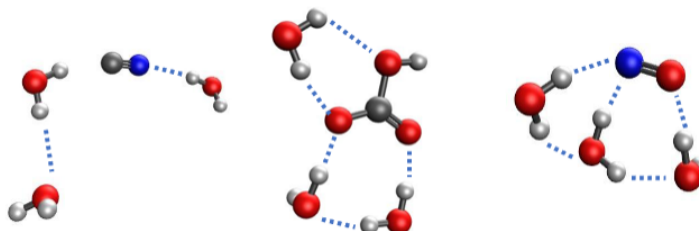


Figure 4.9: Hydrogen bonding (marked with dashed lines) for anionic conformers of CN^- , NO^- , and HCO_3^- with $n=3$ waters. NO^- and HCO_3^- maximize the number of hydrogen bonds formed between guest and water molecules, and thus have larger binding energies than CN^- .

CN^- interacts with H_2O through only one 'true' hydrogen bond, as indicated in Figure 4.9: $\text{CN}\cdots\text{HOH}$ between CN^- and H_2O , and one additional hydrogen bond exists between the additional two water molecules, which form a dimer structure. This dimer interacts with C through a weaker $\text{HOH}\cdots\text{CN}^-$ attraction. In contrast, HCO_3^- and NO^- form five hydrogen bonds both between the water molecules themselves and the guest molecule. Upon complexation with an additional water ($n=4$ H_2O), the minimum energy conformer of HCO_3^- with four waters now forms one extra hydrogen bond than those in the complexes of CN^- and NO^- , giving HCO_3^- a slight edge in binding once again.

Similar to the cationic species, molecules with CH and NH functional groups (CH_3^- and NH_2^-) are the strongest binders of the anion group, with HCO^- also binding strongly after $n=2$ waters.

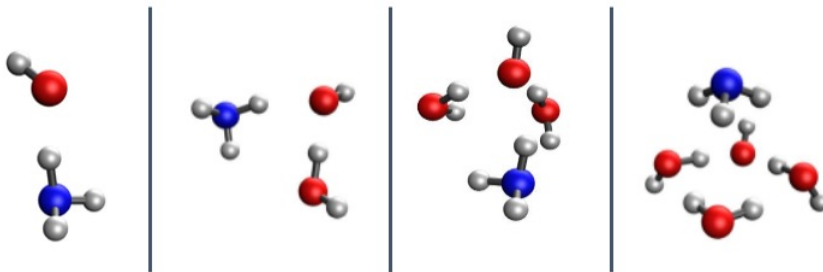


Figure 4.10: NH_2^- reactivity with water clusters of size $n=1-4$. NH_2^- acts as a strong base to barrierlessly deprotonate water, forming NH_3 and OH^- . The resulting hydroxyl anion clusters with the remaining water molecules in familiar structures, while newly formed NH_3 interacts less strongly.

Figure 4.10 shows the result of NH_2^- binding to clusters of $n=1-4$ waters. In all cases, NH_2^- acts as a strong base to spontaneously deprotonate water to form NH_3 and OH^- , resulting in the smoothly increasing binding energies exhibited in Figure 4.8. In the complexes, the water structures (with OH^- now replacing one water) mimic their minima configurations with NH_3 spectating or weakly interacting. CH_3^- follows a nearly identical trend, deprotonating water to form CH_4 and OH^- in very similar structures with the exception of the water trimer. In almost all cases anions produce OH^- after exchanging a hydrogen and charge with water cluster. This leaves a neutral hydride and an active OH^- in the water cluster to take part in further reactions.

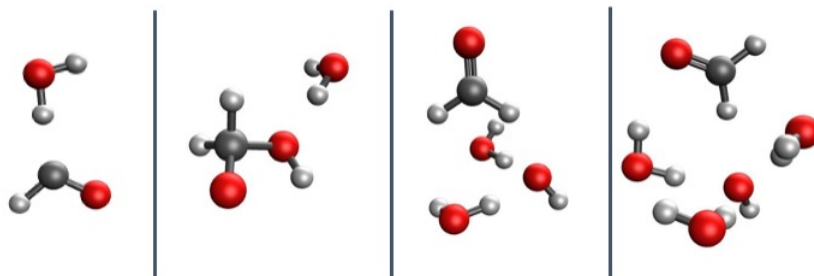


Figure 4.11: Minima geometries of HCO^- interacting and reacting with $n=1-4$ water molecules. Different reactions occur with differing numbers of H_2O ; in the case of $n=2$ waters, HCO^- reacts with one water to form hydroxymethanolate, $\text{H}_2\text{COH}(\text{O})^-$, which is the conjugate base of methane diol, $\text{H}_2\text{C}(\text{OH})_2$. For $n > 3$ waters however, HCO^- deprotonates a water molecule to form formaldehyde and OH^- .

HCO^- has an interesting pattern of reactivity, as shown in Figure 4.11. With just one water, HCO^- has a similar binding energy to its functional group cousin HCO_3^- (~ 19 versus ~ 15 kcal/mol respectively). Unlike NH_2^- and CH_3^- , HCO^- does not react with the water monomer; the hydrogen of H_2O interacts with the negatively charged carbon atom of HCO^- at a distance of 1.69\AA , but the attraction is not strong enough to barrierlessly deprotonate H_2O . However, when interacting instead with the water dimer, one H_2O molecule reacts with HCO^- to form hydroxymethanolate. The relatively electronegative carbon atom of HCO^- deprotonates one water of the dimer to form formaldehyde (H_2CO), leaving OH^- . This hydroxyl anion then reacts with newly formed formaldehyde to form a C–O bond and produce hydroxymethanolate, which interacts with the remaining water through a O–H hydrogen bond.

In the trimer and tetramer structures, HCO^- again deprotonates one water molecule to form formaldehyde and OH^- . Here however, the OH^- is recaptured by the water cluster, which is large enough to form cyclic structures close to those of the water minima with strong hydrogen-bonding networks that mitigate the reactivity of OH^- .

Alternative conformers

For several molecules, alternative low-lying conformers are available in addition to the global minima presented here. The final structure obtained upon minimization depends largely on 1) the initial approach of the guest molecule relative to the cluster, and 2) interaction with an existing cluster versus sequential addition of dispersed water.

Several noteworthy examples arise from ionic species, for which reactivity and interactions with water are more dramatic. Of the cations, NH_2^+ and HCO^+ are two that have at least one low-lying, unique conformer arising from varied starting structures.

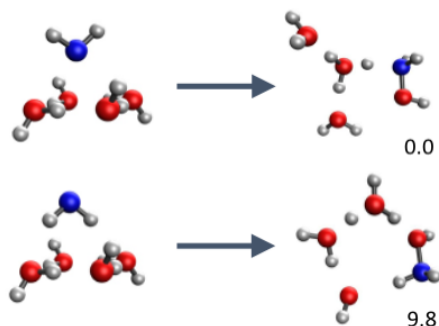


Figure 4.12: Starting structures versus and their resulting optimized geometries for two conformers of NH_2^+ bound to water tetramer. Initial approach of the guest molecule via N results in a different configuration than approach via the H atoms of NH_2^+ . Both conformers form hydroxylamine, but form different composite structures with the remaining waters and shared proton. Energy differences are indicated with respect to the global minimum in kcal/mol.

Figure 4.12 shows two conformers arising from two different starting structures of NH_2^+ with water tetramer. The lowest-energy conformer arises from nitrogen-forward approach by NH_2^+ ; another conformer approx. 9.8 kcal/mol above the minimum arises from hydrogen-forward approach of the guest. For the first, the approaching nitrogen immediately bonds with the oxygen atom of a water molecule in the cluster, and the positive charge shifts to this H_2O , causing proton release as the N–O bond forms. Further rearrangement occurs as new hydrogen bonds form and the free proton is shuttled around the complex. In the second case, a similar process occurs, but the extra reorganization needed to orient NH_2^+ to form the new N–O bond leads to an alternative arrangement of waters and proton.

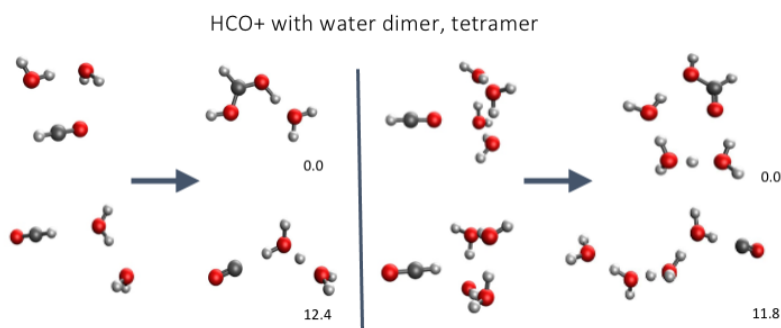


Figure 4.13: Minima and next-lowest conformers of HCO^+ bound to water dimer and tetramer shown in conjunction with their respective starting structures. Energy differences are indicated with respect to the minima in kcal/mol.

Similarly, approach from either the oxygen or hydrogen end of HCO^+ influences the final structure, shown here most plainly for binding to water trimer and tetramer. Approach from

the proton end appears to result in fast deprotonation by the water cluster, and conformers 12.4 and 11.8 kcal/mol above the minimum for water trimer and tetramer respectively. These alternative conformers form CO and a proton shared amongst the water molecules, in contrast to the more dramatic reactions that occur in alternative approaches. The proton reversion channel is only a minor component of the competing reaction channels.

The examples shown above are a small sample illustrating the effects of starting structure on final conformer. Additional examples may be found in the Supplementary Information (Appendix C). The alternative conformers resulting from varied angles of approach by the guest molecule, in addition to having different structures than the minimal energy conformer, bind to water clusters with strengths that can vary from those of the minima anywhere from less than 1 kcal/mol to 10's of kcal/mol depending on the interactions at play. This is especially important to note when considering astrochemical models, as alternative conformers found by reactive molecules may have a wide variety of binding strengths, which thus influence desorption and other surface reaction processes.

Astrochemical Implications

The first step of condensation of molecules on grains may be the formation of molecular complexes, and then the binding to H₂O or CO ice surfaces, which are the dominant ice species in protoplanetary disks. Binding energies (BEs), and other parameters that depend on them, e.g., diffusion energies (DEs), are important input parameters for the disk chemical simulations of interstellar molecular clouds and protoplanetary disks. BEs are only available for a limited number of molecules, radicals and ions. In some cases, while the gas phase BEs for species with individual H₂O molecules are available, binding energies with dimers, trimers, and clusters of water molecules adhering to the surface are not available. Even though binding energies of some major ices have been obtained from laboratory experiments, binding and diffusion energies of key radicals and ions are largely missing because it is difficult to study them in the laboratory due to their high reactivity. Knowing the diffusion energy barriers, in particular for radicals, is critical because they control the reactivity in the ice in disk chemical models. Additionally, at present, the diffusion energy (DE) of a given molecule is considered as a fixed fraction (0.4) of its BE in disk models, because of a lack of experimental and computed DE data for a large number of molecules. However, not all molecules bind equally as we have seen above. Binding energies of molecules as shown here vary significantly during the water freeze out process. Some interactions are weak, which may result in those molecules diffusing easily on the surface of icy grains, while others are more strongly bound, resulting in slower diffusion. Accurate binding energy results during water freeze out process presented here indicate that the DEs of molecules containing different functional groups are going to vary widely given that their BEs with the surface have strong functional group dependence, highlighting again the importance of analyzing binding behavior of a molecule on a case-by-case basis. While the radicals and neutral species bind less strongly than water binds to itself, the binding energies of ions are significantly larger. The ions, therefore, bind permanently or change the nature altogether by reacting with the

water matrix. For some ions the coming in contact with H₂O surface means a spontaneous reaction even at low-temperature. Some of these ions therefore are not likely to diffuse on water surface, but other ions may still be able to diffuse.

Polar molecules, both closed-shell neutrals and open-shell radicals e.g. NH₃, HCN and H₂CO, that bind almost as strongly with H₂O surface as water itself, will sublime at similar disk temperatures as water does. Hydrocarbons will sublime at much lower temperatures. In the context of Enceladus' southern plumes, once the ions come in contact with icy grains they will react and evolve into newer species leaving behind a proton or a hydride.

4.4 Conclusions

In this work, we have computed binding energies for select sets of small neutral closed-shell, neutral open-shell, and ionic closed-shell molecules that are relevant for several astrochemical environments. Grain-surface chemistry, especially involving grains that are covered with thin H₂O ice, are important for dense interstellar medium, proto-planetary disks, exo-planetary atmospheres, and the southern plumes of Enceladus. To simulate the changes in binding energies during the water freeze-out process, accurate binding energies have been evaluated for small water clusters with up to four water molecules.

For neutral closed and open-shell species, binding energies span a relatively small range of values, generally no more than approx. 10 kcal/mol for the strongest binders; predictably, polar molecules with stronger dipoles and more capacity for hydrogen bonding have the largest binding energies. The binding energy values computed for radicals may be of interest to astrochemical modellers, whose models include radical reactions for which data is often missing. The strongest (non-water) open-shell binders HCO[•] and NH₂[•] exhibit short hydrogen bonds with surrounding water molecules, but do not invoke spontaneous deprotonation of the water, and have binding energies only slightly greater in magnitude than their hydrogenated, closed-shell cousins.

The results gathered for cationic and anionic species are particularly intriguing. Many, but not all, of the ions investigated here bind with exceptional strength, especially the cations (some with binding energies above 100 kcal/mol). The most striking examples are NH₂⁺, CH₃⁺, and HCO⁺ for the cations, as well as their anionic counterparts. Each of these molecules undergo barrierless acid-base chemistry to form new species (formaldehyde, methanol, and more) and release H⁺ or OH⁻ into the surrounding water molecules. These reactions occur spontaneously without additional energetic input, indicating radical-free synthetic routes to important astrobiological precursors (especially oxides) in ice grains without the need for energetic processing.

Overall, our computations not only improve existing libraries of binding energy data for neutral closed-shell molecules, but also expand these libraries to include open-shell and ionic species, which have received less attention in previous literature. We have identified important trends in reactivity and a variety of conformers for open-shell and ionic species bound to water clusters, which is particularly important to include in models of astrochemical reac-

tions, as ions and radicals are important synthetic drivers in environments where energetic stimulus is sparse. The binding energies computed here may be included in astrochemical models to improve their quality, and the conformer geometries we have generated should be considered when investigating molecular binding to amorphous ice. We hope that these results will prompt more investigation into the role and fate of ions and other species in cold grains, and how the binding behavior of these species influences production of astrobiological products.

Bibliography

- (1) Schrödinger, E. Quantisierung als Eigenwertproblem. *Ann. Phys.* **1926**, *385*, 437–490.
- (2) Born, M.; Oppenheimer, R. Zur Quantentheorie der Molekeln. *Ann. Phys.* **1927**, *389*, 457–484.
- (3) Sherrill, C. D. An Introduction to Hartree-Fock Molecular Orbital Theory, 2000.
- (4) Szabo, A.; Ostlund, N. S., *Modern Quantum Chemistry: Introduction to Advanced Electronic Structure Theory*; Dover Publications: Mineola, N.Y, 1996.
- (5) Slater, J. A Simplification of the Hartree-Fock Method. *Phys. Rev.* **1950**, *81*, 385–390.
- (6) Roothaan, C. C. J. New Developments in Molecular Orbital Theory. *Rev. Mod. Phys.* **1951**, *23*, 69–89.
- (7) Löwdin, P.-O. In Löwdin, P.-O., Ed.; *Advances in Quantum Chemistry*, Vol. 5; Academic Press: 1970, pp 185–199.
- (8) Hohenberg, P.; Kohn, W. Inhomogeneous Electron Gas. *Phys. Rev.* **1964**, *136*, B864–B871.
- (9) Kohn, W.; Sham, L. J. Self-Consistent Equations Including Exchange and Correlation Effects. *Phys. Rev.* **1965**, *140*, A1133–A1138.
- (10) Thomas, L. H. The calculation of atomic fields. *Math. Proc. Camb. Philos. Soc.* **1927**, *23*, 542–548.
- (11) Dirac, P. A. M. Note on Exchange Phenomena in the Thomas Atom. *Math. Proc. Camb. Philos. Soc.* **1930**, *26*, 376–385.
- (12) Becke, A. D. Perspective: Fifty years of density-functional theory in chemical physics. *J. Chem. Phys.* **2014**, *140*, 18A301.
- (13) Fermi, E. Statistical method to determine some properties of atoms. *Rend. Naz. Lincei* **1927**, *6*, 5.
- (14) Wang, Y. A.; Govind, N.; Carter, E. A. Orbital-free kinetic-energy density functionals with a density-dependent kernel. *Phys. Rev. B* **1999**, *60*, 16350–16358.

- (15) Lignères, V. L.; Carter, E. A. In *Handbook of Materials Modeling: Methods*, Yip, S., Ed.; Springer Netherlands: Dordrecht, 2005, pp 137–148.
- (16) Zhou, B.; Wang, Y. A. Orbital-corrected orbital-free density functional theory. *J. Chem. Phys.* **2006**, *124*, 081107.
- (17) Lehtomäki, J.; Makkonen, I.; Caro, M. A.; Harju, A.; Lopez-Acevedo, O. Orbital-free density functional theory implementation with the projector augmented-wave method. *J. Chem. Phys.* **2014**, *141*, 234102.
- (18) Mardirossian, N.; Head-Gordon, M. Thirty years of density functional theory in computational chemistry: an overview and extensive assessment of 200 density functionals. *Mol. Phys.* **2017**, *115*, 2315–2372.
- (19) Vosko, S. H.; Wilk, L.; Nusair, M. Accurate spin-dependent electron liquid correlation energies for local spin density calculations: a critical analysis. *Can. Journal of Phys.* **1980**, *58*, 1200–1211.
- (20) Perdew, J. P.; Zunger, A. Self-interaction correction to density-functional approximations for many-electron systems. *Phys. Rev. B* **1981**, *23*, 5048–5079.
- (21) Perdew, J. P.; Wang, Y. Accurate and simple analytic representation of the electron-gas correlation energy. *Phys. Rev. B* **1992**, *45*, 13244–13249.
- (22) Ceperley, D. M.; Alder, B. J. Ground State of the Electron Gas by a Stochastic Method. *Phys. Rev. Lett.* **1980**, *45*, 566–569.
- (23) Herman, F.; Van Dyke, J. P.; Ortenburger, I. B. Improved Statistical Exchange Approximation for Inhomogeneous Many-Electron Systems. *Phys. Rev. Lett.* **1969**, *22*, 807–811.
- (24) Herman, F.; Ortenburger, I. B.; Van Dyke, J. P. A method for improving the physical realism of first-principles band structure calculations. *Int. J. Quant. Chem.* **1969**, *4*, 827–846.
- (25) Perdew, J. P.; Burke, K.; Ernzerhof, M. Generalized Gradient Approximation Made Simple. *Phys. Rev. Lett.* **1996**, *77*, 3865–3868.
- (26) Zhao, Y.; Truhlar, D. G. A new local density functional for main-group thermochemistry, transition metal bonding, thermochemical kinetics, and noncovalent interactions. *J. Chem. Phys.* **2006**, *125*, 194101.
- (27) Mardirossian, N.; Head-Gordon, M. ω B97X-V: A 10-parameter, range-separated hybrid, generalized gradient approximation density functional with nonlocal correlation, designed by a survival-of-the-fittest strategy. *Phys. Chem. Chem. Phys.* **2014**, *16*, 9904–9924.
- (28) Mardirossian, N.; Head-Gordon, M. Survival of the most transferable at the top of Jacob’s ladder: Defining and testing the ω B97M(2) double hybrid density functional. *J. Chem. Phys.* **2018**, *148*, 241736.

- (29) Medvedev, M. G.; Bushmarinov, I. S.; Sun, J.; Perdew, J. P.; Lyssenko, K. A. Density functional theory is straying from the path toward the exact functional. *Science* **2017**, *355*, 49–52.
- (30) Kepp, K. P. Comment on "Density functional theory is straying from the path toward the exact functional". *Science* **2017**, *356*, 496–496.
- (31) Tubman, N. M.; Freeman, C. D.; Levine, D. S.; Hait, D.; Head-Gordon, M.; Whaley, K. B. Modern Approaches to Exact Diagonalization and Selected Configuration Interaction with the Adaptive Sampling CI Method. *J. Chem. Theory Comput.* **2020**, *16*, PMID: 32159951, 2139–2159.
- (32) Tubman, N. M.; Lee, J.; Takeshita, T. Y.; Head-Gordon, M.; Whaley, K. B. A deterministic alternative to the full configuration interaction quantum Monte Carlo method. *J. Chem. Phys.* **2016**, *145*, 044112.
- (33) Stanton, J. F. Why CCSD (T) works: a different perspective. *Chem. Phys. Lett.* **1997**, *281*, 130–134.
- (34) Řezáč, J.; Hobza, P. Describing Noncovalent Interactions beyond the Common Approximations: How Accurate Is the "Gold Standard" CCSD(T) at the Complete Basis Set Limit? *J. Chem. Theory Comput.* **2013**, *9*, 2151–2155.
- (35) M, C.; Plesset, M. S. Note on an Approximation Treatment for Many-Electron Systems. *Phys. Rev.* **1934**, *46*, 618–622.
- (36) Goringe, C.; Hernández, E.; Gillan, M.; Bush, I. Linear-scaling DFT-pseudopotential calculations on parallel computers. *Comput. Phys. Commun.* **1997**, *102*, 1–16.
- (37) Fonseca Guerra, C.; Snijders, J.; Velde, G.; Baerends, E. Towards an order-N DFT method. *Theor. Chem. Acc.* **1998**, *99*, 391–403.
- (38) Artacho, E.; Sánchez-Portal, D.; Ordejón, P.; García, A.; Soler, J. M. Linear-Scaling ab-initio Calculations for Large and Complex Systems. *Phys. Status Solidi (b)* **1999**, *215*, 809–817.
- (39) Arita, M.; Arapan, S.; Bowler, D. R.; Miyazaki, T. Large-scale DFT simulations with a linear-scaling DFT code CONQUEST on K-computer. *J. Adv. Sim. Sci. Eng.* **2014**, *1*, 87–97.
- (40) Christensen, A. S.; Kubař, T.; Cui, Q.; Elstner, M. Semiempirical Quantum Mechanical Methods for Noncovalent Interactions for Chemical and Biochemical Applications. *Chem. Rev.* **2016**, *116*, PMID: 27074247, 5301–5337.
- (41) Parr, R. G. A Method for Estimating Electronic Repulsion Integrals Over LCAO MO'S in Complex Unsaturated Molecules. *J. Chem. Phys.* **1952**, *20*, 1499–1499.
- (42) Pople, J. A.; Segal, G. A. Approximate Self-Consistent Molecular Orbital Theory. II. Calculations with Complete Neglect of Differential Overlap. *J. Chem. Phys.* **1965**, *43*, S136–S151.

- (43) Voityuk, A. A. Intermediate neglect of differential overlap for spectroscopy. *WIRES Comput. Mol. Sci.* **2013**, *3*, 515–527.
- (44) Pople, J. A.; Santry, D. P.; Segal, G. A. Approximate Self-Consistent Molecular Orbital Theory. I. Invariant Procedures. *J. Chem. Phys.* **1965**, *43*, S129–S135.
- (45) Porezag, D.; Frauenheim, T.; Köhler, T.; Seifert, G.; Kaschner, R. Construction of tight-binding-like potentials on the basis of density-functional theory: Application to carbon. *Phys. Rev. B* **1995**, *51*, 12947–12957.
- (46) Seifert, G.; Porezag, D.; Frauenheim, T. Calculations of molecules, clusters, and solids with a simplified LCAO-DFT-LDA scheme. *Int. J. Quantum Chem.* **1996**, *58*, 185–192.
- (47) Elstner, M.; Porezag, D.; Jungnickel, G.; Elsner, J.; Haugk, M.; Frauenheim, T.; Suhai, S.; Seifert, G. Self-Consistent-Charge Density-Functional Tight-Binding Method for Simulations of Complex Materials Properties. *Phys. Rev. B* **1998**, *58*, 7260.
- (48) Bannwarth, C.; Caldeweyher, E.; Ehlert, S.; Hansen, A.; Pracht, P.; Seibert, J.; Spicher, S.; Grimme, S. Review GFN_n-xTB. *WIRES Comput Mol Sci* **2021**, *11*, DOI: 10.1002/wcms.1493.
- (49) Hourahine, B. et al. DFTB+, a Software Package for Efficient Approximate Density Functional Theory Based Atomistic Simulations. *J. Chem. Phys.* **2020**, *152*, 124101.
- (50) Spiegelman, F.; Tarrat, N.; Cuny, J.; Dontot, L.; Posenitskiy, E.; Martí, C.; Simon, A.; Rapacioli, M. Density-Functional Tight-Binding: Basic Concepts and Applications to Molecules and Clusters. *Adv. Phys.: X* **2020**, *5*, 1710252.
- (51) Melix, P.; Oliveira, A.; Rüger, R. Spin polarization in SCC-DFTB. *Theor. Chem. Acc.* **2016**, *135*, 232.
- (52) Pracht, P.; Bohle, F.; Grimme, S. Automated exploration of the low-energy chemical space with fast quantum chemical methods. *Phys. Chem. Chem. Phys.* **2020**, *22*, 7169–7192.
- (53) Hendrix, J.; Bera, P. P.; Lee, T. J.; Head-Gordon, M. Cation, Anion, and Radical Isomers of C₄H₄N: Computational Characterization and Implications for Astrophysical and Planetary Environments. *J. Phys. Chem. A* **2020**, *124*, PMID: 32077700, 2001–2013.
- (54) Miller, S. L.; Urey, H. C. Organic Compound Synthesis on the Primitive Earth. *Science* **1959**, *130*, 245–251.
- (55) Strecker, A. Ueber die künstliche Bildung der Milchsäure und einen neuen, dem Glycocoll homologen Körper; *Justus Liebigs Ann. Chem* **1850**, *75*, 27–45.
- (56) Saladino, R.; Dia Mauro, E.; Garcia-Ruiz, J. M. A Universal Geochemical Scenario for Formamide Condensation and Prebiotic Chemistry. *Chem. Eur. J.* **2019**, *25*, 3181–3189.

- (57) Taillades, J.; Beuzelin, I.; Garrel, L.; Tabacik, V.; Bied, C.; Commeyras, A. N-Carbamoyl- α -Amino Acids Rather than Free α -Amino Acids Formation in the Primitive Hydrosphere: A Novel Proposal for the Emergence of Prebiotic Peptides. *Origins of life and evolution of the biosphere* **1998**, *28*, 61–77.
- (58) Gibb, E. L.; Whittet, D. C. B.; Boogert, A. C. A.; Tielens, A. G. G. M. Interstellar Ice: The Infrared Space Observatory Legacy. *ApJS*. **2004**, *151*, 35–73.
- (59) Matthews, C.; Moser, R. E. Peptide Synthesis from Hydrogen Cyanide and Water. *Nature* **1967**, *215*, 1230–1234.
- (60) Roy, D.; Najafian, K.; von Ragué Schleyer, P. Chemical evolution: The mechanism of the formation of adenine under prebiotic conditions. *Proc. Natl. Acad. Sci.* **2007**, *104*, 17272–17277.
- (61) Ferris, J. P.; Hagan, W. J. HCN and chemical evolution: The possible role of cyano compounds in prebiotic synthesis. *Tetrahedron* **1984**, *40*, 1093–1120.
- (62) Dartnell, L. R. Ionizing Radiation and Life. *Astrobiology* **2011**, *11*, PMID: 21774684, 551–582.
- (63) Chyba, C.; Sagan, C. Endogenous production, exogenous delivery and impact-shock synthesis of organic molecules: an inventory for the origins of life. *Nature* **1992**, *355*, 125–132.
- (64) Zamirri, L.; Ugliengo, P.; Ceccarelli, C.; Rimola, A. Quantum Mechanical Investigations on the Formation of Complex Organic Molecules on Interstellar Ice Mantles. Review and Perspectives. *ACS Earth Space Chem.* **2019**, *3*, 1499–1523.
- (65) D.E. Woon The Astrochymist, <http://astrochymist.org/>, Online; accessed 20 November 2019, 2019.
- (66) Kvenvolden, K.; Lawless, J.; Pering, K.; Peterson, E.; Flores, J.; Ponnampereuma, C.; Kaplan, I. R.; Moore, C. Evidence for Extraterrestrial Amino-acids and Hydrocarbons in the Murchison Meteorite. *Nature* **1970**, *228*, 923–926.
- (67) Engel, M.; Macko, S. Isotopic evidence for extraterrestrial non-racemic amino acids in the Murchison meteorite. *Nature* **1997**, *389*, 265–268.
- (68) Engel, M.; Macko, S.; Silfer, J. Carbon isotope composition of individual amino acids in the Murchison meteorite. *Nature* **1990**, *348*, 47–49.
- (69) Callahan, M. P.; Smith, K. E.; Cleaves, H. J.; Ruzicka, J.; Stern, J. C.; Glavin, D. P.; House, C. H.; Dworkin, J. P. Carbonaceous meteorites contain a wide range of extraterrestrial nucleobases. *Proc. Natl. Acad. Sci.* **2011**, *108*, 13995–13998.
- (70) Bera, P.; Nuevo, M.; Milam, S.; Sandford, S.; Lee, T. Mechanism for the Abiotic Synthesis of Uracil via UV-induced Oxidation of Pyrimidine in Pure H₂O Ices under Astrophysical Conditions. *J. Chem. Phys.* **2010**, *133*, 104303.

- (71) Bera, P. P.; Nuevo, M.; Materese, C. K.; Sandford, S. A.; Lee, T. J. Mechanisms for the formation of thymine under astrophysical conditions and implications for the origin of life. *J. Chem. Phys.* **2016**, *144*, 144308.
- (72) Bera, P. P.; Stein, T.; Head-Gordon, M.; Lee, T. J. Mechanisms of the Formation of Adenine, Guanine, and Their Analogues in UV-Irradiated Mixed NH₃:H₂O Molecular Ices Containing Purine. *Astrobiology* **2017**, *17*, PMID: 28708419, 771–785.
- (73) Materese, C. K.; Nuevo, M.; Sandford, S. A. The Formation of Nucleobases from the Ultraviolet Photoirradiation of Purine in Simple Astrophysical Ice Analogues. *Astrobiology* **2017**, *17*, PMID: 28723229, 761–770.
- (74) Sandford, S. A.; Bera, P. P.; Lee, T. J.; Materese, C. K.; Nuevo, M. The Photosynthesis and Photo-Stability of Nucleic Acids in Prebiotic Extraterrestrial Environments. *Top. Curr. Chem.* **2015**, *356*, 123–164.
- (75) Plows, F. L.; Elsilá, J. E.; Zare, R. N.; Buseck, P. R. Evidence that polycyclic aromatic hydrocarbons in two carbonaceous chondrites predate parent-body formation. *Geochim. Cosmochim. Acta* **2003**, *67*, 1429–1436.
- (76) Ehrenfreund, P.; Charnley, S. B. Organic Molecules in the Interstellar Medium, Comets, and Meteorites: A Voyage from Dark Clouds to the Early Earth. *Annu. Rev. Astron. Astrophys.* **2000**, *38*, 427–483.
- (77) Alves, J. F.; Lada, C. J.; Lada, E. A. Internal structure of a cold dark molecular cloud inferred from the extinction of background starlight. *Nature* **2001**, *409*, 159–161.
- (78) Ziurys, L. M. The chemistry in circumstellar envelopes of evolved stars: Following the origin of the elements to the origin of life. *Proc. Natl. Acad. Sci.* **2006**, *103*, 12274–12279.
- (79) Parker, D. S. N.; Kaiser, R. I.; Kostko, O.; Troy, T. P.; Ahmed, M.; Sun, B.-J.; Chen, S.-H.; Chang, A. H. H. On the formation of pyridine in the interstellar medium. *Phys. Chem. Chem. Phys.* **2015**, *17*, 32000–32008.
- (80) Parker, D. S. N.; Kaiser, R. I. On the formation of nitrogen-substituted polycyclic aromatic hydrocarbons (NPAHs) in circumstellar and interstellar environments. *Chem. Soc. Rev.* **2017**, *46*, 452–463.
- (81) Kaiser, R. I.; Parker, D. S.; Mebel, A. M. Reaction Dynamics in Astrochemistry: Low-Temperature Pathways to Polycyclic Aromatic Hydrocarbons in the Interstellar Medium. *Annu. Rev. Phys. Chem.* **2015**, *66*, PMID: 25422849, 43–67.
- (82) Parker, D. S. N.; Yang, T.; Dangi, B. B.; Kaiser, R. I.; Bera, P. P.; Lee, T. J. Low temperature formation of Nitrogen-Substituted Polycyclic Aromatic Hydrocarbons (PANHs) - Barrierless Routes to Dihydroisoquinolines. *ApJ*. **2015**, *815*, 115.

- (83) Hamid, A. M.; Bera, P. P.; Lee, T. J.; Aziz, S. G.; Alyoubi, A. O.; El-Shall, M. S. Evidence for the Formation of Pyrimidine Cations from the Sequential Reactions of Hydrogen Cyanide with the Acetylene Radical Cation. *J. Phys. Chem. Lett.* **2014**, *5*, PMID: 26278451, 3392–3398.
- (84) Hamid, A. M.; El-Shall, M. S.; Hilal, R.; Elroby, S.; Aziz, S. G. Unconventional hydrogen bonding to organic ions in the gas phase: Stepwise association of hydrogen cyanide with the pyridine and pyrimidine radical cations and protonated pyridine. *J. Chem. Phys.* **2014**, *141*, 054305.
- (85) Joblin, C.; Tielens, A.; Cherchneff, I. The formation of Polycyclic Aromatic Hydrocarbons in evolved circumstellar environments. *EAS Publ. Ser.* **2011**, *46*, 177–189.
- (86) Cable, M. L.; Hörst, S. M.; Hodyss, R.; Beauchamp, P. M.; Smith, M. A.; Willis, P. A. Titan Tholins: Simulating Titan Organic Chemistry in the Cassini-Huygens Era. *Chemical Reviews* **2012**, *112*, PMID: 22091924, 1882–1909.
- (87) Brown, R. H.; Lebreton, J.-P.; Waite, J. H., *Titan from Cassini-Huygens*; Springer: New York: 2009.
- (88) Coates, A. J.; Crary, F. J.; Lewis, G. R.; Young, D. T.; Waite Jr., J. H.; Sittler Jr., E. C. Discovery of heavy negative ions in Titan's ionosphere. *Geophys. Res. Lett.* **2007**, *34*.
- (89) Coates, A.; Wellbrock, A.; Lewis, G.; Jones, G.; Young, D.; Crary, F.; Waite, J. Heavy negative ions in Titan's ionosphere: Altitude and latitude dependence. *Planet. Space Sci.* **2009**, *57*, 1866–1871.
- (90) Crary, F.; Magee, B.; Mandt, K.; Waite, J.; Westlake, J.; Young, D. Heavy ions, temperatures and winds in Titan's ionosphere: Combined Cassini CAPS and INMS observations. *Planet. Space Sci.* **2009**, *57*, 1847–1856.
- (91) Cravens, T.; et al. Composition of Titan's ionosphere. *Geophys. Res. Lett.* **2006**.
- (92) Waite, J. H. et al. Ion Neutral Mass Spectrometer Results from the First Flyby of Titan. *Science* **2005**, *308*, 982–986.
- (93) Waite, J. H.; Young, D. T.; Cravens, T. E.; Coates, A. J.; Crary, F. J.; Magee, B.; Westlake, J. The Process of Tholin Formation in Titan's Upper Atmosphere. *Science* **2007**, *316*, 870–875.
- (94) Cravens, T.; et al. Composition of Titan's ionosphere. *Geophys. Res. Lett.* **2006**, *33*.
- (95) Dubois, D.; Carrasco, N.; Bourgalais, J.; Vettier, L.; Desai, R. T.; Wellbrock, A.; Coates, A. J. Nitrogen-containing Anions and Tholin Growth in Titan's Ionosphere: Implications for Cassini CAPS-ELS Observations. *ApJ*. **2019**, *872*, L31.
- (96) Horvath, G.; Aranda-Gonzalvo, Y.; Mason, N. J.; Zahoran, M.; Matejczik, S. Negative ions formed in N₂/CH₄/Ar discharge - A simulation of Titan's atmosphere chemistry. *Eur. Phys. J. Appl. Phys.* **2010**, *49*, 13105.

- (97) Dubois, D.; Sciamma-O'Brien, E.; Fortenberry, R. C. The Fundamental Vibrational Frequencies and Spectroscopic Constants of the Dicyanoamine Anion, NCNCN^- (C_2N_3^-): Quantum Chemical Analysis for Astrophysical and Planetary Environments. *ApJ.* **2019**, *883*, 109.
- (98) Motiyenko, R.; Armieieva, I.; Margulès, L.; Alekseev, E.; Guillemin, J.-C. Rotational spectroscopy of malononitrile and its corresponding monoisocyanide isomer, isocyanacetoneitrile. *Astron. Astrophys.* **2019**, *623*.
- (99) Custer, T.; Szczepaniak, U.; Gronowski, M.; Fabisiewicz, E.; Couturier-Tamburelli, I.; Kołos, R. Density Functional Exploration of $\text{C}_4\text{H}_3\text{N}$ Isomers. *J. Phys. Chem. A* **2016**, *120*, 5928–5938.
- (100) Lattalais, M.; Ellinger, Y.; Matrane, A.; Guillemin, J.-C. Looking for heteroaromatic rings and related isomers as interstellar candidates. *Phys. Chem. Chem. Phys.* **2010**, *12*, 4165–4171.
- (101) Broten, N. W.; MacLeod, J. M.; Avery, L. W.; Irvine, W. M.; Hoglund, B.; Friberg, P.; Hjalmarsen, A. The detection of interstellar methylcyanoacetylene. *ApJ.* **1984**, *276*, L25–L29.
- (102) Lovas, F. J.; Remijan, A. J.; Hollis, J. M.; Jewell, P. R.; Snyder, L. E. Hyperfine Structure Identification of Interstellar Cyanoallene toward TMC-1. *ApJ.* **2006**, *637*, L37–L40.
- (103) Chin, Y.-N.; Kaiser, R. I.; Lemme, C.; Henkel, C. In *Astrochemistry - From Laboratory Studies to Astronomical Observations*, ed. by Kaiser, R. I.; Bernath, P.; Osamura, Y.; Petrie, S.; Mebel, A. M., 2006; Vol. 855, pp 149–153.
- (104) Soorkia, S.; Taatjes, C. A.; Osborn, D. L.; Selby, T. M.; Trevitt, A. J.; Wilson, K. R.; Leone, S. R. Direct detection of pyridine formation by the reaction of CH (CD) with pyrrole: a ring expansion reaction. *Phys. Chem. Chem. Phys.* **2010**, *12*, 8750–8758.
- (105) Sah, C.; Yadav, A. K.; Venkataramani, S. Deciphering Stability of Five-Membered Heterocyclic Radicals: Balancing Act Between Delocalization and Ring Strain. *J. Phys. Chem. A* **2018**, *122*, PMID: 29791155, 5464–5476.
- (106) Holzmeier, F.; Wagner, I.; Fischer, I.; Bodi, A.; Hemberger, P. Pyrolysis of 3-Methoxypyridine. Detection and Characterization of the Pyrrolyl Radical by Threshold Photoelectron Spectroscopy. *J. Phys. Chem. A* **2016**, *120*, PMID: 26698131, 4702–4710.
- (107) Hong, X.; Zhang, L.; Zhang, T.; Qi, F. An Experimental and Theoretical Study of Pyrrole Pyrolysis with Tunable Synchrotron VUV Photoionization and Molecular-Beam Mass Spectrometry. *J. Phys. Chem. A* **2009**, *113*, 5397–5405.
- (108) Mardirossian, N.; Head-Gordon, M. Exploring the limit of accuracy for density functionals based on the generalized gradient approximation: Local, global hybrid, and range-separated hybrid functionals with and without dispersion corrections. *J. Chem. Phys.* **2014**, *140*, 18A527.

- (109) Becke, A. D. Perspective: Fifty years of density-functional theory in chemical physics. *J. Chem. Phys.* **2014**, *140*, 18A301.
- (110) Goerigk, L.; Hansen, A.; Bauer, C.; Ehrlich, S.; Najibi, A.; Grimme, S. A look at the density functional theory zoo with the advanced GMTKN55 database for general main group thermochemistry, kinetics and noncovalent interactions. *Phys. Chem. Chem. Phys.* **2017**, *19*, 32184–32215.
- (111) Najibi, A.; Goerigk, L. The Nonlocal Kernel in van der Waals Density Functionals as an Additive Correction: An Extensive Analysis with Special Emphasis on the B97M-V and ω B97M-V Approaches. *Journal of Chemical Theory and Computation* **2018**, *14*, PMID: 30299953, 5725–5738.
- (112) Gräfenstein, J.; Kraka, E.; Cremer, D. The impact of the self-interaction error on the density functional theory description of dissociating radical cations: Ionic and covalent dissociation limits. *J. Chem. Phys.* **2004**, *120*, 524–539.
- (113) Cohen, A. J.; Mori-Sánchez, P.; Yang, W. Challenges for Density Functional Theory. *Chemical Reviews* **2012**, *112*, 289–320.
- (114) Lee, T. J.; Schaefer, H. F. Systematic study of molecular anions within the self-consistent field approximation: OH^- , CN^- , C_2H^- , NH_2^- , and CH_3^- . *J. Chem. Phys.* **1985**, *83*, 1784–1794.
- (115) Glendening, E.; Badenhop, J.; Karafillogou, P.; Landis, C.; Weinhold, F. NBO 7.0, Theoretical Chemistry Institute, University of Wisconsin, Madison, 2018.
- (116) Raghavachari, K.; Trucks, G.; Pople, J.; Head-Gordon, M. A fifth-order perturbation comparison of electron correlation theories. *Chem. Phys. Lett.* **1989**, *157*, 479–483.
- (117) Feyereisen, M.; Fitzgerald, G.; Komornicki, A. Use of approximate integrals in ab initio theory. An application in MP2 energy calculations. *Chem. Phys. Lett.* **1993**, *208*, 359–363.
- (118) Bernholdt, D.; Harrison, R. Large-scale correlated electronic structure calculations: The RI-MP2 method on parallel computers. *Chem. Phys. Lett.* **1996**, *250*, 477–484.
- (119) Halkier, A.; et al. Basis-set convergence in correlated calculations on Ne, N_2 , H_2O . *Chem. Phys. Lett.* **1998**, *286*, 243–252.
- (120) Behn, A.; Zimmerman, P.; Bell, A.; Head-Gordon, M. Efficient exploration of reaction paths via a freezing string method. *J. Chem. Phys.* **2011**, *135*.
- (121) Baker, J. An algorithm for the location of transition states. *J. Comput. Chem.* **1986**, *7*, 385–395.
- (122) Shao, Y. et al. Advances in molecular quantum chemistry contained in the Q-Chem 4 program package. *Molecular Physics* **2015**, *113*, 184–215.
- (123) Schofield, K., *Hetero-aromatic Nitrogen Compounds: Pyrroles and Pyridines*; Springer Science+Business Media, LLC: 1967.

- (124) Haynes, W. M.; Lide, D. R.; Bruno, T. J., *CRC Handbook of Chemistry and Physics: A Ready-reference Book of Chemical and Physical data*; Boca Raton, Florida: CRC Press: 2016.
- (125) Katritzky, A. R.; Ramsden, C. A.; Joule, J. A.; Zhdankin, V. V., *Handbook of Heterocyclic Chemistry (3rd Edition)*; Elsevier: 2010.
- (126) Jiao, H.; Schleyer, P. v. R.; Mo, Y.; McAllister, M. A.; Tidwell, T. T. Magnetic Evidence for the Aromaticity and Antiaromaticity of Charged Fluorenyl, Indenyl, and Cyclopentadienyl Systems. *J. Am. Chem. Soc.* **1997**, *119*, 7075–7083.
- (127) Gianola, A. J.; Ichino, T.; Hoenigman, R. L.; Kato, S.; Bierbaum, V. M.; Lineberger, W. C. Thermochemistry and Electronic Structure of the Pyrrolyl Radical. *J. Phys. Chem. A* **2004**, *108*, 10326–10335.
- (128) P. F. Lee, E.; G. Wright, T. A study of the lowest-lying triplet and singlet states of the cyclopentadienyl cation ($c\text{-C}_5\text{H}_5^+$). *Phys. Chem. Chem. Phys.* **1999**, *1*, 219–225.
- (129) Wiberg, K. B. Antiaromaticity in Monocyclic Conjugated Carbon Rings. *Chem. Rev.* **2001**, *101*, PMID: 11710223, 1317–1332.
- (130) Breslow, R.; Groves, J.; Ryan, G. Cyclopropenyl cation. *J. Am. Chem. Soc.* **1967**.
- (131) Byun, Y.; Saebo, S.; Pittman Jr, C. An ab initio study of potentially aromatic and antiaromatic three-membered rings. *J. Am. Chem. Soc.* **1991**.
- (132) Kokkila Schumacher, S. I. L.; Bera, P. P.; Lee, T. J. Characterization of the Azirinyll Cation and Its Isomers. *J. Phys. Chem. A* **2016**, *120*, 1275–1282.
- (133) Puzzarini, C.; Bloino, J.; Tasinato, N.; Barone, V. Accuracy and Interpretability: The Devil and the Holy Grail. New Routes across Old Boundaries in Computational Spectroscopy. *Chem. Rev.* **2019**, *119*, PMID: 31187984, 8131–8191.
- (134) Puzzarini, C.; Baiardi, A.; Bloino, J.; Barone, V.; Murphy, T. E.; Drew, H. D.; Ali, A. Spectroscopic Characterization of Key Aromatic and Heterocyclic Molecules: A Route toward the Origin of Life. *AJ* **2017**, *154*, 82.
- (135) Lara, L.; Lellouch, E.; Lopez-Moreno, J.; Rodrigo, R. Vertical distribution of Titan's atmospheric neutral constituents. *J. Geophys. Res.* **1996**, *101*, 23261–23283.
- (136) Toubanc, D.; Parisot, J.; Brillet, J.; Gautier, D.; Raulin, F.; McKay, C. Photochemical modeling of Titan's atmosphere. *Icarus* **1995**, *113*, 2–26.
- (137) Wilson, E. H.; Atreya, S. K. Current state of modeling the photochemistry of Titan's mutually dependent atmosphere and ionosphere. *J. Geophys. Res.: Planets* **2004**, *109*, DOI: 10.1029/2003JE002181.
- (138) Vuitton, V.; Yelle, R.; McEwan, M. Ion chemistry and N-containing molecules in Titan's upper atmosphere. *Icarus* **2007**, *191*, 722–742.
- (139) McGuigan, M.; Waite, J.; Imanaka, H.; Sacks, R. Analysis of Titan tholin pyrolysis products by comprehensive two-dimensional gas chromatography-time-of-flight mass spectrometry. *J. Chromatogr. A* **2006**.

- (140) Gautier, T.; Carrasco, N.; Buch, A.; Szopa, C.; Sciamma-O'Brien, E.; Cernogora, G. Nitrile gas chemistry in Titan's atmosphere. *Icarus* **2011**, *213*, 625–635.
- (141) Blank, D.; North, S.; Lee, Y. The ultraviolet photodissociation dynamics of pyrrole. *Chemical Physics* **1994**, *187*, 35–47.
- (142) Roberts, G. M.; Williams, C. A.; Yu, H.; Chatterley, A. S.; Young, J. D.; Ullrich, S.; Stavros, V. G. Probing ultrafast dynamics in photoexcited pyrrole: timescales for $^1\pi^*$ mediated H-atom elimination. *Faraday Discuss.* **2013**, *163*, 95–116.
- (143) Lippert, H.; Ritze, H.; Hertel, I.; Radloff, W. Femtosecond Time-Resolved Hydrogen-Atom Elimination from Photoexcited Pyrrole Molecules. *Chem. Phys. Chem.* **2004**, *5*, 1423–1427.
- (144) Picconi, D.; Grebenshchikov, S. Y. Photodissociation dynamics in the first absorption band of pyrrole. I. Molecular Hamiltonian and the Herzberg-Teller absorption spectrum for the $^1A_2(\sigma\pi^*) < -\tilde{\chi}A_1(\pi\pi)$ transition. *J. Chem. Phys.* **2018**, *148*, 104103.
- (145) Sobolewski, A. L.; Domcke, W.; Dedonder-Lardeux, C.; Jouvet, C. Excited-state hydrogen detachment and hydrogen transfer driven by repulsive $^1\pi\sigma^*$ states: A new paradigm for nonradiative decay in aromatic biomolecules. *Phys. Chem. Chem. Phys.* **2002**, *4*, 1093–1100.
- (146) Ashfold, M. N. R.; Cronin, B.; Devine, A. L.; Dixon, R. N.; Nix, M. G. D. The Role of $\pi\sigma^*$ Excited States in the Photodissociation of Heteroaromatic Molecules. *Science* **2006**, *312*, 1637–1640.
- (147) Zawadzki, M. M.; Thompson, J. O. F.; Burgess, E. A.; Paterson, M. J.; Townsend, D. Time-resolved photoionization spectroscopy of mixed Rydberg-valence states: indole case study. *Phys. Chem. Chem. Phys.* **2015**, *17*, 26659–26669.
- (148) Ashfold, M. N. R.; King, G. A.; Murdock, D.; Nix, M. G. D.; Oliver, T. A. A.; Sage, A. G. $\pi\sigma^*$ excited states in molecular photochemistry. *Phys. Chem. Chem. Phys.* **2010**, *12*, 1218–1238.
- (149) Kirkby, O. M.; Parkes, M. A.; Neville, S. P.; Worth, G. A.; Fielding, H. H. Non-radiative relaxation dynamics of pyrrole following excitation in the range 249.5–200nm. *Chem. Phys. Lett.* **2017**, *683*, Ahmed Zewail (1946-2016) Commemoration Issue of Chem. Phys. Lett., 179–185.
- (150) Makhov, D. V.; Saita, K.; Martinez, T. J.; Shalashilin, D. V. Ab initio multiple cloning simulations of pyrrole photodissociation: TKER spectra and velocity map imaging. *Phys. Chem. Chem. Phys.* **2015**, *17*, 3316–3325.
- (151) Roberts, G. M.; Stavros, V. G. The role of $\pi\sigma^*$ states in the photochemistry of heteroaromatic biomolecules and their subunits: insights from gas-phase femtosecond spectroscopy. *Chem. Sci.* **2014**, *5*, 1698–1722.

- (152) Wei, J.; Kuczmann, A.; Riedel, J.; Renth, F.; Temps, F. Photofragment velocity map imaging of H atom elimination in the first excited state of pyrrole. *Phys. Chem. Chem. Phys.* **2003**, *5*, 315–320.
- (153) Vuitton, V.; Lavvas, P.; Yelle, R.; Galand, M.; Wellbrock, A.; Lewis, G.; Coates, A.; Wahlund, J. Negative ion chemistry in Titan's upper atmosphere. *Planet. Space Sci.* **2009**, *57*, 1558–1572.
- (154) Agúndez, M.; Cernicharo, J.; Guélin, M.; Kahane, C.; Roueff, E.; Klos, J.; Aoiz, F. J.; Lique, F.; Marcelino, N.; Goicoechea, J. R.; González Garcia, M.; Gottlieb, C. A.; McCarthy, M. C.; Thaddeus, P. Astronomical identification of CN^- , the smallest observed molecular anion. *A&A* **2010**, *517* L2, L2.
- (155) Fuente, A.; Garcia-Burillo, S.; Gerin, M.; Teyssier, D.; Usero, A.; Rizzo, J. R.; de Vicente, P. Photon-dominated Chemistry in the Nucleus of M82: Widespread HOC^+ Emission in the Inner 650 Parsec Disk. *ApJ*. **2005**, *619*, L155–L158.
- (156) Nixon, C. A.; Jennings, D. E.; Bézard, B.; Vinatier, S.; Teanby, N. A.; Sung, K.; Ansty, T. M.; Irwin, P. G. J.; Goriunov, N.; Cottini, V.; Coustenis, A.; Flasar, F. M. Detection of propene in Titan's stratosphere. *ApJ*. **2013**, *776*, L14.
- (157) Kaiser, R. I.; Balucani, N. The Formation of Nitriles in Hydrocarbon-Rich Atmospheres of Planets and Their Satellites: Laboratory Investigations by the Crossed Molecular Beam Technique. *Acc. Chem. Res.* **2001**, *34*, PMID: 11560469, 699–706.
- (158) Dobrijevic, M.; Loison, J.; Hickson, K.; Gronoff, G. 1D-coupled photochemical model of neutrals, cations and anions in the atmosphere of Titan. *Icarus* **2016**, *268*, 313–339.
- (159) Balucani, N.; Asvany, O.; Kaiser, R.-I.; Osamura, Y. Formation of Three $\text{C}_4\text{H}_3\text{N}$ Isomers from the Reaction of CN ($X^2\Sigma^+$) with Allene, H_2CCCH_2 (X^1-A_1), and Methylacetylene, CH_3CCH (X^1A_1): A Combined Crossed Beam and Ab Initio Study. *J. Phys. Chem. A* **2002**, *106*, 4301–4311.
- (160) Bond, T. C. et al. Bounding the role of black carbon in the climate system: A scientific assessment. *J. Geophys. Res. Atmos.* **2013**, *118*, 5380–5552.
- (161) Climate Change 2013: The Physical Science Basis. Working Group I Contribution to the Fifth Assessment Report of the Intergovernmental Panel on Climate Change. 2013.
- (162) Lighty, J. S.; Veranth, J. M.; Sarofim, A. F. Combustion Aerosols: Factors Governing Their Size and Composition and Implications to Human Health. *J. Air Waste Manag. Assoc.* **2000**, *50*, 1565–1618.
- (163) Niranjana, R.; Thakur, A. The toxicological mechanisms of environmental soot (black carbon) and carbon black: Focus on oxidative stress and inflammatory pathways. *Front. Immunol.* **2017**, *8*, DOI: 10.3389/fimmu.2017.00763.

- (164) Heusinkveld, H. J.; Wahle, T.; Campbell, A.; Westerink, R. H.; Tran, L.; Johnston, H.; Stone, V.; Cassee, F. R.; Schins, R. P. Neurodegenerative and neurological disorders by small inhaled particles. *NeuroToxicology* **2016**, *56*, 94–106.
- (165) Pope, C. A.; Dockery, D. W. Health effects of fine particulate air pollution: Lines that connect. *J. Air Waste Manage.* **2006**, *56*, 709–742.
- (166) Donnet, J.-B.; Bansal, R. C.; Wang, M.-J., *Carbon Black: Science and Technology*. 2nd ed. Marcel Dekker, Inc.: New York, NY: 1993.
- (167) Wu, C.-S.; Chang, T.-W.; Teng, H.; Lee, Y.-L. High performance carbon black counter electrodes for dye-sensitized solar cells. *Energy* **2016**, *115*, 513–518.
- (168) Sabbah, H.; Biennier, L.; Klippenstein, S. J.; Sims, I. R.; Rowe, B. R. Exploring the Role of PAHs in the Formation of Soot: Pyrene Dimerization. *J. Phys. Chem. Lett.* **2010**, *1*, 2962–2967.
- (169) D’Anna, A. Combustion-formed nanoparticles. *Proc. Combust. Inst* **2009**, *32*, 593–613.
- (170) Wang, H. Formation of nascent soot and other condensed-phase materials in flames. *Proc. Combust. Inst* **2011**, *33*, 41–67.
- (171) Johansson, K. O.; Head-Gordon, M. P.; Schrader, P. E.; Wilson, K. R.; Michelsen, H. A. Resonance-stabilized hydrocarbon-radical chain reactions may explain soot inception and growth. *Science* **2018**, *361*, 997–1000.
- (172) Michelsen, H. A.; Colket, M. B.; Bengtsson, P.-E.; D’Anna, A.; Desgroux, P.; Haynes, B. S.; Miller, J. H.; Nathan, G. J.; Pitsch, H.; Wang, H. A Review of Terminology Used to Describe Soot Formation and Evolution under Combustion and Pyrolytic Conditions. *ACS Nano* **2020**, *14*, PMID: 32986401, 12470–12490.
- (173) Martin, J. W.; Salamanca, M.; Kraft, M. Soot inception: Carbonaceous nanoparticle formation in flames. *Prog. Energy Combust. Sci.* **2022**, *88*, 100956.
- (174) Mosbach, S.; Celnik, M. S.; Raj, A.; Kraft, M.; Zhang, H. R.; Kubo, S.; Kim, K.-O. Towards a detailed soot model for internal combustion engines. *Combust. Flame* **2009**, *156*, 1156–1165.
- (175) D’Anna, A.; Violi, A. A kinetic model for the formation of aromatic hydrocarbons in premixed laminar flames. *Symposium (International) on Combustion* **1998**, *27*, Twenty-Seventh Symposium (International) on Combustion Volume One, 425–433.
- (176) Saggese, C.; Sánchez, N. E.; Frassoldati, A.; Cuoci, A.; Faravelli, T.; Alzueta, M. U.; Ranzi, E. Kinetic Modeling Study of Polycyclic Aromatic Hydrocarbons and Soot Formation in Acetylene Pyrolysis. *Energy & Fuels* **2014**, *28*, 1489–1501.
- (177) Jin, H.; Frassoldati, A.; Wang, Y.; Zhang, X.; Zeng, M.; Li, Y.; Qi, F.; Cuoci, A.; Faravelli, T. Kinetic modeling study of benzene and PAH formation in laminar methane flames. *Combust. Flame* **2015**, *162*, 1692–1711.

- (178) Raj, A.; Sander, M.; Janardhanan, V.; Kraft, M. A study on the coagulation of polycyclic aromatic hydrocarbon clusters to determine their collision efficiency. *Combust. and Flame* **2010**, *157*, 523–534.
- (179) Martin, J. W.; Hou, D.; Menon, A.; Pascazio, L.; Akroyd, J.; You, X.; Kraft, M. Reactivity of Polycyclic Aromatic Hydrocarbon Soot Precursors: Implications of Localized π -Radicals on Rim-Based Pentagonal Rings. *J. Phys. Chem. C* **2019**, *123*, 26673–26682.
- (180) Menon, A.; Martin, J. W.; Akroyd, J.; Kraft, M. Reactivity of Polycyclic Aromatic Hydrocarbon Soot Precursors: Kinetics and Equilibria. *J. Phys. Chem. A* **2020**, *124*, PMID: 33202128, 10040–10052.
- (181) Nobili, A.; Maffei, L. P.; Baggioli, A.; Pelucchi, M.; Cuoci, A.; Cavallotti, C.; Faravelli, T. On the radical behavior of large polycyclic aromatic hydrocarbons in soot formation and oxidation. *Combust. Flame* **2021**, 111692.
- (182) Faccinetto, A.; Irimiea, C.; Minutolo, P. e. a. Evidence on the formation of dimers of polycyclic aromatic hydrocarbons in a laminar diffusion flame. *Commun. Chem.* **2020**, *3*, 112.
- (183) Gleason, K.; Carbone, F.; Gomez, A. PAHs controlling soot nucleation in 0.101–0.811MPa ethylene counterflow diffusion flames. *Combust. and Flame* **2021**, *227*, 384–395.
- (184) Liu, L.; Xu, H.; Zhu, Q.; Ren, H.; Li, X. Soot formation of n-decane pyrolysis: A mechanistic view from ReaxFF molecular dynamics simulation. *Chemical Physics Lett.* **2020**, *760*, 137983.
- (185) Mitra, T.; Chu, C.; Naseri, A.; Thomson, M. J. Polycyclic aromatic hydrocarbon formation in a flame of the alkylated aromatic trimethylbenzene compared to those of the alkane dodecane. *Combust. Flame* **2021**, *223*, 495–510.
- (186) Jin, H.; Xing, L.; Liu, D.; Hao, J.; Yang, J.; Farooq, A. First aromatic ring formation by the radical-chain reaction of vinylacetylene and propargyl. *Combust. Flame* **2021**, *225*, 524–534.
- (187) Commodo, M.; Picca, F.; Vitiello, G.; De Falco, G.; Minutolo, P.; D’Anna, A. Radicals in nascent soot from laminar premixed ethylene and ethylene-benzene flames by electron paramagnetic resonance spectroscopy. *Proc. Combust. Inst* **2020**, DOI: <https://doi.org/10.1016/j.proci.2020.08.024>.
- (188) Adamson, B. D.; Skeen, S. A.; Ahmed, M.; Hansen, N. Detection of Aliphatically Bridged Multi-Core Polycyclic Aromatic Hydrocarbons in Sooting Flames with Atmospheric-Sampling High-Resolution Tandem Mass Spectrometry. *J. Phys. Chem. A* **2018**, *122*, PMID: 30415549, 9338–9349.
- (189) Vitiello, G.; De Falco, G.; Picca, F.; Commodo, M.; D’Errico, G.; Minutolo, P.; D’Anna, A. Role of radicals in carbon clustering and soot inception: A combined EPR and Raman spectroscopic study. *Combust. Flame* **2019**, *205*, 286–294.

- (190) Rundel, J. A.; Thomas, C. M.; Schrader, P. E.; Wilson, K. R.; Johansson, K. O.; Bambha, R. P.; Michelsen, H. A. Promotion of particle formation by resonance-stabilized radicals during hydrocarbon pyrolysis. *Combust. Flame* **2021**, 111942.
- (191) Couch, D. E.; Zhang, A. J.; Taatjes, C. A.; Hansen, N. Experimental Observation of Hydrocarbon Growth by Resonance-Stabilized Radical-Radical Chain Reaction. *Angew. Chem. Int. Ed.* **2021**, *60*, 27230–27235.
- (192) Frenklach, M.; Wang, H. Detailed modeling of soot particle nucleation and growth. *Symposium (International) on Combustion* **1991**, *23*, Twenty-Third Symposium (International) on Combustion, 1559–1566.
- (193) Frenklach, M. Reaction mechanism of soot formation in flames. *Phys. Chem. Chem. Phys.* **2002**, *4*, 2028–2037.
- (194) Jain, A.; Wang, Y.; Kulatilaka, W. D. Effect of H-atom concentration on soot formation in premixed ethylene/air flames. *Proc. Combust. Inst* **2019**, *37*, 1289–1296.
- (195) Mulla, I. A.; Renou, B. Simultaneous imaging of soot volume fraction, PAH, and OH in a turbulent n-heptane spray flame. *Combust. Flame* **2019**, *209*, 452–466.
- (196) Harris, S. J.; Anita M., W.; Blint, R. J.; Goldsmith, J. Concentration profiles in rich and sooting ethylene flames. *Symposium (International) on Combustion* **1988**, *21*, Twenty-First Symposium (International on Combustion), 1033–1045.
- (197) Frenklach, M.; Clary, D. W.; Gardiner W. C., J.; Stein, S. E. Detailed kinetic modeling of soot formation in shock-tube pyrolysis of acetylene. *Proc. Combust. Inst.* **1985**, *20*, 887–901.
- (198) Miller, J. A.; Klippenstein, S. J. The Recombination of Propargyl Radicals and Other Reactions on a C₆H₆ Potential. *J. Phys. Chem. A* **2003**, *107*, 7783–7799.
- (199) Long, A. E.; Merchant, S. S.; Vandeputte, A. G.; Carstensen, H.-H.; Vervust, A. J.; Marin, G. B.; Van Geem, K. M.; Green, W. H. Pressure dependent kinetic analysis of pathways to naphthalene from cyclopentadienyl recombination. *Combust. Flame* **2018**, *187*, 247–256.
- (200) Jain, A.; Wang, Y.; Kulatilaka, W. D. Simultaneous imaging of H and OH in flames using a single broadband femtosecond laser source. *Proc. Combust. Inst* **2020**, DOI: <https://doi.org/10.1016/j.proci.2020.07.137>.
- (201) Lamoureux, N.; Foo, K. K.; Desgroux, P. Quantitative measurement of atomic hydrogen in low-pressure methane flames using two-photon LIF calibrated by krypton. *Combust. Flame* **2021**, *224*, A dedication to Professor Ronald K. Hanson, 248–259.
- (202) Turns, S., *An Introduction to Combustion Concepts and Applications*, 3rd Ed. McGraw Hill; New York: 2012.
- (203) Simmie, J. M. Detailed chemical kinetic models for the combustion of hydrocarbon fuels. *Prog. Energy Combust. Sci.* **2003**, *29*, 599–634.

- (204) Miller, J. A.; Melius, C. F. Kinetic and thermodynamic issues in the formation of aromatic compounds in flames of aliphatic fuels. *Combust. Flame* **1992**, *91*, 21–39.
- (205) Labbe, N. J.; Sivaramakrishnan, R.; Goldsmith, C. F.; Georgievskii, Y.; Miller, J. A.; Klippenstein, S. J. Weakly Bound Free Radicals in Combustion: "Prompt" Dissociation of Formyl Radicals and Its Effect on Laminar Flame Speeds. *J. Phys. Chem. Lett.* **2016**, *7*, PMID: 26655248, 85–89.
- (206) Miller, J. A.; Sivaramakrishnan, R.; Tao, Y.; Goldsmith, C. F.; Burke, M. P.; Jasper, A. W.; Hansen, N.; Labbe, N. J.; Glarborg, P.; Zádor, J. Combustion chemistry in the twenty-first century: Developing theory-informed chemical kinetics models. *Prog. Energy Combust. Sci.* **2021**, *83*, 100886.
- (207) Chu, Q.; Shi, B.; Wang, H.; Chen, D.; Liao, L. Hydrogen abstraction/addition reactions in soot surface growth. *Phys. Chem. Chem. Phys.* **2021**, *23*, 3071–3086.
- (208) Pejpichestakul, W.; Ranzi, E.; Pelucchi, M.; Frassoldati, A.; Cuoci, A.; Parente, A.; Faravelli, T. Examination of a soot model in premixed laminar flames at fuel-rich conditions. *Proc. Combust. Inst* **2019**, *37*, 1013–1021.
- (209) St. John, P.; Guan, Y.; Kim, Y.; Etz, B.; Kim, S.; Paton, R. Quantum Chemical Calculations for over 200,000 organic radical species and 40,000 associated closed-shell molecules. *Sci. Data* **2020**, *7*, 244.
- (210) Violi, A.; Truong, T. N.; Sarofim, A. F. Kinetics of Hydrogen Abstraction Reactions from Polycyclic Aromatic Hydrocarbons by H Atoms. *J. Phys. Chem. A* **2004**, *108*, 4846–4852.
- (211) Yönder, Ö.; Schmitz, G.; Hättig, C.; Schmid, R.; Debiagi, P.; Hasse, C.; Locaspi, A.; Faravelli, T. Can Small Polyaromatics Describe Their Larger Counterparts for Local Reactions? A Computational Study on the H-Abstraction Reaction by an H-Atom from Polyaromatics. *J. Phys. Chem. A* **2020**, *124*, PMID: 33147026, 9626–9637.
- (212) Tielens, A. Interstellar Polycyclic Aromatic Hydrocarbon Molecules. *Ann. Rev. Astron. Astrophys.* **2008**, *46*, 289–337.
- (213) Kaiser, R. I.; Hansen, N. An Aromatic Universe - A Physical Chemistry Perspective. *J. Phys. Chem. A* **2021**, *125*, PMID: 33826842, 3826–3840.
- (214) Salama, F.; Galazutdinov, G. A.; Krelowski, J.; Biennier, L.; Beletsky, Y.; Song, I.-O. Polycyclic Aromatic Hydrocarbons and the Diffuse Interstellar Bands: A Survey. *Astrophys. J.* **2011**, *728*, 154.
- (215) McCarthy, M. C.; McGuire, B. A. Aromatics and Cyclic Molecules in Molecular Clouds: A New Dimension of Interstellar Organic Chemistry. *J. Phys. Chem. A* **2021**, *125*, PMID: 33749264, 3231–3243.
- (216) Sagan, C.; Khare, B. N.; Thompson, W. R.; McDonald, G. D.; Wing, M. R.; Bada, J. L.; Vo-Dinh, T.; Arakawa, E. T. Polycyclic Aromatic Hydrocarbons in the Atmospheres of Titan and Jupiter. *Astrophys. J.* **1993**, *414*, 399.

- (217) López-Puertas, M.; Dinelli, B. M.; Adriani, A.; Funke, B.; Garcia-Comas, M.; Moriconi, M. L.; D'Aversa, E.; Boersma, C.; Allamandola, L. J. Large Abundances of Polycyclic Aromatic Hydrocarbons in Titan's Upper Atmosphere. *Astrophys. J.* **2013**, *770*, 132.
- (218) Parker, D. S. N.; Zhang, F.; Kim, Y. S.; Kaiser, R. I.; Landera, A.; Kislov, V. V.; Mebel, A. M.; Tielens, A. G. G. M. Low temperature formation of naphthalene and its role in the synthesis of PAHs (Polycyclic Aromatic Hydrocarbons) in the interstellar medium. *PNAS* **2012**, *109*, 53–58.
- (219) Levey, Z. D.; Laws, B. A.; Sundar, S. P.; Nauta, K.; Kable, S. H.; da Silva, G.; Stanton, J. F.; Schmidt, T. W. PAH Growth in Flames and Space: Formation of the Phenalenyl Radical. *J. Phys. Chem. A* **2022**, *126*, PMID: 34936357, 101–108.
- (220) Jochims, H. W.; Ruhl, E.; Baumgartel, H.; Tobita, S.; Leach, S. Size Effects on Dissociation Rates of Polycyclic Aromatic Hydrocarbon Cations: Laboratory Studies and Astrophysical Implications. *Astrophysical Journal* **1994**, *420*, 307.
- (221) Zhen, J.; Castellanos, P.; Paardekooper, D. M.; Ligterink, N.; Linnartz, H.; Nahon, L.; Joblin, C.; Tielens, A. G. G. M. Laboratory Photo-Chemistry of PAHs: Ionization versus Fragmentation. *Astrophys. J.* **2015**, *804*, L7.
- (222) Mardirossian, N.; Head-Gordon, M. Thirty years of density functional theory in computational chemistry: an overview and extensive assessment of 200 density functionals. *Mol. Phys.* **2017**, *115*, 2315–2372.
- (223) Weigend, F.; Ahlrichs, R. Balanced basis sets of split valence, triple zeta valence and quadruple zeta valence quality for H to Rn: Design and assessment of accuracy. *Phys. Chem. Chem. Phys.* **2005**, *7*, 3297–3305.
- (224) Curtiss, L. A.; Redfern, P. C.; Raghavachari, K. Gaussian-4 theory using reduced order perturbation theory. *J. Chem. Phys.* **2007**, *127*, 124105.
- (225) Li, Y.-P.; Gomes, J.; Mallikarjun Sharada, S.; Bell, A. T.; Head-Gordon, M. Improved force-field parameters for QM/MM simulations of the energies of adsorption for molecules in zeolites and a free rotor correction to the rigid rotor harmonic oscillator model for adsorption enthalpies. *J. Phys. Chem. C* **2015**, *119*, 1840–1850.
- (226) Behn, A.; Zimmerman, P. M.; Bell, A. T.; Head-Gordon, M. Efficient exploration of reaction paths via a freezing string method. *J. Chem. Phys.* **2011**, *135*, 224108.
- (227) Baker, J. An algorithm for the location of transition states. *J. Comput. Chem* **1986**, *7*, 385–395.
- (228) Steinfeld, J.; Francisco, J.; Hase, W., *Chemical Kinetics and Dynamics*; Oxford University Press, Oxford, U.K.
- (229) Beyer, T.; Swinehart, D. F. Algorithm 448: Number of Multiply-Restricted Partitions. *Commun. ACM* **1973**, *16*, 379.

- (230) Glowacki, D. R.; Liang, C.-H.; Morley, C.; Pilling, M. J.; Robertson, S. H. MESMER: An Open-Source Master Equation Solver for Multi-Energy Well Reactions. *J. Phys. Chem. A* **2012**, *116*, PMID: 22905697, 9545–9560.
- (231) Crabtree, R. H.; Lei, A. Introduction: CH activation. *Chem. Rev.* **2017**, *117*, 8481–8482.
- (232) Exner, K.; Schleyer, P. v. R. Theoretical bond energies: a critical evaluation. *J. Phys. Chem. A* **2001**, *105*, 3407–3416.
- (233) Bauschlicher, C. W.; Langhoff, S. R. Theoretical study of the C-H bond dissociation energies of CH₄, C₂H₂, C₂H₄, and H₂C₂O. *Chem. Phys. Lett.* **1991**, *177*, 133–138.
- (234) Habibollahzadeh, D.; Murray, J.; Grodziki, M.; Seminario, J.; Politzer, P. C-H Bond-dissociation of Acetylene - Local Density Functional Calculations. *Int. J. Quantum Chem.* **1992**, *42*, 267–272.
- (235) Marshall, P. Thermochemistry of the Ethyl Radical and the C-H Bond Strength in Ethane. *J. Phys. Chem. A* **1999**, *103*, 4560–4563.
- (236) Blanksby, S.; Ellison, G. Bond dissociation energies of organic molecules. *Acc. Chem. Res.* **2003**, *36*, 255–263.
- (237) Richter, H.; Howard, J. B. Formation of polycyclic aromatic hydrocarbons and their growth to soot - a review of chemical reaction pathways. *Prog. Energy Combust. Sci.* **2000**, *26*, 565–608.
- (238) Wang, Y.; Chung, S. H. Soot formation in laminar counterflow flames. *Prog. Energy Combust. Sci.* **2019**, *74*, 152–238.
- (239) Kohse-Höinghaus, K. Combustion in the future: The importance of chemistry. *Proc. Combust. Inst* **2020**, DOI: <https://doi.org/10.1016/j.proci.2020.06.375>.
- (240) Zhao, L.; Kaiser, R. I.; Lu, W.; Ahmed, M.; Oleinikov, A. D.; Azyazov, V. N.; Mebel, A. M.; Howlader, A. H.; Wnuk, S. F. Gas phase formation of phenalene via 10 π -aromatic, resonantly stabilized free radical intermediates. *Phys. Chem. Chem. Phys.* **2020**, *22*, 15381–15388.
- (241) Zhao, L.; Kaiser, R. I.; Lu, W.; Kostko, O.; Ahmed, M.; Evseev, M. M.; Bashkurov, E. K.; Oleinikov, A. D.; Azyazov, V. N.; Mebel, A. M.; Howlader, A. H.; Wnuk, S. F. Gas phase formation of cyclopentanaphthalene (benzindene) isomers via reactions of 5- and 6-indenyl radicals with vinylacetylene. *Phys. Chem. Chem. Phys.* **2020**, *22*, 22493–22500.
- (242) Kalpathy, S. V.; Poddar, N. B.; Bagley, S. P.; Wornat, M. J. Reaction pathways for the growth of polycyclic aromatic hydrocarbons during the supercritical pyrolysis of n-decane, as determined from doping experiments with 1- and 2-methylnaphthalene. *Proc. Combust. Inst* **2015**, *35*, 1833–1841.

- (243) Porfiriev, D. P.; Azyazov, V. N.; Mebel, A. M. Conversion of acenaphthalene to phenalene via methylation: A theoretical study. *Combust. Flame* **2020**, *213*, 302–313.
- (244) Kislov, V. V.; Mebel, A. M. Ab Initio G3-type/Statistical Theory Study of the Formation of Indene in Combustion Flames. I. Pathways Involving Benzene and Phenyl Radical. *J. Phys. Chem. A* **2007**, *111*, PMID: 17260977, 3922–3931.
- (245) Savee, J. D.; Selby, T. M.; Welz, O.; Taatjes, C. A.; Osborn, D. L. Time- and isomer-resolved measurements of sequential addition of acetylene to the propargyl radical. *J. Phys. Chem. Lett.* **2015**, *6*, 4153–4158.
- (246) Gao, Y.; DeYonker, N. J.; Garrett III, E. C.; Wilson, A. K.; Cundari, T. R.; Marshall, P. Enthalpy of formation of the cyclohexadienyl radical and the C-H bond enthalpy of 1, 4-cyclohexadiene: An experimental and computational re-evaluation. *J. Phys. Chem. A* **2009**, *113*, 6955–6963.
- (247) Barckholtz, C.; Barckholtz, T. A.; Hadad, C. M. C-H and N-H Bond Dissociation Energies of Small Aromatic Hydrocarbons. *J. Am. Chem. Soc.* **1999**, *121*, 491–500.
- (248) Aihara, J.-i.; Fujiwara, K.; Harada, A.; Ichikawa, H.; Fukushima, K.; Hirota, F.; Ishida, T. The C-H bond dissociation energies of polycyclic aromatic hydrocarbons. *J. Mol. Struct.* **1996**, *366*, 219–226.
- (249) Truhlar, D. G.; Garrett, B. C. Variational transition state theory. *Ann. Rev. Phys. Chem.* **1984**, *35*, 159–189.
- (250) Burcat, A.; Dvinyaninov, M.; Olchanski, E. Detailed combustion kinetics of cyclopentadiene studied in a shock-tube. *Int. J. Chem. Kinet.* **2001**, *33*, 491–508.
- (251) Bacskay, G. B.; Mackie, J. C. The pyrolysis of cyclopentadiene: quantum chemical and kinetic modelling studies of the acetylene plus propyne/allene decomposition channels. *Phys. Chem. Chem. Phys.* **2001**, *3*, 2467–2473.
- (252) Tokmakov, I.; Moskaleva, L.; Lin, M. Quantum chemical/vRRKM study on the thermal decomposition of cyclopentadiene. *Int. J. Chem. Kinet.* **2004**, *36*, 139–151.
- (253) Wang, H.; Liu, Z.; Gong, S.; Liu, Y.; Wang, L.; Zhang, X.; Liu, G. Experimental and kinetic modeling study on 1,3-cyclopentadiene oxidation and pyrolysis. *Combust. Flame* **2020**, *212*, 189–204.
- (254) Lu, M.; Mulholland, J. A. PAH Growth from the pyrolysis of CPD, indene and naphthalene mixture. *Chemosphere* **2004**, *55*, 605–610.
- (255) Silva, G. d.; Bozzelli, J. W. Indene Formation from Alkylated Aromatics: Kinetics and Products of the Fulvenallene + Acetylene Reaction. *J. Phys. Chem. A* **2009**, *113*, PMID: 19603772, 8971–8978.

- (256) Pousse, E.; Tian, Z. Y.; Glaude, P. A.; Fournet, R.; Battin-Leclerc, F. A lean methane premixed laminar flame doped with components of diesel fuel part III: Indane and comparison between n-butylbenzene, n-propylcyclohexane and indane. *Combust. Flame* **2010**, *157*, DOI: 10.1016/J.COMBUSTFLAME.2010.03.008.
- (257) Cowley, R. E.; Eckert, N. A.; Vaddadi, S.; Figg, T. M.; Cundari, T. R.; Holland, P. L. Selectivity and Mechanism of Hydrogen Atom Transfer by an Isolable Imidoiron(III) Complex. *J. Am. Chem. Soc.* **2011**, *133*, PMID: 21563763, 9796–9811.
- (258) Jin, H.; Xing, L.; Hao, J.; Yang, J.; Zhang, Y.; Cao, C.; Pan, Y.; Farooq, A. A chemical kinetic modeling study of indene pyrolysis. *Combust. Flame* **2019**, *206*, 1–20.
- (259) Léger, A.; d’Hendecourt, L.; Boissel, P.; Desert, F. Photo-thermo-dissociation. I-A general mechanism for destroying molecules. *Astron. Astrophys.* **1989**, *213*, 351–359.
- (260) Wang, Q.-D.; Sun, Y.; Sun, M.-M.; Liang, J.-H. Chemical Kinetics of Hydrogen Atom Abstraction from Propargyl Sites by Hydrogen and Hydroxy Radicals. *Int. J. Mol. Sci.* **2019**, *20*, DOI: 10.3390/ijms20133227.
- (261) Badra, J.; Farooq, A. Site-specific reaction rate constant measurements for various secondary and tertiary H-abstraction by OH radicals. *Combust. Flame* **2015**, *162*, 2034–2044.
- (262) Sumathi, R.; Carstensen, H.-H.; Green, W. H. Reaction Rate Prediction via Group Additivity Part 1: H Abstraction from Alkanes by H and CH₃. *J. Phys. Chem. A* **2001**, *105*, 6910–6925.
- (263) Manion, J. A.; Sheen, D. A.; Awan, I. A. Evaluated Kinetics of the Reactions of H and CH₃ with n-Alkanes: Experiments with n-Butane and a Combustion Model Reaction Network Analysis. *J. Phys. Chem. A* **2015**, *119*, PMID: 25871634, 7637–7658.
- (264) Jin, H.; Yang, J.; Xing, L.; Hao, J.; Zhang, Y.; Cao, C.; Pan, Y.; Farooq, A. An experimental study of indene pyrolysis with synchrotron vacuum ultraviolet photoionization mass spectrometry. *Phys. Chem. Chem. Phys.* **2019**, *21*, 5510–5520.
- (265) Wang, H.; Wen, K.; You, X.; Mao, Q.; Luo, K. H.; Pilling, M. J.; Robertson, S. H. Energy transfer in intermolecular collisions of polycyclic aromatic hydrocarbons with bath gases He and Ar. *J. Chem. Phys.* **2019**, *151*, 044301.
- (266) Stein, S. E.; Fahr, A. High-temperature stabilities of hydrocarbons. *J. Phys. Chem.* **1985**, *89*, 3714–3725.
- (267) Marinov, N. M.; Pitz, W. J.; Westbrook, C. K.; Castaldi, M. J.; Senkan, S. M. Modeling of Aromatic and Polycyclic Aromatic Hydrocarbon Formation in Premixed Methane and Ethane Flames. *Combust. Sci. Technol.* **1996**, *116-117*, 211–287.

- (268) Slavinskaya, N. A.; Riedel, U.; Dworkin, S. B.; Thomson, M. J. Detailed numerical modeling of PAH formation and growth in non-premixed ethylene and ethane flames. *Combust. Flame* **2012**, *159*, 979–995.
- (269) Ono, K.; Matsukawa, Y.; Dewa, K.; Watanabe, A.; Takahashi, K.; Saito, Y.; Matsushita, Y.; Aoki, H.; Era, K.; Aoki, T.; Yamaguchi, T. Formation mechanisms of soot from high-molecular-weight polycyclic aromatic hydrocarbons. *Combust. Flame* **2015**, *162*, 2670–2678.
- (270) Johansson, K.; Lai, J.; Skeen, S.; Popolan-Vaida, D.; Wilson, K.; Hansen, N.; Violi, A.; Michelsen, H. Soot precursor formation and limitations of the stablomer grid. *Proc. Combust. Inst* **2015**, *35*, 1819–1826.
- (271) Mercier, X.; Carrivain, O.; Irimiea, C.; Faccineto, A.; Therssen, E. Dimers of polycyclic aromatic hydrocarbons: the missing pieces in the soot formation process. *Phys. Chem. Chem. Phys.* **2019**, *21*, 8282–8294.
- (272) Zhang, H.-B.; Hou, D.; Law, C. K.; You, X. Role of Carbon-Addition and Hydrogen-Migration Reactions in Soot Surface Growth. *J. Phys. Chem. A* **2016**, *120*, PMID: 26799641, 683–689.
- (273) Swings, P.; Rosenfeld, L. Considerations Regarding Interstellar Molecules. *Astrophys. J.* **1937**, *86*, 483–486.
- (274) McKellar, A. Evidence for the Molecular Origin of Some Hitherto Unidentified Interstellar Lines. *Publ. Astron. Soc. Pac.* **1940**, *52*, 187.
- (275) Cheung, A. C.; Rank, D. M.; Townes, C. H.; Thornton, D. D.; Welch, W. J. Detection of NH₃ Molecules in the Interstellar Medium by Their Microwave Emission. *Phys. Rev. Lett.* **1968**, *21*, 1701–1705.
- (276) Cheung, A. C.; Rank, D. M.; Townes, C. H.; Thornton, D. D.; Welch, W. J. Detection of NH₃ Molecules in the Interstellar Medium by Their Microwave Emission. *Nature* **1969**, *221*, 626–628.
- (277) Snyder, L. E.; Buhl, D.; Zuckerman, B.; Palmer, P. Microwave Detection of Interstellar Formaldehyde. *Phys. Rev. Lett.* **1969**, *22*, 679–681.
- (278) Ishak, B. Introduction to astrochemistry: chemical evolution from interstellar clouds to star and planet formation. *Contemp. Phys.* **2019**, *60*, 262–262.
- (279) Ruaud, M.; Gorti, U. A Three-phase Approach to Grain Surface Chemistry in Protoplanetary Disks: Gas, Ice Surfaces, and Ice Mantles of Dust Grains. *Astrophys. J.* **2019**, *885*, 146.
- (280) Herbst, E. Unusual Chemical Processes in Interstellar Chemistry: Past and Present. *Front. Astron. Space Sci.* **2021**, *8*, DOI: 10.3389/fspas.2021.776942.
- (281) Hama, T.; Watanabe, N. Surface Processes on Interstellar Amorphous Solid Water: Adsorption, Diffusion, Tunneling Reactions, and Nuclear-Spin Conversion. *Chem. Rev.* **2013**, *113*, 8783–8839.

- (282) Wakelam, V.; Bron, E.; Cazaux, S.; Dulieu, F.; Gry, C.; Guillard, P.; Habart, E.; HornekÅŠr, L.; Morisset, S.; Nyman, G.; Pirronello, V.; Price, S. D.; Valdivia, V.; Vidali, G.; Watanabe, N. H₂ formation on interstellar dust grains: The viewpoints of theory, experiments, models and observations. *Mol. Astrophys.* **2017**, *9*, 1–36.
- (283) Hollenbach, D. J.; Werner, M. W.; Salpeter, E. E. Molecular Hydrogen in H i Regions. **1971**, *163*, 165.
- (284) Materese, C. K.; Nuevo, M.; Bera, P. P.; Lee, T. J.; Sandford, S. A. Thymine and Other Prebiotic Molecules Produced from the Ultraviolet Photo-Irradiation of Pyrimidine in Simple Astrophysical Ice Analogs. *Astrobiology* **2013**, *13*, PMID: 24143868, 948–962.
- (285) Bera, P. P.; Nuevo, M.; Milam, S. N.; Sandford, S. A.; Lee, T. J. Mechanism for the abiotic synthesis of uracil via UV-induced oxidation of pyrimidine in pure H₂O ices under astrophysical conditions. *J. Chem. Phys.* **2010**, *133*, 104303.
- (286) Oberg, K. I.; Fayolle, E.; Linnartz, H.; van Dishoeck, E.; Fillion, J.; Bertin, M. In *American Astronomical Society Meeting Abstracts*, 2013; Vol. 222, 202.02, p 202.02.
- (287) Khawaja, N.; Postberg, F.; Hillier, J.; Klenner, F.; Kempf, S.; Nölle, L.; Reviol, R.; Zou, Z.; Srama, R. Low-mass nitrogen-, oxygen-bearing, and aromatic compounds in Enceladean ice grains. *Mon. Notices Royal Astron. Soc.* **2019**, *489*, 5231–5243.
- (288) Waite Jr, J.; Combi, M.; et al. Cassini ion and neutral mass spectrometer: Enceladus plume composition and structure. *Science* **2006**, *311*, 1419–1422.
- (289) Postberg, F.; et al. Macromolecular organic compounds from the depths of Enceladus. *Nature* **2018**, *558*, 564–568.
- (290) He, J.; Acharyya, K.; Vidali, G. Binding energy of molecules on water ice: laboratory measurements and modeling. *Astrophys. J.* **2016**, *825*, 89.
- (291) Enrique-Romero, J.; Rimola, A.; Ceccarelli, C.; Ugliengo, P.; Balucani, N.; Skouteris, D. Quantum Mechanical Simulations of the Radical–Radical Chemistry on Icy Surfaces. *Astrophys. J. Suppl. Ser.* **2022**, *259*, 39.
- (292) Ferrero, S.; Zamirri, L.; Ceccarelli, C.; Witzel, A.; Rimola, A.; Ugliengo, P. Binding Energies of Interstellar Molecules on Crystalline and Amorphous Models of Water Ice by Ab Initio Calculations. *Astrophys. J.* **2020**, *904*, 11.
- (293) Das, A.; Sil, M.; Gorai, P.; Chakrabarti, S. K.; Loison, J. C. An Approach to Estimate the Binding Energy of Interstellar Species. *Astrophys. J. Suppl. Ser.* **2018**, *237*, 9.
- (294) Tentscher, P. R.; Arey, J. S. Geometries and Vibrational Frequencies of Small Radicals: Performance of Coupled Cluster and More Approximate Methods. *J. Chem. Theory Comput.* **2012**, *8*, PMID: 26593847, 2165–2179.
- (295) Tentscher, P. R.; Arey, J. S. On the Nature of Interactions of Radicals with Polar Molecules. *J. Phys. Chem. A* **2013**, *117*, PMID: 24224466, 12560–12568.

- (296) Tentscher, P. R.; Arey, J. S. Binding in Radical-Solvent Binary Complexes: Benchmark Energies and Performance of Approximate Methods. *J. Chem. Theory Comput.* **2013**, *9*, PMID: 26587618, 1568–1579.
- (297) Wakelam, V.; Loison, J.-C.; Mereau, R.; Ruaud, M. Binding energies: New values and impact on the efficiency of chemical desorption. *Mol. Astrophys.* **2017**, *6*, 22–35.
- (298) Bovolenta, G.; Bovino, S.; Vöhringer-Martinez, E.; Saez, D. A.; Grassi, T.; Vogt-Geisse, S. High level ab initio binding energy distribution of molecules on interstellar ices: Hydrogen fluoride. *Mol. Astrophys.* **2020**, *21*, 100095.
- (299) Xantheas, S. S.; Dunning, T. H. Ab initio studies of cyclic water clusters (H₂O)_n, n=1–6. I. Optimal structures and vibrational spectra. *J. Chem. Phys.* **1993**, *99*, 8774–8792.
- (300) Wales, D. J.; Hodges, M. P. Global minima of water clusters (H₂O)_n, n ≤ 21, described by an empirical potential. *Chem. Phys. Lett.* **1998**, *286*, 65–72.
- (301) Maheshwary, S.; Patel, N.; Sathyamurthy, N.; Kulkarni, A. D.; Gadre, S. R. Structure and Stability of Water Clusters (H₂O)_n, n = 8-20: An Ab Initio Investigation. *J. Phys. Chem. A* **2001**, *105*, 10525–10537.
- (302) Shields, R. M.; Temelso, B.; Archer, K. A.; Morrell, T. E.; Shields, G. C. Accurate Predictions of Water Cluster Formation, (H₂O)_n=2–10. *J. Phys. Chem. A* **2010**, *114*, PMID: 20882961, 11725–11737.
- (303) Bannwarth, C.; Ehlert, S.; Grimme, S. GFN2-xTB—An Accurate and Broadly Parametrized Self-Consistent Tight-Binding Quantum Chemical Method with Multipole Electrostatics and Density-Dependent Dispersion Contributions. *J. Chem. Theory Comput.* **2019**, *15*, 1652.
- (304) Werner, H.-J. et al. The Molpro quantum chemistry package. *J. Chem. Phys.* **2020**, *152*, 144107.
- (305) Adler, T. B.; Knizia, G.; Werner, H.-J. A simple and efficient CCSD(T)-F12 approximation. *J. Chem. Phys.* **2007**, *127*, 221106.
- (306) Sylvetsky, N.; Kesharwani, M. K.; Martin, J. M. L. The aug-cc-pVnZ-F12 basis set family: Correlation consistent basis sets for explicitly correlated benchmark calculations on anions and noncovalent complexes. *J. Chem. Phys.* **2017**, *147*, 134106.
- (307) Malaspina, T.; Fileti, E. E.; Riveros, J. M.; Canuto, S. Ab Initio Study of the Isomeric Equilibrium of the HCN–H₂O and H₂O–HCN Hydrogen-Bonded Clusters. *J. Phys. Chem. A* **2006**, *110*, PMID: 16928122, 10303–10308.
- (308) Li, Q.; Wang, X.; Cheng, J.; Li, W.; Gong, B.; Sun, J. Theoretical study on the interlay of hydrogen bonds in the trimers involving HCN and water. *Int. J. Quantum Chem.* **2009**, *109*, 1396–1402.

- (309) Sánchez, E. Q.; Dubernet, M.-L. Theoretical study of HCN–water interaction: five dimensional potential energy surfaces. *Phys. Chem. Chem. Phys.* **2017**, *19*, 6849–6860.
- (310) Bacelo, D. E. Theoretical Study of Microscopic Solvation of Ammonia in Water Clusters: $\text{NH}_3(\text{H}_2\text{O})_n$, $n = 3, 4$. *J. Phys. Chem. A* **2002**, *106*, 11190–11196.
- (311) Sorokin, A.; Dahlke, E. E.; Truhlar, D. G. Application of the Electrostatically Embedded Many-Body Expansion to Microsolvation of Ammonia in Water Clusters. *J. Chem. Theory Comput.* **2008**, *4*, PMID: 26621082, 683–688.
- (312) Zhong, J.; Zhao, Y.; Li, L.; Li, H.; Francisco, J. S.; Zeng, X. C. Interaction of the NH_2 Radical with the Surface of a Water Droplet. *J. Am. Chem. Soc.* **2015**, *137*, PMID: 26325351, 12070–12078.
- (313) Allodi, M. A.; Dunn, M. E.; Livada, J.; Kirschner, K. N.; Shields, G. C. Do Hydroxyl Radical-Water Clusters, $\text{OH}(\text{H}_2\text{O})_n$, $n = 1-5$, Exist in the Atmosphere? *J. Phys. Chem. A* **2006**, *110*, PMID: 17149847, 13283–13289.
- (314) Hernández-Soto, H.; Weinhold, F.; Francisco, J. S. Radical hydrogen bonding: Origin of stability of radical-molecule complexes. *J. Chem. Phys.* **2007**, *127*, 164102.
- (315) Suma, K.; Sumiyoshi, Y.; Endo, Y. The rotational spectrum of the water-hydroperoxy radical ($\text{H}_2\text{O}-\text{HO}_2$) complex. *Science (New York, N.Y.)* **2006**, *311*, 1278–1281.
- (316) Novakovskaya, Y. V.; Stepanov, N. F. Small Charged Water Clusters: Cations. *J. Phys. Chem. A* **1999**, *103*, 3285–3288.
- (317) Shi, Z.; Ford, J. V.; Wei, S.; Castleman, A. W. Water clusters: Contributions of binding energy and entropy to stability. *J. Chem. Phys.* **1993**, *99*, 8009–8015.
- (318) Berg, C.; Achatz, U.; Beyer, M.; Joos, S.; Albert, G.; Schindler, T.; Niedner-Schatteburg, G.; Bondybey, V. E. Chemistry and charge transfer phenomena in water cluster cations. *Int. J. Mass Spectrom. Ion Process.* **1997**, *167-168*, In Honour of Chava Lifshitz, 723–734.
- (319) Rodriguez-Cruz, S. E.; Jockusch, R. A.; Williams, E. R. Binding Energies of Hexahydrated Alkaline Earth Metal Ions, $\text{M}^{2+}(\text{H}_2\text{O})_6$, $\text{M} = \text{Mg}, \text{Ca}, \text{Sr}, \text{Ba}$: Evidence of Isomeric Structures for Magnesium. *J. Am. Chem. Soc.* **1999**, *121*, PMID: 16429613, 1986–1987.
- (320) Vicens, M. C.; López, G. E. Density functional studies of cation–water complexes. *J. Comp. Chem.* **2000**, *21*, 63–68.
- (321) Winter, B.; Weber, R.; Hertel, I. V.; Faubel, M.; Jungwirth, P.; Brown, E. C.; Bradforth, S. E. Electron Binding Energies of Aqueous Alkali and Halide Ions: EUV Photoelectron Spectroscopy of Liquid Solutions and Combined Ab Initio and Molecular Dynamics Calculations. *J. Am. Chem. Soc.* **2005**, *127*, PMID: 15884962, 7203–7214.

- (322) Westbrook, B. R.; Dreux, K. M.; Tschumper, G. S.; Francisco, J. S.; Fortenberry, R. C. Binding of the atomic cations hydrogen through argon to water and hydrogen sulfide. *Phys. Chem. Chem. Phys.* **2018**, *20*, 25967–25973.
- (323) Schwaab, G.; Sebastiani, F.; Havenith, M. Ion Hydration and Ion Pairing as Probed by THz Spectroscopy. *Angew. Chem. Int. Ed.* **2019**, *58*, 3000–3013.
- (324) Miyazaki, M.; Fujii, A.; Mikami, N. Binding Energy of the BenzeneâWater Cluster Cation:â An Ar-Mediated IR Photodissociation Study. *J. Phys. Chem. A* **2004**, *108*, 8269–8272.
- (325) Min, S. K.; Lee, E. C.; Lee, H. M.; Kim, D. Y.; Kim, D.; Kim, K. S. Complete basis set limit of Ab initio binding energies and geometrical parameters for various typical types of complexes. *J. Comp. Chem.* **2008**, *29*, 1208–1221.
- (326) Kim, H.; Lee, H. M. AmmoniaâWater Cation and Ammonia Dimer Cation. *J. Phys. Chem. A* **2009**, *113*, PMID: 19534557, 6859–6864.
- (327) Lu, W.; Mackie, C. J.; Xu, B.; Head-Gordon, M.; Ahmed, M. A Computational and Experimental View of Hydrogen Bonding in Glycerol Water Clusters. *J. Phys. Chem. A* **2022**, *126*, PMID: 35254809, 1701–1710.
- (328) Lee, H. M.; Tarakeshwar, P.; Park, J.; KoÅaski, M. R.; Yoon, Y. J.; Yi, H.-B.; Kim, W. Y.; Kim, K. S. Insights into the Structures, Energetics, and Vibrations of Mono-valent Cation-(Water)₁₋₆ Clusters. *J. Phys. Chem. A* **2004**, *108*, 2949–2958.

Appendix A

Supplementary Information: The cation, anion, and radical isomers of C_4H_4N : Computational characterization and implications for astrophysical and planetary environments

A.1 Vibrational frequencies and IR intensities for A^- , $A\dot{\cdot}$, and F^+

Table A.1: Vibrational frequencies and IR intensities for A^-

Frequency	IR Intensity
642.03	0.0
682.79	57.516
700.95	98.535
733.53	0.0
813.04	25.907
846.01	0.0
884.6	4.451
899.35	0.022
1025.23	31.391
1043.64	11.205
1115.5	20.587
1195.22	1.428
1243.65	1.118
1326.95	1.82
1410.68	0.256
1478.66	10.291
1494.52	38.188
3147.24	54.011
3153.06	33.075
3178.28	109.374
3200.96	39.631

Table A.2: Vibrational frequencies and IR intensities for A[•]

Frequency	IR Intensity
504.23	0.0
548.04	20.378
669.03	5.988
728.16	65.783
853.67	0.0
865.44	0.749
887.04	11.777
946.32	0.0
954.05	0.025
1056.39	0.004
1092.51	5.39
1106.2	38.617
1222.06	1.975
1303.57	0.262
1379.09	53.264
1474.31	24.184
1595.9	1.053
3215.39	17.32
3220.19	1.214
3249.43	5.199
3270.28	1.182

Table A.3: Vibrational frequencies and IR intensities for F^+

Frequency	IR Intensity
135.49	3.846
328.59	7.303
380.9	9.649
396.6	1.265
420.94	156.301
620.68	60.674
648.2	83.026
651.2	5.729
839.07	32.945
952.63	4.092
953.26	48.796
985.17	3.703
1129.33	35.499
1335.8	36.698
1436.34	10.625
2037.81	296.267
2383.97	328.508
3151.32	78.77
3195.48	42.715
3240.67	31.145
3720.83	1006.652

A.2 A comparison of DFT energies and CCSD(T)/CBS results

Table A.4: Relative energies of anionic isomers A-G, calculated both using the CCSD(T)/CBS scheme and the indicated density functional ω B97X-V in the aug-cc-pVTZ basis.

Anion Isomer CCSD(T) CBS	Relative energy CCSD(T) CBS	Anion Isomer ω B97X-V aug-cc-pVTZ	Relative energy ω B97X-V aug-cc-pVTZ
A ⁻	0.00	A ⁻	0.00
E ⁻	33.28	B ⁻	36.69
B ⁻	36.59	E ⁻	40.87
D ⁻	42.72	C ⁻	48.78
C ⁻	46.91	D ⁻	51.06
F ⁻	56.34	F ⁻	58.63
G ⁻	84.26	G ⁻	105.44

Table A.4 compares the energetic ordering of anionic isomers A-G calculated using two different methods: CCSD(T)/CBS and density functional theory (ω B97X-V/aug-cc-pVTZ). Comparing these results, the magnitude of sequential energetic differences between isomers is quite similar between the two schemes. In fact, the differences calculated with ω B97X-V in the large, augmented basis set are within 1 kcal/mol of those computed in CCSD(T)/CBS for isomers A-E. The fact that ω B97X-V is in such good agreement with CCSD(T)/CBS, largely considered the 'gold standard' when it comes to energetic calculations need to confirm this, speaks to the performance of this range-separated hybrid. With structures such as F⁻ and G⁻, which are strained and energetically disfavored on the anionic PES, we observe growing discrepancy between the DFT and CCSD(T) schemes, indicating that these are more difficult cases. Between the two schemes, energetic ordering of isomers with respect to the global minimum A⁻ did not change.

Table A.5: Relative energies of radical isomers A-G, calculated both using the CCSD(T)/CBS scheme and the indicated density functional ω B97X-V in the aug-cc-pVTZ basis. Structures were optimized using the latter DFT methodology, except in the cc-pVTZ basis.

Radical Isomer CCSD(T) CBS	Relative energy CCSD(T) CBS	Radical Isomer ω B97X-V aug-cc-pVTZ	Relative energy ω B97X-V aug-cc-pVTZ
A \cdot	0.00	A \cdot	0.00
C \cdot	24.73	C \cdot	23.07
E \cdot	24.79	E \cdot	24.06
B \cdot	25.12	B \cdot	31.06
D \cdot	28.81	D \cdot	36.10
F \cdot	44.29	F \cdot	50.29
G \cdot	53.91	G \cdot	56.90

Similarly to the anionic case, Table A.5 compares energetic differences calculated using the two indicated schemes. Re-calculation of energies using CCSD(T)/CBS on the radical surface did not result in any stability shuffling of isomers A-G. Again, we observe that the relative magnitude of energetic spacing does not change drastically, though the difference between DFT and CCSD(T) is slightly greater for radicals than the anionic case for A-E (between \sim 1-2 kcal/mol). We see that DFT and CCSD(T) again have the greatest disagreement for G \cdot , though the discrepancy is smaller here than for anionic G $^-$.

Table A.6: Relative energies of cationic isomers A-G, calculated both using the CCSD(T)/CBS scheme and the indicated density functional ω B97X-V in the aug-cc-pVTZ basis. Structures were optimized using the latter DFT methodology, except in the cc-pVTZ basis.

Cation Isomer CCSD(T) CBS	Relative energy CCSD(T) CBS	Cation Isomer ω B97X-V aug-cc-pVTZ	Relative energy ω B97X-V aug-cc-pVTZ
F $^+$	0.00	F $^+$	0.00
G $^+$	25.27	G $^+$	17.50
A $^+$	26.40	A $^+$	21.22
C $^+$	35.24	C $^+$	25.80
B $^+$	36.66	B $^+$	28.91
E $^+$	39.02	E $^+$	39.66
D $^+$	39.53	D $^+$	41.38

Energetic comparisons for cation isomers are shown in Table A.6. Interestingly, the magnitude of relative energy spacing between isomers is slightly more variable with the cations

between DFT and CCSD(T). While these were quite similar in the anions and radicals, DFT appears to estimate systematically lower relative stabilities of each isomer compared to the CCSD(T)/CBS scheme. Consequently, cationic isomers exhibit the largest difference between the two methods of calculation, on the order of ~ 2 -4 kcal/mol. Energetic ordering did not change with calculations involving CCSD(T)/CBS.

A.3 Optimized geometries for C_4H_4N

The following coordinates are optimized geometries for all C_4H_4N isomers.

- Anionic Isomers

A⁻

N -0.9624802558 0.6135819411 -0.3526541983
C 0.2668264351 1.1062912978 -0.0507659217
C 1.1594842426 0.0995237914 0.3272879094
C 0.4190488854 -1.1057490126 0.2511777676
C -0.8600467194 -0.7280559656 -0.1667123571
H 0.4655607851 2.1734306171 -0.1168627600
H 2.1984466906 0.2206276036 0.6164789950
H 0.7661501785 -2.1104397792 0.4699350787
H -1.7153202422 -1.3766704937 -0.3412445135

B⁻

N -0.9033907331 0.5762801707 -0.3310519950
C 0.3033419266 1.2131780174 -0.0522272959
C 1.1162596173 0.1261969790 0.3116517225
C 0.3958916609 -1.1088951686 0.2446367956
C -0.8784439457 -0.7960393671 -0.1639595771
H 2.1579141132 0.2151559590 0.6057044676
H 0.7561027996 -2.1084923897 0.4661549121
H -1.7448208477 -1.4209317369 -0.3443494421
H -1.7198545911 1.0776875363 -0.6281895877

C⁻

N -0.9401826089 0.5864419420 -0.3427445961
C 0.3231692301 1.1110994545 -0.0350303467
C 1.2220531651 0.1315723777 0.3421629133
C 0.4054480945 -1.0662231504 0.2424379389
C -0.8787734393 -0.7728306536 -0.1667437177
H 0.4485245796 2.1877070057 -0.1237187902
H 0.7388378094 -2.0791670349 0.4576688059
H -1.7481019343 -1.3958504016 -0.3482111216
H -1.7529248961 1.0960304607 -0.6401310858

D⁻

N -1.1122894575 -1.0578997366 0.2381823344
 C -1.7714827652 -0.7363697724 -0.6512493494
 C -2.5837444227 -0.3437886381 -1.8112622315
 H -2.1329514086 0.5821308802 -2.1897298199
 H -2.4271453528 -1.1239823920 -2.5859766057
 C -4.0560970168 -0.0814088210 -1.4691763877
 C -4.8799799372 -0.7496880127 -2.2921854933
 H -5.9663107925 -0.6618019376 -2.2202585505
 H -4.5305888467 -1.4349015698 -3.0918638963

E⁻

N -0.7503012118 -0.5530276260 0.1193076668
 C -1.6599257479 -0.6759504346 -0.5875552545
 C -2.7502596051 -0.8819498458 -1.4993050200
 H -2.5457617261 -1.6749555394 -2.2403223841
 C -3.8995972954 -0.1696187899 -1.4436442534
 C -4.8909449128 -0.5743805837 -2.5136869335
 H -5.8339273078 -0.8930361148 -2.0509969686
 H -4.5498337829 -1.3884248156 -3.1901709906
 H -5.1492984102 0.2936737497 -3.1338658620

F⁻

N -1.0303994730 -0.3382241056 -0.4653133644
 C -1.9303513063 -0.9159048756 -1.2120495607
 C -2.3582549102 -1.9804674492 -1.9639435329
 H -2.1878075499 -2.9672185703 -2.3701769672
 C -3.2325285303 -0.8942645244 -1.8608380834
 C -4.3950046594 -0.2389327366 -2.1187093924
 H -5.1717828461 -0.6840261095 -2.7350322240
 H -4.5726340581 0.7514286574 -1.7115525852
 H -1.3913966668 0.5737297138 -0.1902042898

G⁻

N -3.3597566270 0.6232007279 1.6769972932
 C -4.0660680243 0.2563168566 0.6686105823
 C -2.7874382953 0.0988248229 0.2530561232
 C -1.6032426934 -0.1338582189 -0.3690520345
 C -0.3024761652 0.0360585428 0.1084791768
 H -0.1193765576 0.4032347205 1.1123454562
 H 0.5460500775 -0.1995673442 -0.5244406825
 H -1.7101876612 -0.5083704477 -1.3916438818
 H -5.1340540534 0.1783103401 0.4441979671

- Radical Isomers

A[•]

N -0.9775147133 0.6231795275 -0.3584348114
C 0.2363992306 1.1039344510 -0.0592435893
C 1.1688042751 0.0572158447 0.3348616399
C 0.4604332948 -1.0957640250 0.2621911096
C -0.8712792272 -0.6991638899 -0.1732249433
H 0.4468373683 2.1656505860 -0.1214775382
H 2.2014934805 0.1961533515 0.6203555672
H 0.7891840428 -2.1025757978 0.4755220864
H -1.7166877516 -1.3560900480 -0.3439095209

B[•]

N -0.9379607715 0.5857614604 -0.3420852061
C 0.2805067645 1.0955567562 -0.0454029958
C 1.1547925697 0.1200003359 0.3235933103
C 0.3937489756 -1.0936742104 0.2423011624
C -0.8756310062 -0.7829192772 -0.1647900486
H 2.1870079971 0.2327656817 0.6121186495
H 0.7596585253 -2.0854491135 0.4647190904
H -1.7374900898 -1.4067198318 -0.3440880781
H -1.7416329647 1.1088181986 -0.6379958841

C[•]

N -0.9190615112 0.5880012645 -0.3365654120
C 0.3038377143 1.1541375875 -0.0458076556
C 1.1075014907 0.1140702192 0.3101797420
C 0.4074521227 -1.1091299446 0.2483978085
C -0.8616595394 -0.7672438009 -0.1628892042
H 0.4747604134 2.2154624314 -0.1194594208
H 0.7643132698 -2.1025876714 0.4684719535
H -1.7255842027 -1.3892106187 -0.3430997104
H -1.7335097576 1.0952805329 -0.6335381009

D[•]

N -1.3303368533 -1.0395051942 0.4041145085
C -1.8195794727 -0.7481530751 -0.5930926047
C -2.4304193677 -0.3768031907 -1.8769739891
H -1.9499604237 0.5408678978 -2.2293624816
H -2.2028683759 -1.1651982349 -2.6080781547
C -3.8984561501 -0.1892744760 -1.7806742998
C -4.9677658618 -0.7177812039 -2.3081487436
H -5.9650545881 -0.3606686846 -2.0698446651

H -4.8961489066 -1.5511938384 -3.0114595697
 E[•]
 N -0.8625347295 -0.2861580542 0.2240612829
 C -1.6488274805 -0.5977934252 -0.5561363658
 C -2.6039420227 -1.0176756014 -1.5445969368
 H -2.3025109022 -1.8553365162 -2.1772846679
 C -3.7755642128 -0.4422149886 -1.6953197804
 C -4.9728825827 -0.5574646425 -2.5330899727
 H -5.8533222471 -0.7619542613 -1.9188470380
 H -4.8583441834 -1.3718530175 -3.2611012768
 H -5.1519216390 0.3727805069 -3.0779252446
 F[•]
 N -0.9541710136 -0.2402439301 -0.2535562030
 C -1.3706023115 -0.8365298882 -1.2479211905
 C -2.5389689006 -1.5658491724 -1.6506068773
 H -2.4198730073 -2.6364525523 -1.7925317959
 C -3.6749566525 -0.9818414975 -1.9768795287
 C -4.7715471748 -0.3892979476 -2.3443364468
 H -4.8950771132 -0.0151773465 -3.3567890706
 H -5.5942250733 -0.2503511454 -1.6494563803
 H -0.0507387531 0.2218634800 -0.3557425069
 G[•]
 N -3.2506102776 0.5956036929 1.5815988547
 C -4.0644871384 0.2510716842 0.6430111723
 C -2.7570226013 0.1108508271 0.2839689901
 C -1.5999617273 -0.1504846449 -0.4044288994
 C -0.3434366803 0.0407510907 0.1269999122
 H -0.2195736889 0.4149802809 1.1360065502
 H 0.5434096577 -0.1789286205 -0.4526521051
 H -1.7109598863 -0.5262669607 -1.4173764061
 H -5.1339076577 0.1965726504 0.4814219312

- Cationic Isomers

A⁺
 N -0.9986170612 0.6362631940 -0.3656402549
 C 0.2101341858 1.1021076832 -0.0675527425
 C 1.1940670948 0.0237137640 0.3464433892
 C 0.5015403462 -1.1041157166 0.2746292877
 C -0.8819809245 -0.6739442104 -0.1799202063
 H 0.4242469141 2.1686260701 -0.1286299119
 H 2.2226350010 0.1999843008 0.6270971224

H 0.7957913525 -2.1236018533 0.4793562592
H -1.7301469086 -1.3364932318 -0.3491429429
B⁺
N -0.9560221545 0.6020365157 -0.3494463575
C 0.2449576831 1.0848280311 -0.0543844298
C 1.1663216444 0.0745485391 0.3321675927
C 0.4380086984 -1.0877436501 0.2546359118
C -0.8852097403 -0.7641114030 -0.1700535512
H 2.1968481709 0.2221134599 0.6161455479
H 0.7847242994 -2.0884013469 0.4725565904
H -1.7417254172 -1.4021755656 -0.3458352371
H -1.7649031842 1.1330454199 -0.6474160670
C⁺
N -0.9379594001 0.5927100371 -0.3426615498
C 0.2865320548 1.1460913202 -0.0504495622
C 1.1224779061 0.0722583896 0.3198588958
C 0.4535523643 -1.1035770881 0.2611580405
C -0.8782644706 -0.7388571605 -0.1714880112
H 0.4753598260 2.2087034827 -0.1185833158
H 0.7876903121 -2.1083347823 0.4761783777
H -1.7349644987 -1.3780558484 -0.3472273632
H -1.7563740938 1.1078416497 -0.6410955117

D⁺
N -2.2071039434 -0.6114787984 0.5246078961
C -2.1429332244 -0.6122867020 -0.6230954436
C -2.1943643505 -0.6144422781 -2.1023380372
H -1.7474948703 0.2996107771 -2.5063951138
H -1.7322108279 -1.5217643569 -2.5043497478
C -3.6333442483 -0.6266072411 -2.2074288648
C -4.8979630853 -0.6369746333 -2.2114704443
H -5.4686643469 -0.6413261395 -1.2776365958
H -5.4365111030 -0.6424406278 -3.1654136489

E⁺
N -1.1786413813 0.0137180816 0.2126837218
C -1.7730022090 -0.5275277201 -0.6076017428
C -2.5121695179 -1.2033640724 -1.6301073366
H -2.0902508912 -2.0809075248 -2.1378360910
C -3.6814163899 -0.8240078456 -1.9964111956
C -4.9581703338 -0.4788046345 -2.4565929352
H -5.7434866696 -0.6225131436 -1.7079413258

H -5.1077718430 -1.2734967383 -3.2312966082
 H -4.9849407643 0.4792335977 -2.9851364866
 F⁺
 N -0.7104140358 -0.2426819134 -0.5790386691
 C -1.5623194062 -0.8398424427 -1.0523525210
 C -2.5967652410 -1.5952845426 -1.6319595653
 H -2.4346912309 -2.6631135312 -1.7450544312
 C -3.7024085986 -0.9674798281 -2.0046690452
 C -4.7896367302 -0.3883067907 -2.3773877593
 H -4.8878168755 0.0046998660 -3.3859183333
 H -5.6249400654 -0.2870987798 -1.6894834174
 H 0.0388321836 0.2852279626 -0.1619562582

G⁺
 N -3.1492529721 0.5752065282 1.5237569173
 C -4.0556093915 0.2492686057 0.6362829612
 C -2.7442402781 0.1216291494 0.3111033275
 C -1.5847621024 -0.1654625106 -0.4434693354
 C -0.3884907980 0.0436271006 0.1350494602
 H -0.3067537223 0.4208605391 1.1502464043
 H 0.5327761971 -0.1610972972 -0.4000741845
 H -1.7080872065 -0.5403390429 -1.4516691539
 H -5.1321297262 0.2104569278 0.5173236031

- Other geometries

CN⁻
 C -0.0066988810 2.0275749722 0.0000000000
 N 1.1623288810 2.0998250278 0.0000000000
 CN[•]
 C -0.0020021193 2.0278652487 0.0000000000
 N 1.1576321193 2.0995347513 0.0000000000
 CH₃CCH
 C 0.9315029884 3.8196151807 0.0000012179
 C 0.5144221333 2.6963041658 0.0000344222
 H 1.3020741595 4.8178481822 -0.0000245175
 C 0.0056284086 1.3249918863 0.0000022324
 H -0.5497838183 1.1207682941 0.9179603345
 H 0.8279840203 0.6096399461 -0.0695462845
 H -0.6626978918 1.1626923448 -0.8484274050
 CN[•]/CH₃CCH complex
 N 0.7065375211 3.9923216928 2.9283206014

C 0.8058141647 3.9312577408 1.7829771206
C 0.9215648572 3.8327052759 0.3494314129
H 1.3107291144 4.6995565278 -0.1751815629
C 0.5665600324 2.7306388679 -0.2750475032
C 0.0258437545 1.4014764873 0.0234464307
H -0.9263041163 1.2489446745 -0.4903786475
H 0.7167956385 0.6220834484 -0.3067491207
H -0.1364709666 1.2924852846 1.1040812687
CN^{*}/CH₃CCH transition state
N 0.7935563669 4.4439318256 2.9780325571
C 0.8647763324 4.1655076652 1.8643016741
C 0.9641226718 3.8171741723 0.4728784569
H 1.3996304699 4.5540036850 -0.1948431960
C 0.5472857115 2.6599208100 0.0285457238
C 0.1075937290 1.4815994839 -0.3385614117
H -0.8948206140 1.3710538930 -0.7375954824
H 0.7929212606 0.6464801690 -0.4344815719
H -0.5592459280 0.6161982960 1.2973132501
CH₂CCHCN (cyanoallene)
N -0.5431985940 -0.2207507161 -0.8026836132
C -1.4639894836 -0.7973108656 -1.1806537338
C -2.5935505402 -1.5509169760 -1.6471470290
H -2.4901152869 -2.6302837232 -1.6845016320
C -3.7078211215 -0.9694619750 -2.0154223218
C -4.8169960817 -0.4077888214 -2.3815492076
H -4.9706044277 -0.1028958488 -3.4111435234
H -5.6093344645 -0.2257810739 -1.6634189392
Pyrrole
N -0.9180212282 0.5851864730 -0.3363163123
C 0.3020713831 1.1332804619 -0.0436268375
C 1.1432975142 0.1140759571 0.3208378542
C 0.3991453520 -1.0973080074 0.2442940616
C -0.8685241723 -0.7722000817 -0.1638875281
H 0.4694929969 2.1966575742 -0.1184346660
H 2.1777204521 0.2226157376 0.6104620889
H 0.7555370707 -2.0924154604 0.4643752977
H -1.7341890464 -1.3904875577 -0.3448392399
H -1.7265303220 1.1005949034 -0.6328647186

Appendix B

Supplemental Information: Hydrogen ejection from hydrocarbons: Characterization and relevance in soot formation and interstellar chemistry

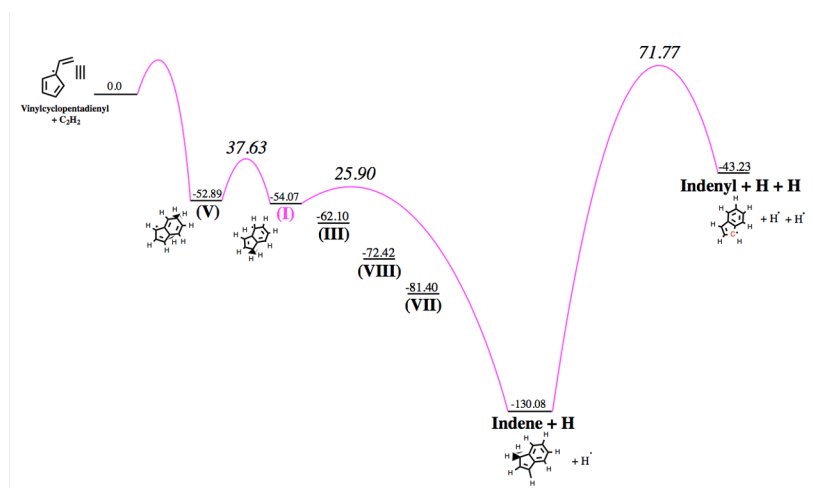


Figure B.1: Potential energy surface (PES) for sample CHRCR reaction sequence from vinylcyclopentadienyl to indenyl. Energetic barriers are expressed in kcal/mol. Isomerization barriers are shown for species (I).

Table B.1: Canonical RRKM rate constants for C₁₃H₁₁ (II)

Species	C13H11 (II) ZZ		C13H11 (II) FE	
Temp (K)	Barrier (kcal/mol)	Rate (s ⁻¹)		
500	29.86	0.9220	50.14	1.26E-9
600	29.85	168	50.13	6.870E-6
700	29.83	7110	50.11	3.3E-3
800	29.79	121000	50.08	0.34599
900	29.75	1120000	50.05	13.2
1000	29.7	6720000	50.01	246
1100	29.65	29500000	49.96	2720
1200	29.58	102000000	49.9	20400
1300	29.52	296000000	49.84	113000
1400	29.44	739000000	49.77	496000
1500	29.37	1640000000	49.7	1790000
1600	29.29	3330000000	49.63	5540000
1700	29.21	6230000000	49.55	15100000
1800	29.12	10900000000	49.48	36900000
1900	29.04	18100000000	49.4	82400000
2000	28.95	28600000000	49.31	170000000

Table B.2: Canonical RRKM rate constants for C₁₃H₁₁ (IV)

Species	C13H11 (IV) ZZ		C13H11 (IV) FE	
Temp (K)	Barrier (kcal/mol)	Rate (s ⁻¹)		
500	34.6599	7.3899E-3	74.62	2.52E-20
600	34.65	3	74.599	8.4100E-15
700	34.6199	226	74.56	7.6599E-11
800	34.5900	5910	74.52	7.3199E-8
900	34.5499	76300	74.4599	1.56E-5
1000	34.51	599000	74.39	1.15E-3
1100	34.450	3280000	74.31	3.939E-2
1200	34.39	13600000	74.22	0.75900
1300	34.32	46000000	74.13	9.34
1400	34.25	131000000	74.03	81
1500	34.17	328000000	73.92	530
1600	34.0900	735000000	73.81	2760
1700	34.01	1500000000	73.69	11900
1800	33.92	2860000000	73.5699	43800
1900	33.83	5080000000	73.45	141000
2000	33.74	8570000000	73.33	405000

Table B.3: Canonical RRKM rate constants for C₁₃H₁₀ (II)

Species	C13H10 (II) ZZ		C13H10 (II) FE	
Temp (K)	Barrier (kcal/mol)	Rate (s ⁻¹)		
500	67.64	2.8299E-17	80.73	5.3700E-23
600	67.62	2.94E-12	80.70999	4.9900E-17
700	67.58	1.16E-8	80.6800	9.4400E-13
800	67.52	5.95999E-6	80.63	1.56E-9
900	67.45999	7.78999E-4	80.58	5.0900E-7
1000	67.39	3.91000E-2	80.51000	5.2899E-5
1100	67.3	0.97499	80.44	2.3900E-3
1200	67.2099	14.4	80.36	5.800E-2
1300	67.11	141	80.27	0.86899
1400	67.0100	1010	80.17	8.91
1500	66.900	5600	80.06999	67.400
1600	66.78	25200	79.97	398
1700	66.66	95400	79.86	1920
1800	66.5400	313000	79.75	7780
1900	66.42	908000	79.64	27400
2000	66.2900	2380000	79.52	85200

Table B.4: Canonical RRKM rate constants for C₁₃H₁₀ (IV)

Species	C13H10 (IV) ZZ		C13H10 (IV) ZZ	
Temp (K)	Barrier (kcal/mol)	Rate (s ⁻¹)		
500	17.98	144000	65.53	2.3800E-16
600	17.97	3560000	65.5	1.7300E-11
700	17.95	36400000	65.4599	5.32E-8
800	17.91	213000000	65.41	2.26E-5
900	17.87	857000000	65.34	2.5500E-3
1000	17.82	2660000000	65.2600	0.114
1100	17.7600	6770000000	65.1800	2.58
1200	17.7	14900000000	65.08	35.1
1300	17.64	29300000000	64.97	324
1400	17.57	52700000000	64.86	2190
1500	17.5	88200000000	64.7399	11500
1600	17.4200	139000000000	64.62	49700
1700	17.3500	209000000000	64.4899	181000
1800	17.27	300000000000	64.36	575000
1900	17.18	418000000000	64.23	1620000
2000	17.100	564000000000	64.09	4130000

Table B.5: Canonical RRKM rate constants for C₉H₉ (V)

Species	C9H9 (V) FE		C9H9 (V) ZZ	
Temp (K)	Barrier (kcal/mol)	Rate (s ⁻¹)		
500	50.51	8.6999E-10	44.64	3.200E-7
600	50.5	5.0599E-6	44.62	6.99E-4
700	50.48	2.5300E-3	44.59	0.17499
800	50.46	0.27300	44.56	11.2
900	50.44	10.6	44.53	289
1000	50.45	196	44.5	3920
1100	50.49	2130	44.48	33400
1200	50.53	15700	44.48	198000
1300	50.57	85300	44.52	889000
1400	50.62	366000	44.56	3230000
1500	50.67	1290000	44.61	9900000
1600	50.73	3920000	44.66	26400000
1700	50.83	10300000	44.73	63000000
1800	50.96	24400000	44.8	137000000
1900	51.09	52600000	44.87	273000000
2000	51.23	105000000	44.95	510000000

Species	C9H9 (V) ZZ Barrier (kcal/mol)	G4(MP2) Rate (s ⁻¹)	C9H8 (V)	FE	C9H8 (V) ZZ
500	45.78	1.01E-7	59.1	1.53E-13	35.21
600	45.77	2.6699E-4	59.07	3.8099E-9	35.21
700	45.74	7.6600E-2	59.02	5.4600E-6	35.22
800	45.7	5.46	58.96	1.31E-3	35.22
900	45.65	154	58.88	9.4500E-2	35.2299
1000	45.6	2260	58.79	2.96	35.24
1100	45.53	20600	58.69	50.2	35.24
1200	45.47	131000	58.58	537	35.25
1300	45.39	634000	58.46	4030	35.26
1400	45.31	2460000	58.33	22900	35.2700
1500	45.23	8040000	58.2	104000	35.28
1600	45.14	22700000	58.07	390000	35.29
1700	45.06	57200000	57.93	1270000	35.299
1800	44.96	130000000	57.78	3620000	35.31
1900	44.87	273000000	57.64	9280000	35.32
2000	44.77	534000000	57.49	21800000	35.33

Table B.6: Canonical RRKM rate constants for C₉H₉ (V) and C₉H₈ (V)

Species	C9H9 (III) FE Barrier (kcal/mol)	Rate (s ⁻¹)	C9H9 (I) FE	C9H9 (I) ZZ	C9H9 (I) ZZ
500	31.91	0.11700	55.72	4.5899E-12	26.56
600	31.9	30	55.71	6.4000E-8	26.55
700	31.88	1620	55.68	6.02E-5	26.52
800	31.86	33000	55.65	1.05000E-2	26.48
900	31.82	351000	55.6	0.59	26.43
1000	31.78	2360000	55.55	15.1	26.37
1100	31.74	11300000	55.5	216	26.31
1200	31.69	42300000	55.43	2010	26.23
1300	31.64	130000000	55.36	13400	26.16
1400	31.58	342000000	55.29	68300	26.07
1500	31.53	797000000	55.21	282000	25.99
1600	31.47	1680000000	55.13	983000	25.9
1700	31.41	3250000000	55.05	2970000	25.8
1800	31.35	5860000000	54.96	7960000	25.71
1900	31.28	9980000000	54.87	19300000	25.61
2000	31.22	16200000000	54.78	43000000	25.51

Table B.7: Canonical RRKM rate constants for C₉H₉ isomers

Species	indene	cyclopentadiene	propyne
Temp (K)	Barrier (kcal/mol)	Rate (s^{-1})	
500	76.33	4.5200E-21	2.08E-24
600	75.8499	2.94E-15	3.600E-18
700	75.38	4.2500E-11	1.0799E-13
800	74.92	5.700E-8	2.54E-10
900	74.45	1.56E-5	1.09E-7
1000	74.02	1.39E-3	1.43E-5
1100	73.59	5.5E-2	7.799E-4
1200	73.19	1.17	2.2200E-2
1300	72.8	15.7	0.38100
1400	72.44	143	4.400
1500	72.099	977	36.9
1600	71.77	5250	239
1700	71.47	22900	1250
1800	71.2	85000	5450
1900	70.9300	275000	20500
2000	70.6800	787000	67600
		83.96	86.88
		83.85	86.19
		83.7	85.46
		83.53	84.72
		83.33	84.1
		83.12	83.48
		82.89	82.85
		82.65	82.21
		82.4	81.5699
		82.13	80.930
		81.87	80.3199
		81.59	79.8199
		81.31	79.33
		81.02	78.87
		80.73	78.400
		80.44	77.98
			1.100E-25
			5.0300E-19
			3.0300E-14
			1.2E-10
			7.0799E-8
			1.19E-5
			7.9500E-4
			2.6700E-2
			0.52400
			6.78
			61.9
			417
			2240
			9970
			37900
			126000

Table B.8: Canonical RRKM rate constants for indene, cyclopentadiene, and propyne.

Table B.9: Canonical RRKM rate constants for triplet cyclopentadiene and triplet toluene

Species	triplet cyclopentadiene		triplet toluene	
Temp (K)	Barrier (kcal/mol)	Rate (s ⁻¹)		
500	27.56	9.34	29.12	1.95
600	27.45	1260	29.08	320
700	27.3	43800	29.02	12700
800	27.12	649000	28.95	206000
900	26.93	5430000	28.86	1840000
1000	26.71	30300000	28.76	10800000
1100	26.48	125000000	28.66	46500000
1200	26.24	416000000	28.54	159000000
1300	25.99	1160000000	28.41	453000000
1400	25.73	2810000000	28.28	1120000000
1500	25.47	6090000000	28.15	2480000000
1600	25.19	12100000000	28.01	4990000000
1700	24.92	22200000000	27.86	9280000000
1800	24.63	38300000000	27.71	16200000000
1900	24.35	62600000000	27.56	26800000000
2000	24.06	97900000000	27.4	42200000000

Table B.10: Ordered energy barriers to ejection at 1600K

Molecule	Barrier (kcal/mol)	Ejection rate @ 1600K
propyne	89.146199700747133	417
cyclopentadiene	80.995772828244341	239
indene	79.029378318482912	5250
phen_edge_first	78.906932153509359	2760
c0_benz_edge	51.734000997748382	983000
c0_edge_first	48.200260604995293	3920000
alt_edge_first	43.27439456573984	5540000
c0_bay_first	39.656023116752834	26400000
phen_bay_first	25.765455064012883	735000000
c1	23.481738094482694	1680000000
alt_bay_first	19.323193595220403	3330000000
c0_benz_bay	18.323188450006	9670000000

Species	Avg E	Avg E cutoff 500	Monte Carlo no cutoff	Monte Carlo cutoff 500	BDE
I	9440000000	119000000000	134000000000	166000000000	28.38
III	20400000000	380000000000	308000000000	574000000000	32.659999999999997
VII	11900000000	223000000000	241000000000	453000000000	49.72
V	3690000000	393000000000	129000000000	133000000000	49.25
VIII	78100000000	1160000000000	1380000000000	2040000000000	41.5

Table B.11: Microcanonical rate constants for select species. "Cutoff 500" indicates that a low frequency cutoff was included - frequencies less than 500 are set to 500cm^{-1} . Monte Carlo sampling was used to determine the vibrational energy of reactant species preceding C_9H_9 . "Avg E" indicates the average thermal energy of reactants, and BDE indicates the barrier to dissociation in kcal/mol.

Table B.12: $k(E)$ calculated using MESMER for C_9H_9 (V)

Reaction	$k(E)$	Bath Gas	Method
V -j, $C_9H_8 + H$	2208991000000000	He	RRKM

Appendix C

**Supplementary Information:
Computational exploration of the
binding motifs and binding energies of
neutral molecules, radicals and ions
with small water clusters**

C.1 Binding Energies of lowest-energy conformers

Neutral closed-shell

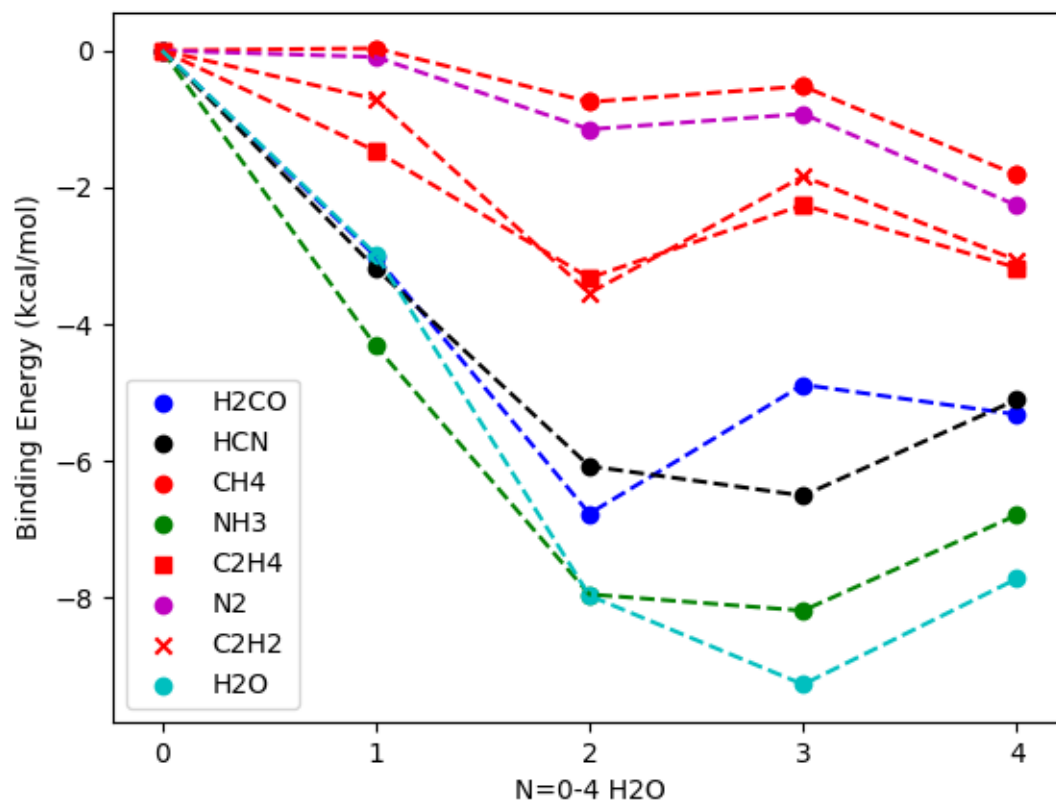


Figure C.1: DFT binding energies for closed-shell neutral molecules, zero point corrected.

Table C.1: Tabulated binding energies (in kcal/mol) for closed-shell neutral molecules with clusters of size $n=1-4$, zero point corrected.

Molecule	Monomer	Dimer	Trimer	Tetramer
H ₂ CO	-3.009	-6.768	-4.884	-5.319
HCN	-3.184	-6.074	-6.505	-5.103
CH ₄	-0.032	-0.752	-0.522	-1.820
NH ₃	-4.315	-7.948	-8.185	-6.788
C ₂ H ₄	-1.468	-3.323	-2.258	-3.174
N ₂	-0.095	-1.152	-0.926	-2.265
C ₂ H ₂	-0.711	-3.545	-1.840	-3.065
H ₂ O	-2.974	-7.966	-9.264	-7.719

Neutral open-shell

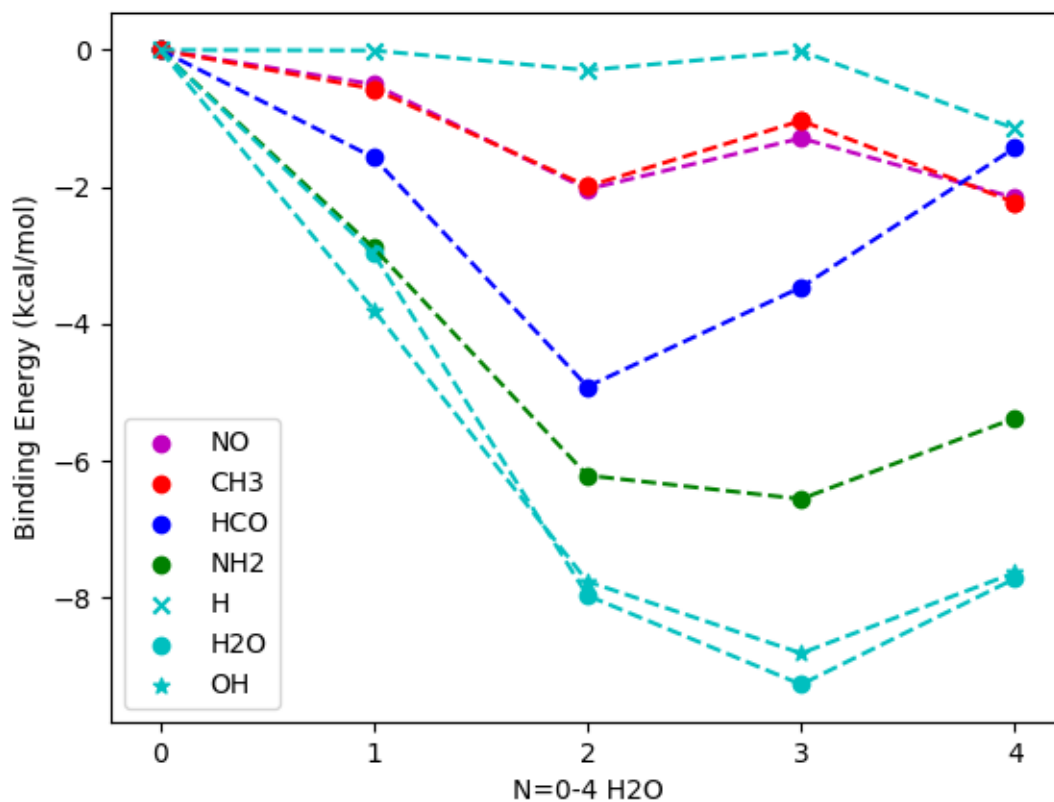


Figure C.2: DFT binding energies for open-shell neutral molecules, zero point corrected.

Table C.2: Tabulated binding energies (in kcal/mol) for open-shell neutral molecules with clusters of size $n=1-4$, zero point corrected.

Molecule	Monomer	Dimer	Trimer	Tetramer
NO [•]	-0.504	-2.035	-1.290	-2.161
CH ₃ [•]	-0.571	-1.993	-1.035	-2.229
HCO [•]	-1.571	-4.916	-3.465	-1.430
NH ₂ [•]	-2.890	-6.213	-6.557	-5.377
H [•]	-0.009	-0.297	-0.018	-1.149
OH [•]	-3.793	-7.761	-8.808	-7.633

Cationic closed-shell

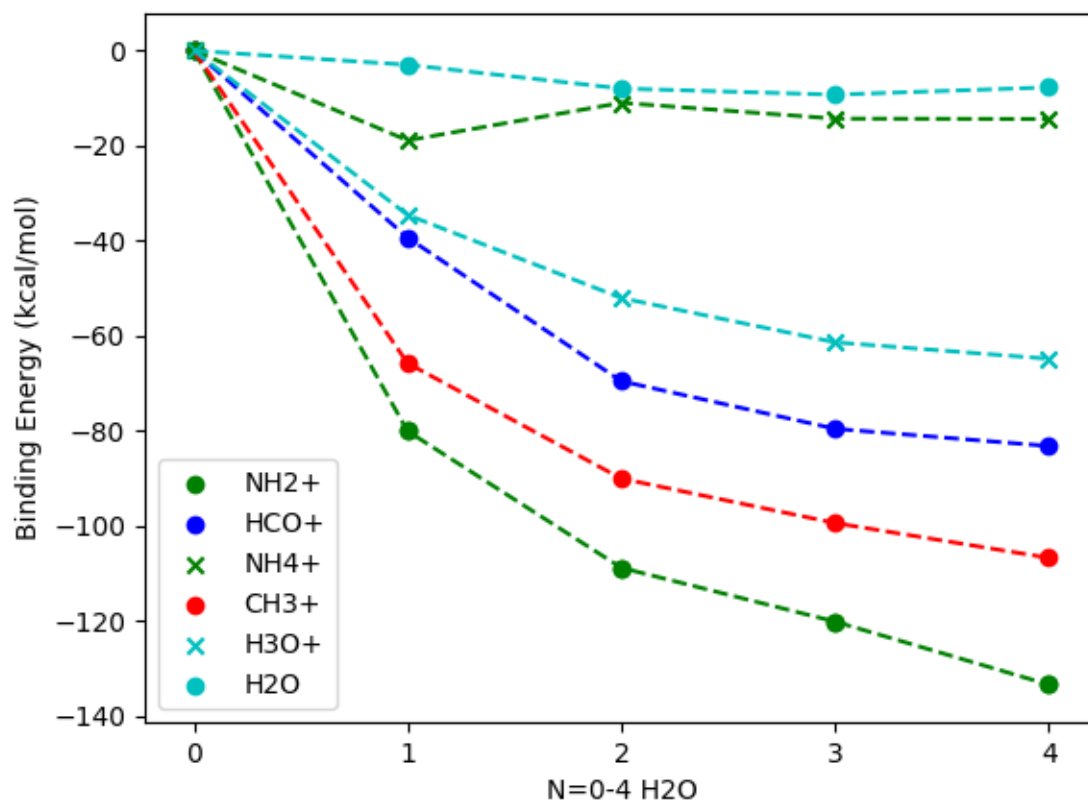


Figure C.3: DFT binding energies for closed-shell cationic molecules, zero point corrected.

Table C.3: Tabulated binding energies (in kcal/mol) for closed-shell cationic molecules with clusters of size $n=1-4$, zero point corrected.

Molecule	Monomer	Dimer	Trimer	Tetramer
NH ₂ ⁺	-80.090	-108.863	-120.199	-133.460
HCO ⁺	-39.355	-69.578	-79.602	-83.229
NH ₄ ⁺	-18.889	-10.975	-14.310	-14.389
CH ₃ ⁺	-65.806	-90.079	-99.448	-106.776
H ₃ O ⁺	-34.586	-52.064	-61.393	-64.860

Anionic closed-shell

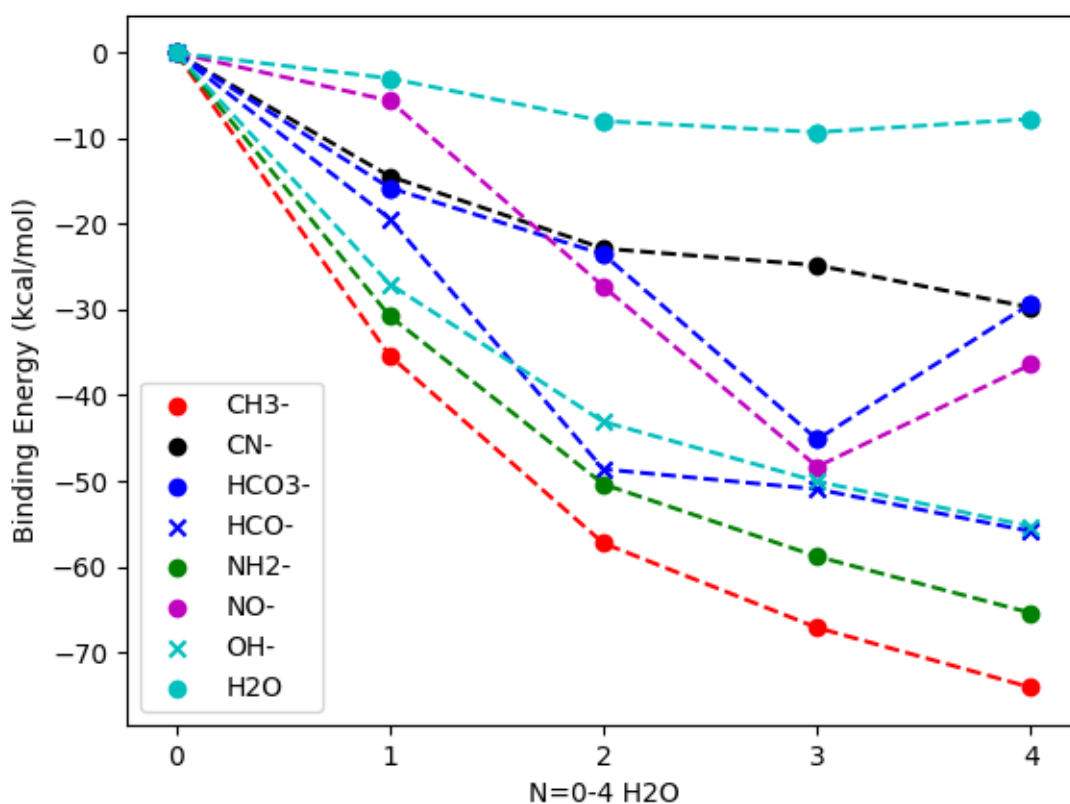


Figure C.4: DFT binding energies for closed-shell anionic molecules, zero point corrected.

Table C.4: Tabulated binding energies (in kcal/mol) for closed-shell anionic molecules with clusters of size $n=1-4$, zero point corrected.

Molecule	Monomer	Dimer	Trimer	Tetramer
CH ₃ ⁻	-35.367	-57.278	-67.147	-74.132
CN ⁻	-14.414	-22.854	-24.815	-29.743
HCO ₃ ⁻	-15.764	-23.530	-45.154	-29.286
HCO ⁻	-19.358	-48.638	-50.970	-55.895
NH ₂ ⁻	-30.741	-50.384	-58.835	-65.423
NO ⁻	-5.585	-27.290	-48.334	-36.399
OH ⁻	-27.001	-43.096	-50.065	-55.317

C.2 Coordinates for lowest energy conformers

Neutrals

Monomer

C2H2

H	2.804010641	-0.7676124665	0.0034732209
H	2.804661443	0.7670739775	0.0034754763
O	2.223230458	-0.0000231839	-0.0009334386
C	-2.280667129	-0.0001318207	0.0001263366
C	-1.072431095	0.0002545882	-0.0000364063
H	-3.356159537	-0.0004836197	0.0001946926
H	0.0076819719	0.0005599972	-0.0002842056

C2H4

H	-2.557680811	0.5754627337	-0.7628266896
H	-1.19266165	0.2631661049	-0.13494507
O	-2.120780177	0.4207858635	0.0805042297
C	1.044637996	-0.7940520911	0.1769394388
C	1.313219213	0.5004351782	-0.008426317
H	1.227993865	-1.534701106	-0.607312847
H	0.6360359097	-1.162987123	1.122755008
H	1.729772338	0.8683376912	-0.9510258117
H	1.134625302	1.238819731	0.7791991486

CH4

H	0.7857511354	0.0129455843	0.0137596563
H	2.168400144	0.6687433496	0.0054634444
O	1.725960303	-0.182012537	0.0890348733
C	-1.746808358	0.0137930585	-0.0118775933
H	-2.834173329	-0.1323274519	0.011330918
H	-1.457524084	0.3929404783	-1.002481525
H	-1.253266966	-0.950094671	0.1792163309
H	-1.465070192	0.7384488952	0.7655679038

H2CO

APPENDIX C. SUPPLEMENTARY INFORMATION: BINDING ENERGIES AND MOTIFS FOR ASTROCHEMICALLY RELEVANT MOLECULES

138

H	2.553062824	0.2096880354	-0.0234844281
H	1.024659424	0.4231331102	-0.0091409043
O	1.714488329	-0.2584119246	-0.0216785574
C	-1.348828745	-0.371279663	0.0022731605
O	-0.9310138852	0.7615735626	0.0100934347
H	-2.441251745	-0.5814911701	0.0077209405
H	-0.6560310134	-1.241734484	-0.0105471734

HCN

H	2.639012977	-0.7683203129	0.0007050755
H	2.637318021	0.7704207964	0.0006853622
O	2.059440041	0.0004111055	-0.0034907462
C	-1.054760908	-0.0002935582	0.0007236264
N	-2.208238879	0.0002270426	0.0062110705
H	0.0340791857	-0.0006839095	-0.0049786643

N2

H	2.623894485	-0.7388342145	0.0029373162
H	1.261448751	-0.0381299115	-0.0017948107
O	2.209948148	0.129684055	-0.0002393491
N	-2.124929845	0.0346159864	0.0006969385
N	-1.030707144	-0.0560739514	-0.0007752242

NH3

H	1.925969485	-0.773897111	0.0047643202
H	0.5732503691	-0.0270242996	-0.001663148
O	1.540742765	0.106737786	-0.0036144694
N	-1.3790347	-0.0108787681	-0.000011829
H	-1.673121942	0.5369223586	0.80576471
H	-1.680284053	0.4892676358	-0.8336268873
H	-1.88637106	-0.8923024059	0.0278865721

Dimer

C2H2

H	0.7266145758	2.109004357	-0.7539962544
---	--------------	-------------	---------------

APPENDIX C. SUPPLEMENTARY INFORMATION: BINDING ENERGIES AND MOTIFS FOR ASTROCHEMICALLY RELEVANT MOLECULES

139

H	-0.1777951849	1.264058082	0.1542844697
O	0.7204063828	1.618279799	0.0745485416
H	1.674423517	-0.0482066531	0.0545028362
H	2.704033479	-1.185749285	0.2795066746
O	1.807761835	-1.009685678	-0.0177539709
C	-2.351110626	-0.2218167132	0.0378205995
C	-1.30446834	-0.8270178618	-0.005684819
H	-3.29478955	0.293985374	0.0772460078
H	-0.3485463097	-1.334188572	-0.0353945495
C2H4			
H	2.484005386	-1.203728151	-0.9046698661
H	1.63673512	-0.0896508952	-0.2531732745
O	1.662937773	-1.04435202	-0.4320154862
O	0.8734214567	1.615711084	0.2026807831
H	1.048995138	2.072377802	1.031529305
C	-1.833622769	-0.1175222567	-0.5401680432
C	-1.488749078	-0.6977537904	0.6127637011
H	-1.202908261	-0.219550461	-1.428996797
H	-2.757469855	0.4601859134	-0.6404693281
H	-0.5676392481	-1.283657484	0.6898281912
H	-2.122143571	-0.6158273796	1.501562366
H	-0.0161462502	1.240648768	0.2915853525
CH4			
H	1.263228405	0.4901919635	-0.0943000997
H	2.051141254	1.807251674	-0.2544111786
O	1.182850282	1.456185122	-0.0401861511
H	-0.0687211089	-1.371451418	-0.2182822324
H	1.037327506	-1.861459919	0.7236810317
O	0.8897365576	-1.4049694	-0.1113693287
C	-2.123646051	0.129296457	0.0078516701
H	-1.2745362	0.8258649783	0.0399409021
H	-3.062613235	0.6975214994	-0.0013352193
H	-2.110741126	-0.5207961687	0.8956508514
H	-2.075366746	-0.4803410864	-0.9076341899

H₂CO

H	-0.6097499898	-2.750756216	-0.393673419
H	-0.8983398483	-1.257564204	-0.0980448481
O	-0.2022495162	-1.941325084	-0.0753709614
H	-2.328387947	0.6999819339	0.5840286658
H	-0.9151327499	0.9509189435	0.0043090418
O	-1.718579624	0.4058869698	-0.099133175
C	1.68418467	0.6676986366	0.1941388977
O	0.8372301236	1.533961623	0.1983498085
H	1.418763843	-0.4058585075	0.0897084364
H	2.759408994	0.9349959727	0.2962102577

HCN

H	1.102469079	0.8361007668	-0.0572692214
H	1.402842132	2.344492418	-0.2684004637
O	0.7032520989	1.725071173	-0.0463180093
H	0.4211758065	-1.438166089	-0.1127015265
H	1.750167137	-1.532626612	0.6564256463
O	1.306344829	-1.052599966	-0.0501473166
C	-1.679214663	0.0472102737	0.03922806
N	-1.937442251	-1.077652477	0.0455948393
H	-1.342666548	1.080890264	0.0266929432

N₂

H	1.21804135	0.8754565712	0.0827999819
H	1.160969498	2.393831913	0.3461366606
O	0.6367060489	1.651462377	0.033328203
H	2.131032196	-1.357262228	-0.7255194095
H	0.8210975529	-1.308507319	0.0751594907
O	1.735388229	-0.9983572139	0.0754452943
N	-1.391953083	-0.7475297994	0.0185764009
N	-2.348357221	-0.2082481397	0.0111229326

NH₃

APPENDIX C. SUPPLEMENTARY INFORMATION: BINDING ENERGIES AND
MOTIFS FOR ASTROCHEMICALLY RELEVANT MOLECULES

141

H	0.0585613676	-2.172045014	-0.6443813013
H	-0.6326444847	-0.9438503718	0.0244539046
O	0.1326393959	-1.562942722	0.0960185521
H	1.231130194	-0.041950787	0.065260824
H	2.351990186	1.0119074	0.2715107053
O	1.424368853	0.9147833159	0.0433066776
N	-1.578400365	0.6559800918	0.0001528538
H	-2.101967145	0.9411156281	-0.8238709568
H	-2.152587576	0.8564712026	0.815570494
H	-0.7395489988	1.236920975	0.055420759

Trimer

C2H2

O	-1.401486917	1.272041662	-0.1513499042
H	-1.559496852	0.5076962492	-0.7428533559
H	-2.207557793	1.795742088	-0.1542884943
O	-0.3995947332	-1.011941013	1.343521798
H	0.5539490217	-0.8618426527	1.357132475
H	-0.778992626	-0.1229402742	1.244939605
O	-1.458046412	-1.256684923	-1.21898093
H	-1.021906352	-1.480382912	-0.372371124
H	-0.9075009702	-1.62330951	-1.917154841
C	1.774450283	0.971991572	0.0297761669
C	2.849280227	0.4699492669	0.2647085286
H	0.8012977722	1.4021273	-0.1644212208
H	3.813874257	0.0371980418	0.4661257514

C2H4

O	-1.194688003	-1.497506861	0.5252314524
H	-1.852339134	-2.13534268	0.8157640389
H	-1.479258095	-0.6273458899	0.8617573399
O	-0.5723860178	0.1563369998	-1.696592318
H	-0.7680002204	-0.6683818853	-1.218094359
H	0.387981375	0.239731059	-1.63785965
O	-1.535379279	1.264370615	0.64215631

APPENDIX C. SUPPLEMENTARY INFORMATION: BINDING ENERGIES AND MOTIFS FOR ASTROCHEMICALLY RELEVANT MOLECULES

142

H	-2.260185198	1.895616139	0.6416376529
H	-1.265428957	1.139858472	-0.2914652701
C	2.176456673	-0.5893637014	0.1641966572
C	2.023574285	0.711758813	0.4237647969
H	2.818100967	1.43265968	0.2077977913
H	1.101632134	1.098812567	0.8694733064
H	3.10222953	-0.9771103765	-0.271688443
H	1.383339025	-1.308626614	0.3925516453

CH4

O	-0.5073907947	-1.57776307	0.7212278437
H	-0.8712998467	-1.205612747	-0.1039350818
H	-1.13192312	-2.245210839	1.019007457
O	-0.3225421516	1.154301245	1.299589195
H	0.5928500861	1.446642779	1.355721778
H	-0.2942724189	0.185570194	1.414732583
O	-1.24208385	0.3339073099	-1.191356083
H	-2.084037654	0.6680350609	-1.513366544
H	-0.9913689751	0.8969037036	-0.4320467419
C	2.301154095	0.0599027518	-0.7139940548
H	2.615208112	0.9774966179	-0.1948052093
H	3.144358464	-0.3174416279	-1.307994424
H	1.452356689	0.2807369856	-1.375193636
H	1.997547062	-0.7022805766	0.0168484322

H2CO

O	-1.603950187	-1.299878041	-0.2183380049
H	-2.113863413	-2.106535894	-0.1148541996
H	-0.7099666621	-1.546582709	-0.5326816992
O	-1.553237254	1.408118227	0.2072122758
H	-1.957329764	1.799495661	-0.5733375429
H	-1.710747166	0.4459004863	0.122209555
O	1.223105218	1.544637168	0.3856156033
H	0.2464137617	1.591591711	0.3302502703
H	1.514575952	2.408624725	0.6876855302
C	1.694776917	-1.053170227	0.0474630508

APPENDIX C. SUPPLEMENTARY INFORMATION: BINDING ENERGIES AND
MOTIFS FOR ASTROCHEMICALLY RELEVANT MOLECULES

143

O	1.047981008	-1.508347001	-0.8700602232
H	1.262479207	-0.9253359382	1.060483595
H	2.755339833	-0.758980566	-0.0857040244
HCN			
O	2.395562685	-0.0204224315	-0.2104396266
H	3.1676893	0.3330613571	-0.658562347
H	1.766376616	0.7221308626	-0.0899837661
O	-2.149994345	0.6784234377	0.1173230267
H	-2.853263325	0.8212031321	-0.523313077
H	-2.050639591	-0.2834507347	0.2043611141
O	0.3830031309	1.816430324	0.2103480386
H	-0.5266381186	1.467638273	0.1123152264
H	0.3764125917	2.329871699	1.023873888
C	0.1238846722	-1.808407047	0.1220878176
N	-0.9966380293	-2.050895781	0.2554178594
H	1.163349715	-1.492238995	-0.0180398601
N2			
O	1.551030423	-0.3521967872	1.099114327
H	1.495675373	0.4867973473	0.599283898
H	2.417554637	-0.3712471235	1.514694236
O	0.320016349	-1.201701811	-1.240942017
H	0.6209703537	-1.931576843	-1.789153607
H	0.7997023397	-1.267752484	-0.3941737219
O	0.9266415009	1.50918635	-0.8628214349
H	0.1098597358	1.988335059	-0.6876243319
H	0.6470110531	0.6881200641	-1.308750623
N	-1.943274583	-0.4090699203	1.263123309
N	-1.685247546	0.5286477873	0.7518623827
NH3			
O	1.26513004	1.4252594	0.0323911301
H	1.830335883	1.827829915	0.6976562913
H	1.482735838	0.4547752415	0.0172174742
O	-1.428305463	-1.414242958	0.0786696208

APPENDIX C. SUPPLEMENTARY INFORMATION: BINDING ENERGIES AND MOTIFS FOR ASTROCHEMICALLY RELEVANT MOLECULES

144

H	-1.554426045	-0.441568719	0.0546898733
H	-2.2206083	-1.778279966	0.4813193018
O	-1.453416358	1.346486535	0.0103121691
H	-0.4818511161	1.495583382	0.0628299847
H	-1.741915245	1.798402137	-0.7882314577
N	1.548954088	-1.330442419	-0.0972266033
H	1.860733797	-1.664411747	-1.006572405
H	2.073088924	-1.843450639	0.6080294821
H	0.5604184511	-1.58403525	0.0023715262

Tetramer

C2H2

O	-2.02343058	-0.6945210994	1.382644795
H	-1.833932119	-0.5976381837	2.320581636
H	-2.102162155	0.2183191234	1.021335425
O	-1.908946336	1.727813877	0.1668721363
H	-2.602759795	2.153471302	-0.3448417591
H	-1.176815088	1.533079123	-0.4623160926
O	-0.2910938229	-1.774610044	-0.3938015415
H	-0.6802217005	-2.54344535	-0.8206790456
H	-0.923916769	-1.495124026	0.3093508149
O	0.0708179004	0.7973976491	-1.451938926
H	-0.0345373584	-0.1550361347	-1.25642877
H	0.9848427264	0.9960192602	-1.213819094
C	3.44392117	0.3869521398	0.1850579201
C	2.580163942	-0.4588472895	0.1632957516
H	4.222381935	1.129225137	0.2134895768
H	1.788471406	-1.194232464	0.1256088469

C2H4

O	-0.7260237318	0.0619789788	1.884938475
H	0.1915776655	-0.0048738216	2.171309961
H	-0.895294282	-0.7477923802	1.356798048

APPENDIX C. SUPPLEMENTARY INFORMATION: BINDING ENERGIES AND
MOTIFS FOR ASTROCHEMICALLY RELEVANT MOLECULES

145

O	-1.076610365	-1.947338106	0.0334219911
H	-1.004266834	-1.366763905	-0.7595109297
H	-1.869322224	-2.478036998	-0.0820944568
O	-1.079941578	1.945396537	-0.0434782425
H	-1.874779018	2.474433622	0.0648403287
H	-1.013600425	1.364944939	0.750071751
O	-0.7089852475	-0.0631935237	-1.891814162
H	-0.8844939014	0.7461571668	-1.365060622
H	0.2111770903	0.0052297267	-2.169476075
C	2.249150972	-0.6655255728	0.0292453814
C	2.248420451	0.6693339932	-0.0089696114
H	3.185466598	-1.231027983	0.049952674
H	1.320823098	-1.244938179	0.0418195946
H	3.184123987	1.236078624	-0.0218976575
H	1.319458515	1.247515304	-0.029250189
CH4			
O	-0.627798616	-1.041895243	1.612451044
H	0.1471613556	-1.256974162	2.14050465
H	-0.6470480685	-0.0610068203	1.545246694
O	-0.6323862464	1.633631763	1.029494792
H	-0.5843833725	1.568450371	0.0481482794
H	-1.383957245	2.200130826	1.225477691
O	-0.6690677328	-1.602244379	-1.055347686
H	-0.656513081	-1.538474632	-0.0728360249
H	-1.438923195	-2.131934442	-1.281079609
O	-0.5120382232	1.06961998	-1.635118738
H	-0.5818029484	0.0909028037	-1.569770647
H	0.2945783264	1.245912309	-2.12904133
C	2.427454229	-0.0583278282	0.0473660161
H	3.093016006	0.4688112353	-0.6505202688
H	1.79901528	0.6709721128	0.5760599791
H	3.036658923	-0.6167774723	0.7718512365
H	1.786569196	-0.7565174694	-0.5077327549
H2CO			

APPENDIX C. SUPPLEMENTARY INFORMATION: BINDING ENERGIES AND MOTIFS FOR ASTROCHEMICALLY RELEVANT MOLECULES

146

O	0.3916126167	0.141904563	1.764919273
H	1.27264204	0.1868019533	1.355709867
H	-0.0968461342	0.887149104	1.366507763
O	-0.9949436784	1.882256022	0.0665069349
H	-1.44177987	1.208824967	-0.4865337182
H	-1.623576038	2.595479525	0.2045702566
O	-1.784871696	-0.3500496202	-1.320423704
H	-1.593340992	-1.053247862	-0.6571612367
H	-2.564316638	-0.6253318028	-1.809485736
O	-0.8565756637	-1.943495126	0.6354891256
H	-1.23727943	-2.561638999	1.264626958
H	-0.3844512017	-1.248974801	1.162327798
C	1.820012634	0.0843569556	-1.172345149
O	2.484918953	0.1705251561	-0.1666895989
H	2.3031361	0.0628781805	-2.174484778
H	0.711126156	0.0240455176	-1.145319716
HCN			
O	0.8210017528	-1.750359827	-0.4757872344
H	0.0835391516	-1.93309529	-1.071414409
H	0.4083278036	-1.585414094	0.3951382429
O	-0.225662835	-0.6881298905	1.864025505
H	-0.2277569391	0.2735205603	1.700017519
H	-0.944480432	-0.8771624879	2.473083684
O	1.783129603	0.7419461663	-0.8421348364
H	2.73364143	0.7801245171	-0.9760735069
H	1.533032665	-0.2136349075	-0.7969669836
O	-0.0173126591	1.875050195	0.7625983213
H	0.7637542662	1.617490944	0.2135378954
H	0.1779434234	2.7326627	1.150169477
C	-1.724944715	0.1775787516	-1.163597846
N	-2.064166042	-0.75423368	-1.75384938
H	-1.366640886	1.027761668	-0.5849616486
N2			
O	0.0276679071	-0.9274662562	1.813081231

APPENDIX C. SUPPLEMENTARY INFORMATION: BINDING ENERGIES AND MOTIFS FOR ASTROCHEMICALLY RELEVANT MOLECULES

147

H	0.8169709041	-0.871343822	1.226985642
H	0.1884598602	-1.65783906	2.417355759
O	-1.959931128	-0.7215683244	-0.0481042322
H	-1.356629149	-0.8490719671	0.7177150172
H	-2.472121765	0.0680417315	0.1530394454
O	-0.0269897797	-0.5502427633	-1.961820887
H	-0.1892480647	-1.145606262	-2.69914337
H	-0.816440268	-0.6095902437	-1.376267144
O	1.960411127	-0.7183635034	-0.0965904768
H	1.357612863	-0.6916332622	-0.8728809341
H	2.472431857	0.0955742389	-0.1367755633
N	0.5455669343	2.172681203	0.1661776881
N	-0.547940894	2.162178173	0.2745620116
NH3			
O	-1.439361779	-1.756198344	-0.1477804193
N	-2.297933582	0.8633446089	0.0300831309
H	-2.836231583	1.242036931	-0.7463577844
O	2.298086782	0.4873769293	-0.2107708736
O	0.2964017646	2.325868145	0.1585131788
O	1.222499269	-1.963713285	0.2332293024
H	-1.790506649	-0.8231425909	-0.114406601
H	-1.899396165	-2.203028751	-0.8636888176
H	1.036271346	1.699166091	0.0026666309
H	0.6754193133	3.067337753	0.6373359538
H	1.346452637	-2.433117705	1.063041241
H	0.2487596879	-1.930885838	0.0788750415
H	1.956973488	-0.4166678082	-0.0196089772
H	2.760848499	0.4207559884	-1.051005444
H	-1.445209255	1.429061263	0.1131928707
H	-2.847397489	1.014278538	0.8736625812

Waters

1 H₂O

H	-1.966791369	-0.032544997	0.7357820357
H	-0.5967835665	0.0111193412	0.0556869653
O	-1.541813065	0.0048656558	-0.127074001

2 H₂O

H	-1.952444862	-0.0226870845	0.7397786684
H	-0.5766544826	0.0037487093	0.0518100216
O	-1.5306734	-0.0003253802	-0.1240350385
H	1.737845533	0.775504486	-0.3359706079
H	1.718018583	-0.7586896293	-0.3923715001
O	1.361215629	-0.0034391013	0.0876404564

3 H₂O

H	8.871674113	-2.302441003	-0.1479359748
O	7.960600045	-1.954978116	-0.1103272445
H	7.455124119	-2.560896406	0.4386181204
O	10.74372497	-1.945616527	-0.2075882374
H	10.5582384	-1.001782673	-0.0372385661
H	11.44518832	-2.198944376	0.3992096713
O	9.354488888	0.4137671842	0.282371004
H	8.611285603	-0.2155251413	0.2134492007
H	9.17337554	1.112017056	-0.3538579736

4 H₂O

O	-1.918192432	-0.1659027893	-0.0698529222
H	-2.475390867	-0.3678755499	-0.827123346
H	-1.269493146	-0.902102081	-0.0003316406
O	0.1659027894	-1.918192432	0.0698529222
H	0.9021020812	-1.269493146	0.0003316405
H	0.36787555	-2.475390866	0.8271233461
O	-0.1659027894	1.918192432	0.0698529222
H	-0.36787555	2.475390866	0.8271233461
H	-0.9021020811	1.269493146	0.0003316405

APPENDIX C. SUPPLEMENTARY INFORMATION: BINDING ENERGIES AND
MOTIFS FOR ASTROCHEMICALLY RELEVANT MOLECULES

149

O	1.918192432	0.1659027893	-0.0698529222
H	1.269493146	0.902102081	-0.0003316406
H	2.475390867	0.3678755499	-0.827123346
5 H ₂ O			
O	-1.979164662	-0.9752464684	-0.1333940393
H	-2.724196115	-1.580212744	-0.1508093896
H	-1.155967732	-1.515221071	-0.1552687427
O	-1.656148278	1.69908488	0.0929915574
H	-2.040397496	1.958476358	0.9356754278
H	-1.857245545	0.7420033593	-0.0109674338
O	2.204771167	-0.3545974462	0.2854394542
H	2.708157039	-0.2533876182	1.098120629
H	1.824705835	0.5315921519	0.0826485579
O	0.3852046751	-2.30653277	-0.162353734
H	0.6857677217	-2.750827259	-0.9607295662
H	1.079994559	-1.639296841	0.046915864
H	1.171097472	2.54409113	-1.00257239
H	0.040081115	1.959549778	-0.1022849594
O	1.018035054	2.027045272	-0.2066417847

Guest Molecules

Neutral

C2H2

C	-0.5728415213	-3.454064902	3.471021629
C	-1.747248847	-3.479192102	3.192841729
H	0.4735815828	-3.431659456	3.719051555
H	-2.793721215	-3.501573539	2.945015087

C2H4

C	0.9568011024	0.00318	0.08197
C	2.289218898	0.00318	0.08197
H	0.3849229642	-0.7562021851	-0.4593338408
H	0.3849229643	0.7625621851	0.6232738408
H	2.861097036	-0.7562021852	-0.4593338408
H	2.861097036	0.7625621852	0.6232738408

CH4

C	0.9739298629	-0.0645022604	-0.0718313213
H	2.072465064	-0.0644987968	-0.0718297382
H	0.60775815	-0.9376276186	-0.6289216124
H	0.6077488058	0.8545102251	-0.5494368022
H	0.6077481177	-0.1103915493	0.9628594741

H2CO

C	1.109492394	0.0147072554	0.0811775544
O	2.311939674	0.0147106785	0.0811790468
H	0.5217721935	0.1823962238	1.014633524
H	0.5217757383	-0.1529841577	-0.8522801265

HCN

C	1.640294635	0.3550975628	-0.0519835043
N	1.421714728	-0.7575716612	0.0568516003
H	1.833556339	1.388401309	-0.1547014903

APPENDIX C. SUPPLEMENTARY INFORMATION: BINDING ENERGIES AND
MOTIFS FOR ASTROCHEMICALLY RELEVANT MOLECULES

151

N ₂			
N	1.027357379	-0.09019	-0.02861
N	2.126032621	-0.09019	-0.02861
NH ₃			
N	1.035230477	-0.0388327073	0.0626743277
H	2.051629585	-0.0271809059	0.0965853727
H	0.7133298329	0.9016266234	0.2777791901
H	0.7133301053	-0.6485030101	0.8103611095
Openshell			
CH ₃			
C	0.93655	-0.05171	-0.05745
H	0.57988	0.68543	-0.74616
H	0.57989	-1.01672	-0.35147
H	2.00655	-0.05171	-0.05745
H			
H	2.00655	-0.05171	-0.05745
HCO			
C	1.07457	0.06658	-0.00246
H	0.53957	-0.73645	-0.46487
O	2.34547	0.06658	-0.00246
NH ₂			
N	1.04338	-0.03134	0.08448
H	2.06338	-0.03134	0.08448
H	0.70338	0.91253	0.26861
NO			
N	1.073542937	0.6106898649	0.0009044974
O	1.667972733	-0.3686721357	-0.0010639941

OH			
H	0	0	0.8663813032
O	0	0	-0.1099422262

Cation

CH3+			
C	0.0000032714	-0.0000298969	-0.0775354001
H	0.9546621483	0.5529802657	-0.0775924844
H	-0.9566234571	0.5495697024	-0.0775971166
H	0.0019757875	-1.103237593	-0.0775111932

H3O+			
O	-0.0000130167	0.0000075768	0.0312951382
H	0.9320559438	-0.1730151368	-0.2225543038
H	-0.3161903233	0.8937058763	-0.2225510194
H	-0.6158494911	-0.7206979722	-0.222552912

HCO+			
C	0	0	-0.5081244415
O	0	0	0.5992067956
H	0	0	-1.617130354

NH2+			
N	0	0	0.155203168
H	-0.8541799782	0	-0.4702005647
H	0.8541799782	0	-0.4702005647

NH4+			
N	0.0000010615	-0.0000042117	-0.0000016166
H	1.011796512	-0.0594179469	-0.1774732573
H	-0.2767944621	0.9878049442	0.0798368867
H	-0.2239408969	-0.4908364427	0.8761776007
H	-0.5110572944	-0.4375581728	-0.7785434033

Anion

CH3-			
C	0.0000033078	-0.0001167086	0.2799500535
H	0.8768930854	0.5081535415	-0.1968200298
H	-0.8786926057	0.5050173603	-0.1968278113
H	0.0018139626	-1.013771715	-0.1965384068
CN-			
C	0	0	-0.6353371601
N	0	0	0.5383394678
HCO3-			
C	0.1083974472	0.0187565268	0
O	-0.0141217151	1.264542503	0
O	-1.137498121	-0.6777243746	0
O	1.105335913	-0.7118356825	0
H	-1.780255678	0.0409183835	0
HCO-			
C	0.6030125635	-0.2707777334	0
H	1.288532498	0.7198222887	0
O	-0.5934685434	0.0819339428	0
NH2-			
N	0	0	0.1709897847
H	-0.7973723654	0	-0.4780938731
H	0.7973723654	0	-0.4780938731
NO-			
N	0	0	0.6686855969
O	0	0	-0.5923093182
OH-			
H	0	0	2.071788549
O	0	0	1.106491931

Radicals

Monomer

CH3

H	0.64522163	-0.0789415549	0.005139095
H	1.920378308	0.7693709269	-0.0107190611
O	1.609986718	-0.1414977007	0.0072642871
C	-1.663086147	0.0384930628	-0.0004484815
H	-1.552444526	-1.047239551	0.007044264
H	-1.771369254	0.5659424858	-0.9491960834
H	-1.776929855	0.5784367186	0.9405810279

H

H	0.8843644093	-0.8045705162	0.0001870074
H	-0.3668622801	0.0763729619	0.0003419075
O	0.5950541685	0.1135017021	0.0003888223
H	-3.109579602	-0.1077048725	-0.0003890996

HCO

H	2.497825579	0.2889925158	-0.3127685739
H	1.015687299	0.6735793641	-0.1645533194
O	1.61964652	-0.0788379842	-0.1815477431
C	-1.3585437	-0.6261883118	0.2690409785
H	-0.5066984516	-1.362242204	0.2144840892
O	-1.231262463	0.5390468526	0.1381422858

NH2

H	2.333365809	0.5239278743	0.1331029314
H	0.9551737207	-0.1217597824	-0.0998400416
O	1.911090397	-0.2873485127	-0.1634453564
N	-1.031857732	-0.0890083665	-0.0741271582
H	-1.512145043	-0.9577188427	-0.3448197411
H	-1.785888118	0.5776304338	0.1352463784

NO

APPENDIX C. SUPPLEMENTARY INFORMATION: BINDING ENERGIES AND MOTIFS FOR ASTROCHEMICALLY RELEVANT MOLECULES

155

H	2.758476396	0.5029612006	0.1722020849
H	1.272131876	0.1459853959	0.0603093822
O	2.157852865	-0.2329936673	0.0182572067
N	-0.9865836267	0.5429403242	0.0491600369
O	-1.792666888	-0.252727851	-0.1083514178

OH

H	1.55238691	-0.8068755158	0.0898342471
H	1.730246161	0.7255939553	-0.003031995
O	1.072323176	0.0233999373	0.0113368136
H	-0.7840014845	0.2453183683	0.0264101494
O	-1.759526943	0.3706176169	0.0343974326

Dimer

CH3

H	0.8121014483	0.9488753294	-0.0895759328
H	0.1908172548	2.116446795	0.6941115925
O	0.08042665	1.585792452	-0.1019268525
H	-2.539511388	-0.6506024201	-0.2861046681
H	-1.266561079	0.1972421975	-0.0710912347
O	-1.623766696	-0.7035935849	-0.0002289413
C	1.789713927	-1.103893808	-0.0104596988
H	2.381106561	-1.059801455	0.9059571413
H	2.291388348	-1.002846185	-0.9748263428
H	0.7340797948	-1.384278235	0.0293520033

H			
H	1.986982405	-0.5333258467	-0.2443650656
H	0.4987245105	-0.1710431028	-0.1011836594
O	1.386140965	0.2140739204	-0.1757033966
H	-1.726320724	-0.3290040247	0.9212196221
H	-1.907612054	-0.2293415036	-0.5995993067
O	-1.369834815	-0.6443220465	0.0835876354
H	-0.7154407822	2.85214162	-0.1665936407

APPENDIX C. SUPPLEMENTARY INFORMATION: BINDING ENERGIES AND
MOTIFS FOR ASTROCHEMICALLY RELEVANT MOLECULES

156

HCO			
H	1.008583211	-0.9881491131	0.0534790058
H	2.304809143	-0.4731447753	-0.6031658544
O	1.674429948	-0.2846409493	0.0991983974
H	0.561647587	1.223684417	0.0937674249
H	-0.0199819177	2.631747901	0.3905820232
O	-0.25260581	1.758769434	0.0636744279
C	-1.777045489	-0.9675886551	-0.1482601332
O	-0.8649963335	-1.721013334	-0.1205782558
H	-1.676454269	0.1519142375	-0.0680161833
NH2			
H	0.9189905379	-0.8439553305	0.1372147659
H	2.19257243	-0.2421702117	-0.5116358042
O	1.551053625	-0.0987982171	0.1904268034
H	-0.8628353186	2.31821994	0.1224684509
H	0.0995552739	1.104358255	0.0398126612
O	-0.8347943076	1.372464965	-0.0409169855
N	-0.8456609504	-1.589218103	0.0188461858
H	-1.420670176	-0.7330522027	-0.0135687907
H	-1.498265047	-2.380774479	0.0137250102
NO			
H	-1.18580102	1.113249457	0.114186941
H	-2.403395584	0.8595095751	-0.7911984716
O	-1.987792703	0.5795087135	0.0308967211
H	-0.9447588571	-1.054488102	0.098754896
H	-0.327082505	-2.39085041	0.5658220218
O	-0.1189900083	-1.564972448	0.1201559352
N	1.084878411	1.059560576	0.3916126055
O	1.946328071	0.8709681203	-0.3357909553
OH			
H	0.1337929788	-2.21218928	0.3683863541
H	-0.6601130101	-1.017006571	-0.2269627852
O	0.2133551747	-1.448643784	-0.2110124123

APPENDIX C. SUPPLEMENTARY INFORMATION: BINDING ENERGIES AND
MOTIFS FOR ASTROCHEMICALLY RELEVANT MOLECULES

157

H	-2.28562082	1.181084859	-0.3726437225
H	-0.8042341116	1.163784051	0.1047175519
O	-1.602936445	0.6189679987	0.0030867647
H	1.10256427	0.0927708211	0.166650989
O	1.216864014	1.067042523	0.3229388424

Trimer

CH3

O	0.3742896226	0.3701542195	1.04458665
H	1.227812695	0.2609427762	0.602830909
H	-0.0795608773	-0.4852251987	0.9386844777
O	-1.474089753	-1.479148182	0.0464094083
H	-1.880157694	-0.6488112516	-0.2666418891
H	-2.190579199	-2.093635714	0.2251036439
O	-1.761732961	1.236220481	-0.4908046787
H	-2.322336082	1.913786225	-0.1018747363
H	-0.9479573656	1.208935249	0.0529310595
C	3.016446822	-0.1287219851	-0.7422393838
H	3.461812468	-0.8616926918	-0.0678456412
H	3.325058588	0.9165898212	-0.6890227159
H	2.348064792	-0.4581838933	-1.539342989

H			
O	1.525684724	-0.5784224301	-0.3595635754
H	1.226273165	0.3285721183	-0.1568043111
H	2.055357464	-0.5108531088	-1.159700668
O	-0.1583437082	1.576914625	0.1448873803
H	-0.8195505649	0.8594967535	0.117070787
H	-0.3547355115	2.102493054	0.9255782134
O	-1.227829429	-0.9628862652	-0.2518568382
H	-1.570948516	-1.646224314	0.3311388857
H	-0.2744245516	-1.145589849	-0.3606967972
H	0.4750712363	-0.6526218694	3.035572797

HCO

APPENDIX C. SUPPLEMENTARY INFORMATION: BINDING ENERGIES AND
MOTIFS FOR ASTROCHEMICALLY RELEVANT MOLECULES

158

O	1.860211345	0.9950073015	-0.0184892341
H	1.060271856	1.515057872	0.1611579837
H	2.431568754	1.546376951	-0.5606270297
O	1.268053397	-1.695933159	-0.07606844
H	1.685253165	-2.08099568	0.7005352054
H	1.575694014	-0.7674292099	-0.10939046
O	-1.482818786	-1.433507393	-0.1552784132
H	-0.5223745363	-1.627218102	-0.1441775045
H	-1.904562722	-2.170587515	-0.604704997
C	-1.725683108	1.608505388	0.4853574799
H	-1.824072242	0.5049688	0.2690014787
O	-0.7051783237	2.211004017	0.5010325222
NH2			
O	-1.472467945	-1.383356101	0.0271611571
H	-1.868189106	-1.931944223	-0.6560100436
H	-0.5195251806	-1.630637624	0.0734227023
O	1.51392917	1.321764036	-0.1271157647
H	0.5413887889	1.447258707	-0.096104498
H	1.875981839	2.104062698	-0.5505517368
O	-1.24677865	1.342179649	-0.0053775615
H	-1.442186256	0.3793746457	-0.0384318626
H	-1.677793807	1.666381265	0.7911293005
N	1.306023968	-1.600381008	0.1542098468
H	2.115717397	-2.211231833	0.30723903
H	1.671634668	-0.6394993312	0.0362408346
NO			
O	-1.224290651	1.430956328	-0.6466670647
H	-0.6819108409	2.071480714	-0.174970489
H	-0.5904486014	0.7808922544	-1.002466894
O	0.2341535183	-0.9648436914	-0.9386120124
H	0.2544757463	-1.601412003	-1.658874317
H	-0.4858243998	-1.245295613	-0.3391404387
O	-2.008014093	-0.9064291939	0.6680769736
H	-1.981822707	0.0329760191	0.39994012

APPENDIX C. SUPPLEMENTARY INFORMATION: BINDING ENERGIES AND
MOTIFS FOR ASTROCHEMICALLY RELEVANT MOLECULES

159

H	-2.054576617	-0.9154643657	1.628560092
N	1.298476708	0.6899055244	1.243290049
O	2.392729895	0.3553734169	1.232551738
OH			
O	-1.87219485	0.0623758017	-0.0637160157
H	-2.708980656	-0.102798469	-0.5061695368
H	-1.390085959	-0.7882583061	-0.0275242395
O	-0.06618481	-2.079943235	-0.0262835062
H	0.7335857658	-1.477922757	-0.0092114187
O	0.1325248051	1.916533163	-0.0565923411
H	0.0317926477	2.48859547	0.7103448577
H	-0.6918361002	1.387369425	-0.1079741858
O	1.84643656	-0.1927229201	0.0064808934
H	1.356387303	0.6603598473	-0.02490644
H	2.628555293	-0.0962302885	-0.5439423884

Tetramer

CH3			
O	0.1564308159	1.768027652	0.2335304202
H	0.5702947041	2.501536786	0.6975908192
H	0.8744387832	1.314454802	-0.2639902966
O	2.041056984	0.1957900182	-0.943503392
H	1.839405991	-0.6570282858	-0.495420362
H	2.08231419	0.0034581899	-1.88478074
O	-0.9285683295	-0.4930787714	1.38831786
H	-1.779090728	-0.5978038202	0.9445745223
H	-0.6063527812	0.3875814551	1.099205499
O	1.130925964	-1.976221558	0.4152852495
H	0.3396061539	-1.559612309	0.829199139
H	1.586869147	-2.451764887	1.115591416
C	-2.822624877	0.3928852374	-1.124143152
H	-2.042215177	1.129890333	-0.9244237523
H	-2.606698773	-0.4745623679	-1.749881208
H	-3.838588337	0.5549278822	-0.7605768651

APPENDIX C. SUPPLEMENTARY INFORMATION: BINDING ENERGIES AND
MOTIFS FOR ASTROCHEMICALLY RELEVANT MOLECULES

160

H			
O	-1.675689862	0.7827401541	-0.2416331675
H	-2.154975087	0.7924166554	-1.075314528
H	-1.497667178	-0.1630322685	-0.0377688799
O	-0.7862664927	-1.741582023	0.2828571206
H	0.1776206776	-1.54970137	0.3299075951
H	-0.9978806812	-2.253859167	1.068750602
O	0.8556439671	1.729555104	0.1038172684
H	0.8715083321	2.414294869	0.7787621307
H	-0.0926443493	1.527168511	-0.0631488258
O	1.775941184	-0.817651361	0.4071759889
H	2.450459866	-1.002176195	-0.252936608
H	1.577410099	0.1433197099	0.3362901463
H	0.4112651881	-0.4800957021	-2.90736772
HCO			
O	2.18936586	1.110925934	-0.327347397
H	1.367618116	1.556590041	-0.0288514243
H	2.712533071	1.784315327	-0.7703388789
O	-0.1590726214	2.283389016	0.4597457036
H	-0.9625575319	1.766129213	0.2302653393
H	-0.3028941131	2.623329249	1.347493777
O	-1.653064047	-1.905775364	-0.0031581675
H	-2.098445359	-2.622164146	0.4580347852
H	-0.7201430544	-2.162615506	-0.0809457654
O	-2.333762142	0.7478520765	-0.1457410678
H	-2.136010724	-0.2090117416	-0.0771187744
H	-2.796285267	0.8657828787	-0.9807700335
C	2.144160541	-1.98633254	-0.306044764
H	2.230001456	-0.8603835877	-0.3569046869
O	1.133688879	-2.596546708	-0.1975521891
NH2			
O	2.173130033	0.6962975994	0.0379552787
H	1.477004986	1.345791427	-0.2149533469

APPENDIX C. SUPPLEMENTARY INFORMATION: BINDING ENERGIES AND
MOTIFS FOR ASTROCHEMICALLY RELEVANT MOLECULES

161

H	2.615082657	1.063739276	0.8087722129
O	0.1497099527	2.38488806	-0.5865626479
H	0.1029878679	2.887375466	-1.404769787
H	-0.721837886	1.930005095	-0.481088765
O	-1.469629265	-1.880543422	0.4339158137
H	-1.64846682	-2.511382639	1.136275821
H	-0.5007270674	-1.920374961	0.2745852949
O	1.230842324	-1.851144633	0.0098931652
H	1.633193771	-2.271494319	-0.7554567015
H	1.606643897	-0.9418997066	0.0489864074
N	-2.175402649	0.9106917364	-0.2043933187
H	-2.05211533	-0.0829660848	0.0633953303
H	-3.186475987	1.085850727	-0.215979935
NO			
O	-0.2433139345	1.761605441	-0.7889712351
H	0.4378327515	2.241290096	-0.3071916712
H	0.1951203388	0.9515348631	-1.13101823
O	0.7887667883	-0.6985691645	-1.405192585
H	0.1560325609	-1.258369321	-0.8964692487
H	0.8653795702	-1.096272693	-2.27711997
O	-2.215369148	0.4981454684	0.6130399127
H	-3.089988687	0.7986393733	0.3498613244
H	-1.569950931	1.074011204	0.143953451
O	2.010093061	0.7310878955	1.271013146
H	-1.607619308	-1.138918866	0.352474966
H	-0.7431471368	-2.257773864	0.9831496693
N	1.482171069	-0.2554012939	1.515917069
O	-1.074017107	-1.936674649	0.1382619267
OH			
O	-0.1241481676	-2.283450377	0.1832000209
H	-0.8909993154	-1.698595553	-0.0030953685
H	-0.3115713939	-2.705793861	1.026490061
O	2.146252224	-0.8491004035	-0.1686764986
H	2.551879169	-1.159961869	-0.9832752396

APPENDIX C. SUPPLEMENTARY INFORMATION: BINDING ENERGIES AND
MOTIFS FOR ASTROCHEMICALLY RELEVANT MOLECULES

162

H	1.358652498	-1.42319764	-0.0198741447
O	-2.127792722	-0.4949212859	-0.2134791171
H	-2.989064491	-0.5352337495	-0.6368913443
H	-1.879316791	0.4506051301	-0.1468390204
O	1.399516145	1.720104073	0.1332447126
H	2.0838164	2.216544431	0.588849552
H	1.728241713	0.7979437213	0.0092581176
H	-0.2271726554	2.029984992	0.0946749852
O	-1.225171511	2.121422705	0.0422787854

Cations

Monomer

CH₃⁺

H	0.9150121735	-0.6570102874	0.4086282663
H	0.9686385911	0.8542772316	-0.1397193279
O	0.4819058904	0.0082907328	-0.1593391964
C	-1.011895725	0.1092951915	-0.0336750244
H	-1.313774993	0.7975619762	-0.8292733485
H	-1.249458033	0.4778937664	0.9703790028
H	-1.378202004	-0.9055452907	-0.2168015942

H₃O⁺

H	1.263296544	-0.8378137571	0.5030938625
H	1.441060649	0.5468970072	-0.2816284241
O	0.8244109319	-0.0317818015	0.1919551261
O	-1.525828341	0.1463716486	-0.2071479321
H	-0.3506605441	0.0152619278	-0.0183074212
H	-2.01360206	-0.3868178108	-0.8524532026
H	-2.111298722	0.4921859513	0.4833451678

HCO⁺

H	2.393717076	-0.8030314375	-0.0977991462
H	2.374773463	0.8168474	-0.074269479
O	1.92412049	-0.0027019375	0.2050741581
C	-0.782010699	-0.0115139473	-0.0134431491
O	-1.900362939	-0.0016621099	-0.0578479957
H	0.8807124406	-0.0114863301	0.079622966

NH₂⁺

H	1.301278023	-0.8130278102	-0.27965196
H	1.320249836	0.7479358791	-0.0219740282
O	0.8595566391	-0.0870656417	0.214216486
N	-0.5445222536	-0.0269775495	-0.2758792749
H	-0.9782837105	-0.7745161695	0.2809405172

APPENDIX C. SUPPLEMENTARY INFORMATION: BINDING ENERGIES AND MOTIFS FOR ASTROCHEMICALLY RELEVANT MOLECULES

164

H	-0.8788741106	0.8538980691	0.1350334386
NH ₄ ⁺			
H	1.958538489	-0.4684745803	-0.2793657292
H	1.785706084	1.007366888	0.160549999
O	1.300374873	0.1980401067	-0.0443272691
N	-1.364161137	-0.1380817114	0.0293149876
H	-1.593233909	-1.127495858	0.1713429503
H	-1.771755767	0.4084929415	0.7954246008
H	-1.771819622	0.1748332344	-0.8583815139
H	-0.3064460352	-0.0073835701	0.0092363789
Dimer			
CH ₃ ⁺			
H	-2.096900495	0.2945716827	0.9585991374
H	-2.305875221	0.3053063324	-0.6020174737
O	-1.657908085	0.1833895514	0.1050124059
H	0.8718209523	-1.405979103	-0.1347977855
H	-0.3466463769	-0.2140753132	-0.1143407598
O	0.6566958247	-0.483865671	-0.3466792537
C	1.71099335	0.4847801963	-0.0111196378
H	1.33823466	1.455793268	-0.3528183506
H	1.885183053	0.4750699292	1.071438662
H	2.60356969	0.1917508776	-0.5734178133
H ₃ O ⁺			
H	0.114674995	-1.653129933	0.1137834121
H	-0.7378641883	-0.2064480951	-0.0503802408
O	0.1332873233	-0.7480898377	-0.2292766586
H	-2.547784934	0.7820636281	-0.6217644055
H	-2.362745266	0.847870848	0.9334538992
O	-1.964914467	0.540797098	0.1092768201
O	2.333761764	0.3945564618	-0.0373589969
H	2.806627342	0.6706868616	0.7576165195
H	2.891413865	0.5760478947	-0.8045865994

APPENDIX C. SUPPLEMENTARY INFORMATION: BINDING ENERGIES AND
MOTIFS FOR ASTROCHEMICALLY RELEVANT MOLECULES

165

H	1.049029943	-0.2674127388	-0.1117472951
HCO+			
H	1.032207275	-2.468253767	0.0987964411
H	1.748712512	1.837755448	0.2165416269
O	0.8467262087	-1.513700828	0.0775996222
H	0.4585597603	2.742228084	0.1580979533
H	-0.0293704175	0.7458177738	-0.0471338744
O	0.7877462773	1.834343647	0.1265975998
C	-0.3879294651	-1.219110741	-0.1453428081
O	-0.7594556105	-0.036725969	-0.1956871682
H	-1.133000576	-2.016036756	-0.2959841449
NH2+			
H	1.100099455	1.52213686	1.241092485
H	1.189344812	1.848212978	-0.3008870226
O	0.8495987826	1.223575236	0.3555845388
H	-0.1375184426	0.3740046457	0.0852961253
H	-1.754669471	-0.3064659348	0.2703460345
O	-0.9033327488	-0.3582285337	-0.1978314162
N	-0.5236998733	-1.734302622	-0.2945017288
H	0.2966115899	-1.853931057	0.3027291064
H	-0.2613755021	-1.859464948	-1.273330369
NH4+			
H	-3.065916448	-0.3280493211	0.5359704696
H	-2.412408499	-1.254029656	-0.5141558916
O	-2.258578017	-0.4702217603	0.0270783775
H	3.049221243	-0.3211087542	-0.6451323944
H	2.454706028	-1.251846286	0.4353815123
O	2.270341368	-0.4669286129	-0.0946276009
N	0.0060649595	1.088801797	0.0262530159
H	-0.8579845759	0.4899561457	0.0318441263
H	0.0374104712	1.654229057	0.8789516753
H	-0.024931928	1.717536134	-0.7809150764
H	0.8699167241	0.4919618426	-0.0251191835

Trimer

CH₃⁺

H	0.0416155955	0.0269291104	-0.5364053097
O	-0.6336392615	-1.048297651	-0.9238175976
H	-0.2095454129	-1.851380316	-1.24878754
O	0.5111479882	0.949949704	-0.1874938709
H	0.896262147	0.9875557482	0.7618713699
H	1.06307131	1.411312103	-0.8339449403
O	1.400199261	1.106427427	2.165312331
H	2.157116598	0.6565543491	2.559943915
H	1.021888019	1.695932243	2.829154919
C	-2.057721042	-1.022670411	-1.172591547
H	-2.425570112	-0.0699214737	-0.7747170012
H	-2.252591142	-1.079221767	-2.251679721
H	-2.536914264	-1.857899833	-0.6456299306

H₃O⁺

H	1.501576094	2.58179569	-0.9080817161
O	1.264137653	2.168762865	-0.0697112835
H	1.587831216	2.73588014	0.6403089173
O	-2.506520363	0.0050317724	-0.1157317831
H	-2.969048372	0.0240309382	-0.9616291957
H	-3.171162946	-0.0165108857	0.5830781538
O	1.256306173	-2.166307787	-0.1027964793
H	1.503901549	-2.56162102	-0.946747508
H	1.577903285	-2.744669644	0.5990679613
O	-0.003119361	0.0003407031	0.3694801088
H	0.4899477398	0.8601347131	0.1583407737
H	-0.9900448316	-0.0023666532	0.1399034467
H	0.496436026	-0.8522525676	0.1455264204

HCO⁺

H	-1.489308507	-0.6095717347	-0.9655319215
O	-0.9772265177	0.1586816052	-0.6747830701

APPENDIX C. SUPPLEMENTARY INFORMATION: BINDING ENERGIES AND
MOTIFS FOR ASTROCHEMICALLY RELEVANT MOLECULES

167

H	-0.1229040709	-0.091247209	-0.0959308515
O	2.016965436	-1.736740125	-0.5651611821
H	-2.808837352	2.093724634	1.08408453
H	2.832181008	-2.257904324	-0.6243801699
O	-2.442005342	1.997806115	0.1967607418
H	-1.576618975	0.9049383499	-0.2896106614
H	-2.629306044	2.805229592	-0.2975922179
C	1.954254889	-1.00235019	0.5193076355
O	0.9903366306	-0.2898480847	0.7418186687
H	2.804332232	-1.055334791	1.222761313
NH ₂ ⁺			
H	-0.6494744317	-1.835557419	-0.2604371561
O	-0.6273723586	-0.867625928	-0.2642958817
H	-1.467377946	-0.4430145425	0.1684746733
O	-2.684269835	0.1719248202	0.6982052982
H	-3.387007442	0.538688025	0.1471767408
H	-2.943024698	0.2651437139	1.623554486
O	1.56162533	0.1392446944	0.2026466936
H	0.3204918653	-0.4518001472	-0.0290864728
H	2.113183142	0.0500357917	0.9910534988
N	2.348117021	0.8077153299	-0.7716055481
H	1.820374409	1.638126619	-1.039455865
H	2.414522396	0.1776669487	-1.570896986
NH ₄ ⁺			
H	0.7846170889	1.073796671	0.3082627915
O	0.0336544179	1.661511879	0.5036967591
H	0.3849466905	2.527336242	0.7369121505
O	1.816072479	-0.4693591059	-0.1587436125
H	2.400051095	-0.3777649085	-0.9236749844
H	2.372728214	-0.8181512876	0.5503476442
O	-0.7634532608	-1.65033464	-0.5161325691
H	0.1846510951	-1.436426472	-0.4664512951
H	-0.8496411368	-2.564597189	-0.80647197
N	-2.342454263	0.4263467669	0.1758933964

APPENDIX C. SUPPLEMENTARY INFORMATION: BINDING ENERGIES AND
MOTIFS FOR ASTROCHEMICALLY RELEVANT MOLECULES

168

H	-1.902837389	-0.4827764614	-0.1217961508
H	-2.944115583	0.7935472415	-0.5645468556
H	-1.533312052	1.076286516	0.3518070697
H	-2.888761385	0.2959013917	1.030044561

Tetramer

CH3+

O	3.527969681	-0.4015606909	-0.4677619021
H	4.187506614	0.2770951813	-0.6505011385
H	3.88550851	-1.237703953	-0.787086816
O	1.261979348	-0.0506504303	0.8430923464
H	2.109715346	-0.1867548966	0.3467889818
H	1.420615166	-0.1704433788	1.785144031
O	-0.8845271321	0.373065989	-0.2446966778
H	0.032099358	0.1639811065	0.254231394
H	-1.600886463	-0.3306085131	-0.1447167828
O	-2.775745894	-1.348706501	-0.0881667878
H	-3.076844078	-1.863990227	-0.8461259937
H	-3.289876133	-1.629090144	0.677982168
C	-1.368970844	1.732938299	-0.1049411626
H	-1.723261764	1.90556006	0.9197283681
H	-0.5308140087	2.395847591	-0.3441779375
H	-2.179518887	1.870237316	-0.8287151458

H3O+

O	-2.393227161	-1.911714695	-0.2882561074
H	-2.628431593	-2.383492019	-1.095614662
H	-2.851726198	-2.340772804	0.4430684622
O	1.403097402	-0.2227044559	0.8167499435
H	2.257807484	-0.2738715299	0.3245286488
H	1.576954311	-0.3300449569	1.757117006
O	-1.925511451	2.405476959	0.101907144
H	-2.031674388	3.053637544	-0.6040455067
H	-2.305860131	2.783493054	0.9028848281
O	3.711718669	-0.3559503278	-0.5091503403

APPENDIX C. SUPPLEMENTARY INFORMATION: BINDING ENERGIES AND MOTIFS FOR ASTROCHEMICALLY RELEVANT MOLECULES

169

H	4.133083001	-1.152617244	-0.8501254924
H	4.309796762	0.3780433601	-0.6882095766
O	-0.7924246631	0.1141328571	-0.2635152181
H	0.1258558433	-0.0302453707	0.2175537008
H	-1.420429009	-0.6690494282	-0.2396131235
H	-1.237489584	0.9971315121	-0.0887817533
HCO+			
O	2.264178036	-0.9567543147	-0.1631929458
H	3.195170727	-1.222922226	-0.1744867501
H	0.4082836159	-1.753659859	-0.3131537651
O	-0.5449924855	-1.926972759	-0.3407349248
H	-1.557173965	-0.8915112635	-0.0800307626
H	-0.6999560707	-2.789301492	-0.7419349743
O	-1.380681524	2.107609948	0.0191278464
H	-1.726976186	2.848740796	-0.4915663465
H	-0.4100532006	2.078124387	-0.050457928
O	-2.274780542	-0.1734413629	0.1210878935
H	-1.916923301	0.8318743951	0.0471520095
H	-2.698297134	-0.3389034792	0.9758625572
C	2.097972303	0.366148791	-0.0575638022
O	0.9905576144	0.8322593622	-0.026335308
H	3.030270703	0.9609749188	-0.0048066886
NH2+			
O	1.420358166	2.64526603	-0.0772997167
H	1.755453559	3.304297036	0.5422398965
H	1.662552765	2.934021147	-0.9646741449
O	-1.661380256	-1.39775321	-0.4496667456
H	0.803545723	-2.336407832	-0.7727396357
H	-2.483722316	-1.851308155	-0.6846764342
O	0.497966881	0.35847828	0.7004450471
H	-0.5439672765	0.2351822173	0.5724808158
H	0.861180903	1.234249561	0.3660151071
O	1.46439042	-1.735908677	-0.4080564648
H	0.9730230992	-0.437072971	0.2971300194

APPENDIX C. SUPPLEMENTARY INFORMATION: BINDING ENERGIES AND
MOTIFS FOR ASTROCHEMICALLY RELEVANT MOLECULES

170

H	2.297731077	-2.213772289	-0.3325796631
N	-1.964301924	-0.2581823919	0.3129632242
H	-2.459324389	-0.5393904826	1.163117536
H	-2.564633736	0.3651150871	-0.2321748336
NH4+			
O	-0.7295513807	0.319193306	-1.968312254
H	-0.8135281869	0.4162660763	-2.922997267
H	-0.427948048	-0.5879638938	-1.794699958
O	-0.1800185891	-1.863947999	-0.2905485363
H	0.5882143028	-1.579426232	0.2515163169
H	-0.1447953133	-2.822553915	-0.3845009662
O	0.1359512132	1.84766437	0.0544213101
H	0.2811987768	2.800343564	0.0362256053
H	-0.0071203857	1.540875452	-0.8677924671
O	1.284280793	-0.3538874615	1.369129015
H	1.308127777	0.542193538	0.9943699741
H	2.086279264	-0.468752906	1.890117342
N	-1.762982993	0.0423709677	0.948057618
H	-1.832689389	-0.0900571148	1.959563461
H	-1.143696309	0.8613121166	0.7371960367
H	-2.691575622	0.2007223716	0.5502318764
H	-1.32638452	-0.8043725685	0.5108475779

Anions

Monomer

CH₃-

H	-0.401611876	0.082287574	0.0480837255
H	2.500150428	0.5237808922	-0.0614572073
O	1.553807548	0.3503518068	-0.0223389114
C	-1.501824419	-0.0703158358	0.0789478524
H	-1.833860774	-0.607410393	-0.8247102066
H	-2.016098569	0.9037853464	0.1242993008
H	-1.778333658	-0.6615866618	0.9673638196

CN-

H	2.134898042	-0.8347222497	-0.0275238937
H	0.9667144673	0.146568632	0.0750224185
O	1.966931104	0.1058479921	0.0741691343
C	-1.935661421	-0.0773982138	-0.0021259872
N	-0.7660110737	-0.0002480215	0.0529874214

HCO₃-

H	2.275254556	-0.2898887475	0.2651764045
H	1.975409618	1.060327706	-0.202910847
O	2.754005181	0.5342732823	0.0577694612
C	-0.278653626	-0.1868340658	-0.0678240436
O	0.4709067536	-1.11780755	0.3164225842
O	-1.643322622	-0.5221213467	-0.1180970902
O	-0.0087014378	0.9745664869	-0.4074843208
H	-1.658594609	-1.440789313	0.1748256988

HCO-

H	1.129436742	0.3057088525	0.0290657951
H	2.303838362	-0.7576370279	-0.0852826519
O	2.195587569	0.1940244493	0.0094213093
C	-0.5555700649	0.3728381014	0.0458287644
H	-1.165486082	1.377981978	0.1234067983

APPENDIX C. SUPPLEMENTARY INFORMATION: BINDING ENERGIES AND
MOTIFS FOR ASTROCHEMICALLY RELEVANT MOLECULES

172

O	-1.321498843	-0.6001279259	-0.024182921
NH ₂ -			
H	-0.220388971	0.1488846231	-0.1372051745
H	2.059557099	0.404577276	-0.213269389
O	1.367537134	0.2155225394	0.4302880147
N	-1.268338867	0.0764673985	-0.3391852371
H	-1.698755172	0.7390572535	0.3066117239
H	-1.536556405	-0.8400059048	0.0204893043
NO-			
H	1.809677294	-0.9694321384	0.1461162013
H	1.025897279	0.3232643454	-0.0363556093
O	1.973441429	-0.0306231304	0.0158167873
N	-0.679470098	0.5689278134	-0.0750034113
O	-1.240635018	-0.537206085	0.0741613527
OH-			
H	0.4285077874	-0.2744352955	-0.0357816139
H	2.077713468	0.5152187308	-0.3552078121
O	1.738439994	-0.1565387709	0.2450872344
H	-1.052106918	0.1239371514	0.5203407193
O	-0.6751974979	-0.3468524148	-0.2282461624
Dimer			
CH ₃ -			
H	1.753469053	-0.6639112168	1.128188066
H	1.239119881	0.0471660954	-0.1986414119
O	1.813570045	-0.7848269947	0.1765144907
H	-1.371986177	0.1796832117	-0.2010747887
H	1.038517185	1.842290323	-0.9280358016
O	0.4431724002	1.159803166	-0.605249726
C	-2.215857097	-0.4734479534	0.0868141042
H	-2.652220177	-0.1297614361	1.038349941
H	-1.846678129	-1.502955167	0.2083900229

APPENDIX C. SUPPLEMENTARY INFORMATION: BINDING ENERGIES AND
MOTIFS FOR ASTROCHEMICALLY RELEVANT MOLECULES

173

H	-2.994261559	-0.4560412672	-0.6930624303
CN-			
H	0.0527071543	0.8787506625	0.3615333579
H	-0.5228633943	2.073446885	-0.4112412192
O	-0.6132896207	1.622968794	0.4334056785
H	-1.848048555	-0.0120667089	0.0108137034
H	-1.045815464	-1.220235652	-0.3540082001
O	-1.969743687	-0.92301972	-0.2993328271
C	1.62941429	-1.425195219	-0.4078271805
N	1.035878247	-0.4909448464	-0.0118552317
HCO ₃ -			
H	2.340095196	-0.1663962578	-0.0206477164
H	3.792373129	0.2768631255	0.0217064687
O	3.263809331	-0.5204495595	-0.0721955386
H	-2.385208112	-0.5149881945	0.1336544207
H	-3.601239114	-0.3856887232	-0.8238908965
O	-3.363901741	-0.2703412498	0.1003259473
C	-0.238491788	0.594823923	0.1320329976
O	0.9670497613	0.8814562611	0.0863342745
O	-1.099224792	1.680619042	0.2143893954
O	-0.7805491325	-0.5433259809	0.113147053
H	-2.001939267	1.325817059	0.2419763828
HCO-			
H	2.752496511	-0.9289089263	1.022837065
H	1.819508804	-0.278688613	-0.0006889884
O	2.638221042	-0.8386883644	0.072901901
H	-0.8766509165	-0.8313676332	-0.274971851
H	0.3592986573	1.473243387	-0.4821080207
O	0.451272738	0.7253827571	0.1231260751
C	-0.9960185537	0.228953105	0.0906394396
H	-1.2487721	0.1784839832	1.189535533
O	-1.738256836	1.010970748	-0.6371994018

APPENDIX C. SUPPLEMENTARY INFORMATION: BINDING ENERGIES AND
MOTIFS FOR ASTROCHEMICALLY RELEVANT MOLECULES

174

NH₂-

H	-0.8206318288	-2.31284734	-0.2796970312
H	-0.7769973143	-0.7596935495	0.0691499459
O	-0.2657841512	-1.691759557	0.1990055389
H	0.341577084	1.153060091	-0.0512555033
H	-2.004901482	0.6865567215	0.5994064424
O	-1.444329705	0.4946049837	-0.1589490522
N	1.380479921	1.202535527	-0.0658886643
H	1.641667513	0.2344402145	0.1280615169
H	1.617650874	1.340427609	-1.048140255

NO-

H	0.0864503981	0.8881432937	-0.2603025902
H	-0.4557110135	2.035905392	0.6013768512
O	-0.4967467116	1.707004954	-0.3013201364
H	-1.094307578	-1.156168981	0.1744187223
H	-1.974592046	0.0191483823	-0.1103144504
O	-2.046069111	-0.916228479	0.1258050591
N	0.7840817616	-0.6710038844	0.0720161163
O	1.945324208	-1.097453508	0.0399702029

OH-

H	2.03543296	0.7219839425	-0.2845329829
H	0.8379566677	-0.1349571629	0.237842515
O	1.604239838	0.4977880586	0.5445197699
H	-1.509355369	-0.0328017464	-0.279612601
H	-1.752029723	1.381214573	0.2848191221
O	-2.229535908	0.6966936618	-0.1936073118
H	-0.4097064067	-1.78823115	0.1791978971
O	-0.2807330941	-0.9857431804	-0.3349211928

Trimer

CH₃-

H	-1.216883816	-0.7340157594	-1.369834648
O	-1.07484777	-1.525834807	-0.8383187686

APPENDIX C. SUPPLEMENTARY INFORMATION: BINDING ENERGIES AND
MOTIFS FOR ASTROCHEMICALLY RELEVANT MOLECULES

175

H	1.47957485	-0.0910314624	0.598627834
O	-0.8271185413	1.67862614	-0.5249143404
H	-0.7822988176	1.007139097	0.2632117439
H	0.0995628078	1.81804271	-0.7392742125
O	-0.5876781277	-0.0954175749	1.311663538
H	-0.8912279082	-1.103167409	0.0629587276
H	-1.30059784	-0.0943774916	1.955785145
C	2.387084959	-0.1040426836	-0.0273450114
H	3.240428923	-0.4944891531	0.5490395851
H	2.625015736	0.9149420635	-0.3722536591
H	2.203262166	-0.7509636814	-0.897057648
CN-			
H	0.7517639602	0.907607769	0.8676237686
O	0.7175155112	1.679280709	0.2842282803
H	-0.1544550896	1.557671354	-0.1327888653
O	0.2378149451	-1.228142501	0.7778981007
H	-0.1416568736	-1.775443558	1.468883859
H	-0.54621216	-0.7888448039	0.3196201492
O	2.611922758	-0.4327170508	-0.6613605812
H	2.213788666	0.4510720786	-0.6641522567
H	1.921036957	-0.9555098935	-0.2216406049
C	-2.626216515	0.8465099325	-0.7226562255
N	-1.764403866	0.1360869123	-0.3555864553
HCO3-			
H	2.907625053	1.525594784	0.0853115637
O	2.363547899	2.319653044	0.1191691904
H	1.46627644	1.92207172	0.1359007423
O	-3.129536223	-1.335540092	0.1377032147
H	-2.164500782	-1.483298341	0.0838610185
H	-3.179401197	-0.3678383233	0.1820595161
O	-2.523765204	1.555514574	0.0093882798
H	-2.603181339	1.719374727	-0.9348161764
H	-1.584264623	1.257074197	0.1131268575
C	0.3929654564	-0.4412012906	0.0521467027

APPENDIX C. SUPPLEMENTARY INFORMATION: BINDING ENERGIES AND
MOTIFS FOR ASTROCHEMICALLY RELEVANT MOLECULES

176

O	-0.3002157532	-1.469396777	-0.0080420137
O	1.774068374	-0.6409705889	0.0378884101
O	0.0524754994	0.7622771591	0.1226279059
H	1.875614116	-1.59839412	-0.0119314569
HCO-			
H	-1.355301497	-0.7770466772	-0.0864235307
O	-1.531934361	-0.7923275139	-1.108316571
H	-1.369385016	-1.703817236	-1.363271948
O	-0.9564425923	-0.6507498722	1.371594487
H	-0.9078935507	0.9459231481	1.09356613
H	-1.683914133	-0.8527322902	1.965485996
O	-0.889031805	1.893527849	0.7344660518
H	-1.276864698	1.777980478	-0.1393699839
H	1.05581266	0.6607244159	-0.8920129155
C	1.543426018	-0.2012525543	-0.3839555092
H	0.9728837205	-0.6358003106	0.465749847
O	2.624879001	-0.6187275371	-0.7499327807
NH2-			
H	-0.9373136526	-0.4861695416	1.604815178
O	-1.672506763	-0.447408427	0.9810856089
H	-0.6735542565	1.746168667	0.1347172383
O	1.508700097	-0.4941673658	0.9959137641
H	0.9665994734	-0.8011052142	0.199355197
H	1.539916628	0.4586076472	0.8434533565
O	-0.0925903553	-0.9420591985	-1.043603992
H	-1.193283615	-0.6974772615	0.1242090109
H	-0.0984277757	-1.784267604	-1.503058304
N	0.1064330971	1.879567546	-0.5105249858
H	0.155944043	0.9701875875	-0.9970127786
H	-0.1997697933	2.567972021	-1.194666403
NO-			
H	2.064543852	-0.8882816395	-0.4491867651
O	2.576865375	-0.0860050752	-0.6290471361

APPENDIX C. SUPPLEMENTARY INFORMATION: BINDING ENERGIES AND MOTIFS FOR ASTROCHEMICALLY RELEVANT MOLECULES

177

H	1.981542854	0.5970909497	-0.2643862366
O	0.2902413462	-1.627891344	0.5743974803
H	0.3550976085	-0.6755644919	0.8291636808
H	-0.4975494634	-1.615938259	0.0101551444
O	-2.250039857	-0.5518707693	-0.593061395
H	-2.751097414	-0.665586702	0.2199818656
H	-1.716312496	0.2664572777	-0.4143477839
N	0.290447019	1.213423933	0.7155499361
O	-0.7543280237	1.574601398	0.1360618804

OH-

H	-1.15957984	-0.6832562844	0.1972460565
O	-1.596395221	-0.8135558602	-0.6967897855
H	-0.8332706646	-1.081853921	-1.223665816
O	-0.0137278105	-0.330832422	1.344686607
H	0.0274857694	1.163404567	0.6263000865
H	-0.0307608765	-0.5391713668	2.279792198
O	-0.0358093708	1.879361998	-0.0743203152
H	-0.7481397526	1.52367399	-0.6202274086
H	1.520382135	0.1569994754	-0.9387412804
H	1.087970161	-0.7649470087	0.1763761597
O	1.582513623	-0.775317723	-0.6956068774

Tetramer

CH3-

O	-0.7315099523	1.08448143	1.280426696
H	-0.4224607329	0.8811932569	2.168023309
H	0.3874834963	1.450069882	0.3941776755
O	1.132247791	1.694098832	-0.3048343609
H	0.8798341969	2.566429926	-0.6169015297
O	-1.848498428	-0.8723332073	0.1417501686
H	-2.718940587	-0.5321298748	-0.0788564145
H	-1.392516247	-0.0825860289	0.6592618275
O	-0.0669806095	-0.2624425501	-2.075148069
H	-0.7057761964	-0.5763111754	-1.407649258

APPENDIX C. SUPPLEMENTARY INFORMATION: BINDING ENERGIES AND
MOTIFS FOR ASTROCHEMICALLY RELEVANT MOLECULES

178

H	0.4382085952	0.4097880429	-1.579369803
C	1.538116418	-1.662836663	0.8477933029
H	2.105331468	-2.409473944	0.2719230211
H	0.4618381957	-1.810077004	0.6884171614
H	1.795030736	-0.6532552101	0.501128537
H	1.773450364	-1.760702274	1.918832188
CN-			
O	0.2759696421	1.093209683	-1.207172394
H	-0.0434175601	1.431902876	-0.3526341883
H	0.4360696973	0.1567909776	-0.9939207787
O	3.002546261	0.1919993452	0.1918089219
H	2.521619226	0.8297928891	-0.3497033964
H	2.319164565	-0.4817427828	0.3793756453
O	-2.557322464	-0.0691090075	-0.7940575014
H	-1.873987571	0.3783850456	-1.315384706
H	-2.102955602	-0.8950526587	-0.5206299193
O	-1.028476322	1.114693428	1.400017782
H	-0.4898798755	0.3118597848	1.490192131
H	-1.776370378	0.8016334591	0.8609244994
C	-0.4568788786	-1.881596257	0.1739061059
N	0.6140173999	-1.455453792	0.4020813643
HCO ₃ -			
O	3.707673716	-1.42818292	-0.0455808252
H	3.537323076	-0.4774396553	-0.1306614608
H	2.815578834	-1.796564964	-0.148080088
O	2.092322487	0.9785460747	-0.6383780605
H	1.578547543	0.1594189597	-0.7325905384
H	1.571040459	1.517640425	-0.0161563569
O	0.2225756379	2.325091346	1.155862061
H	-0.2261649836	1.445772558	1.225079275
H	-0.4003035537	2.827083692	0.619901469
O	0.8194903751	-1.722679067	-0.3631701038
H	0.3179266509	-1.257712062	0.3439500736
H	0.1106937962	-1.832751209	-1.014683786

APPENDIX C. SUPPLEMENTARY INFORMATION: BINDING ENERGIES AND
MOTIFS FOR ASTROCHEMICALLY RELEVANT MOLECULES

179

C	-1.692938491	-0.0240383071	-0.1231396605
O	-1.860772661	-0.8524330025	-1.031247193
O	-2.413688394	1.163675066	-0.2195022074
O	-0.9411380859	-0.0849827994	0.8830038825
H	-2.91511121	1.077011488	-1.038998857

HCO-

O	-0.3697040462	-2.00335847	-0.5349475171
H	-1.125704519	-1.60526791	-0.0841975708
H	0.1171538791	-1.225625492	-0.9311806143
O	0.9493960559	0.206085701	-1.294064002
H	0.9204539237	1.423079114	-0.1763103155
H	1.407709069	0.2904471057	-2.132913607
O	2.156029519	-0.8670799185	0.8465890202
H	1.873857471	-0.4433053435	-0.010820712
H	1.489017047	-1.561312446	0.9236684317
O	0.8336818709	1.959115888	0.6669682937
H	1.24273983	1.359686441	1.303806053
H	-1.032306639	0.7247172687	-0.6795273872
C	-1.803938288	0.9252128181	0.0948561582
H	-2.013431392	1.99256722	0.3374560175
O	-2.400014469	0.0341697387	0.6659667172

NH2-

O	0.9587006518	1.544350248	0.3614074909
H	0.7992716016	2.056575452	1.159129504
H	1.374433284	0.1562419538	0.626007499
O	1.632640062	-0.8537173659	0.7357863074
H	0.4558561543	-1.401752088	-0.7008608773
H	2.549664505	-0.8948199968	0.4540147918
O	-1.045667876	1.299540892	-1.137694455
H	-0.8354141422	1.817467341	-1.918237716
H	-0.2268984351	1.446176902	-0.4958057288
O	-0.2191358868	-1.473552968	-1.402831325
H	-0.5837378452	-0.5684692196	-1.430963493
H	-1.627219599	-1.364257262	0.7386211833

APPENDIX C. SUPPLEMENTARY INFORMATION: BINDING ENERGIES AND
MOTIFS FOR ASTROCHEMICALLY RELEVANT MOLECULES

180

N	-1.653821566	-0.6234298455	1.440268387
H	-0.6818586715	-0.5535072631	1.744906
H	-1.796942756	0.2209474439	0.8838917742
NO-			
O	-2.097535294	0.6098875096	1.12761268
H	-2.301338349	0.1561348409	0.2921780126
H	-1.145526815	0.4135195251	1.22607672
O	3.165998005	-0.7739451045	1.766454675
H	2.34895914	-0.3356880046	1.429735356
H	3.142548795	-1.615325866	1.300156141
O	-0.5488511208	2.226407169	-0.8311619732
H	-1.263134147	2.188316705	-0.1777672353
H	0.0904150329	1.588160352	-0.442109846
O	-1.723238542	-0.3762818837	-1.622062882
H	-0.9374758393	-0.8077574843	-1.227656324
H	-1.419142513	0.5408962232	-1.719987798
N	0.7535997765	-0.0093266084	0.4850269876
O	0.6013817734	-1.042940438	-0.1878756473
OH-			
O	0.032071792	-0.0315701647	-1.280514427
H	0.053207243	-0.0501259946	-2.2394438
H	1.503093927	-0.1086853572	-0.3538872802
O	2.14088384	-0.0552303024	0.4056663161
H	1.815894932	0.739446209	0.8496950823
H	0.7157945859	-1.8281158	0.8639446402
O	-2.157524508	0.0493281851	0.2955209188
H	-1.855519373	-0.7296758588	0.7815853254
H	-1.481320204	0.0790453868	-0.4314819973
O	0.044657921	2.146378673	0.3164123591
H	-0.7544177719	1.838373017	0.764630692
H	0.1076745755	1.477769749	-0.4150703213
H	-0.0851437573	-1.507984774	-0.3695066968
O	-0.0597886581	-2.151951051	0.3864909018

C.3 Alternative conformers and relative energies

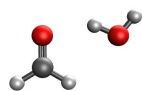
APPENDIX C. SUPPLEMENTARY INFORMATION: BINDING ENERGIES AND
MOTIFS FOR ASTROCHEMICALLY RELEVANT MOLECULES

182

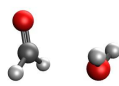
Distinct conformers - Neutral Monomer

dE with respect to minima in kcal/mol

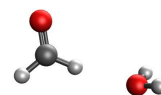
H₂CO



0

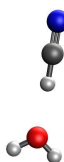


3.025



3.703

HCN

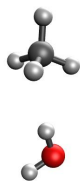


0

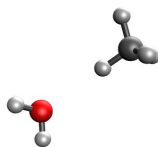


0.947

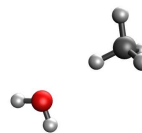
CH₄



0

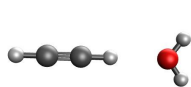


0.373

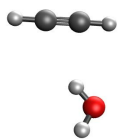


0.289

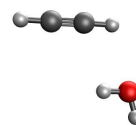
C2H2



0

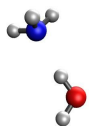


0.663



0.702

NH3

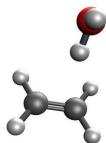


0

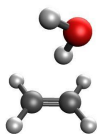


4.823

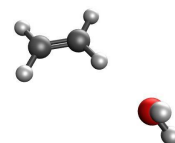
C2H4



0

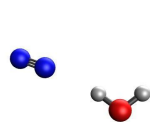


0.07



1.542

N₂

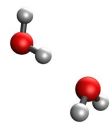


0



0.704

H₂O



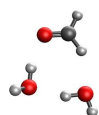
0

APPENDIX C. SUPPLEMENTARY INFORMATION: BINDING ENERGIES AND
MOTIFS FOR ASTROCHEMICALLY RELEVANT MOLECULES

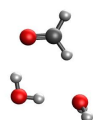
185

Distinct conformers - Neutral Dimer

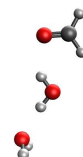
H₂CO



0

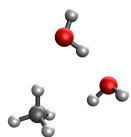


5.356

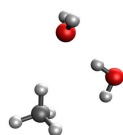


4.649

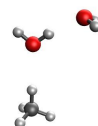
CH₄



0



0.005



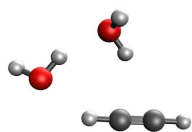
1.125

HCN



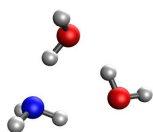
0

C2H2

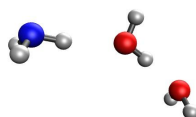


0

NH₃

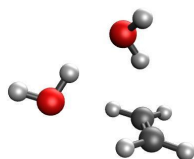


0

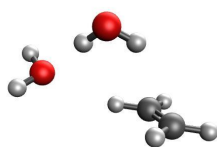


8.588

C₂H₄

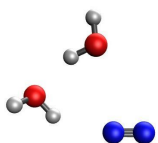


0

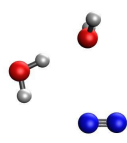


2.374

N₂

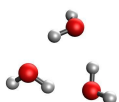


0

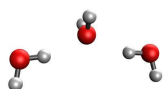


1.139

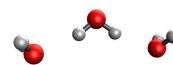
H₂O



0



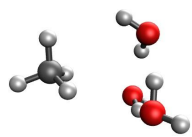
7.409



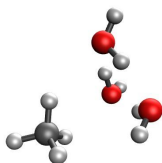
7.586

Distinct Conformers - Neutral Trimer

CH₄

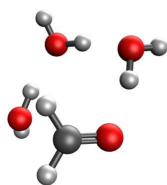


0

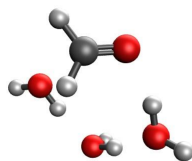


0.002

H₂CO

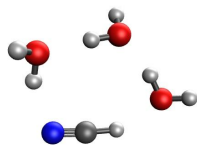


0



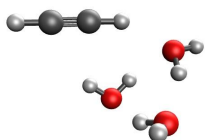
0.575

HCN



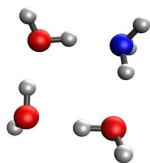
0

C2H2



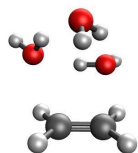
0

NH3

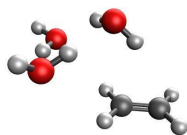


0

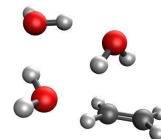
C2H4



0

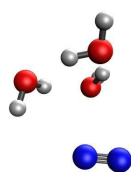


0.27



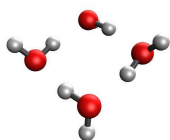
0.636

N₂

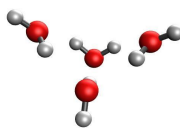


0

H₂O



0

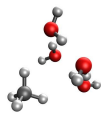


5.027

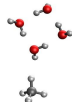
APPENDIX C. SUPPLEMENTARY INFORMATION: BINDING ENERGIES AND MOTIFS FOR ASTROCHEMICALLY RELEVANT MOLECULES

Distinct Conformers - Neutral Tetramer

CH₄



0



1.701



1.185

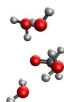
H₂CO



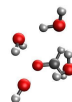
0



2.674



3.475

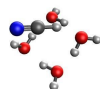


2.493



3.561

HCN



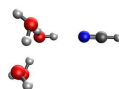
0



0.608

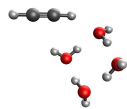


0.027



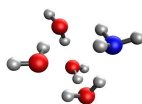
2.061

C₂H₂

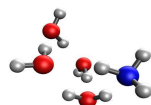


0

NH₃



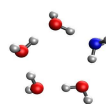
0



0.47

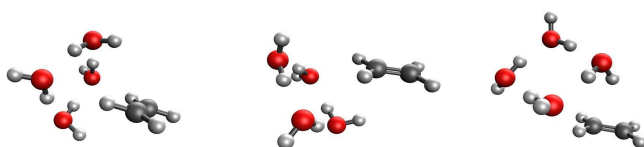


1.018



0.583

C₂H₄

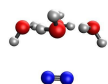


0

0.626

0.885

N₂



0

H₂O



0

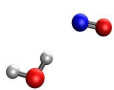
0.946

APPENDIX C. SUPPLEMENTARY INFORMATION: BINDING ENERGIES AND MOTIFS FOR ASTROCHEMICALLY RELEVANT MOLECULES

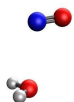
193

Distinct conformers - Neutral open-shell monomer

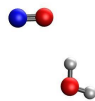
NO



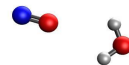
0



0.475

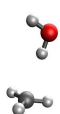


0.64

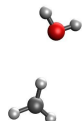


0.957

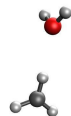
CH3



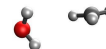
0



0.833



0.796

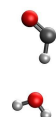


1.319

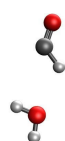
HCO



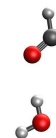
0



0.805

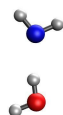


1.038

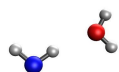


1.295

NH2

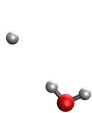


0



1.68

H



0



0.106



0.116



0.15

OH



0



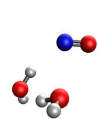
2.711

APPENDIX C. SUPPLEMENTARY INFORMATION: BINDING ENERGIES AND MOTIFS FOR ASTROCHEMICALLY RELEVANT MOLECULES

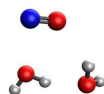
195

Distinct Conformers - Neutral open-shell dimer

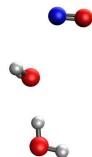
NO



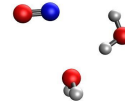
0



0.708

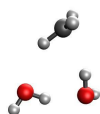


2.085

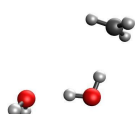


1.634

CH3



0

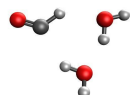


1.985

HCO

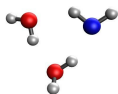


0



1.639

NH2

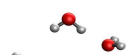


0

H



0



0.13

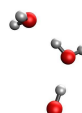
OH



0



0.149



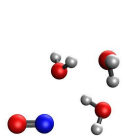
2.595

APPENDIX C. SUPPLEMENTARY INFORMATION: BINDING ENERGIES AND MOTIFS FOR ASTROCHEMICALLY RELEVANT MOLECULES

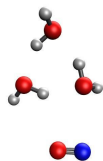
197

Distinct Conformers - Neutral open-shell trimer

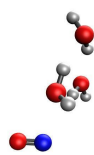
NO



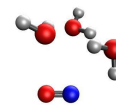
0



0.695

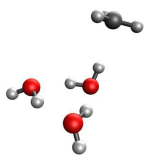


0.424

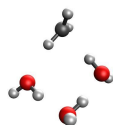


0.102

CH3

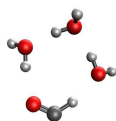


0

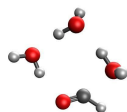


1.186

HCO

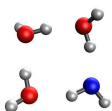


0

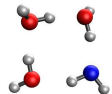


1.456

NH2

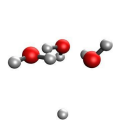


0

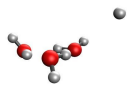


0.016

H

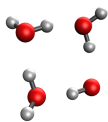


0

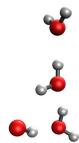


0.1

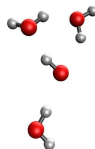
OH



0



6.342



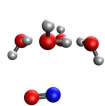
8.164

APPENDIX C. SUPPLEMENTARY INFORMATION: BINDING ENERGIES AND MOTIFS FOR ASTROCHEMICALLY RELEVANT MOLECULES

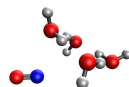
199

Distinct Conformers - Neutral open-shell tetramers

NO



0



0.091

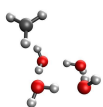


0.959

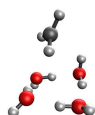


1.078

CH3

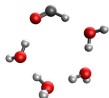


0



0.748

HCO



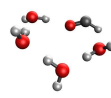
0



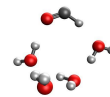
2.655



1.748

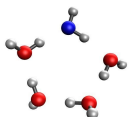


1.301

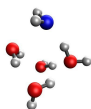


0.854

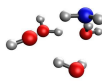
NH2



0



2.945

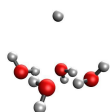


1.96



3.053

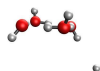
H



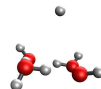
0



0.227



0.162



1.031

OH



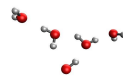
0



1.365



0.989



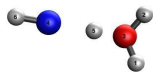
11.437

Distinct Conformers - Cationic monomers

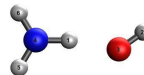
NH₂⁺



0



39.371

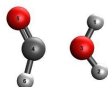


34.982

HCO⁺



0



10.646

NH₄⁺

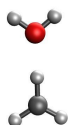


0

CH₃ +

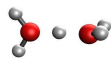


0



55.804

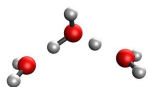
H₃O +



0

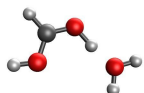
Distinct Conformer - Cationic dimer

H₃O⁺

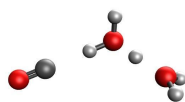


0

HCO⁺

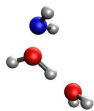


0

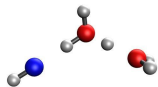


12.38

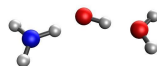
NH₂⁺



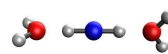
0



46.333

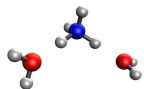


50.963



55.484

NH₄⁺

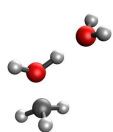


0

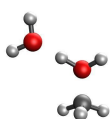


2.45

CH₃⁺



0



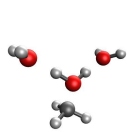
0.841

APPENDIX C. SUPPLEMENTARY INFORMATION: BINDING ENERGIES AND MOTIFS FOR ASTROCHEMICALLY RELEVANT MOLECULES

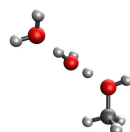
205

Distinct Conformers - Cationic trimer

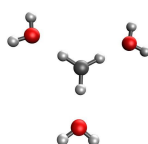
CH₃⁺



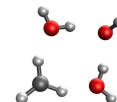
0



3.261

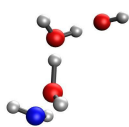


79.176

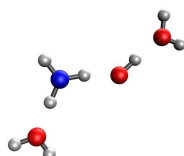


78.291

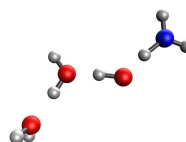
NH₂⁺



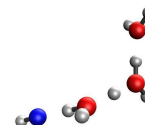
0



53.882

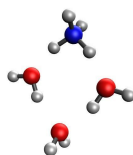


59.268

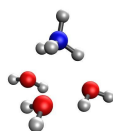


49.743

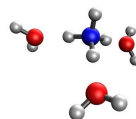
NH₄⁺



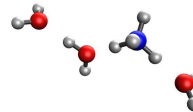
0



3.25

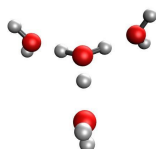


0.726

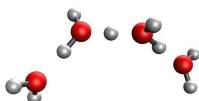


2.155

H₃O⁺

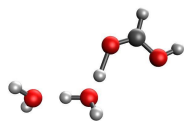


0

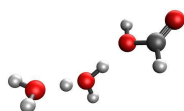


3.518

HCO⁺



0



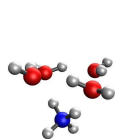
13.028

APPENDIX C. SUPPLEMENTARY INFORMATION: BINDING ENERGIES AND MOTIFS FOR ASTROCHEMICALLY RELEVANT MOLECULES

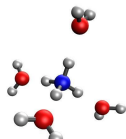
207

Distinct Conformers - Cationic tetramer

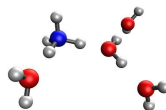
NH₄⁺



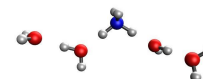
0



0.125

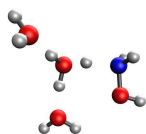


3.111

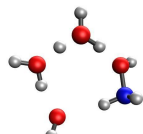


1.595

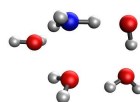
NH₂⁺



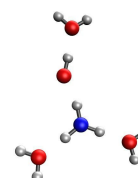
0



9.804

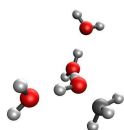


68.23

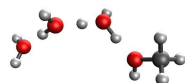


63.214

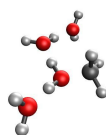
CH₃⁺



0

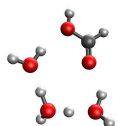


3.084

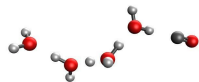


0.4

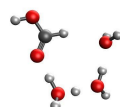
HCO⁺



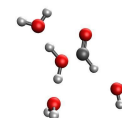
0



11.801

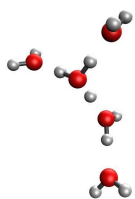


0.547

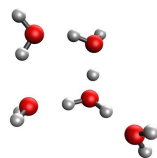


19.324

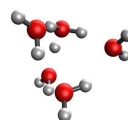
H₃O⁺



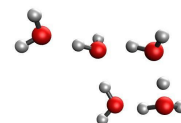
0



1.868



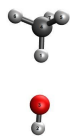
2.461



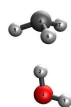
3.55

Distinct Conformers - Anionic monomer

CH₃ -



0

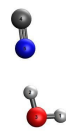


25.13

CN -

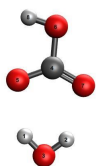


0

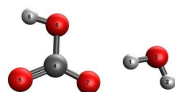


0.036

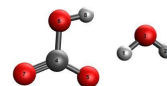
HCO₃ -



0

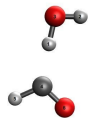


3.133

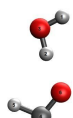


2.715

HCO -

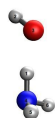


0

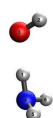


5.47

NH₂ -

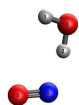


0

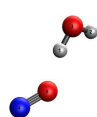


0.563

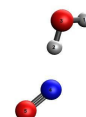
NO -



0

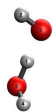


3.169



0.604

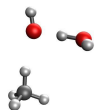
OH -



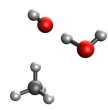
0

Distinct Conformers - Anionic dimers

CH₃-

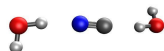


0

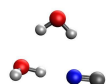


0.463

CN-

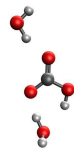


0

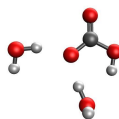


0.064

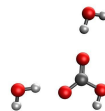
HCO₃-



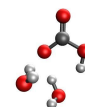
0



0.591



3.218

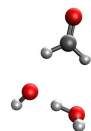


0.491

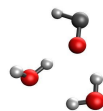
HCO-



0



10.73

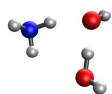


29.8

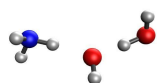
0 1,2

3

NH₂-



0

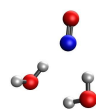


0.385



7.78

NO-



0

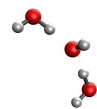


3.354

OH-



0



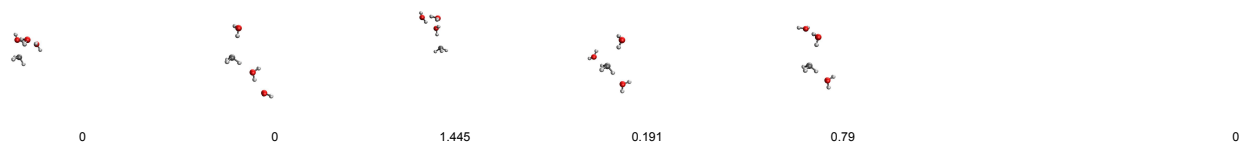
0.014

APPENDIX C. SUPPLEMENTARY INFORMATION: BINDING ENERGIES AND MOTIFS FOR ASTROCHEMICALLY RELEVANT MOLECULES

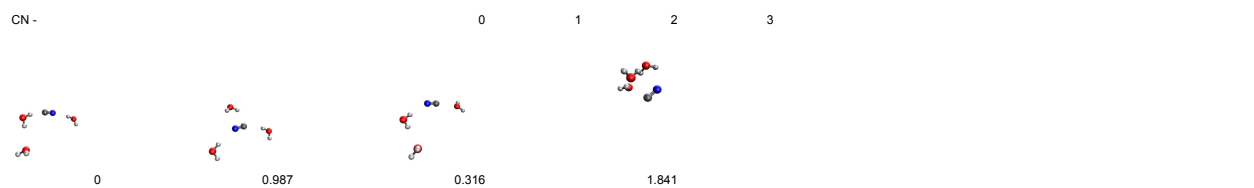
213

Distinct Conformers - Anionic trimer

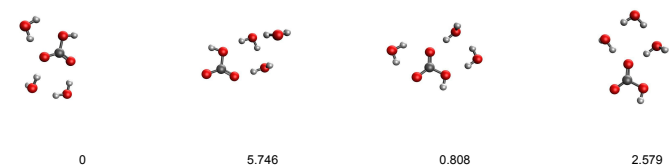
CH₃ -



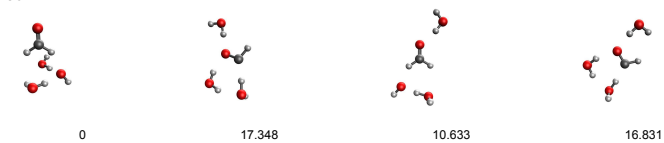
CN -



HCO₃ -



HCO -



NH₂ -



0



3.169



11.002

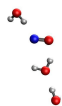


5.739

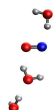
NO -



0



4.379



3.788

OH -



0



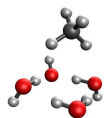
0.399



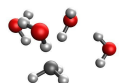
1.898

Distinct Conformers - Anionic tetramer

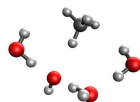
CH₃ -



0

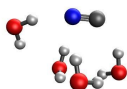


31.79



2.497

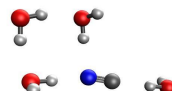
CN -



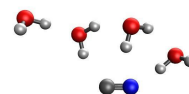
0



0.436

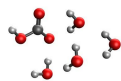


1.993

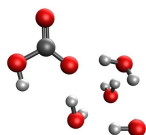


3.435

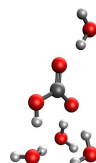
HCO₃ -



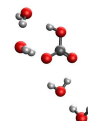
0



3.091

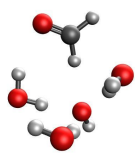


4.181

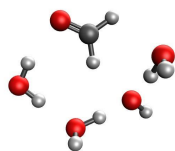


1.9

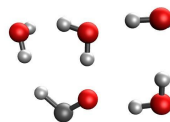
HCO -



0

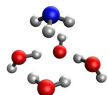


2.762

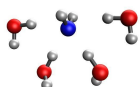


35.153

NH2 -

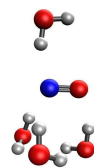


0

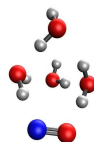


13.379

NO -

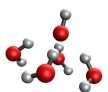


0

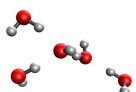


5.245

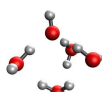
OH -



0



5.185



0.69